Tracking the activity of supermassive black holes and the habitats of their hosts

Charutha Krishnan

The University of Nottingham

Thesis submitted to the University of Nottingham
for the degree of Doctor of Philosophy

May 2019

"Per aspera ad astra"

– Lucius Annaeus Seneca

Supervisors:	Prof. Omar Almaini
	Dr. Nina Hatch
Examiners:	Prof. David Alexander *(University of Durham)*
	Dr. Simon Dye *(University of Nottingham)*
Submitted:	10 May 2019
Examined:	05 Jul 2019
Final version:	TBA

Contents

List of Figures

Abstract

In this thesis, we explore the connections between active galactic nuclei (AGN) and the environments of their host galaxies across cosmic time, as viewed using three complementary angles. Much of this thesis is based on recently available, state-of-the-art data. Our galaxy catalogues comprise deep, multi-wavelength data provided by the UKIDSS Ultra Deep Survey (UDS) and Cosmic Evolution Survey (COSMOS). The UDS field contains a dense structure at $z \sim 1.6$ with additional narrow-band imaging tailored to its redshift, allowing for the selection of protocluster members using precise photometric redshifts (Hatch et al. 2016). Both the UDS and COSMOS have coverage from X-ray telescopes such as *Chandra* and *XMM-Newton*, enabling the clean selection of AGN. This thesis also makes use of galaxy classifications (such as star-forming, passive, and post-starburst) based on principal component analysis (PCA) of broad-band photometry.

In our first study, we investigate the prevalence of AGN in the Cl 0218.3–0510 protocluster at $z = 1.62$. Analyses using imaging from the *Chandra* X-ray Telescope reveal a large overdensity of AGN in the protocluster by a factor of 23 ± 9 times the field density of AGN. The overdensity of massive galaxies in the protocluster is a factor of 11 ± 2, accounting for roughly half of the measured AGN overdensity. Likewise, we find that $17^{+6}_{-5}\%$ of massive galaxies ($M_* > 10^{10}\,\mathrm{M}_\odot$) in the protocluster host an X-ray luminous AGN, compared to $8 \pm 1\%$ in the field, corresponding to an enhancement of AGN activity in massive protocluster galaxies by a factor of 2.1 ± 0.7. This AGN overdensity is centrally concentrated, located within 3 arcmin and most pronounced within 1 arcmin of the centre of the protocluster. We find no significant differences in the distributions of AGN properties such as X-ray luminosity and hardness ratio, between AGN in the protocluster and the field. Using visually classified morphologies, we find tentative evidence that the fraction of "irregular" galaxies is also enhanced in the protocluster with respect to the field. From these results, we conclude that there is a reversal in the local anti-correlation between galaxy density and AGN activity, and that there is tentative evidence for a correlation between galaxy interactions and AGN activity.

Adopting a statistical approach, in our second study we investigate the relationship between AGN and dark matter halo mass using clustering techniques. We

present evidence that X-ray selected AGN in the UDS and COSMOS fields show a clustering signal likely determined by the properties of their host galaxies, at all epochs from $z \sim 4.5$ to $z \sim 0.5$. Consistent with previous studies, we find that AGN are on average hosted by galaxies in dark matter halos of $10^{12} - 10^{13}$ $M_{\odot}$, corresponding to group-like environments. However, we show that the same clustering signal can be produced by inactive (i.e. non-AGN) galaxies closely matched to the AGN in spectral class, stellar mass and redshift. We find that AGN in higher mass galaxies have a higher clustering signal, but that this stellar mass dependence disappears when passive host galaxies are removed. The strength of clustering is also largely independent of AGN X-ray luminosity. Therefore, the most important property that determines the clustering in a given AGN population appears to be the fraction of passive host galaxies. From these results we infer that AGN luminosity is likely not driven by environmental triggering, and conclude that AGN may be a stochastic phenomenon without a strong dependence on large-scale environment.

Finally, our third study presents a preliminary analysis of the properties of galaxy neighbours within 500 kpc of X-ray selected AGN between $z \sim 2.5$ and $z \sim 0.5$ in the UDS and COSMOS fields. At all epochs, we find consistent number densities of neighbours around AGN and control galaxies, suggesting that AGN do not live in special environments. At the highest redshifts ($1.5 < z < 2.5$), the neighbours of AGN are indistinguishable from those of control galaxies, since the star-forming properties of neighbours around AGN in passive/star-forming hosts are consistent with control passive/star-forming galaxies. We find that the star-formation activity of neighbours of AGN is more complex at lower redshifts, since we see opposite trends below and above $z = 1$. At $1.0 < z < 1.5$ we find that the star-formation activity in the neighbours of AGN is enhanced (at 2.3σ) with respect to neighbours of control galaxies, while this is reversed at $0.5 < z < 1.0$ (at 4.3σ). This study must be repeated in smaller redshift intervals in order to develop a deeper understanding of these trends and to draw robust conclusions.

In conclusion of the work presented in this thesis, the majority of AGN (hosted by normal, star-forming galaxies) are likely triggered by the stochastic accretion of cold gas, without a dominant influence from the environment. It appears that galaxy mergers and interactions *can* play a role in triggering AGN, especially in passive host galaxies, but that they are not a crucial parameter for the vast majority of the AGN population.

Acknowledgements

First and foremost, I would like to thank my supervisors, Omar and Nina, for your patient guidance throughout my PhD. You have helped me navigate through the terrain of research and pushed me to do my best. Thank you for your commitment, your encouragement, your advice, and of course your time over the past years. I am certainly lucky to have supervisors who cared so much about my work, were so prompt in responding to my questions, and were so enthusiastic about science.

I would also like to thank my collaborators, especially Dave, Aaron and Lizzie, for your advice and support. I am grateful to the entire UDS crew for providing invaluable discussions of various topics ranging from confusing plots, to women in astronomy, to time management. Amelia, Ulli, and Dave, thank you very much for your career advice. Many thanks also to Alfonso and Meghan for your journal club talks, which had a big impact on my relationship with my work.

I'm very grateful for all the science (and non-science) discussions with my academic sibling, Miguel. I'm eternally indebted to you and Mehdi for your support whilst I was on crutches at the Garching conference. Thanks to Fahad, Berta, Rachana, Felipe, Miguel, Lizzie, Mehdi, Jake and Rachel for tea/coffee breaks. Next up, I'd like to thank my officemates for creating a lively environment, with special credit to Finlay (+Tom), Jake, Fahad, Roan, and Amy. As promised, "Finlay is my proof-reader and he is great. Thanks Finlay."

Many thanks to my wonderful school friends Nivy, Sharanya, Sunila, and Silpa for being yourselves and for being part of my support network. Nishith, I will always be grateful that the University of Nottingham sent me your forms by accident and worked as a conversation starter between us. Mandeep, thank you for the many many cups of Masala Chai you have made over the years.

Finally, Amma and Achan, thank you so much for being so wonderful to me. I know everyone says this, but you are truly the best parents ever! My grandparents have played a huge role in shaping who I am today, even if only one of you remains. Thank you.

Published work

Much of the work in this thesis also appears in the following papers:

I Krishnan C., Hatch N. A., Almaini O., Kocevski D., Cooke, E. A., Hartley W. G., Hasinger G., Maltby D. T., Muldrew S. I., Simpson C., 2017, *"Enhancement of AGN in a protocluster at z = 1.6"*, MNRAS, 470, 2170

II Krishnan C., Almaini O., Hatch N. A., Wilkinson A., Maltby D. T., Conselice C. J., Kocevski D., Suh H., Wild, V., 2019, *"The clustering of X-ray AGN at 0.5 ¡ z ¡ 4.5: host galaxies dictate dark matter halo mass"*, MNRAS, resubmitted.

Paper I contains much of the work detailed in Chapter 3 of this thesis. Paper II describes the work presented in Chapter 4.

The vast majority of the work presented in this thesis was performed by the author, with advice from the paper co-authors listed above. Where the material presented is the result of more collaborative work, this is mentioned at the beginning of the relevant chapter.

Chapter 1

Introduction

1.1 Galaxy evolution

1.1.1 The field of extragalactic astronomy

The field of extragalactic astronomy was a late-bloomer compared to other branches of astronomy such as the study of the solar system, stars and our own Galaxy. Back in the early 1700s, it was still widely believed that the Milky Way was the extent of our Universe. It all began with Immanuel Kant's suggestion of "island universes" or galaxies external to the Milky Way, which gave rise to the hypothesis that observed galaxies are more than "nebulae of an unknown nature". The debate as to whether or not these systems were part of our Galaxy was the hot topic of the era. A major breakthrough took the form of Edwin Hubble's calculations of distances to candidate "spiral nebulae" galaxies using Cepheid variable stars (Hubble 1925). This placed some of these nebulae at distances over 200 kpc, well outside the boundaries of our own Galaxy. It was thus concluded that these astronomical objects were indeed "extragalactic" in nature. Like all exciting discoveries, this opened up more scientific questions than it solved. The field of *extragalactic astronomy* was only in its infancy, and researchers to this day continue their attempts of understanding fundamental questions such as:

- What are the different types of observed galaxies?
- Why are galaxies distributed throughout the Universe the way they are?
- How do galaxies form and evolve?
- What physical processes are responsible for the differences in galaxy types?

Hubble made rapid progress on the first question and managed to classify over 400 galaxies based on their morphology and complexity (Hubble 1926, 1936). He also created a classification scheme now known as "the Hubble Sequence", which remains

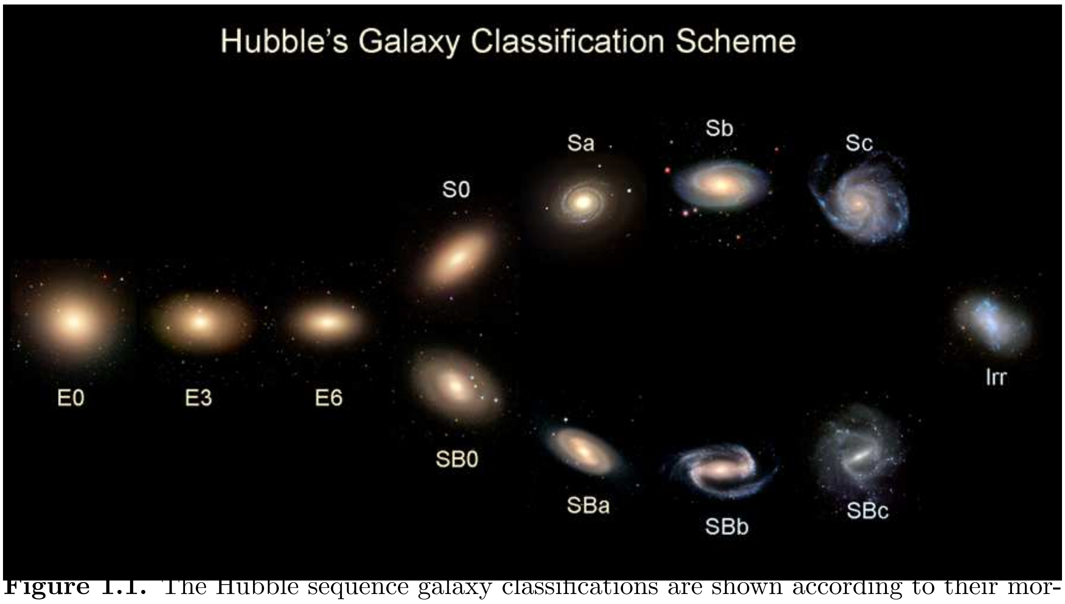

Figure 1.1. The Hubble sequence galaxy classifications are shown according to their morphology into spiral, elliptical (E), and lenticular (S0) galaxies (Hubble 1925). The spirals branch out into "normal" spirals on the top, and "barred" spirals on the bottom. This image was produced using the Sloan Digital Sky Survey (SDSS, York et al. 2000) galaxies, classified by participants of the GalaxyZoo project (Lintott et al. 2008).

widely used today (see Figure 1.1). The galaxies on the left of the diagram are known as ellipticals or "early-types" although it must be stressed that this nomenclature does not reflect the evolutionary stage of the galaxy. Lenticulars are found in the middle, and the spirals or "late-types" are found branching out on the right side.

1.1.2 Galaxy environments

It was clear to the pioneers of extragalactic astronomy that galaxies are not distributed randomly in the Universe, and hence a question that has long been pondered is: *Why are galaxies distributed throughout the Universe the way they are?* Since the 1930s, it has been observed that galaxies are typically found to be in close proximity to other galaxies (Hubble & Humason 1931; Shapley 1933; Abell 1965). Observations of this "clustering" and of interacting galaxies thus led to the interesting hypothesis that galaxies may be influenced by their surrounding environments.

The terminology of "galaxy environments" generally refers to local galaxy densities. These environments can take several forms, such as cosmic voids, the field (isolated galaxies), galaxy groups, and massive galaxy cluster cores, in increasing order of local galaxy density. These galaxy environments originated from structure formation, which we review in the next section.

1.1.3 Structure formation

Before reviewing the theory of structure formation, we must first take a step back and consider the cosmology of the Universe, since this governs the formation and evolution of galaxies.

Cosmology

The currently favoured standard cosmological model of the Universe, the ΛCDM paradigm, describes the Universe dominated by a cosmological constant (Λ) and cold dark matter (CDM). This model successfully reproduces several observed properties of the Universe, such as the large scale structure of the Universe (Springel, Frenk & White 2006), the power spectrum of the Cosmic Microwave Background (CMB; remnant blackbody radiation from the Big Bang that permeates the Universe; Peebles et al. 1991), and the abundances of common elements (Peebles et al. 1991).

The Universe is thought to be spatially flat since the density of the Universe is observed to be equal to the critical density (Planck Collaboration et al. 2018). The ratio of these is defined by the density parameter for species i, $\Omega_i = \frac{\rho_i}{\rho_c}$. The value of this parameter today Ω_0 is given by the sum of its parts:

$$\Omega_0 = \Omega_{\gamma,0} + \Omega_{\Lambda,0} + \Omega_{\mathrm{m},0}, \tag{1.1}$$

where Ω_γ is the radiation density, Ω_Λ is the dark energy density, Ω_m is the matter density of the Universe, and the subscript 0 indicates that the values correspond to the present epoch. The radiation density is negligible today ($\Omega_{\gamma,0} \simeq 0$), but the model predicts it to have dominated at early times. The most up-to-date measurements of cosmological parameters are $\Omega_m = 0.311 \pm 0.006$ and $\Omega_\Lambda = 0.689 \pm 0.006$ (Planck Collaboration et al. 2018). The dark energy density $\Omega_{\Lambda,0}$ represents the most mysterious component of our Universe. The favoured explanation of its nature is a form of vacuum energy that is the expected driver of the accelerated expansion of the Universe (Riess et al. 1998; Perlmutter et al. 1999).

The matter density $\Omega_{m,0}$ of the Universe is the sum of two types of matter: baryonic and dark matter. Baryonic matter refers to the observable matter of our Universe, including the matter we detect from its interactions with light, such as stars and galactic and intergalactic gas. The latest estimates are that $\sim 5\%$ and $\sim 26\%$ of the density of the Universe correspond to these observable components and dark matter respectively (Planck Collaboration et al. 2018). There is a plethora of indirect evidence for dark matter such as the flat rotation curves of disk galaxies (Zwicky 1933; Rubin, Ford & Thonnard 1978), mass measurements of galaxy clusters (Zwicky 1933, 1937), and gravitational lensing (e.g., Clowe et al. 2006). Nevertheless, direct detection of dark matter particles has not been possible, despite numerous attempts from the cosmology community (Bertone, Hooper & Silk 2005).

Hierarchical assembly

Under the ΛCDM paradigm, dark matter is assumed to govern the formation of structures such as galaxies and galaxy clusters. The seeds of structure formation are thought to be primordial density fluctuations in the early Universe, observed as temperature anisotropies in the CMB. These primordial fluctuations are then amplified during inflation, after which they collapse due to gravitational instabilities and evolve through the accretion of dark matter (Peacock 1999). Under the standard model, dark matter is cold (i.e. non-relativistic), and hence structures form in a bottom-up manner (Davis et al. 1985). The first structures to form are dark matter clumps on small scales, followed by low-mass dark matter halos. As the Universe evolves, these halos merge and collapse into more massive halos through a process known as hierarchical aggregation (Lacey & Cole 1993). This process is demonstrated by Figure 1.2. These models have been found to successfully reproduce the observed dark matter halo distribution (e.g. Springel, Di Matteo & Hernquist 2005). On the other hand, simulators have been able to rule out "monolithic collapse" models with relativistic hot dark matter, where the largest structures would have formed first in a top-down approach. This is due to inconsistencies between observations and predictions of structure in the Universe (White, Frenk & Davis 1983).

Clustering

The large scale distribution of galaxies in the Universe as observed by galaxy surveys is well reproduced by the distribution of dark matter as modelled by N-body simulations (Springel, Frenk & White 2006). The striking similarity between the distributions of observed galaxies and those from dark matter based simulations is evident in Figure 1.3, suggesting that the distribution and evolution of galaxies closely follows that of dark matter. It is commonly assumed that galaxies are encased in the central regions of dark matter halos, and that galaxies are a "biased" tracer of the underlying dark matter distribution (Kaiser 1984; Bardeen et al. 1986).

The spatial distribution of a galaxy population can be statistically described by its "clustering". The study of how galaxies are distributed in the Universe is one of the first scientific questions explored in extragalactic astronomy, and galaxy clustering is a well-studied technique in this field (e.g. Coil 2013). While there are a number of techniques used to study the clustering of a given population, the 2-point correlation function remains the most commonly used statistical estimator, and traces the amplitude of galaxy clustering as a function of scale.

As shown by the following equation, the 2-point correlation function $\xi(r)$ is defined as the excess probability (above random) of finding two galaxies in infinitesimal volume elements, δV_1 and δV_2, separated by a distance r (Groth & Peebles 1977;

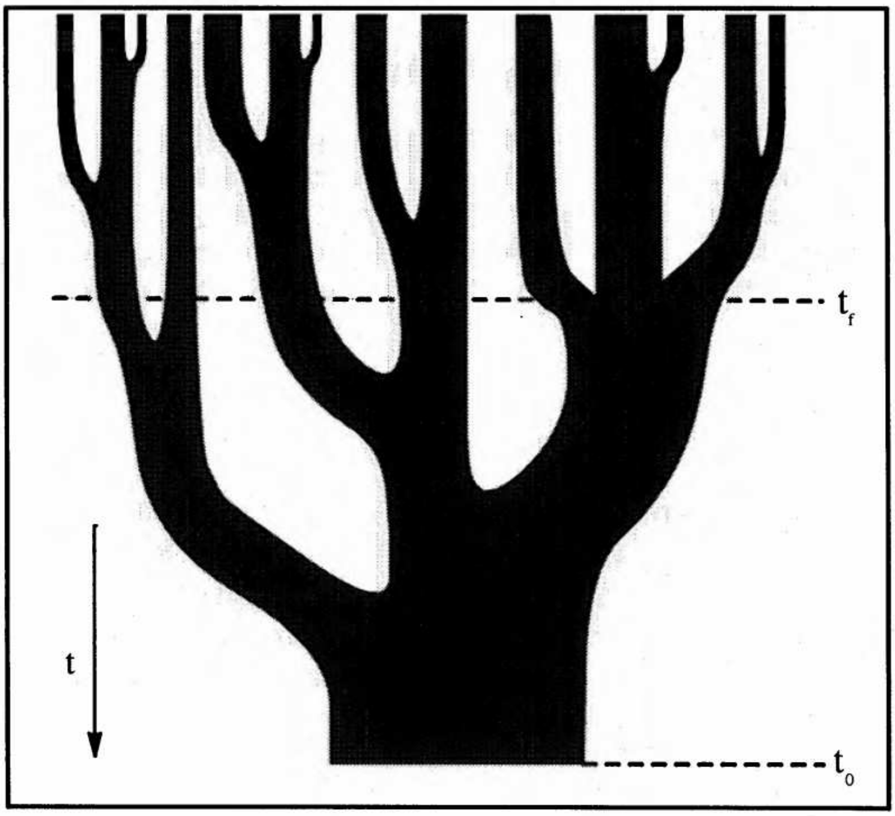

Figure 1.2. Schematic illustrating the dark matter halo merger tree (Lacey & Cole 1993). The growth of dark matter halos as a result of a series of mergers is depicted from a formation time t_{f} (top) to the present epoch t_0 (bottom).

Peebles 1980):

$$\delta^2 P = n_g^2[1 + \xi(r_{12})]\delta V_1 \delta V_2. \tag{1.2}$$

$\xi(r)$ can be estimated numerically from the data by comparing counts of pairs of galaxies to randoms, making use of a random catalogue sampling the same volume and same selection function as the galaxy catalogue. The simplest form of such an estimator is:

$$\xi(r) = \frac{DD(r)}{RR(r)} - 1, \tag{1.3}$$

where $DD(r)$ and $RR(r)$ are the (normalised) pairs of galaxies and randoms as a function of separation r, such that $\xi = 0$ indicates a random distribution of galaxies.

However, this requires knowledge of the 3D positions of galaxies. The angular version of the 2-point correlation function allows for the measurement of clustering based on the 2D projected sky. The equivalent excess probability $\delta^2 P_{\mathrm{ang}}$ of finding two galaxies in solid angle elements $\delta\Omega$, as a function of angular separation θ is given by:

$$\delta^2 P_{\mathrm{ang}} = n_\Omega^2[1 + w(\theta_{12})]\delta\Omega_1 \delta\Omega_2, \tag{1.4}$$

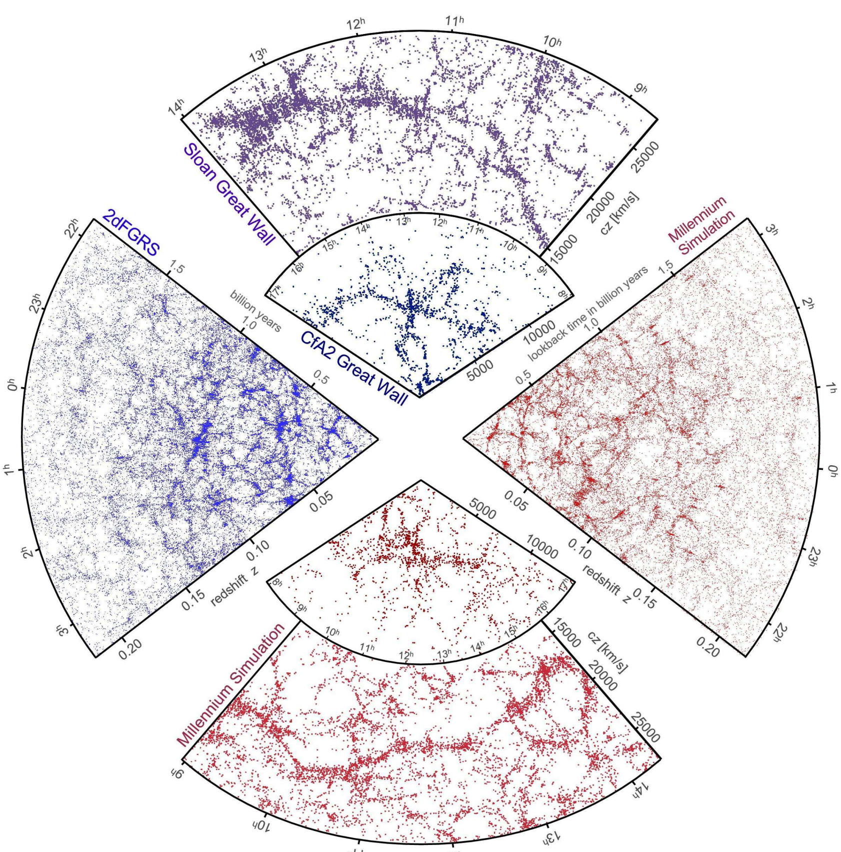

Figure 1.3. A direct comparison between the distribution of galaxies in observational spectroscopic surveys (including CfA2, 2dFGRS, and SDSS) and that of galaxies predicted by dark-matter-only simulations. The top and left sectors (blue and purple) show the large scale structure observed by the 2dFGRS and the Sloan Great Wall respectively. This figure displays the striking similarity of the simulated large scale structure in the Millenium simulation, shown bottom and right sectors (red). Figure credit: Springel, Frenk & White (2006).

and the equivalent estimator measuring pair counts as a function of *angular* separation (as opposed to a physical separation) is:

$$w(\theta) = \frac{DD(\theta)}{RR(\theta)} - 1. \quad (1.5)$$

This clustering technique has been widely used in the field to study the link between galaxy evolution and large scale structure, and we provide details on our implementation in Section 4.3. Measuring the clustering of galaxy populations in this way allows for the estimation of dark matter halo masses for typical galaxy populations, since the two are intimately related. We know that galaxies form in the centres of dark matter halos, and that dark matter halos are more clustered (i.e. a more biased tracer of) than the underlying dark matter distribution (forming its densest peaks; Bardeen et al. 1986). The clustering strength (bias) of a given galaxy population thus determines its typical dark matter halo mass. As shown by Mo & White (1996), this "bias" increases with redshift (at early times galaxies collapsed in the most overdense regions of space, whereas galaxies start forming in less dense regions as the Universe evolves) and halo mass (since more massive dark matter halos form the densest peaks in the dark matter distribution). Therefore, clustering analyses are invaluable in the study of galaxy evolution and large scale structure.

Galaxy formation

There has been much progress on the question: *How do galaxies form and evolve?* Galaxies are thought to form as gas collapses due to the gravitational potential well of dark matter halos. As halos accrete, shock heating gives rise to temperatures $\gtrsim 10^4$K in the gas within halos, in turn leading to ionisation. This ionised gas has the pressure required to support itself against gravitational collapse. As the gas cools however, it collapses under its own gravity and fragments to form stars, and eventually galaxies. As the Universe evolves, the dark matter halos hosting these galaxies can merge such that multiple galaxies are encased in the same parent halo, leading to galaxy groups and clusters (Lacey & Cole 1993; De Lucia et al. 2006). The galaxies themselves can also merge (revisited in Section 1.1.6), resulting in the formation of ever more massive galaxies such as Brightest Cluster Galaxies (BCGs, Lidman et al. 2013).

This simple picture alone, however, is insufficient to accurately describe galaxy formation and evolution. This is evident from comparisons of the observed and CDM-motivated predicted mass/luminosity function (i.e. the number densities of galaxies as a function of mass/luminosity), as shown by the schematic in Figure 1.4 from Silk & Mamon (2012). As shown by this schematic, it appears that simulations and models allow gas to *over-cool*, leading to the creation of higher numbers of galaxies at both high and low masses. To overcome this issue, feedback mechanisms, such as stellar processes at low masses (Efstathiou 2000) and active galactic nuclei (AGN) feedback (Croton et al. 2006) at high masses, are invoked in order to heat gas and regulate star formation. Applying these feedback mechanisms, the latest semi-analytical models of galaxy formation and evolution have managed to successfully reproduce the observed stellar mass function at $z = 0$ (e.g., Guo et al. 2011; Bower, Benson & Crain 2012), although it appears that inconsistencies still exist at higher redshift (Fontanot et al. 2009; Guo et al. 2011; Asquith et al. 2018).

While the nature of dark matter remains a mystery, its physics is somewhat understood and so is easier to model (as collisionless particles following Newtonian gravity). On the other hand, there is no clear explanation for the physics of the visible but elusive baryonic matter. Nevertheless, the complexity of baryonic processes leads to the formation of galaxies with drastic variation in properties such as morphology, size, colour, and spectral energy distribution (SED).

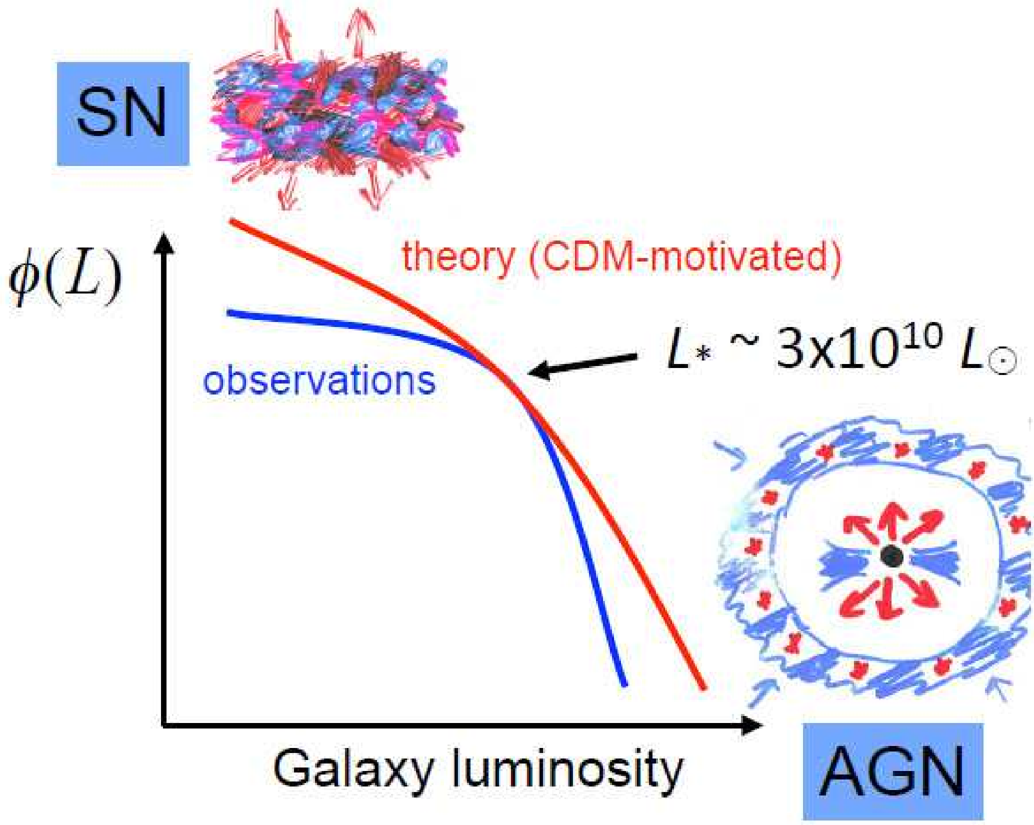

Figure 1.4. Diagram from Silk & Mamon (2012), demonstrating the discrepancy between the observed luminosity function and that predicted from dark matter simulations. To overcome this discrepancy, feedback processes are invoked to prevent over-cooling. At low masses, stellar feedback regulates star-formation to prevent over-production of galaxies, while AGN feedback does the same job at high masses.

1.1.4 Galaxy bimodality

Since Hubble's work in classifying galaxies by their morphologies, astronomers have gone on to study various properties of galaxies. The distributions of these galaxy properties tend to be bimodal in nature. The majority of galaxies in the local Universe fall into one of two broad categories: the more numerous "blue cloud" galaxies and the secondary peak of "red-sequence" galaxies, named after their features on the colour-magnitude diagram (red/blue and cloud/sequence based on scatter/tightness). The most studied galaxy properties that show bimodality corresponding to these two populations are:

1. *Star-formation activity*: Galaxy bimodality is clearly shown by the star-forming main sequence, which is a diagram of star-formation rate (SFR) vs stellar mass. Star-forming galaxies lie on the expected line (e.g., Brinchmann et al. 2004). Those that fall roughly an order of magnitude below (forming far fewer stars than expected for their mass) fall into the category of passive galaxies. These passive galaxies are typically more massive than star-forming galaxies.

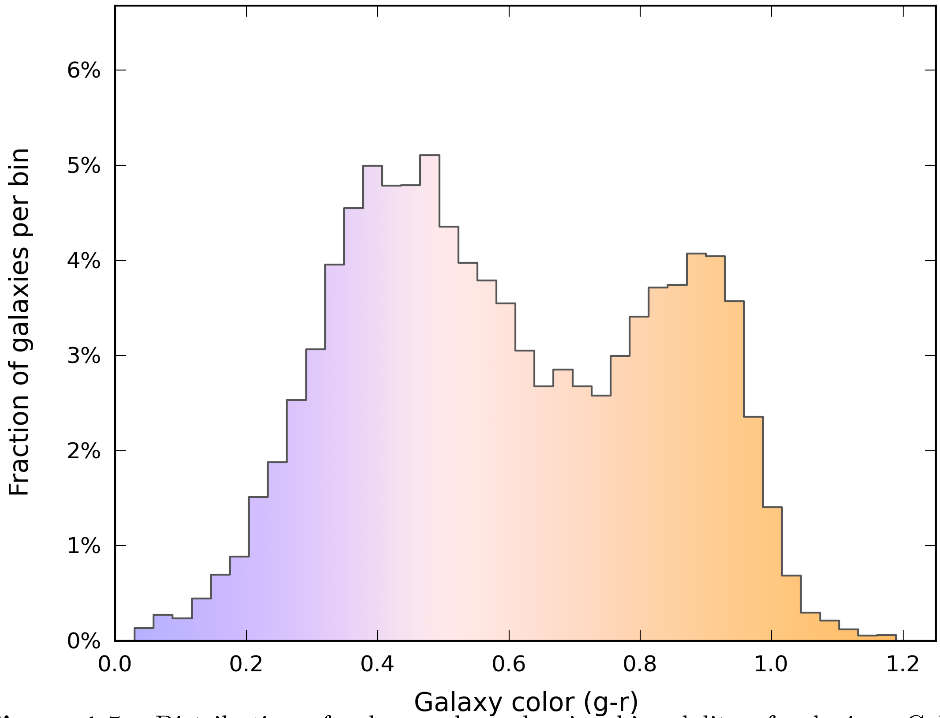

Figure 1.5. Distribution of galaxy colour showing bimodality of galaxies. Colours are chosen to somewhat reflect reality. Plot created using $> 180,000$ SDSS galaxies from Blanton et al. (2003). Figure credit: Markus Pössel.

A linked galaxy property that also shows bimodality is galaxy colour, defined as the difference between the magnitudes of two wavelength bands. The presence of hot, young O and B stars leads to the blue colour of star-forming galaxies. Conversely, passive galaxies are red in colour because of the long time since star-formation and the dominance of the old and low-mass stars. An important caveat is that dusty star-forming galaxies appear red due to dust absorption of high energy photons, followed by re-emission at longer wavelengths.

2. *Colour*: Galaxy colour bimodality can be seen in the example colour distribution of $> 180,000$ SDSS galaxies shown by Figure 1.5. The primary and secondary peaks correspond to the blue cloud (star-forming) and red-sequence (passive) galaxy populations respectively. Colour-mass diagrams show that there is a strong bimodality corresponding to the two populations, with a clear "red-sequence" and a "blue cloud" (with slightly more scatter). It can also be seen that blue galaxies tend to be less massive than red galaxies. This colour bimodality is well-established at $z = 0$ and has been found to exist out to $z \sim 2$, albeit less distinctively (e.g., Bell et al. 2004; Faber et al. 2007).

3. *Morpoholgy & structure*: Galaxies can be separated based on the complexity of their morphology. A strong morphological bimodality has been observed

where featureless and smooth "early-type" morphologies tend to correspond to the massive, passively evolving galaxies, whereas complex, spiral, barred, or irregular "late-type" galaxies make up the lower mass, star-forming population (e.g., Strateva et al. 2001). Visual morphologies have also been parametrised using structural parameters such as the Sérsic index n (Sérsic 1963), and structural bimodality appears to exist out to $z \sim 2$ (Ravindranath et al. 2004; Bell et al. 2004; Nair & Abraham 2010; Buitrago et al. 2013; Mortlock et al. 2013).

Thus the blue cloud consists of galaxies with low stellar masses, high star-formation rates, bluer colours, and late-type morphologies. In contrast, the red sequence is made up of massive, passively evolving galaxies with low SFRs, redder colours, and early-type morphologies. This is a broad generalisation, however, as studies have shown the existence of blue ellipticals (Schawinski et al. 2009) and red spirals (Masters et al. 2010). Dusty star-forming galaxies also appear red due to dust absorption.

1.1.5 Galaxy properties vs environment

Having introduced the concept of galaxy environments and discussed galaxy bimodality, in this section we review the correlations between the properties of galaxies and their environments.

1. *Morphology-density relation*: Since the early days of extragalactic astronomy, it has been noted that there is a clear contrast between the galaxy morphologies of high density cluster cores (early-types) and low density field environments (spirals, Hubble & Humason 1931; Abell 1965). This relationship was first quantified at $z = 0$ by Dressler (1980), as shown by Figure 1.6. He showed that the fraction of early type galaxies (E and S0 in the figure) steadily increases as a function of galaxy density, while the fraction of late-type galaxies (S + Irr in the figure) falls steeply.

2. *Colour-density relation*: The colours of galaxies have also revealed a strong correlation with environment (e.g., Kodama et al. 2001; Blanton et al. 2005; Baldry et al. 2006). While the significance of this result decreases with redshift, it has been detected out to $z \sim 1.5$ (e.g., Cooper et al. 2007; Chuter et al. 2011).

3. *SFR-density relation*: Similarly, a distinct correlation has been observed between the SFR of galaxies and their local galaxy density in the low-redshift Universe: high density environments have galaxies with much lower star-formation rates than low density environments (e.g., Lewis et al. 2002; Gómez et al. 2003). This relationship has been found to exist out to $z \sim 1.5$, and clustering studies suggest that passive galaxies are more clustered than star-forming galaxies

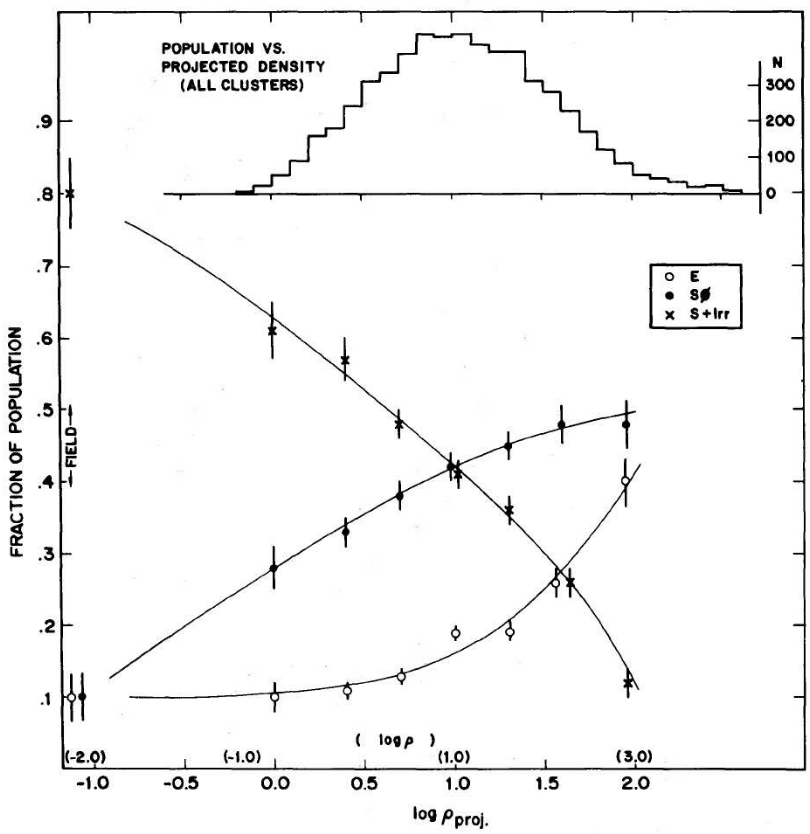

Figure 1.6. The morphology-density relationship, showing the fraction of elliptical (E), lenticular (S0), and spiral and irregular (S + Irr) galaxies as a function of galaxy density at $z = 0$. The fraction of early-type galaxies (ellipticals and lenticulars) increases with local galaxy density, while the fraction of late types (spirals and irregulars) decrease. Figure credit: Dressler (1980).

out to $z \sim 3$ (e.g., Hartley et al. 2013; Wilkinson et al. 2017). In addition, curious correlations have been observed between the star-formation activity of galaxies that are at the centre of their groups ("centrals"), and that of the surrounding galaxies ("satellites", Wirth 1983; Ramella et al. 1987; Weinmann et al. 2006; Ann, Park & Choi 2008; Kawinwanichakij et al. 2014; Hartley et al. 2015). This effect, also known as "galactic conformity", was first detected in a systematic manner by Weinmann et al. (2006), where red central galaxies were found to have a higher fraction of red satellites. We investigate the role that AGN play in this picture in Chapter 5.

4. *AGN-density relation*: In the local Universe, the AGN fraction appears to be suppressed in galaxy clusters (Dressler, Thompson & Shectman 1985; Kauffmann et al. 2004) with respect to low-density field environments. However, the relationship between AGN activity and galaxy environment is far from certain and hotly debated to date. This is explored further in Section 1.3.2 and motivates the three projects presented in this thesis.

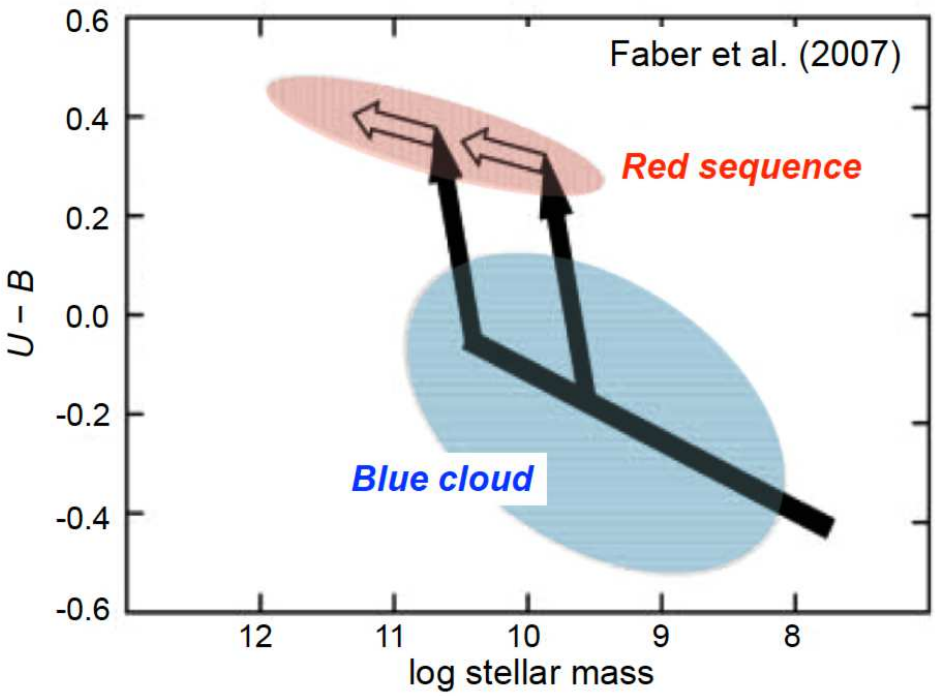

Figure 1.7. Transformation of galaxies from the blue cloud into the red sequence. A variety of physical processes may be responsible for this, including secular processes (mass quenching) and environmental processes (environmental quenching). Figure adapted from (Faber et al. 2007).

These correlations between galaxy properties and environment suggest an evolutionary link: are environmental processes responsible for the transformation of galaxies from the blue cloud into the red sequence?

1.1.6 Quenching of star-formation

The bimodality of galaxies, and the strong correlations between galaxy properties and environment, raise the fundamental question: *what physical processes are responsible for some galaxies to become old, red, passive, early-type galaxies as opposed to young, blue star-forming late-type galaxies?*

Astronomers have come to believe that galaxies are transformed from the blue cloud to the red sequence via a variety of "quenching" mechanisms, as discussed in the following subsections. A schematic representing the journey of galaxies between the two distinct populations is shown in Figure 1.7. These can be classified into two broad categories: environmental processes ("nurture") and secular evolution ("nature").

Environmental processes

Several quenching mechanisms have been proposed to account for the observed correlations between galaxy properties and environment. These mechanisms include galaxy-galaxy interactions such as galaxy mergers and tidal interactions, but also interactions with the intra-cluster medium (ICM) of galaxy clusters, such as ram-pressure stripping, strangulation, and thermal evaporation:

1. *Galaxy mergers* result in the merging of stellar distributions of two galaxies (Icke 1985), and are most common in small galaxy groups with low velocity dispersions (Ostriker 1980). *Major* mergers occur where the two participant galaxies have similar masses, resulting in significant modification of the structure of both galaxies (Toomre & Toomre 1972). *Minor* mergers, on the other hand, occur where galaxies of mass ratio 4:1 or higher merge, resulting in total disruption of the smaller galaxy, and minor structural changes to the more massive galaxy (Younger et al. 2007). These mergers are able to disrupt the star-formation processes that take place in the galaxies, resulting in quenching. *Wet* mergers refer to the merging of two gas-rich galaxies, where the interaction of gas causes a significant fraction of kinetic energy to be dissipated (Mihos & Hernquist 1996). It is thought that gas is funnelled into the central regions of the galaxy, leading to quenching following a starburst or AGN feedback (see next section).

2. *Tidal interactions* refer to gravitational interactions between galaxies. These are most severe in galaxy groups, as galaxies interact with other galaxies with low relative velocities, leading to tidal stripping. On the other hand, *galaxy harassment* occurs as repeated galaxy interactions with high relative velocities (Moore et al. 1996) result in the quenching of star-formation due to long-term disturbance of the gas content.

3. *Ram-pressure stripping* occurs when the cold gas reservoir of a galaxy is removed by the ram pressure exerted by the ICM (Gunn & Gott 1972), resulting in the deprivation of fuel necessary for star-formation. *Strangulation* comes into play when this ram pressure is not sufficient to remove the cold gas reservoir, but is enough to drive the circumgalactic medium (which replenishes this cold gas reservoir) away, eventually leading to quenching once the cold gas reservoir is used up (Larson, Tinsley & Caldwell 1980). For example, *tidal truncation* of outer galactic regions can occur due to the potential well of the cluster, leading to the removal of the outer hot gas reservoir (Merritt 1983).

4. *Thermal evaporation* can also take place due to the heating of the interstellar medium of a galaxy upon interaction with the hot ICM, such that gas does

not collapse into stars (Cowie & Songaila 1977).

Secular processes

The star-formation properties of galaxies have been found to correlate strongly with stellar mass (Peng et al. 2010), leading to the common nomenclature of "mass quenching". This secular channel includes mechanisms such as hot halo quenching, disk instabilities, and stellar and AGN feedback processes.

1. *Hot halo* quenching of intergalactic gas occurs due to the conversion of gravitational energy into heat (Birnboim & Dekel 2003; Kereš et al. 2005). Such infalling gas is unable to cool in dark matter halos more massive than 10^{12} $M_{\odot}$, resulting in shock heating of any further cold gas accretion. However, the hot halo hypothesis alone cannot explain quenching as these halos are expected to cool eventually, thus restarting the process of star formation.

2. *Disk instabilities* have also been proposed to develop as gas-rich disks grow above a certain mass threshold (Dekel, Sari & Ceverino 2009). These unstable disks could then trigger a starburst followed by rapid depletion of cold gas, leading to quenching of star formation.

3. *Stellar feedback* processes may regulate star formation in the form of strong outflows that inject large amounts of energy to surrounding cold gas (e.g., Chevalier & Clegg 1985). In models of galaxy formation and evolution, stellar feedback processes from supernovae explosions and stellar winds are invoked in order to prevent the over-formation of low-mass galaxies (e.g., Efstathiou 2000). These processes are also thought to play a part in regulating star formation in more massive systems (e.g. Diamond-Stanic et al. 2012).

4. *AGN feedback* comes into play as the energetic jets and outflows of gas from the supermassive black hole in the galactic centre are able to inject immense amounts of heat into (and even expel) the interstellar medium. This can lead to the quenching of star formation (Silk & Rees 1998), or to the maintenance of the quenched state of a galaxy (typically known as "radio-mode feedback", e.g. Croton et al. 2006).

1.2 Active galactic nuclei

Although the fields of neither active galactic nuclei (AGN) nor extragalactic astronomy were born at the time, the evidence for AGN dates back to 1908, when Edward Fath obtained spectra of star clusters and "spiral nebulae" and found that the spectrum of source NGC 1068 exhibited strong emission lines (Fath 1909). This did not receive much attention, until 1943 when Carl Seyfert obtained optical spectra for twelve galaxies with a high central concentration of light similar to NGC 1068. He discovered that six of these galaxies had strong, broad emission lines indicative of typical velocities between $500 - 4000$ km s^{-1} (Seyfert 1943), which led to the nomenclature of "Seyfert galaxies" to refer to similar objects. However, the field was still moving at a very slow pace until the discovery of radio-loud quasars two decades later (Schmidt 1963), when a whole new branch of extragalactic astronomy opened up. Over the next decade an interesting hypothesis started to take root: that quasars were the higher redshift, higher luminosity analogues of local Seyferts. Although this idea suffered much debate, it has eventually become the accepted paradigm, such that the umbrella term of AGN now encompasses both Seyferts and quasars, along with several other classes of interesting populations.

Today, the astronomical community is in consensus that essentially all massive galaxies host super-massive black holes (SMBHs), that are observed as AGN during their phases of intense mass accretion. This section reviews our understanding of black holes and AGN.

1.2.1 Black holes

The idea of black holes originated from a geologist and clergyman John Michell in 1783, who was the first to show using Newtonian physics that the escape velocity from the surface of a massive enough star would be greater than the speed of light. For a while the prospect of giant but invisible stars lurking in plain sight raised excitement, but this died down over time as light started to become understood as wave-like, since it was uncertain whether gravity could influence these light waves from escaping.

More than a century later, Einstein showed that gravity does influence the motion of light and published his theory of general relativity (Einstein 1916). Only a few months later, Karl Schwarzchild found the first modern solution of general relativity (Schwarzschild 1916). However, it was only in 1958 that David Finkelstein presented the interpretation that a black hole was a region of space from which no particle could ever escape (Finkelstein 1958). In the following decade it was shown that black holes were in fact a prediction of general relativity. It was in this era that the term "black hole" was coined.

There is much evidence for the existence of black holes, a few examples of which are outlined below:

1. The recent news (10th April 2019) of the first ever image of a black hole has prompted a wave of excitement through the astronomical community. The black hole in the centre of the M87 galaxy was captured by the Event Horizon Telescope, in the act of accreting hot gas with its strong gravitational influence

Figure 1.8. The supermassive black hole at the centre of the nearby elliptical galaxy M87, as depicted in the first ever image of a black hole, released by the Event Horizon Telescope on 10th April 2019 (Event Horizon Telescope Collaboration et al. 2019).

(Event Horizon Telescope Collaboration et al. 2019). This hot gas can be seen as the "ring" around the central black hole in Figure 1.8.

2. A similar wave of excitement was experienced during the first ever direct observation of gravitational waves in 2015 (Abbott et al. 2016). With comparisons to theoretical predictions, the signal was found to be consistent with a merger of two black holes of approximately 30 $M_\odot$ each. From the inferred separation of the two objects prior to the merger of only 350km, it was concluded that the objects must have been extremely compact, rendering black holes as the most plausible explanation.

3. There is also strong evidence for the black hole in our own Milky Way, Saggitarius A*. High resolution observations of the proper motions of stars in the Galactic centre show that the central light day contains a mass of $\sim 4 \times 10^6$ $M_\odot$ (Gillessen et al. 2009).

4. The nuclei of many nearby massive galaxies (e.g. M87, M84) also reveal Keplerian gas motion, implying central objects with masses of 10^7–10^9 $M_\odot$ (e.g., Ford et al. 1994; Bower et al. 1998).

Formation and growth into SMBHs

It has been proposed that the collapse of very massive stars in the early Universe resulted in "stellar mass" black holes (Madau & Rees 2001; Volonteri 2010). These black holes grow via the continuous accretion of matter such as gas and interstellar dust, or merging with stars or other black holes (e.g. Volonteri, Haardt & Madau 2003). Hence it has been proposed that these stellar mass black holes were the initial seeds of supermassive black holes that are now thought to lurk in the centres of all massive galaxies (Park et al. 2016; Pacucci et al. 2017). These SMBHs also provide strong evidence for black holes as they can be observed as AGN with characteristic observational properties.

1.2.2 Observational characteristics of AGN

Rapidly accreting SMBHs share some common observational properties, that drive our physical understanding of AGN and survey designs:

1. *Broad continuum emission*: "Normal galaxies" emit most of their radiation over a relatively narrow range of frequencies, and their spectral shape is typically dominated by the superposition of stellar blackbody spectra. On the other hand, as shown by Figure 1.9, most AGN display a fairly flat continuum shape (in terms of νf_ν) throughout much of the electromagnetic spectrum, from infrared wavelengths to hard X-rays. AGN can therefore outshine typical galaxies by an order of magnitude (or more). At X-ray wavelengths, the light from AGN can be up to four orders of magnitude brighter than non-active galaxies.

2. *Emission lines*: Significant line emission due to high excitation transitions has also been classed as a key characteristic of AGN. Common lines include ionised lines of H, He, C, O, Ne, Mg, Si, and Fe in optical and UV wavelengths, and the 6.4 keV Fe line in X-rays. Flux from broad-band filters can be significantly dominated by the strong nature of the line emission. These observed lines may be narrow and/or broad depending on the class of AGN (see Section 1.2.3), including permitted, semi-forbidden, and forbidden transitions.

3. *Variability* of the continuum and line emission across multiple wavelengths is one of the most characteristic traits of AGN. The timescales of the aperiodic flux variability of AGN ranges from minutes to years, with faster variability in shorter frequency wavebands. For example, at X-ray wavelengths, AGN display significant variability on minute scales whereas at optical/near-infrared wavelengths, AGN vary on monthly or yearly timescales.

4. *Compact, luminous nucleus*: AGN generate an immense amount of power in an extremely compact central region. AGN luminosities typically vary between $10^{42} < L < 10^{48}$ erg s^{-1}, outshining a typical non-AGN galaxy by up to a factor of 10^4 in X-rays. Studies of variability suggest that the upper limit on the size of the emitting region of 10^{-4}–10 pc.

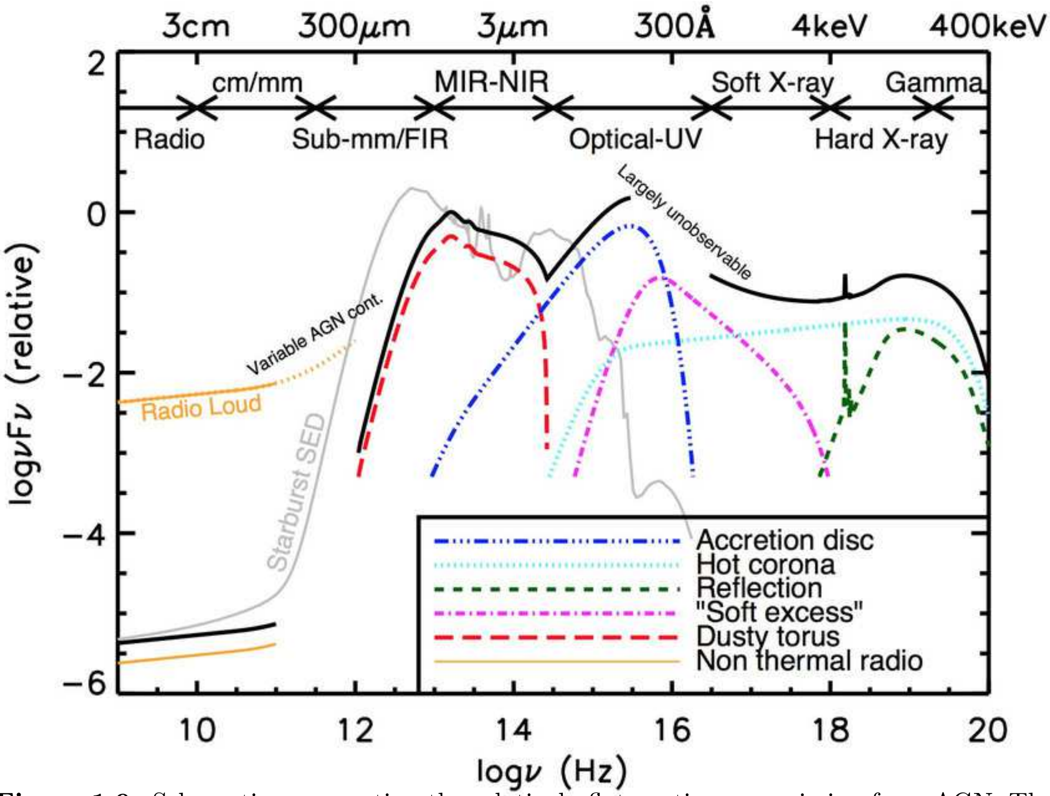

Figure 1.9. Schematic representing the relatively flat continuum emission from AGN. The black solid curve denotes the total spectral energy distribution and the coloured lines (offset for clarity) show the constituent components. Figure credit: Harrison (2014).

1.2.3 Basic model

The most widely accepted model of AGN structure, consistent with these observational characteristics of AGN, is presented in this section. In the currently accepted paradigm (Antonucci 1993; Urry & Padovani 1995), AGN are powered by mass accretion on to the growing central black hole. Less efficient processes such as nuclear burning in stars are not as likely due to the enormous amounts of fuel required and the tensions with observations such as luminosities, sizes, and lifetimes. The luminosity due to accretion is given by $L_{\rm AGN} = \eta \dot{M} c^2$, where η is the conversion efficiency of mass to energy, $\dot{M}$ is the rate of mass accretion, and c is the speed of light.

A theoretical maximal limit on this $L_{\rm AGN}$ can be derived (Rybicki & Lightman 1979), assuming isotropic accretion on to a black hole, and balancing the inward force of gravity and the radiation pressure from the emitted luminosity of accretion. This upper limit, known as the *Eddington luminosity*, is given by

$$L_{\rm Edd} = 1.26 \times 10^{38} (M_{\rm BH}/M_{\odot}) \text{ erg s}^{-1}, \tag{1.6}$$

for spherically symmetric accretion onto a black hole of mass $M_{\rm BH}$.

The Eddington ratio $\lambda_{\rm Edd}$ is often used to relate the AGN luminosity to the

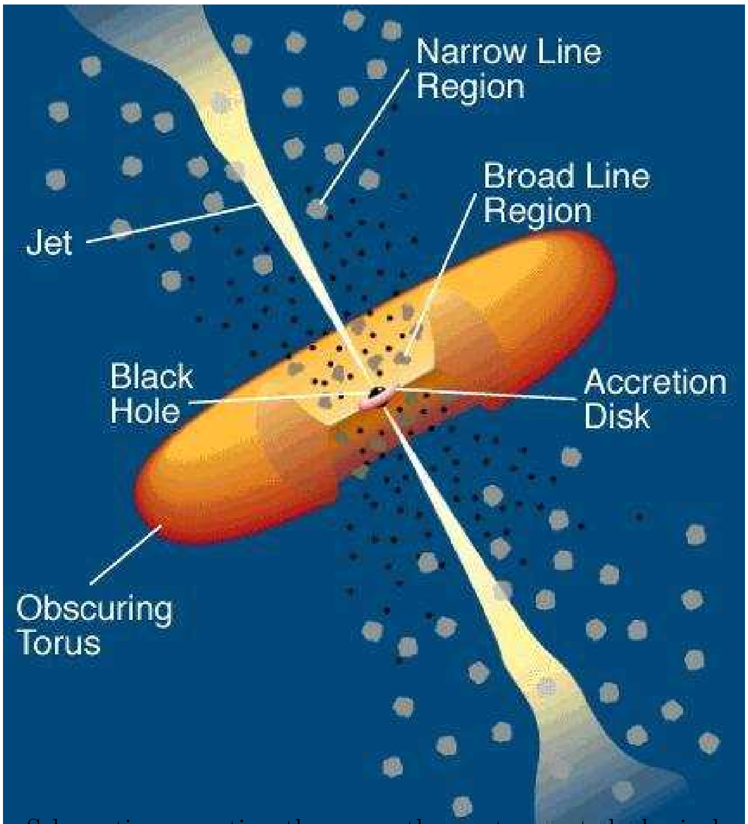

Figure 1.10. Schematic presenting the currently most accepted physical model of AGN (adapted from Urry & Padovani 1995). The accretion disk that surrounds the central engine (SMBH) is shown in pink. An optically thick dusty torus surrounds the accretion disk, and the gaseous envelope above and below the accretion disk is known as the "corona". The "Broad Line Region" refers to the region with observable broad line emission (due to the gravitational effects from the black hole). The "Narrow Line Region" extends over much larger scales and is not so sensitive to this gravitational influence. Thin radio jets can launch near the accretion disk, as observed in radio-loud quasars.

Eddington limit as follows,

$$\lambda_{\mathrm{Edd}} = \frac{L_{\mathrm{AGN}}}{L_{\mathrm{Edd}}}. \tag{1.7}$$

Unified model

The physical model of AGN structure is demonstrated by the schematic in Figure 1.10, adapted from Urry & Padovani (1995). In this figure, the accretion disk that surrounds the central engine (SMBH) is shown in pink. The gaseous envelope above and below the accretion disk is known as the "corona", and an optically thick dusty torus surrounds the accretion disk. As suggested by its name, the "Broad Line Region" refers to the region with observable broad line emission, due to the gravitational influence of the SMBH. The "Narrow Line Region" is not so sensitive to the gravitational effects of the black hole, and extends over much larger scales. This model also explains radio-loud quasars as a result of thin radio jets being launched near the accretion disk.

Type 1 Seyfert galaxies (or Type 1 AGN) are those with significantly broader permitted emission lines than forbidden emission lines. In contrast, Type 2 sources have permitted and forbidden emission lines of similar strength. The unified model (Antonucci 1993; Urry & Padovani 1995) explains that these two classes of AGN merely represent different viewing angles, thus dictating whether or not the dusty torus obstructs the broad emission lines from being observed. While it has been suggested that this model requires modifications, it has been largely successful in explaining the observational characteristics, the types of AGN, and the multi-wavelength and line emission of AGN.

1.2.4 Emission and observations of AGN

Having described the key observational characteristics of AGN and introduced the standard model of AGN, we draw these together in this section to explain the physical origin of nuclear emission, as well as discussing the observation (and selection) of AGN in different methods. These selection methods have different selection biases and key capabilities (e.g., Padovani et al. 2017). We note that these different types of AGN have significant variation in the relative contributions of emission to the broad-band continuum. A schematic representation of the SED of a typical radio-quiet AGN is shown in Figure 1.9.

UV/optical continuum

Emission: Under the assumption that the accretion disk is optically thick, the spectrum of the continuum is expected to reflect thermal blackbody emission that peaks in the ultraviolet (UV). Consistent with this prediction, the UV/optical spectrum is characterised by the “big blue bump” and broad continuum emission from $\sim 4000\,\text{Å}$ through to at least $1000\,\text{Å}$.

Observations: Since a significant fraction of the bolometric luminosity of the AGN is expected to be in the UV, it is unfortunate that this part of the electromagnetic spectrum cannot easily be observed from Earth due to the stratospheric ozone layer.

Since the 1980s, optically selected AGN have been identified using colour diagnostics in photometric surveys (Schmidt & Green 1983; Boyle et al. 1990), using the UV excess (caused by the “big blue bump”), as determined by e.g. U-B colour. Since optical diagnostics are disadvantaged by significant non-AGN contamination, cleaner samples can be obtained by following up using spectroscopy or other selection techniques.

X-ray continuum

Emission: Above and below the optically thick accretion disk, it is proposed that there is an optically-thin hot corona of gas. Optical/UV continuum photons that are produced in the accretion disk are inverse-Compton scattered by the hot electrons in this corona. The boost in the energies of the photons leads to the power-law spectrum of hard X-ray continuum. To first order, this power law can be modelled as $S_\nu \propto \nu^{-\alpha}$, where the energy index $\alpha = 1$.

There is often an additional X-ray continuum feature known as the "soft excess", when fluxes are seen at lower X-ray energies. Inverse Compton scattering of the UV/optical photons have been proposed to account for this soft excess, but the origin of this emission is subject to much debate, as it has also been interpreted as a blend of X-ray emission lines (Turner et al. 1991).

Intervening gas in the circumnuclear torus can modify the X-ray spectra of AGN due to photoelectric absorption. The number of surviving soft photons in the spectrum thus depends on the optical density of this gas absorbing column. The optical depth depends on the number density of hydrogen atoms N_H. Therefore, by comparing the flux of an AGN in the hard and soft bands, we can obtain a measure of the gas obscuration of the circumnuclear torus using the hardness ratio (HR), given by:

$$\mathrm{HR} = \frac{h-s}{h+s}. \tag{1.8}$$

Observations: Since the 1970s, significant numbers of AGN have been found to emit energetically in X-rays (Elvis et al. 1978). It is now evident that luminous X-ray selected AGN ($L_X \gtrsim 10^{42}$ erg s^{-1}) dominate source counts in deep X-ray surveys (over other sources such as stars and X-ray binaries). X-ray surveys are thus an invaluable tool in providing clean, uniform samples of AGN, especially at higher redshifts. AGN are typically matched to near-infrared/optical counterparts at the same position within some search radius, depending on the resolution of the X-ray imaging. This thesis primarily concerns X-ray selected AGN, and we discuss the relevant X-ray surveys in Chapter 2.

Infrared continuum

Emission: A second broad bump marks the infrared (IR) continuum as νF_ν starts to rise at $\sim 1\mu$m and has a steep decline at longer wavelengths (where the emission is dominated by star-formation in the host galaxy and little AGN contribution). As the dust in the torus around the accretion disk is heated from the absorption of photons, it re-emits thermal radiation in the infrared region of the spectrum.

Observations: IR-selected AGN are frequently identified using mid-IR to near-IR colour diagnostics from photometric surveys. The most advantageous facet of IR-selected AGN is its lack of sensitivity to obscuration and orientation effects, allowing for the detection of the most obscured AGN out to high redshift. On the other hand, it is disadvantaged by its susceptibility to contamination, since the signal of thermal re-radiation from AGN could be mixed with the signal from dusty star formation. Extensive multi-component SED fitting is often required to independently model the relative contributions from AGN and the host galaxy (Mullaney et al. 2011).

Radio

Emission: In radio-loud objects, radio emission is thought to originate from relativistic jets that are launched near accretion disk (Merloni & Heinz 2007; Best & Heckman 2012; Heckman & Best 2014). Approximately 10–20% of all quasars are radio-loud (Kellermann et al. 1989; Urry & Padovani 1995; Ivezić et al. 2002). In radio-quiet objects, the processes that drive the more compact radio emission are less clear, although proposed mechanisms include simply more compact radio jets and a corona close to the accretion disk (e.g. Polletta et al. 2000).

Observations: Radio-selected AGN represent one of the oldest selection techniques and radio surveys have been widely used to identify AGN. The main advantages of this selection method are that: (a) radio AGN are mostly missed by other techniques (Heckman & Best 2014; Alexander & Hickox 2012), and (b) the orientation of AGN may not play a significant role in the detection of radio emission. Radio AGN have been suggested to represent active black holes with relatively low radiative efficiencies, with host galaxies that are characteristically more massive and passive (Hickox et al. 2009; Goulding et al. 2014). However, it has also been found that "high-excitation" radio AGN sample host galaxies similar to AGN selected at other wavelengths, and seem to have higher radiative efficiencies (Hardcastle, Evans & Croston 2007; Smolčić 2009).

Broad and narrow lines

Emission: Broad line emission comes from permitted transitions in highly dense ($n_e \sim 10^9$ cm^{-3}), photoionised clouds very close to the black hole (between the central engine and the dusty torus). These transitions are Doppler-broadened due to the direct gravitational influence of the SMBH. Forbidden lines are not observed in the broad-line region because the de-excitation occurs due to collision rather than emission of a photon.

In the narrow line region, the photons that escape the inner regions within the torus are able to ionise gas in low density regions with far lower electron densities

($n_e < 10^6$ cm^{-3}) at much larger radii. The emission lines in this region are narrow, and both forbidden and permitted emission lines are observed in this region.

Observations: From observations of their spectra, AGN can be classified into type 1 or type 2 depending on the presence or absence of broad permitted emission lines in addition to narrow (forbidden and permitted) emission lines.

The presence of high-excitation emission lines in the infrared regime (Weedman et al. 2005; Goulding & Alexander 2009) enables the use of IR spectroscopy to successfully select AGN. Optical spectroscopic surveys allow for the selection of AGN using (a) extremely luminous or broad emission lines and (b) emission-line ratio diagnostics, i.e. comparing the relative strengths of different emission lines. At low redshift, a common diagnostic is the "Baldwin, Phillips & Telervich" (BPT) diagram, which distinguishes (different types of) AGN from star-forming galaxies (Baldwin, Phillips & Terlevich 1981).

1.3 AGN and galaxy evolution

Several lines of observational evidence point towards a close relationship between the evolution of AGN and that of galaxies, such as the correlation between the mass of SMBHs and those of host galaxy bulges (e.g., Ferrarese & Merritt 2000; Gebhardt et al. 2000) and the similar evolution in the cosmic star-formation rate and accretion rate densities (e.g., Boyle et al. 1998). These connections are reviewed in the following subsection.

1.3.1 Co-evolution of black holes and galaxies

$M_{\rm BH} - \sigma$ relationship

It is now widely accepted that in the local Universe, the masses of SMBHs ($M_{\rm BH}$) are tightly connected to the velocity dispersion of their host galaxy bulges (σ). Remarkably, this relationship holds over four orders of magnitude (Ferrarese & Merritt 2000; Gebhardt et al. 2000). Similarly, there is an intimate relationship between SMBH mass and the mass of the bulge, shown by Figure 1.11. This is surprising given that accretion onto the SMBH takes place on scales $\ll 0.1$ pc while the formation of galaxy bulges occurs on scales of kiloparsecs. The likely interpretation was that there must be some intrinsic physical connection between the formation of black holes and that of galaxy bulges.

Cosmic star formation vs black hole accretion

In addition to the M–σ relation at low redshift, the global density of black hole growth and star-formation appear to follow a common trend throughout cosmic

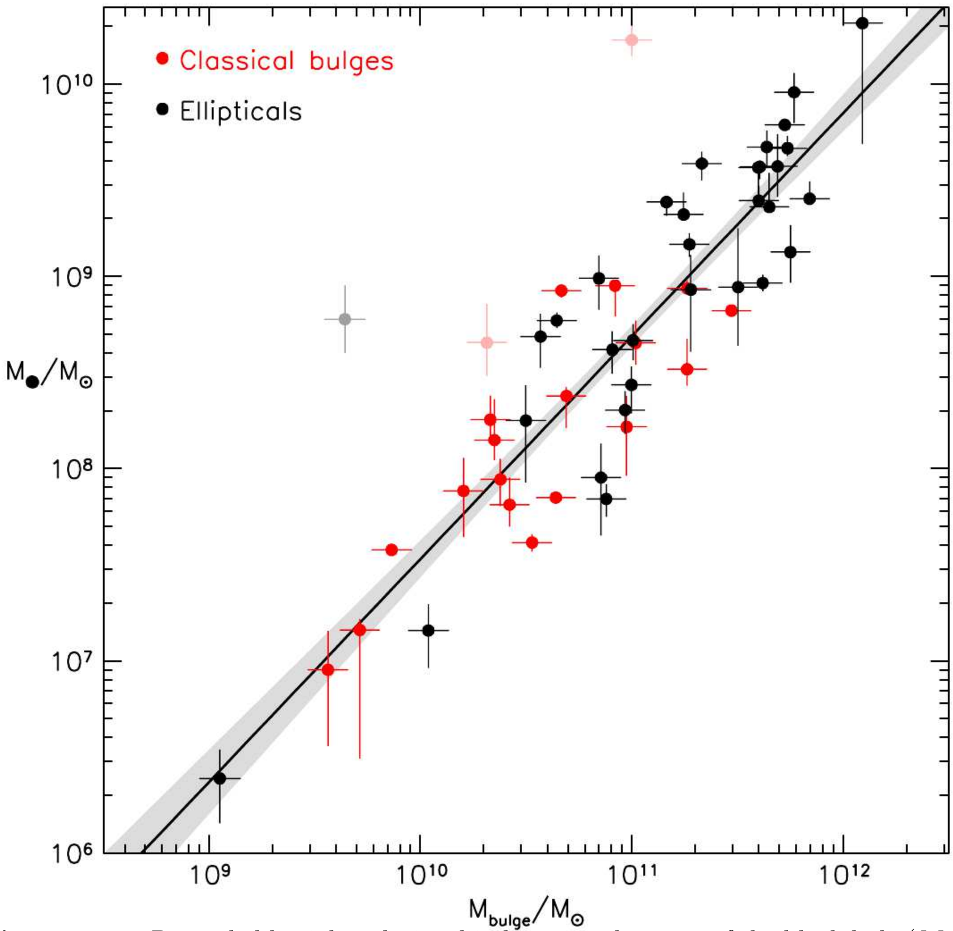

Figure 1.11. Remarkably tight relationship between the mass of the black hole ($M_\bullet$) vs the mass of the bulge ($M_{\rm bulge}$) spanning several orders of magnitude. Figure credit: Kormendy & Ho (2013).

time. A representative model of cosmic black hole growth (Aird et al. 2010) is depicted in Figure 1.12 (reproduced from Harrison 2014). As shown by this figure, Aird et al. (2010) found that scaling the SMBH mass accretion density by ~ 5000 (blue shaded region) matches observations of cosmic SFR density out to cosmic dawn ($z \sim 6$). Both cosmic star formation and black hole accretion were evidently increasing as the Universe was evolving at early times, until the peak at $z = 1$–2. After this epoch, both global SFR and BH growth slow down rapidly. This striking similarity between the growth of star-formation and black hole accretion therefore suggests that there may have been a causal connection between the two.

Furthermore, there is an apparent preferential association of AGN with star-forming galaxies. Several studies find that optical, X-ray, and infrared selected AGN are preferentially located in star-forming galaxies (Kauffmann et al. 2003; Alexander et al. 2005; Mullaney et al. 2012; Rosario et al. 2013). Using a Bayesian analysis, Aird, Coil & Georgakakis (2017) find that the probability of a quiescent galaxy hosting an AGN is generally lower than that of a star-forming galaxy out to $z \sim 2$.

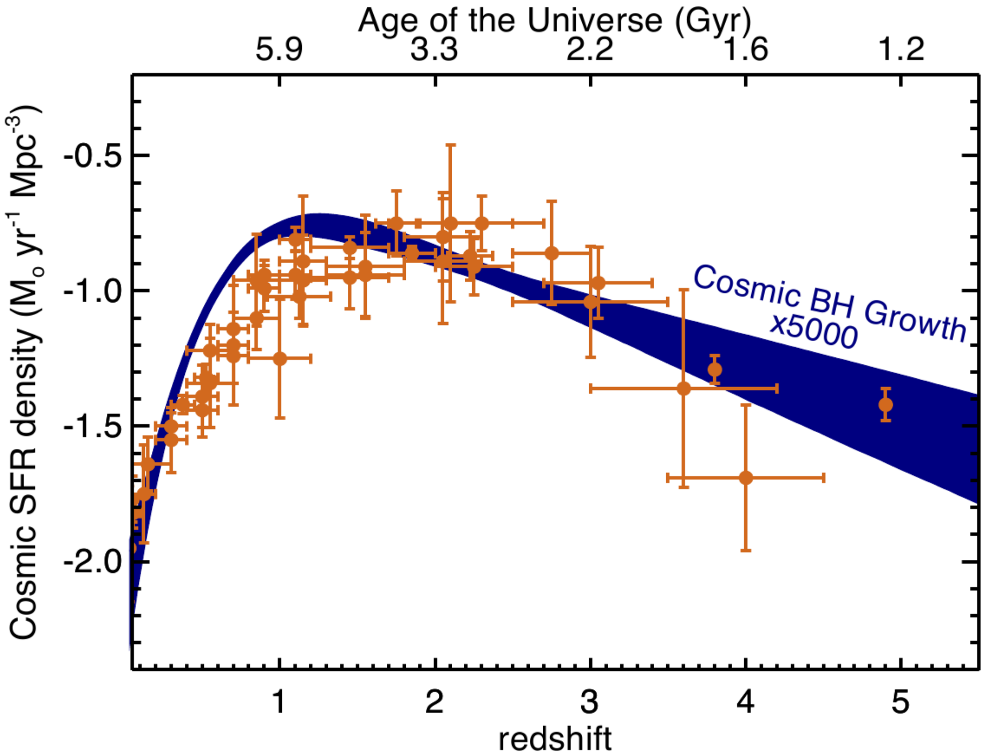

Figure 1.12. The similar shapes of the evolution of densities of cosmic star formation and black hole accretion. The orange points show the redshift evolution of the volume averaged cosmic SFR density as compiled by Madau & Dickinson (2014). The blue shaded region denotes the model of cosmic black hole growth from Aird et al. (2010), which shows the mass accretion density scaled by ~ 5000. Figure credit: Harrison (2014).

While there is significant evidence suggesting that AGN activity is intimately linked to star formation, we note that there are several exceptions, such as radio-selected AGN, that have much lower star formation rates (Heckman & Best 2014). In addition, the flat relationship between X-ray luminosity and star-formation rate (Stanley et al. 2015) may suggest that global star formation is decoupled from AGN activity, although it has been proposed that large X-ray variability on short timescales can dilute intrinsic correlations (Hickox et al. 2014).

1.3.2 AGN host galaxy environments

Given the apparent evolutionary connection between AGN host galaxies and their central SMBHs, the study of AGN as a function of host galaxy environment is well-suited to constraining the parameters that govern the physical triggering of AGN, as well as the links of AGN with star formation and galaxy evolution. If the availability of cold gas drives both star formation and AGN activity, one might expect the correlations between host galaxy environment and AGN to mimic the observed SFR-density relationship (e.g., Gisler 1978). Indeed, it has been known for over three decades that only 1% of massive galaxies in local galaxy clusters show spectroscopic signatures of AGN activity, compared to 5% of the corresponding population in the field (Dressler, Thompson & Shectman 1985). More recently, larger samples have allowed for the confirmation of this trend to higher significances, for example, Kauffmann et al. (2004) found that twice as many galaxies host AGN with strong [OIII] emission in low-density regions as in high density regions. Therefore, there appears to be anti-correlation between galaxy density and AGN activity, parallel to the SFR-density relationship.

Along with the availability of cold gas, however, there are additional physical processes that could affect the rate of accretion onto the SMBH. For instance, in the cluster environment, gas may be removed through environmental processes such as ram-pressure stripping (Gunn & Gott 1972), and tidal effects due to the cluster potential (Farouki & Shapiro 1981) and other galaxies (Richstone 1976). On the other hand, processes such as harassment (Moore et al. 1996) may perturb the galaxy and lead to AGN triggering. From a theoretical viewpoint, less massive groups have been proposed as the ideal environment for AGN activity due to an increased likelihood of mergers (Hopkins et al. 2008a,b). However, observational evidence that mergers are linked to AGN triggering remains mixed (Ellison et al. 2013; Kocevski et al. 2015; Villforth et al. 2017; Hewlett et al. 2017).

1.3.3 Motivations for this work

While much progress has been made in the study of AGN, the fundamental question of how exactly they are triggered remains unanswered. There are apparent connections between AGN activity and host galaxy environment, but clear explanations, both for AGN triggering and the interplay between SMBHs and their host galaxies, remain elusive. To complicate matters further, literature suggests that the suppression of AGN in low redshift clusters reverses at high redshift (Lehmer et al. 2009; Digby-North et al. 2010), although these studies were based only on star-forming galaxies, which could bias the results if there is a strong dependence of AGN activity on host galaxy type. The study of AGN activity in high redshift (proto)clusters has been stunted due to the challenges of identifying them while minimising biases at high redshifts. Once protocluster samples are identified, additional requirements are a clean method of selecting AGN within these protoclusters, and a comparable control field galaxy sample at similar redshift.

The astronomy community has also attempted to study the connection between AGN activity and typical (large-scale) environments from a statistical viewpoint using clustering techniques, as touched upon in Section 1.1.3. Previous clustering studies suggest that X-ray AGN are associated with group-like halo masses of $10^{12-13}\,M_{\odot}$ across a wide range of redshifts (Croom et al. 2005; Ross et al. 2009; Shen et al. 2009; Krumpe et al. 2012; Allevato et al. 2016; Powell et al. 2018), consistent with the interpretation that mergers, which are enhanced in groups, trigger AGN activity. However, recent literature suggests that host galaxy properties play a key role (Mendez et al. 2016; Powell et al. 2018) in driving the clustering signal. There is also much debate on whether AGN triggering is dependent on environment at all and instead stochastically triggered (Aird, Coil & Georgakakis 2017). This ambiguity motivates the need for clustering studies of AGN as a function of redshift, taking into careful consideration the impact of host galaxies.

Additionally, the study the nearby neighbours of AGN is well-motivated, as it could facilitate the disentanglement of AGN triggering scenarios of stochasticity vs environmental triggering. AGN host galaxies are in a unique and complex position in that it has been proposed both that they influence their neighbours via feedback (Croton et al. 2006), as well as be influenced by their neighbours via environmental triggering (Hopkins et al. 2008a,b). Finally, the star-formation properties of the small scale neighbours of AGN have not been given much attention to date. While the star-formation properties of satellite galaxies have been found to "conform" to those of centrals, the role that AGN plays in this picture remains untested.

To tackle the potential connection between AGN activity and host galaxy environments, we identify three outstanding questions that motivate the work presented in this thesis:

- What happens to AGN activity in dense structures at high redshift?
- What role do host galaxies play in the connection between AGN and large scale structure?
- What can the small scale environments of AGN tell us about triggering?

1.4 Thesis structure

This thesis investigates AGN activity in different galaxy environments using three complementary methods: a detailed case study of a dense structure at high redshift, statistical clustering analyses to identify their larger scale structure, and aperture techniques to study the neighbours of AGN within 500 kpc.

- In Chapter 2, we describe the data catalogues used in this thesis, the majority of which were not produced by me. These include the UDS and COSMOS multiwavelength galaxy catalogues, protocluster galaxy catalogue, galaxy classification catalogues, and X-ray catalogues from *Chandra* and *XMM-Newton* observatories.
- In Chapter 3, we explore the prevalence of AGN in the high-redshift protocluster Cl 0218.3–0510 at $z = 1.62$. Using imaging from the *Chandra* X-ray

Telescope, we find a large overdensity of AGN in the protocluster. We study the AGN fraction in massive protocluster galaxies and compare this to the field, and investigate the radial profiles of the AGN overdensity. We also compare the properties of AGN in the protocluster to the field. This work is published in Krishnan et al. (2017).

- In Chapter 4, we study the relationship between AGN and dark matter halo mass using statistical clustering techniques. Our study is based on a cross-correlation analysis applied to X-ray selected AGN in the COSMOS and UDS fields, spanning redshifts from $z \sim 4.5$ to $z \sim 0.5$. We investigate the role of host galaxy properties by measuring the clustering signal of inactive (i.e. non-AGN) galaxies closely matched to the AGN in spectral class, stellar mass and redshift. We also investigate the link between AGN luminosity and clustering. This work is submitted for publication (Krishnan et al. submitted).

- In Chapter 5, we present a preliminary analysis of the properties of galaxy neighbours within 500kpc of X-ray AGN between $z \sim 2.5$ and $z \sim 0.5$ in the UDS and COSMOS fields. We investigate the number densities and passive fractions of AGN compared to a closely matched sample of control galaxies. This preliminary work is as yet unpublished.

- We summarise our results, present our conclusions, and suggest relevant future work in Chapter 6.

All magnitudes throughout this thesis are in the AB magnitude system.

Chapter 2

Description of the data

In this chapter, we describe the data catalogues that made possible the work presented in this thesis. The structure of the chapter is as follows. In Section 2.1, we describe the UKIDSS Ultra Deep Survey (UDS), and its galaxy catalogues. This includes two K-band selected catalogues based on the 8th and 11th data releases (DR8 and DR11). Also included in this section are details of a well-identified protocluster catalogue, and of the X-ray surveys (*Chandra* and *XMM-Newton*) providing coverage of the field. Both the UDS DR11 catalogue and *Chandra* UDS catalogue have been made available during the course of my PhD, allowing us to use state-of-the-art data to probe the scientific questions outlined in Chapter 1. The DR11 catalogue is used in Chapter 4 and Chapter 5. In Section 2.2, we outline the Cosmic Evolution Survey (COSMOS), along with X-ray observations of the field from the COSMOS *Chandra*-Legacy Survey. We discuss the comparability of these two fields in Section 2.3. Section 2.4 presents our galaxy classification technique, and finally, Section 2.5 describes our determination of stellar mass completeness limits.

I did not carry out the majority of this work presented in this chapter, but the catalogues described provide the fundamental basis for the work presented in this thesis. We accredit the relevant authors in each section.

2.1 Ultra Deep Survey

The UKIRT Infrared Deep Sky Survey (UKIDSS, Lawrence et al. 2007) Ultra Deep Survey (UDS) is a deep photometric survey centred on RA = 02:17:48, DEC = -05:05:57, covering a survey area of 0.8 deg^2 after removing masked regions such as bright stars and image artefacts. The UDS is the deepest K-band survey over such a large, contiguous area. UKIDSS uses the UKIRT Wide Field Camera (WFCAM, Casali et al. 2007). Please see Hewett et al. (2006) and Hodgkin et al. (2009) for details on the photometric system and the calibration respectively. The UDS is a mosaic comprised of 16 sub-regions corresponding to four pointings of the four detectors of WFCAM. The full details of the UDS stacking and optimisation will be provided in Almaini et al. (in prep). For the DR11, additional deep Y -band observations are provided by the VISTA Deep Extragalactic Observations (VIDEO) survey (Jarvis et al. 2013), reaching a 5σ depth of 24.4 mag. The UDS also benefits from deep optical observations from the Subaru XMM-Newton Deep Survey (SXDS, Furusawa et al. 2008), with 5σ depths of 27.8, 27.2, 27.0, 27.0 and 26.0 in B, V, R, i', z' in $2''$ apertures, as well as IRAC 3.6μm and 4.5μm coverage from the Spitzer UDS Legacy Program (SpUDS, PI:Dunlop) to a depth of 24.2μJy and 24.0μJy, respectively. The unmasked area with 12-band photometric coverage is 0.62 deg^2.

K-band selected galaxy catalogues were created because the observations were optimised for this wavelength band (in the interest of optimally selecting high redshift galaxies by stellar mass).

2.1.1 UDS DR8

In Chapter 3, we use the 8th data release of the Ultra Deep Survey (UDS DR8). The near-infrared data were the deepest over such a large area at the time, reaching AB magnitude depths of $J = 24.9$, $H = 24.2$ and $K = 24.6$ (see e.g., Hartley et al. 2013; Simpson et al. 2013).

Stellar masses and photometric redshifts in the UDS DR8 catalogue have been determined by fitting the Spectral Energy Distributions (SEDs) of templates to observed photometry. The publicly available code EAZY was used to do so, and further details can be found in (Simpson et al. 2013). Bruzual & Charlot (2003) stellar population templates were used, assuming a Chabrier (2003) initial mass function (IMF). These photometric redshifts have a normalised median absolute deviation of $\sigma_{\rm NMAD} = 0.027$.

2.1.2 UDS DR11

In Chapter 4 and Chapter 5, we use the 11th data release of the UDS (UDS DR11). The 5σ limiting depths in $2''$ diameter apertures are 25.6, 25.1 and 25.3 mag in the J, H, and K-bands, respectively (Almaini et al. in prep).

Improvements from DR8

Beyond the fainter depths that are probed by the UDS DR11 catalogue, several aspects of catalogue preparation have been significantly improved compared to the DR8. We outline these most important systematic effects below:

- DR11 benefits from deep Y-band imaging from VIDEO, allowing for more accurate photometric redshifts at $z > 1$.
- IRAC masks were included, in addition to improved masking of the remaining wavebands.

- Deeper IRAC data were added from the *Spitzer* Extended Deep Survey (SEDS; Ashby et al. 2013).

- Background sky levels were more carefully determined and subtracted, resulting in more accurate photometry for faint objects.

- The WFCAM zeropoint was recalibrated according to each of the four detectors to account for variation across the field.

Photometric redshifts and stellar masses

Photometric redshifts were determined using the method outlined in Simpson et al. (2013), by fitting 12-band photometry using a library of templates built from the Bruzual & Charlot (2003) models with ages of 30 Myr to 10 Gyr, a range of metallicities, and three templates dust-reddened using a Small Magellanic Cloud extinction law. These photometric redshifts have a normalised median absolute deviation of $\sigma_{\rm NMAD} = 0.019$ as compared to ~ 7000 secure spectroscopic redshifts. Spectroscopic redshifts are used when available.

Stellar masses were also calculated using the method described in Simpson et al. (2013) using SED-fitting of a much finer grid of synthetic SEDs. We refer the reader to Almaini et al. (in prep) for further details on the UDS DR11 catalogue.

Completeness simulations

Statistical studies of galaxies must take into account the Malmquist bias (Malmquist 1922, 1925), since astronomical objects at fainter magnitude are less likely to be detected due to survey limits. Monte Carlo simulations, where test images are populated with fake galaxies, are used in order to quantify the "completeness" as a function of galaxy magnitude. Running source detection software (SExtractor; Bertin & Arnouts 1996) on these images allows us to compute completeness curves as a function of magnitude. The magnitude completeness limit corresponding to 2σ or 3σ can then be derived.

I have played a role in the completeness simulations of the UDS DR11 catalogue preparation. I contributed to the investigation of issues such as the effect of placing fake sources at random positions on the real DR11 image as opposed to the typically used blank image (since blending may play a role in recovering galaxies), the influence of galaxy type in the completeness simulations (since passive galaxies tend to have a more compact morphology leading to an increased SExtractor detectability), and the optimisation of SExtractor parameters (to maximise the counts of galaxies while minimising spurious sources).

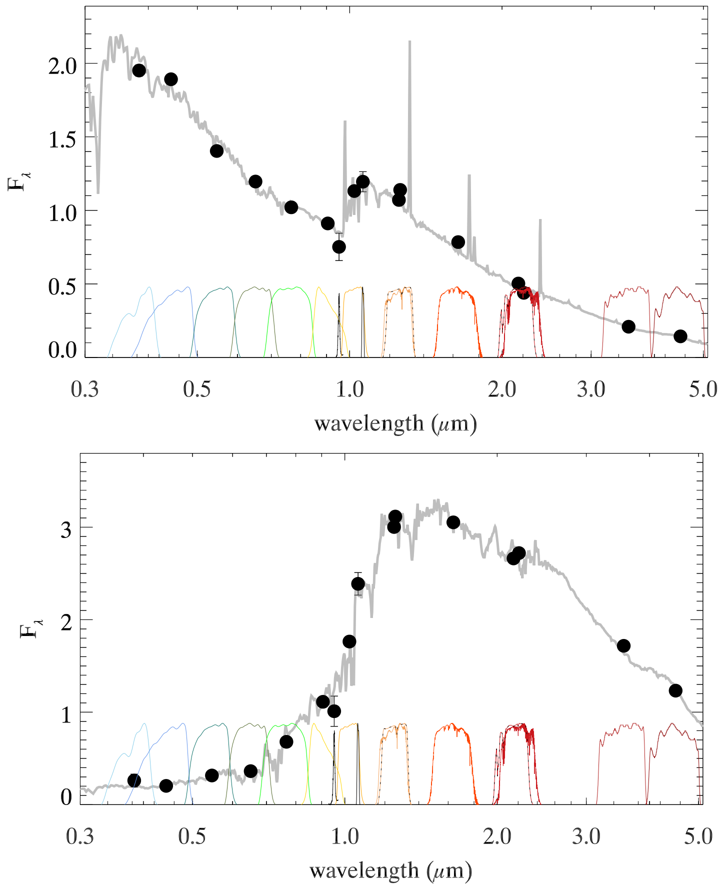

Figure 2.1. SED fits to the observed fluxes from multi-wavelength imaging for a star-forming galaxy (upper panel) and passive galaxy (lower panel). The solid black circles denote the photometric measurements in bands used to derive photometric redshifts and galaxy properties. Corresponding filter transmission curves are plotted on the bottom. The grey line depicts the best-fitting template assigned to the galaxy. Figure credit: Hatch et al. (2016).

2.1.3 Cl 0218.3–0510 protocluster at $z = 1.6233$

Chapter 3 details our case study of AGN in a high-redshift protocluster. For this study we made use of the Cl 0218.3–0510 protocluster at $z = 1.6233$ in the UDS field (Papovich et al. 2010; Tanaka, Finoguenov & Ueda 2010). In addition to the photometry available in the UDS DR8 catalogue, Hatch et al. (2016) obtained multiwavelength imaging for this protocluster, including doubly sampled J and K imaging, as well as imaging in two narrow-band filters (ESO/VLT FORS [SIII]+65 and HAWK-I 1.06μm NB1.06). The two narrowband filters were chosen such that they bracketed the Balmer break and the 4000 Å break of the protocluster galaxies. This enabled the calculation of accurate photometric redshifts and stellar masses. Exemplary fits of the modelled spectral energy distribution (SED) to the observed fluxes from multi-wavelength imaging are shown in Figure 2.1.

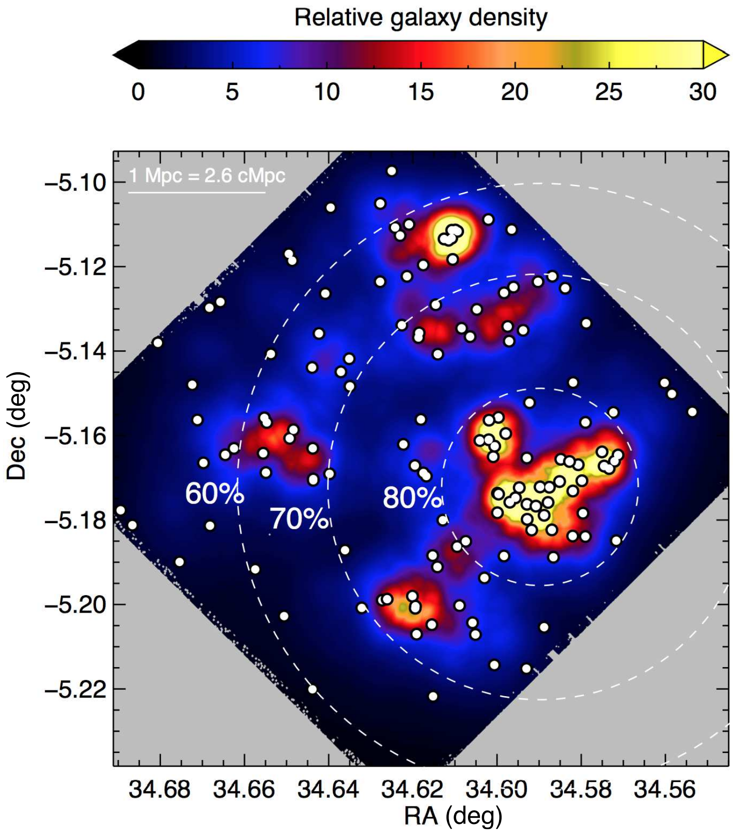

Figure 2.2. Galaxy density map of the Cl 0218.3–0510 protocluster (shown by background colour scale), with protocluster galaxy candidates shown by white circles, and dashed circles marking where 80, 70 and 60% of the galaxies are likely to become cluster members by $z = 0$. Figure credit: Hatch et al. (2016).

Hatch et al. (2016) found that, for 16 protocluster members with existing spectroscopic redshifts, the dispersion of $z_{\rm phot} - z_{\rm spec}$ was $\Delta z/(1+z) = 0.013$. This high-precision redshift data enables the accurate selection of protocluster members using photometry. The "Goldilocks" sample from Hatch et al. (2016) consists of protocluster member galaxies that have been optimised to minimise contamination from field galaxies, as well as maximise completeness of protocluster members. Protocluster members in this sample were defined out to 5 arcmin (2.6 physical Mpc) from the central Brightest Cluster Galaxy (BCG) at RA = 2h 18m 21.5s, $Dec = -5° \, 10' \, 19.8''$. Beyond this radius, the probability of Goldilocks protocluster candidates becoming cluster members is below 50% and decreases rapidly with radius (Hatch et al. 2016). A galaxy density map of this protocluster annotated with the probability that galaxies become cluster members is illustrated in Figure 2.2.

Protocluster galaxy properties such as redshifts and masses have been determined through SED-fitting using Bruzual & Charlot (2003) stellar population templates and assuming a Chabrier (2003) initial mass function (IMF), as described in Hatch et al. (2016). The comoving volume of the full protocluster volume probed by these observations is $10.2 \times 10.2 \times 34.0$ Mpc^3 (Hatch et al. 2016).

2.1.4 UDS *Chandra*

X-ray source catalogue

In Chapter 3, we select AGN using the UDS *Chandra* X-ray source catalogue, as described in this section. We make use of *Chandra* X-ray imaging from the X-UDS program (PI: G. Hasinger; Kocevski et al. 2018), which covers the central 0.33 deg^2 of the UDS field (Almaini et al. in prep; described in Section 2.1). The coverage includes the section of the UDS field that was observed as part of the Cosmic Assembly Near-infrared Deep Extragalactic Legacy Survey (CANDELS) with the *Hubble Space Telescope* (Grogin et al. 2011; Koekemoer et al. 2011). The X-UDS survey consists of 25 ACIS-I pointings with a total integration time of 1.25 Ms (Kocevski et al. 2018). The observations are tiled in a mosaic to achieve an average depth of ~ 600 ksec in the central CANDELS region and ~ 200 ksec in the remainder of the field. The final X-ray point source catalog contains 868 unique detections. A threshold was applied to avoid false point source detections and to select only sources detected in any band with a false detection probability less than 1×10^{-4}, corresponding to 3.7σ detections and above. Further details are provided in (Kocevski et al. 2018).

In Chapter 3 we assume that optical/infrared sources within 1 arcsec of X-ray point sources are AGN. We compare the AGN to the X-UDS optical counterparts catalogue and find that this method is robust; 6/6 protocluster AGN and 20/20 field AGN within the CANDELS region are identical to the counterparts catalogue.

X-ray AGN counterpart catalogue

In Chapter 4 and Chapter 5, we use AGN catalogues that identify optical/NIR counterparts for X-ray sources using a maximum likelihood approach.

As mentioned in the previous section, the final UDS *Chandra* X-ray source catalogue amounts to 868 sources (Kocevski et al. 2018). Counterparts to these X-ray sources were matched to the CANDELS H-band and UDS DR10 K-band catalogues using the likelihood ratio technique of Sutherland & Saunders (1992), following the method outlined in Civano et al. (2012). Spectroscopic redshifts are available for ~ 400 sources. See Hasinger et al. (in prep) for further details on the counterpart matching procedure.

2.1.5 UDS *XMM-Newton*

X-ray source catalogue

The UKIDSS UDS survey is also observed by the Subaru-XMM-Newton Deep Survey (SXDS), centred at RA=02:18:00, DEC=-05:00:00, which is mapped by seven pointings with XMM-Newton covering the 0.2–10 keV band. Combined images from European Photon Imaging Camera (EPIC) pn and MOS cameras on XMM-Newton allows the detection of 866, 1114, 645, and 136 sources in the 0.5–2, 0.5–4.5, 2–10, and 4.5–10 keV bands, respectively. The X-ray source catalogue in the Subaru/XMM-Newton deep survey is presented in Ueda et al. (2008), amounting to 1245 unique sources.

X-ray AGN counterpart catalogue

XMM counterparts have been obtained using the likelihood ratio method to R-band, 3.6μm, near-UV, and 24μm source catalogues. Spectroscopic observations allow the identification of 597 out of 896 total AGN. The remaining AGN have redshifts derived using 15 band photometry, where separate SED templates of QSOs and galaxies are applied to each counterpart. See Akiyama et al. (2015) for further details.

2.1.6 Combining UDS *Chandra* and *XMM-Newton*

As described above, the UDS field has wide but shallow *XMM-Newton* observations, as well as deep *Chandra* coverage of a smaller fraction of the field. Therefore we use the counterparts to the *Chandra* point sources, but supplement this with *XMM-Newton* point source counterparts outside the *Chandra* covered region (see Section 2.1.5), taking into account the flux limits of the surveys.

2.2 Cosmic Evolution Survey

The Cosmic Evolution Survey (COSMOS) field (Scoville et al. 2007) is a comparable survey to the UDS that reaches shallower depths but covers a larger area of 1.5 deg^2 in the UltraVISTA-DR2 region centred on RA = 10:00:28, DEC = +02:12:21. We draw our galaxy sample from *COSMOS2015* published in Laigle et al. (2016), with PSF-matched photometry from Subaru SuprimeCam reaching 5σ limiting depths in 2$''$ diameter apertures of 26.6, 27.0, 26.3, 26.4, 26.3 and 25.8 mag in the u^+, B, V, r, i, and z^{++} bands. UltraVISTA (McCracken et al. 2012) using the VIRCAM instrument on the VISTA telescope provide NIR photometry in the Y, J, H, and K_s bands. In addition to the “deep” coverage of the full field, there are “ultra-deep” stripes of the survey with deeper near-infrared observations. However, we limit our sample with K-band completeness limits corresponding to "deep" regions to maximise number statistics while selecting galaxies uniformly across the field. The UltraVISTA observations in the deep field have 5σ limiting depths in $2''$ diameter apertures of 24.7, 24.6, 24.3 and 23.9 mag, respectively. Additionally, Y band imaging is included from Subaru Hyper Suprime-Cam (HSC) with a depth of 24.3 mag. Also included are Spitzer IRAC observations in 3.6μm and 4.5μm bands, with 5σ limiting depths of 24.9 mag in $2''$ diameter apertures.

The object selection method in this field was a χ^2 sum of the combined $YJHK_S$ and z^{++} images, in order to maximise the completeness for blue and high redshift ($z > 2$) galaxies.

We use photometric redshifts from Laigle et al. (2016), which are derived using the LePhare code (Arnouts et al. 2002; Ilbert et al. 2006) following the method of Ilbert et al. (2013). An array of 31 templates was used in the fitting, including spiral and elliptical galaxies from Polletta et al. (2007) and a set of 12 templates of young blue star-forming galaxies using Bruzual & Charlot (2003) models. Extinction was implemented as a free parameter ($E(B-V) < 0.5$) following a variety of prescriptions. The uncertainty of the photometric redshifts is $\sigma_{\rm NMAD} = 0.021$. We use spectroscopic redshifts when available.

This code also allowed for the determination of stellar masses using a Chabrier (2003) IMF. The reader is referred to Laigle et al. (2016) for further details on *COSMOS2015*.

2.2.1 *Chandra* COSMOS-Legacy

X-ray source catalogue

The Chandra COSMOS-Legacy is the product of 4.6 Ms of Chandra observations over the 2.2 deg^2 COSMOS area. The X-ray source catalogue is described in Civano et al. (2016) and amounts to 4016 unique sources. Each source was detected in at least one of three bands (full; 0.5–7 keV, soft; 0.5–2 keV, or hard; 2–7 keV) down to a threshold corresponding to a background fluctuation probability of $P \sim 5 \times 10^{-5}$. Fluxes have also been calculated in the hard band corresponding to 2–10 keV for comparison with other surveys.

X-ray AGN counterpart catalogue

Marchesi et al. (2016) identify counterparts to the X-ray sources using the approach of Civano et al. (2012), making use of three different bands: i band ($\sim$ 7600 A) from the Subaru photometric catalogue (Capak et al. 2007), K_S band (2.15 μm) from UltraVISTA (Laigle et al. 2016), and 3.6 μm, and the *Spitzer* IRAC catalog from Sanders et al. (2007). Of the 4016 sources, $\sim$ 97% have optical/near-infrared counterparts, and $\sim 54\%$ have spectroscopic redshifts. See Marchesi et al. (2016) for further details on the counterpart catalogue.

2.3 Combining UDS and COSMOS

2.3.1 Multiwavelength observations

In Chapter 4 and Chapter 5, we combine results from the UDS and COSMOS fields to increase our number statistics. These two fields are comparable in their multi-wavelength imaging. While the UDS achieves fainter K-band limiting magnitudes, the COSMOS is larger and dominates number statistics. Some (not all) of the filters used in the derivation of photometric redshifts and stellar masses are shown in Figure 2.3. For clarity we only plot the comparable filters between UDS and COSMOS (excluding narrow-band and broad-band imaging). Flux measurements in these wavebands are used in the classification of galaxies, as described in the next section.

Throughout this thesis, we take care to ensure uniformity in magnitude and mass completeness limits when combining these two datasets. We note that the UDS has deeper near-infrared data leading to more accurate photometric redshifts at $z \geq 1.5$ in comparison to COSMOS. On the other hand, COSMOS has additional optical bands, leading to more accurate redshift determination at $z \leq 1$ than the UDS. We take care to ensure that this does not affect our results by making consistency checks using the surveys independently (such as the correlation functions in Chapter 4) before combining the results.

2.3.2 X-ray observations

We note that the X-ray surveys described in previous sections (UDS *Chandra* and *XMM-Newton* & COSMOS *Chandra*) are comparable in the hard band ($2-10$ keV) and we thus only study AGN detected in this band in Chapter 4. The flux limit maps of these X-ray images are shown in Figure 2.4, where colours are comparable between the three surveys.

In Chapter 4 and Chapter 5, photometric and spectroscopic redshifts of the X-ray sources were provided by the most likely counterpart. We note that we use the spectroscopic redshift when available, in all cases.

2.4 Galaxy classification

In order to classify galaxies into star-forming and passive in Chapter 4 and Chapter 5, we make use of the principal component analysis (PCA) technique outlined in this

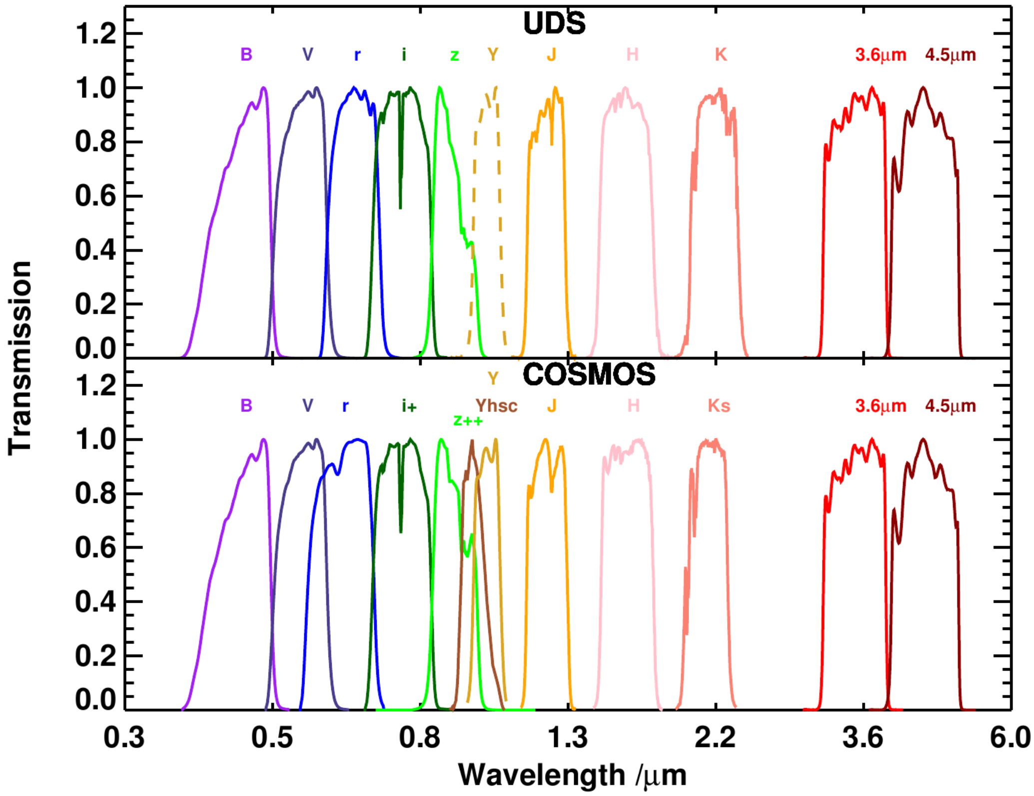

Figure 2.3. Transmission response curves for the filters used in the UDS (top) and COSMOS (bottom) data sets. For clarity we only plot the comparable filters used in our galaxy classification technique, as described by Section 2.4. Figure credit: Aaron Wilkinson.

section. Using this technique, Wild et al. (2014) and Wild et al. (2016) showed that galaxies can be reliably classified using the shape of the SED.

The PCA technique identifies the features of the SED that vary the most between modelled galaxies, and then derives the principal components ("eigenvectors") that produce the variance of these features. The eigenvectors for the PCA are built from a library of Bruzual & Charlot (2003) spectral synthesis models with a variety of ages, metallicities and star formation histories. As outlined in Wild et al. (2014) and Wild et al. (2016), the PCA is applied to the differences of these model SEDs from the mean spectrum (m_λ). They find that linear combinations of only three eigenvectors ($e_{i\lambda}$) can represent $>99.9\%$ of the variance in the model SED library. As shown by the following equation, a normalised galaxy SED ($\frac{f_\lambda}{n}$) can be accurately reproduced by linear combinations of these three eigenvectors:

$$\frac{f_\lambda}{n} = m_\lambda + \sum_{i=1}^{3} a_i e_{i\lambda}, \tag{2.1}$$

where a_i are the amplitudes of the eigenvectors, called "super-colours" (SC). Therefore each galaxy can be represented using a combination of weights of each of the eigenvectors (SC1, SC2, and SC3). These eigenvectors, along with the mean spec-

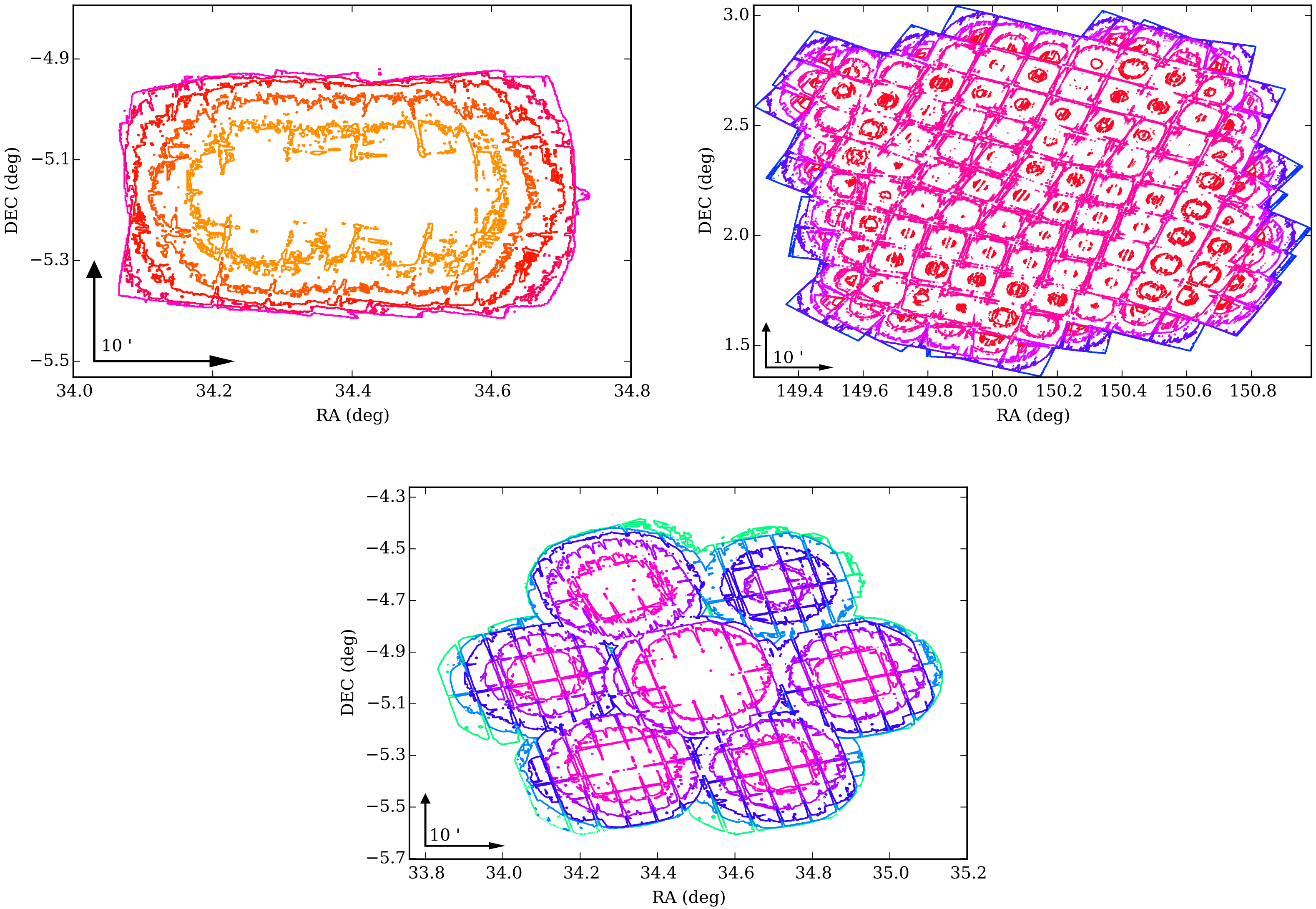

Figure 2.4. Flux limit maps (hard band) in order of X-ray survey sensitivity from highest to lowest. **Left**: (a) *Chandra* coverage of the UDS field, where contours represent 6.15×10^{-16} erg s^{-1} cm^{-2} (inner contour, orange) to 3.38×10^{-15} erg s^{-1} cm^{-2} (outer contour, magenta). **Right**: (b) *Chandra* coverage of the COSMOS field, where contours represent 2.24×10^{-15} erg s^{-1} cm^{-2} (inner contour, red) to 1.38×10^{-14} erg s^{-1} cm^{-2} (outer contour, blue). **Bottom**: (c) *XMM-Newton* coverage of the UDS field, where contours represent 4.61×10^{-15} erg s^{-1} cm^{-2} (inner contour, pink) to 2.22×10^{-14} erg s^{-1} cm^{-2} (outer contour, light green). Colours are comparable between the three surveys. For reference, the black arrows in the bottom left corners show a scale of $10'$.

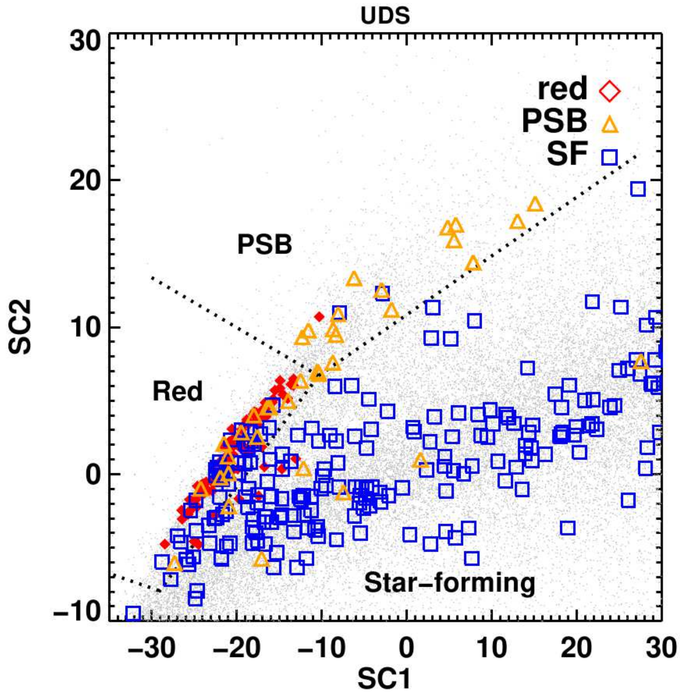

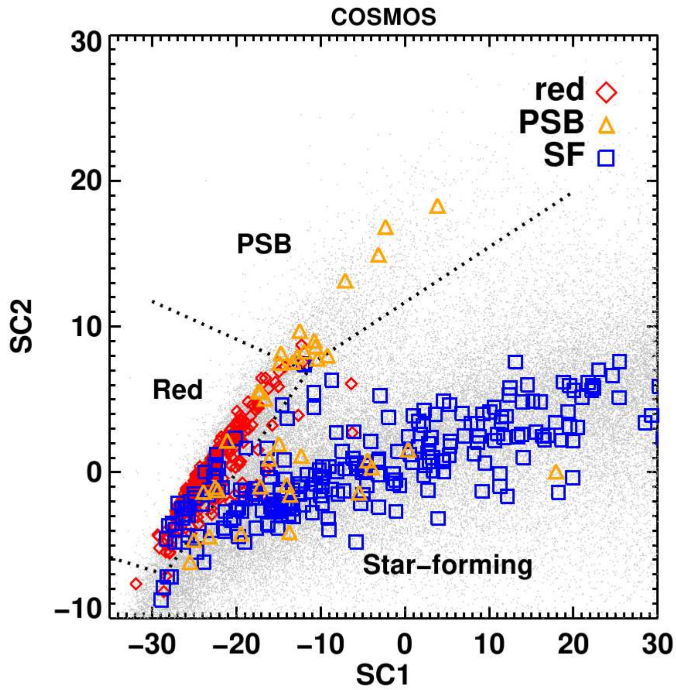

Figure 2.5. Supercolour diagram (SC1-SC2) for UDS (top panel) and COSMOS (bottom panel) showing the boundaries used to classify galaxies as red, star-forming, and post-starburst (PSB). Galaxies with spectroscopy are overplotted in red, blue, and yellow respectively, with photometrically selected samples in grey. Figure credit: Wilkinson et al. (in prep).

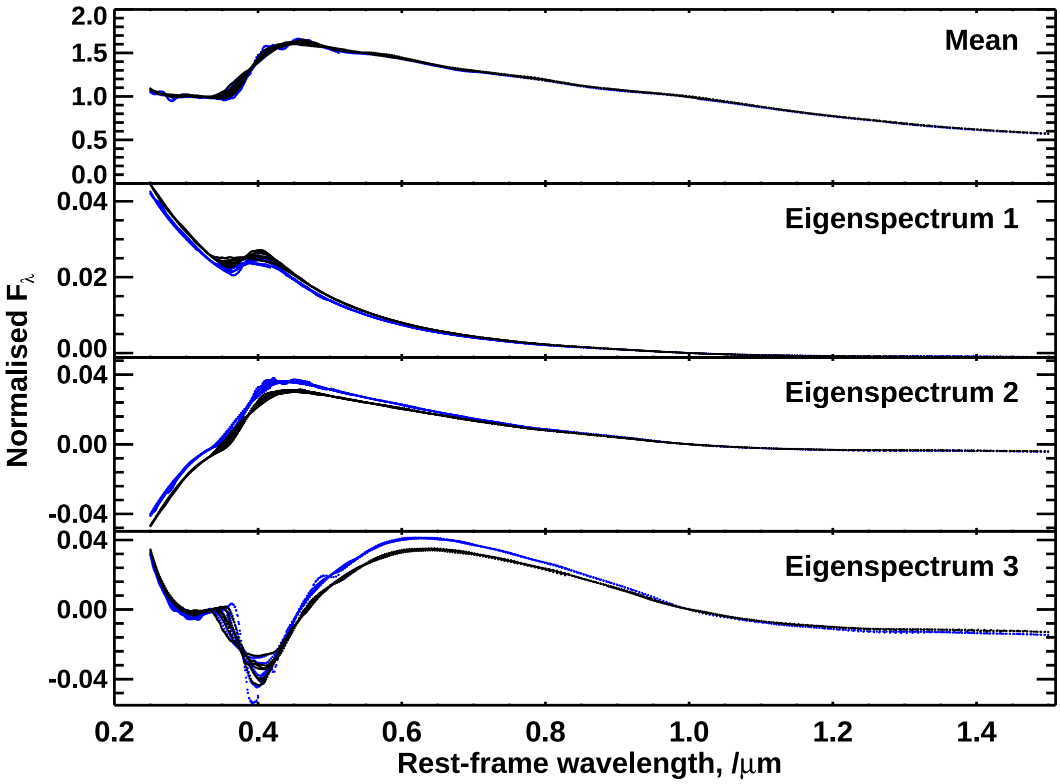

Figure 2.6. The mean and first three eigenvectors derived from the PCA of a library of Bruzual & Charlot (2003) models, for UDS (black) and COSMOS (blue). The addition of the mean and these eigenvectors enables the construction of galaxy SEDs of varying shapes. Figure credit: Aaron Wilkinson.

trum, for both UDS and COSMOS, are shown in Figure 2.6. The first eigenvector (SC1) parameterises the red-blue slope of the SED, while the remaining two eigenvectors (SC2 and SC3) determine the strength and shape of the 4000 Å/Balmer break region. The SC3 is mostly used for singling out low-metallicity candidates.

Galaxies can be split into passive (red and post-starburst), and star-forming (including dusty systems) depending on the where they lie on the supercolour diagram (SC1-SC2). Wilkinson et al. (in prep) present updated super-colour boundaries based on those in Wild et al. (2014) and Wild et al. (2016), primarily to extend the methodology to $z > 2$ using the deeper optical/near-infrared photometric data in the UDS and COSMOS fields. As the broadband filters are slightly different between the UDS and COSMOS fields, the PCA technique is applied separately on each field, resulting in different eigenvectors. Wilkinson et al. (in prep) ensure consistency in the classification boundaries in SC space between the two fields, as shown in Figure 2.5. We make use of these updated classifications in the UDS and COSMOS to classify our galaxies and AGN hosts as either passive or star-forming. These galaxy classifications are hereafter referred to as "spectral class". Stacked spectra from the red, PSB, and SF regions of the supercolour diagram are shown in Figure 2.7.

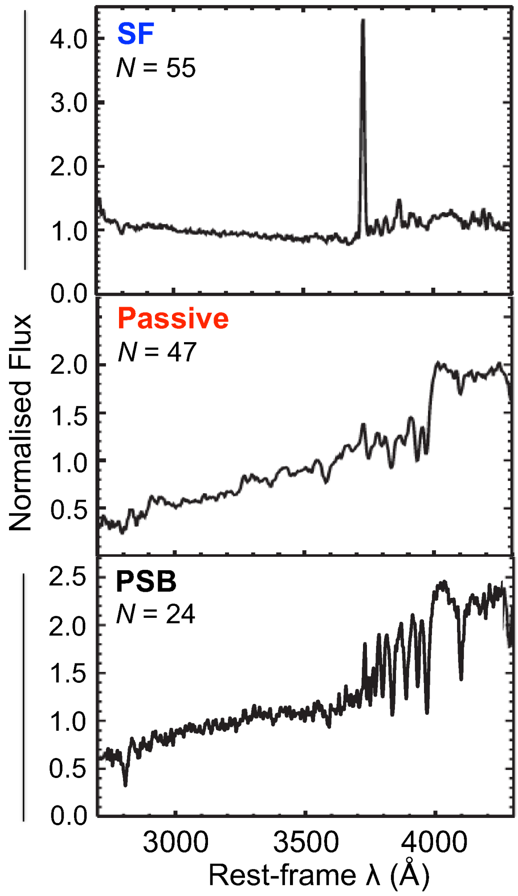

Figure 2.7. Stacked spectra from red, PSB and SF regions of the supercolour diagram. Figure credit: David Maltby.

2.5 Stellar mass completeness limits

As discussed in Section 2.1.2, K-band magnitude limits can be obtained from completeness curves. By removing sources that are fainter than this limit, we avoid biases due to incomplete samples. Since the mass-to-light ratio is not constant across galaxy types, this K-band magnitude limit translates to various stellar mass limits for different galaxy populations. In this thesis, several galaxy samples are subject to an additional *stellar mass* completeness limit, such that incomplete samples of low mass objects are not included.

To calculate the 90% stellar mass completeness limit, we use the method described in Pozzetti et al. (2010). At a given redshift, the limiting mass $M_{\rm lim}$ is defined as the stellar mass a galaxy would have if its magnitude was that of the limiting magnitude of the survey, $K_{\rm lim}$:

$$\log(M_{\rm lim}) = \log(M_*) + 0.4(K - K_{\rm lim}), \tag{2.2}$$

where M_* and K are the stellar mass and K-band magnitude of the galaxy, respectively. To obtain a representative limit for our sample as a function of redshift, we follow the methodology of Pozzetti et al. (2010) and use the $M_{\rm lim}$ of the faintest 20% (in K) of galaxies within the catalogue in a given redshift slice. The 90% stellar mass completeness limit is then defined as the 90th percentile of the resulting M_{lim} distribution. Using this method we obtain (second order polynomial) curves for the redshift-dependent stellar-mass completeness limits for our galaxy catalogues. Applying this method to galaxies in the COSMOS field at a limiting magnitude of $K_{\rm lim} = 23.7$ yields stellar mass completeness limits of $\log(M_*) \geq -0.11z^2 + 1.04z + 8.32$ (as used in Chapter 4).

Chapter 3

Enhancement of AGN in a protocluster at $z = 1.6$

In this chapter we investigate the prevalence of AGN in the high-redshift protocluster Cl 0218.3–0510 at $z = 1.62$. Using imaging from the *Chandra* X-ray Telescope, we find a large overdensity of AGN in the protocluster; a factor of 23 ± 9 times the field density of AGN. Only half of this AGN overdensity is due to the overdensity of massive galaxies in the protocluster (a factor of 11 ± 2), as we find that $17^{+6}_{-5}\%$ of massive galaxies ($M_* > 10^{10}\,\mathrm{M_\odot}$) in the protocluster host an X-ray luminous AGN, compared to $8\pm1\%$ in the field. This corresponds to an enhancement of AGN activity in massive protocluster galaxies by a factor of 2.1 ± 0.7. We also find that the AGN overdensity is centrally concentrated, located within 3 arcmin and most pronounced within 1 arcmin of the centre of the protocluster. Our results confirm that there is a reversal in the local anti-correlation between galaxy density and AGN activity, so there is an enhancement of AGN in high-redshift protoclusters. We compare the properties of AGN in the protocluster to the field and find no significant differences in the distributions of their stellar mass, X-ray luminosity, or hardness ratio. We therefore suggest that triggering mechanisms are similar in both environments, and that the mechanisms simply occur more frequently in denser environments.

The entirety of the work presented in this chapter is published in Krishnan et al. (2017).

3.1 Introduction

There is plenty of evidence supporting a correlation between the growth of supermassive black holes (SMBHs) and the formation of their host galaxies. For instance, there is a well known M–σ relation in the local Universe (Ferrarese & Merritt 2000; Gebhardt et al. 2000; Tremaine et al. 2002), and a similar rate of evolution in the emissivity from AGN and star formation from $z \sim 2$ to $z \sim 0$ (Boyle et al. 1998; Franceschini et al. 1999; Silverman et al. 2008). In addition to the correlation between SMBHs and host galaxies, there is also a connection between AGN activity and larger-scale environment. In the local Universe, Dressler, Thompson & Shectman (1985) found that the AGN fraction in local massive field galaxies is 5%, while only 1% of local cluster galaxies show such nuclear activity. More recently, Kauffmann et al. (2004) found that twice as many galaxies host AGN with strong [OIII] emission in low-density regions as in high-density regions. This anti-correlation between galaxy density and AGN activity in the local Universe mimics the anti-correlation between galaxy density and the fraction of star forming galaxies.

In dense environments, there are several physical processes that could affect the rate of accretion onto the SMBH. Both the availability of cold gas and the mechanisms that funnel the gas into black holes may differ between a galaxy cluster and the field. For instance, in the cluster environment, gas may be removed through environmental processes such as ram-pressure stripping (Gunn & Gott 1972), and tidal effects due to the cluster potential (Farouki & Shapiro 1981) and other galaxies (Richstone 1976). These processes, as well as the absence of new infall of cold gas (Larson, Tinsley & Caldwell 1980), could lead to a shortage of cold gas reservoirs (Giovanelli & Haynes 1985), resulting in the suppression of AGN activity (Kauffmann et al. 2004), reduced star formation activity (Gisler 1978), and the abundance of post-starburst galaxies (Dressler et al. 1999) in local galaxy clusters.

Studies of AGN as a function of galaxy density and redshift are important as they give insights into the fuelling mechanisms behind AGN triggering. Models and simulations of galaxy formation currently require AGN feedback as an important mechanism for quenching star formation (e.g., Croton et al. 2006), but the connection between AGN activity and large-scale galaxy environment is not fully understood. Recent studies show that clusters at high redshift appear to host more star formation and AGN activity compared to the local Universe (e.g., Martini, Sivakoff & Mulchaey 2009; Galametz et al. 2009; Alberts et al. 2016; Bufanda et al. 2017). In addition, X-ray selected AGN are strongly clustered at $z \sim 1$ (e.g., Miyaji et al. 2007; Bradshaw et al. 2011), and radio loud AGN (RLAGN) preferentially reside in denser environments at high redshift, compared to similarly massive non-active galaxies (Hatch et al. 2014).

Previous studies have found an increasing AGN fraction in clusters with redshift up to $z \sim 1.25$ (Martini et al. 2013; Kocevski et al. 2009). However, studies at $z > 1.5$ have been limited to investigating X-ray emission from protocluster galaxies selected based on techniques using rest-frame UV light, such as the BX/MD colour-colour methods (see e.g., Adelberger et al. 2004; Steidel et al. 2003, 2004), Lyman-alpha emitters (LAEs), and Lyman-break galaxies (LBGs, Lehmer et al. 2009; Digby-North et al. 2010; Lehmer et al. 2013; Saez et al. 2015). This means that only limited (star-forming) protocluster galaxies were investigated, potentially biasing the AGN fraction if there is a strong dependence of AGN activity on host galaxy type. In addition, most of these studies cannot readily be compared to cluster AGN fractions at lower redshifts, as the X-ray observations are not deep enough to match the lower luminosity cuts in lower redshift studies.

In this chapter, we present a comparison of the AGN fractions and AGN properties in the Cl 0218.3–0510 protocluster at $z = 1.6233$, and a control field sample. The Cl 0218.3–0510 protocluster (Papovich et al. 2010; Tanaka, Finoguenov & Ueda 2010) is an ideal high-redshift structure to probe AGN activity due to the deep multiwavelength data available. This protocluster benefits from 14 band photometry and a clean yet highly complete sample of protocluster members (Hatch et al. 2016), as well as sensitive *Chandra* data allowing us to probe X-ray luminosities as faint as 10^{43} erg s^{-1} at $z \sim 1.6$.

The outline of the chapter is as follows. We describe the sample selection in Section 3.2. In Section 3.3, we calculate AGN fractions and spatial distributions using uniformly selected X-ray AGN in cluster and field samples. In Section 3.4, we compare the properties of protocluster AGN and field AGN. A discussion of the evolution of the AGN fraction in (proto)clusters from $z \sim 3.09$ to $z \sim 0.25$ follows in Section 3.6. We adopt a WMAP9 cosmology (Hinshaw et al. 2013), with $\Omega_{\rm m} = 0.29$, $\Omega_\Lambda = 0.71$, and $h = 0.69$. All X-ray luminosities quoted are calculated in rest-frame bands using a power-law model with a photon index $\Gamma = 1.7$ to be consistent with comparison work (Martini et al. 2013). We note that the effect of Galactic absorption on our fluxes is negligible.

3.2 Sample selection

3.2.1 X-ray selected AGN

We have selected our AGN using X-ray point source matching and a full band (0.5–7 keV) X-ray luminosity cut of $L_X > 10^{42}$ erg s^{-1}. We make use of *Chandra* X-ray imaging from the X-UDS program (PI: G. Hasinger; Kocevski et al. 2018; described in Section 3.2.1). This deep catalogue enables us to identify X-ray selected AGN at faint X-ray luminosities ($L_X \lesssim 10^{44}$ erg s^{-1}), at the redshift of the protocluster.

In this work we assume that optical/infrared sources within 1 arcsec of X-ray point sources are AGN for both cluster and control field samples (described in Section 3.2.2 and Section 3.2.3 respectively). We compare the AGN to the optical counterparts catalogue and find that this method is robust; 6/6 protocluster AGN and 20/20 field AGN within the CANDELS region are identical to the counterparts catalogue.

We adopt a full band (0.5–7 keV) X-ray flux limit of 6×10^{-16} erg s^{-1} cm^{-2}, defined using the flux limit map for the corresponding band. We choose this conservative value because the protocluster lies towards the edge of the *Chandra* field, so we take care to ensure a uniform flux limit for the control field and protocluster region. Figure 3.1 shows that the protocluster lies in a region of varying flux limit, and we find that the flux limit of 6×10^{-16} erg s^{-1} cm^{-2} maximises both the depth of the data, and the coverage area available for the both cluster and control field samples. We test all the results presented in this chapter using various flux limits and find that the results are consistent within quoted uncertainties.

3.2.2 Protocluster sample

For our protocluster sample, we use the Cl 0218.3–0510 protocluster at $z = 1.6233$ in the UDS field (Papovich et al. 2010; Tanaka, Finoguenov & Ueda 2010). We use the protocluster catalogue detailed in Chapter 2. The field of view in which protocluster members were defined is marked by the diamond in Figure 3.1. Protocluster members in this sample were defined out to 5 arcmin (2.6 physical Mpc) apertures, shown by the circle centred on the protocluster core.

The comoving volume of the full protocluster is $10.2 \times 10.2 \times 34.0$ Mpc^3 (Hatch et al. 2016). Adopting the flux limit defined in Section 3.2.1 results in a comoving volume of 2600 Mpc^3 for the protocluster sample.

To define our protocluster sample, we use only the most massive members ($M_* > 10^{10}\,\mathrm{M}_\odot$) of the Goldilocks sample. We account for two effects before defining this mass cut. Firstly, we calculate the limiting mass of a galaxy starting from the X-ray flux, assuming that accretion on to the SMBH is at the Eddington rate, and that the bolometric correction from X-ray to total light is a factor of 10. We find that this is $\sim 10^9\mathrm{M}_\odot$, assuming that the mass of the black hole is equal to 0.15% of the mass of the host galaxy (Kormendy 2000). Secondly, the 99% flux completeness limit for red galaxies at $z = 1.62$ corresponds to $M_* > 10^{9.7}\,\mathrm{M}_\odot$ (Hatch et al. 2017).

The final protocluster sample contains 46 massive protocluster galaxies, which are shown as red points in Figure 3.1, where AGN are highlighted with black squares. We find 8 X-ray selected AGN in the protocluster sample, out of which 6 AGN have secure spectroscopic redshifts. We note that a further possible AGN is located at $RA = $ 2h 18m 21.0s, $Dec = -5^\circ\,10'\,20.1''$, the detection of which depends sensitively on the X-ray source detection parameters. We discard this source from our AGN sample, however, as this object was not detected a-priori in our *Chandra* source catalogue. There is also a further AGN at $RA = $ 2h 18m 21.8s, $Dec = -5^\circ\,14'\,55.3''$, that has been spectroscopically identified as a protocluster member (Hasinger et al. in prep). As this galaxy is outside the narrowband field of view, it is not part of the Goldilocks sample and, as a consequence, this AGN is not included in our analysis.

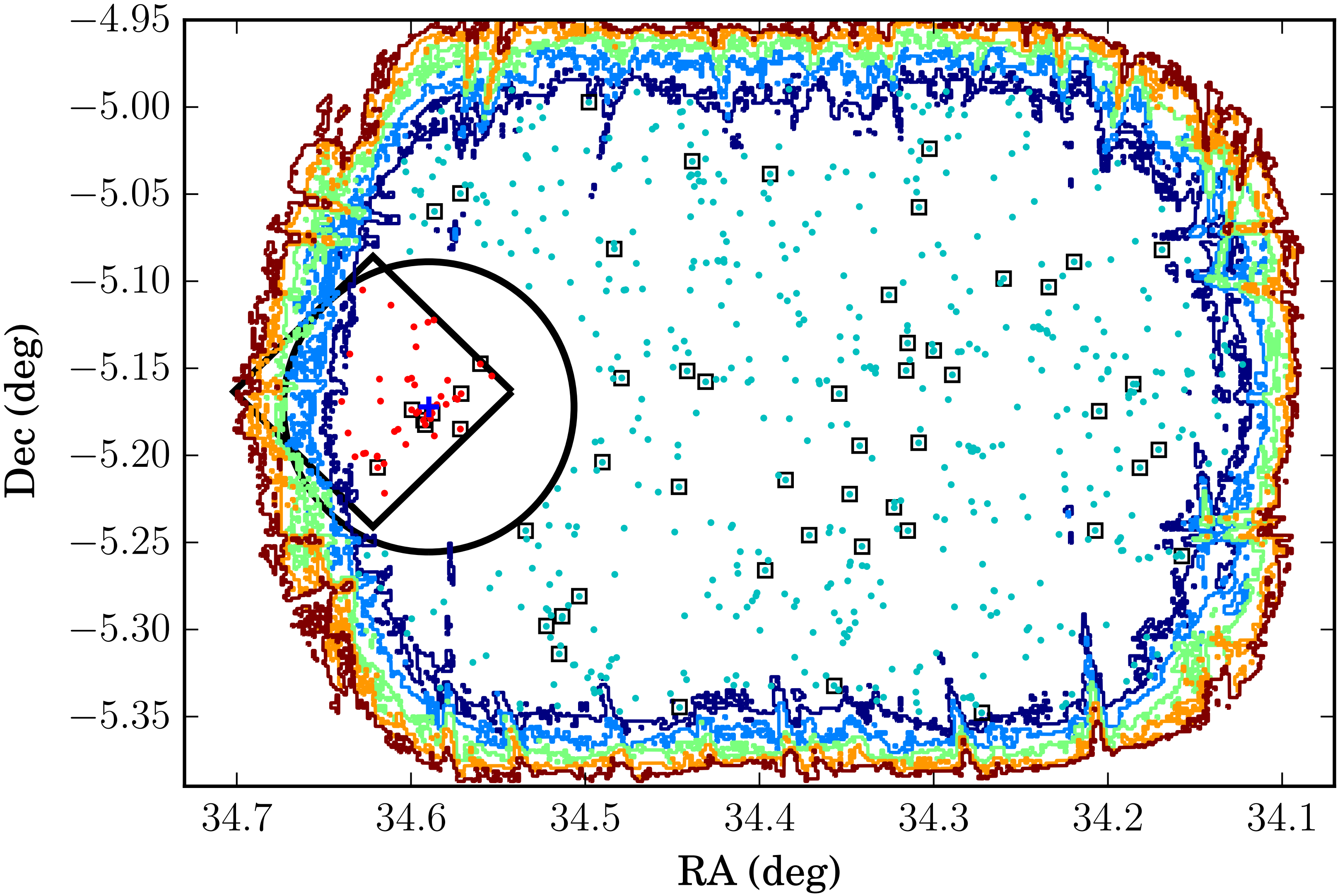

Figure 3.1. This figure shows the distribution of protocluster and field samples in the sky. The "Goldilocks" protocluster sample with $M_* > 10^{10}\,\mathrm{M}_\odot$ is shown as red points, protocluster AGN as red points with black squares, control field galaxies as cyan points, and control field AGN as cyan points with black squares. The plotted galaxies are only those within the adopted flux limit, and the navy, light blue, green, orange, and red contour lines depict flux limits of $(6, 7, 8, 9,$ and $10) \times 10^{-16}$ erg s^{-1} cm^{-2} respectively. The diamond represents the field of view of the narrowband images of the protocluster, and the BCG is marked by the blue cross. The circle represents the excluded region in order to avoid contaminating the field sample with protocluster galaxies, and the empty white space within the circle (but not within the diamond), is a region where protocluster membership is unclear because it lacks the narrowband data.

3.2.3 Control field sample

The data used are from the 8th data release of the Ultra Deep Survey (UDS DR8), described in Chapter 2. We ensure that the field sample is not affected by the presence of the protocluster by excluding a circular region within 5 arcmin (corresponding to 6.80 comoving Mpc) of the protocluster centre. The Brightest Cluster Galaxy (BCG), marked by the blue cross, and the corresponding circle, are shown in Figure 3.1. The BCG, with co-ordinates $RA = 2\text{h } 18\text{m } 21.5\text{s}$, $Dec = -5^\circ\, 10'\, 19.8''$, is taken to be the highest mass galaxy in the protocluster member sample.

To create a similarly selected field comparison sample, we select galaxies more massive than $10^{10}\,\mathrm{M}_\odot$ with photometric redshifts in the range $1.5 < z < 1.7$. We note that masses and photometric redshifts in the UDS DR8 and protocluster catalogues were both determined using SED fitting (Simpson et al. 2013), also using Bruzual & Charlot (2003) stellar population templates and assuming a Chabrier (2003) IMF. The selected field sample is as complete as the protocluster sample, and contains 550 galaxies that are shown in cyan points in Figure 3.1, with the 46 AGN depicted as black squares. The size of the field region ($0.146\ \mathrm{deg}^2$) was kept as high as possible to maximise the sample size, while ensuring uniform X-ray coverage. The comoving volume of the field sample, taking into consideration the flux limit, is $\sim 350,000$ Mpc^3.

3.3 AGN activity in protocluster and field

3.3.1 AGN overdensity in protocluster

We first investigate the abundance of AGN in the Cl 0218.3–0510 protocluster. Plotted in Figure 3.2 is the photometric redshift distribution of AGN (within the flux limit region) in the control field (blue dashed line) and in the narrowband field around the protocluster (red solid line), normalized by the total number of AGN in their respective samples. There is a clear excess of AGN at the redshift of the protocluster ($z \sim 1.62$), in the protocluster field compared to the control field, suggesting that there is indeed an overdensity of AGN associated with the protocluster.

The AGN density in the protocluster is $(3.13 \pm 1.11) \times 10^{-3}\ \mathrm{Mpc}^{-3}$, and that of the field is $(1.33 \pm 0.20) \times 10^{-4}\ \mathrm{Mpc}^{-3}$. Errors are calculated using Poisson statistics. Thus the overdensity in the protocluster is 23 ± 9 times the field density. We perform a robustness check on this result as described in Section 3.5.

As seen in Figure 3.1, the AGN are concentrated around the BCG (marked by the blue cross). We plot the AGN surface density as a function of distance from the BCG in Figure 3.3. The field value has been normalised to account for the difference in comoving volumes between the control field and the protocluster. We find that the AGN overdensity is present in the protocluster up until 3 arcmin, although it is

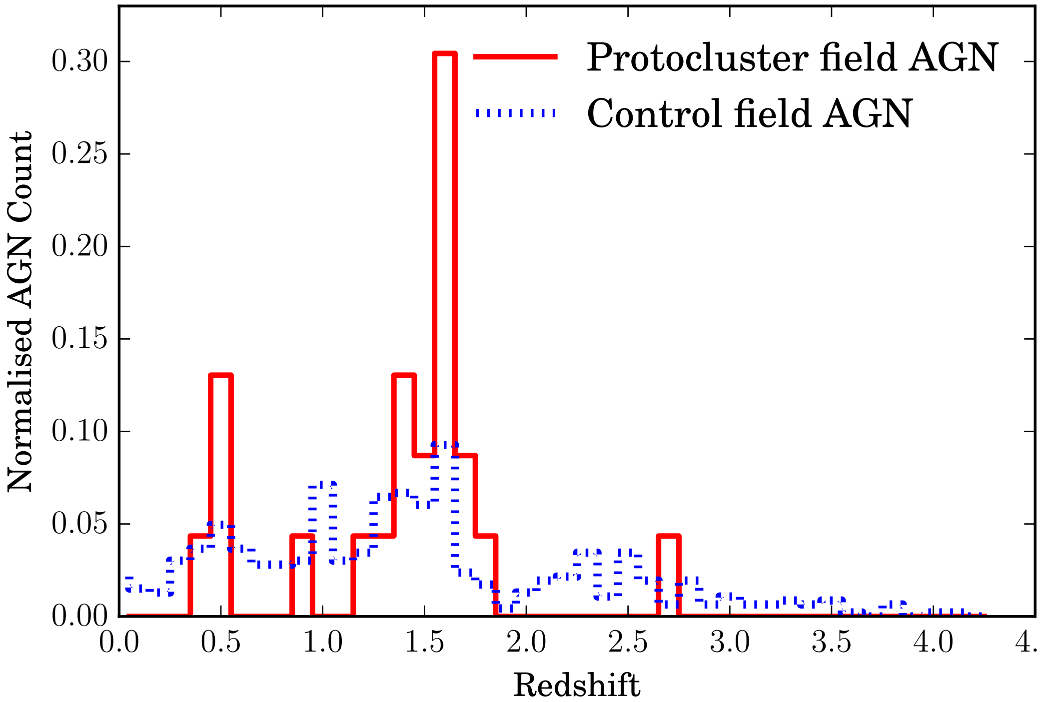

Figure 3.2. Photometric redshift distribution of protocluster field AGN (in red) and control field AGN (in blue), normalised by the total number of AGN in their respective samples. At the redshift of the protocluster, $z = 1.62$, there is a clear excess of AGN.

most significant within the central arcmin of the protocluster.

3.3.2 Fraction of AGN in $M_* > 10^{10}\,\mathrm{M}_\odot$ galaxies

We find an overdensity of AGN by a factor of ~ 23 in the protocluster relative to the field. This overdensity could be because there is a higher AGN fraction in protoclusters, or simply because protoclusters contain a higher fraction of massive galaxies, which are more likely to host AGN (Hatch et al. 2011; Cooke et al. 2014). Therefore, we calculate, in both protocluster and field environments, the fraction of massive galaxies ($M_* > 10^{10}\,\mathrm{M}_\odot$) that are AGN. We find that the AGN fraction in the protocluster is $0.17^{+0.06}_{-0.05}$, while that of the field is 0.08 ± 0.01, meaning that the fraction of massive galaxies that host AGN in the protocluster is double that of the field. The errors are obtained using Wilson intervals, where the uncertainty δf_i ($f_i = N_i/N_{\mathrm{tot}}$) is determined using the Wilson (1927) binomial confidence interval

$$f_i \pm \delta f_i = \frac{N_i + \kappa^2/2}{N_{\mathrm{tot}} + \kappa^2} \pm \frac{\kappa\sqrt{N_{\mathrm{tot}}}}{N_{\mathrm{tot}} + \kappa^2}\sqrt{f_i(1 - f_i) + \frac{\kappa^2}{4N_{\mathrm{tot}}}}, \tag{3.1}$$

where κ is the $100(1 - \alpha/2)$th percentile of a standard normal distribution (α is the error percentile corresponding to the 1σ level; see Brown, Cai & DasGupta 2001 for further details). We obtain an AGN enhancement in the protocluster at 1.6σ

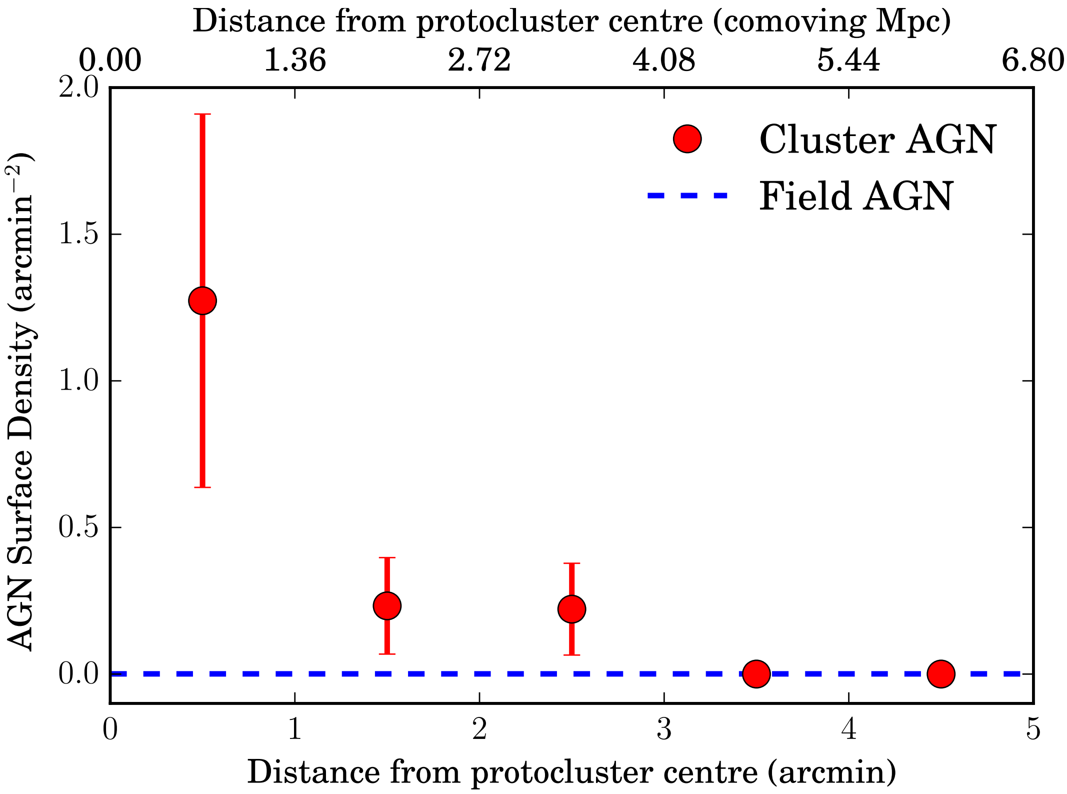

Figure 3.3. Radial plot of AGN surface density in the field (blue dashed line), and protocluster (red circles). There is a significant surface density of AGN in the central arcmin of the protocluster. The field value has been normalised to account for the difference in comoving volumes between the control field and the protocluster.

significance, and the errors are large as the sample size is small.

We also investigate whether the central concentration of AGN we find in Figure 3.3 could be attributed to the distribution of massive galaxies within the protocluster. In Figure 3.4, we plot the surface overdensity,

$$\text{Surface Overdensity} = \frac{\text{Protocluster Surface Density}}{\text{Field Surface Density}} \tag{3.2}$$

of both AGN and galaxies in the protocluster, as a function of the radius from the BCG. The green circles show the density excess of protocluster AGN as a function of radius from the BCG, and the black squares show the density excess of massive protocluster galaxies ($M_* > 10^{10}\,\mathrm{M}_\odot$). This figure shows that there is indeed a higher number of massive galaxies in the core of the protocluster relative to the field, but there is a slightly greater enhancement in the AGN fraction. However, as the number statistics are low, a larger sample of clusters is required to test the significance of this result.

In conclusion, there is an enhancement of AGN activity in this protocluster by a factor of 2.1 ± 0.7, above and beyond the overdensity of massive galaxies. This enhancement lies within 3 arcmin and mainly within the central arcmin of the

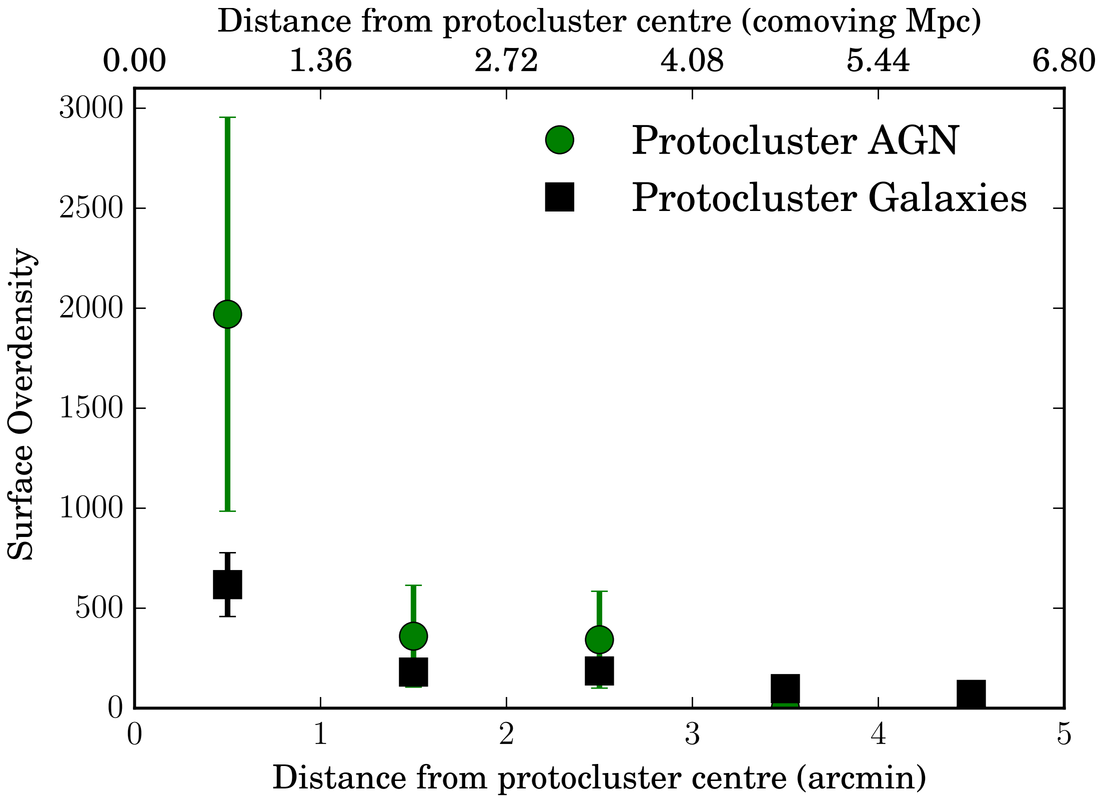

Figure 3.4. Radial plot of the surface overdensity of protocluster AGN and protocluster galaxies. The green circles indicate the protocluster AGN surface density divided by the field AGN surface density, and the black squares indicate the protocluster galaxy surface density divided by the field galaxy surface density for massive galaxies ($M_* > 10^{10}\,\mathrm{M}_\odot$). There is a slight relative excess of AGN surface density compared to massive galaxy surface density, particularly in the central arcmin of the galaxy protocluster.

protocluster (1 arcmin corresponds to 1.36 comoving Mpc).

3.4 Comparison between properties of protocluster and field AGN

We compare the properties of protocluster AGN to field AGN to see if the excess of AGN we find in the protocluster is correlated with differences in their properties, and to investigate whether environment affects the properties of these AGN. We test the null hypothesis that the distributions of the properties of field and protocluster AGN are sampling the same underlying distributions using Kolmogorov-Smirnov (KS) tests.

Firstly, X-ray luminosity functions were produced in order to compare the X-ray properties of field and protocluster AGN. X-ray luminosities were calculated using the X-ray fluxes in the full band (0.5–7 keV). The luminosity functions, as shown in Figure 3.5, were computed using the number of AGN corresponding to each luminosity bin within the comoving volume of the sample. Comparing AGN

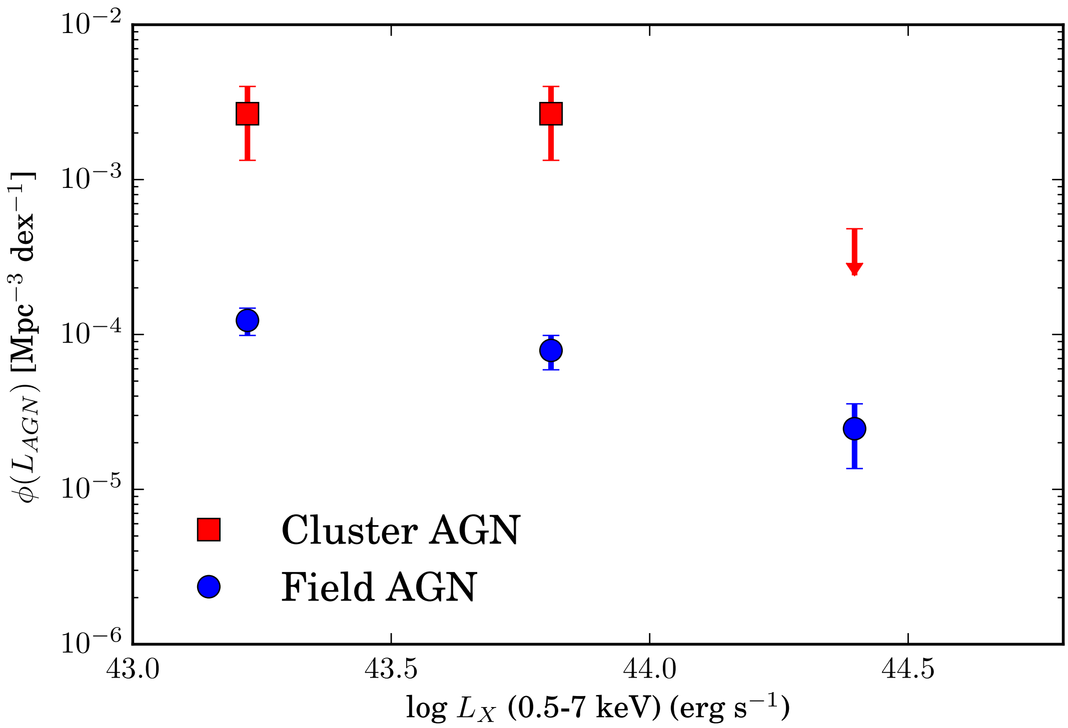

Figure 3.5. Full band (0.5–7 keV) X-ray luminosity function for AGN in the protocluster (red squares) and field (blue circles). Errors are calculated using Poisson statistics.

number densities at different X-ray luminosities allows us to compare the accretion rates in the two populations. The number density of protocluster AGN is, on average, 28 ± 6 times higher than that of the field AGN in the range of 10^{43} to 10^{45} erg s^{-1}, confirming the level of overdensity found in Section 3.3.1. We observe that the X-ray luminosity functions of protocluster and field AGN appear to have the same shape. We test the null hypothesis that the individual X-ray luminosities are sampling the same underlying distribution using a KS test, resulting in $p = 0.82$. Therefore, we find that the shapes of the X-ray luminosity distributions are indistinguishable, and we find no evidence to suggest that the distributions of accretion rates of field and protocluster AGN are different.

Secondly, we examined the hardness ratio (HR), defined by,

$$\mathrm{HR} = \frac{h - s}{h + s}, \tag{3.3}$$

where h is the flux in the hard band (2–10 keV)and s is the flux in the soft band (0.5–2 keV). This was done in order to compare the obscuration by gas in field and protocluster AGN; more obscured AGN result in soft X-rays being absorbed. A KS test on the HR of the two populations does not show a significant difference; with $p = 0.22$. Therefore, this implies that the obscuration by gas within AGN does not significantly differ between AGN in field and protocluster environments.

Thirdly, we investigated the X-ray luminosity to stellar mass ratio of protocluster and field AGN. A lower ratio might imply that the AGN are running out of fuel, or that they are accreting less efficiently. The probability that the populations sample the same underlying distribution is $p = 0.93$. Therefore, we find no evidence that protocluster and field AGN are at different stages of fuel consumption.

The observed $z - J$ colour corresponds to the rest-frame $U - B$ colour, bracketing the 4000 Å break (Papovich et al. 2010). It is thus a proxy for mean stellar age of the galaxies, although it is also affected by dust obscuration. Using a colour cut of $z - J > 1.4$ to define red galaxies, Figure 3.6(a) shows that the colours of protocluster AGN (red squares) are significantly redder than field AGN (blue circles). The probability that the colours of protocluster AGN and field AGN are drawn from the same distribution is $p = 0.03$ as given by a KS test.

The protocluster galaxy population as a whole, however, is redder than the field, so the difference in colour between AGN in the protocluster and AGN in the field could be due to the environment and not the AGN. In Figure 3.6(b), we plot the colour–mass diagram of galaxies within the protocluster that do not host AGN and field galaxies that do not host AGN. We find that 100% of our protocluster AGN are red, whereas only 57% of protocluster non-AGN are red. However, a KS test on the $z - J$ colours of protocluster AGN and non-AGN results in $p = 0.14$, and on field AGN and non-AGN results in $p = 0.35$. Therefore, with the current data, we find no significant evidence that the $z - J$ colours differ from those of normal galaxies, in both environments. Hence, although the colours of AGN are redder in the protocluster as compared to the field, this is possibly due to the fact that protocluster galaxies are redder than field galaxies.

In conclusion, we find that the environment does not appear to impact most of the properties of AGN. We find no evidence that the properties of field and protocluster AGN differ significantly in terms of stellar mass distribution, hardness ratio, and X-ray luminosities. We find that colour is the only property affected by the different environments, as we find a significant difference between the colours of AGN in the protocluster and the field. However, we also find that the colours of field and protocluster AGN are not significantly different from typical field and protocluster galaxies, so these properties appear to randomly sample their parent distributions. In summary, by comparing the properties between field and protocluster AGN, we find no significant evidence that they are different. As there is no compelling theoretical reason to assume that the processes responsible for triggering/fuelling AGN activity are different in these two environments, we suggest that these processes simply occur more frequently in dense environments. Our study is based on a small AGN sample within a single protocluster, however, so larger sample sizes will be required to verify these interpretations.

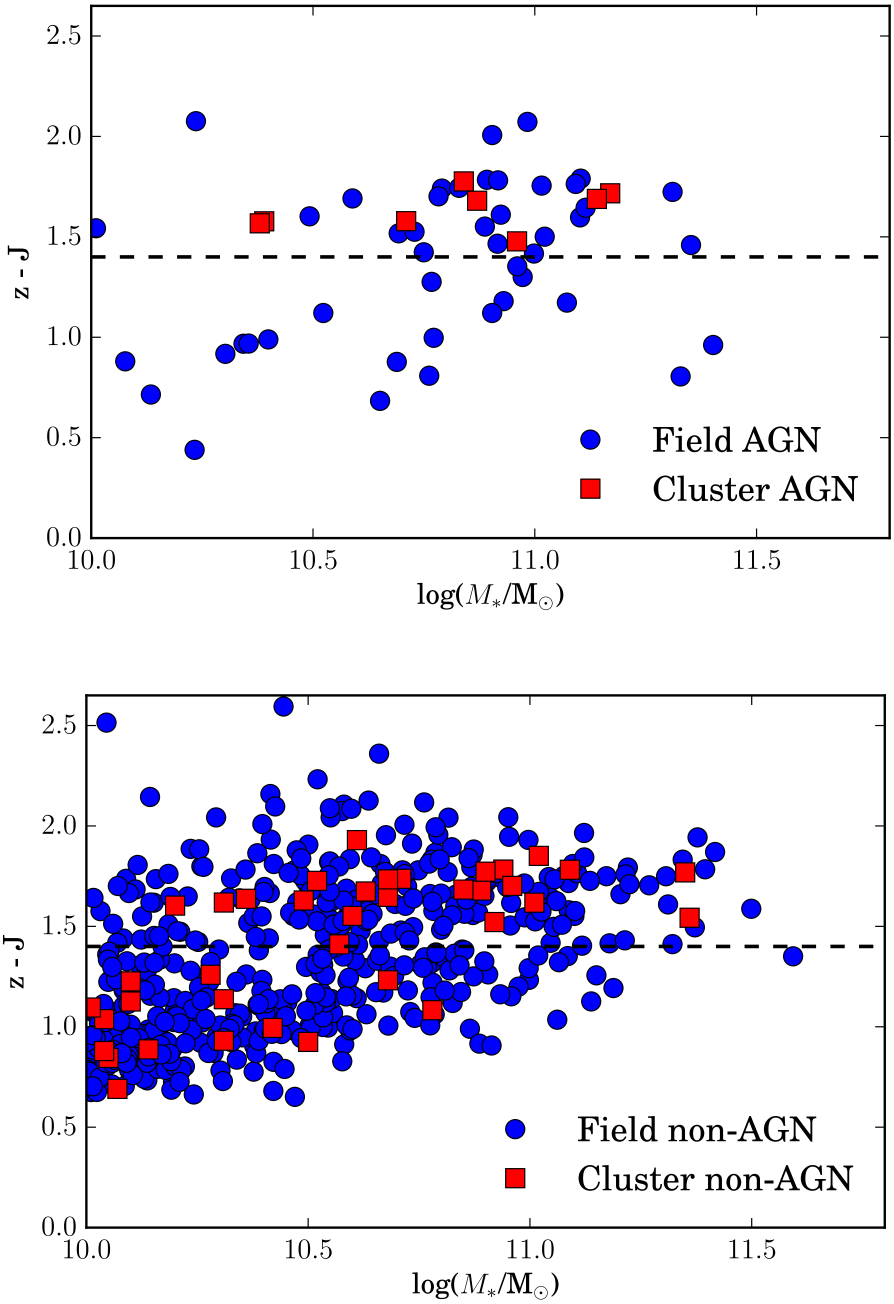

Figure 3.6. Left: (a) $z-J$ colour-mass diagram for field AGN (blue circles) vs protocluster AGN (red squares). **Right:** (b) $z-J$ colour-mass diagram for field non-AGN (blue circles) vs protocluster non-AGN (red squares). The black dashed line shows $z-J = 1.4$.

3.5 Robustness

It is important to consider that our analyses are affected by the issue of completeness of protocluster membership. This is a result of the selection technique used to define the "Goldilocks" sample, which depends on both galaxy magnitude and colour. Redder galaxies are fainter than bluer galaxies of the same mass, resulting in broader redshift probability functions due to higher fractional flux errors. Hence, fainter and redder galaxies are less likely to be selected as protocluster galaxies (Hatch et al. 2017). As described in Section 3.4, we found that protocluster AGN are redder than field AGN, with 100% of protocluster AGN being red ($z - J > 1.4$), and the probability of sampling the same underlying colour distributions being $p = 0.03$ as given by a KS test. Although these red AGN host galaxies are less likely to be selected as part of the "Goldilocks" sample, we still see an excess of protocluster AGN over the field AGN.

However, we perform a robustness check, disregarding the "Goldilocks" sample, to test the AGN enhancement in the protocluster. We define the test protocluster sample to be massive galaxies ($M_* > 10^{10}\,\mathrm{M}_\odot$) in the UDS field with redshifts at $1.5 < z < 1.7$, within a circle of radius 5 arcmin centred on the BCG. We find 14 AGN in this protocluster region (within the flux limit area), and subtract off the number of AGN in the field corresponding to the same area. We find a formal excess of 8.04 AGN, and assume that this is associated with the protocluster. This is consistent with the 8 AGN found using the "Goldilocks" sample in Section 3.2.2. Therefore, we conclude that our result of the AGN enhancement in the protocluster is robust to the protocluster member selection technique used in Hatch et al. (2017).

We find an AGN fraction of $0.17^{+0.06}_{-0.05}$ in massive protocluster galaxies, as described in Section 3.3.2. This fraction is likely to be robust as there are no significant differences in the $z - J$ colours of protocluster galaxies and protocluster AGN, as found in Section 3.4.

We also find that the AGN picked out as part of the test protocluster sample, and not the "Goldilocks" sample, are either massive and red, or blue. They all lie within the region of the colour-mass diagram where $> 75\%$ of protocluster members would be correctly identified (Hatch et al. 2017). It is therefore unlikely that we are missing any protocluster AGN due to the protocluster membership selection criterion.

3.6 Discussion

In summary of our results, we find that the AGN fraction in the $z \sim 1.62$ protocluster is twice that of the field, and that the AGN enhancement lies within the central 3 arcmin (4.08 comoving Mpc) region of the protocluster. We find that the properties of field and protocluster AGN are not significantly different. As there is no significant evidence suggesting that they are triggered/fuelled in different ways, we infer that the processes responsible for triggering/fuelling AGN are possibly more frequent in denser environments.

To frame our results in the context of recent literature on (proto)clusters at higher and lower redshifts, we plot the AGN fraction and the ratio of cluster AGN fraction to field AGN fraction as a function of redshift in Figure 3.7 and Figure 3.8 respectively. The cut in X-ray luminosity is 10^{43} erg s^{-1}, except for the two highest redshift studies at $z = 2.30$ and $z = 3.09$, in which the cuts are 4.6×10^{43} erg s^{-1} and 3.2×10^{43} erg s^{-1} respectively. Figure 3.7 shows that there is an increasing cluster AGN fraction with redshift. It rises to $\sim 17\%$ at $z \sim 1.6$ and then flattens; it is uncertain beyond $z \sim 2$, however, because of the different luminosity limits applied. This increase in the cluster AGN fraction with redshift has also been found by several recent studies (e.g., Galametz et al. 2009; Martini, Sivakoff & Mulchaey 2009; Alberts et al. 2016; Bufanda et al. 2017). The AGN fraction in the field, however, also increases with redshift (e.g., Merloni & Heinz 2013). To study the influence of environment we compare the cluster AGN fractions to field AGN fractions. Figure 3.8 shows that the relative AGN activity in clusters compared to the field increases with redshift. The AGN fraction in clusters is lower than the field at $z < 1$, but we find a larger AGN fraction in the $z \sim 1.62$ protocluster compared to the field. We therefore find evidence for a reversal in the local anti-correlation between galaxy density and AGN fraction, confirming the results of Martini et al. (2013).

The AGN fraction in the $z \sim 1.62$ protocluster is slightly higher than those of two protoclusters at $z = 2.30$ (Digby-North et al. 2010) and $z = 3.09$ (Lehmer et al. 2009), even though it is consistent within error-bars. This is possibly because they use different techniques to select the protocluster members, such as Lyman-alpha emitters (LAEs), Lyman-break galaxies (LBGs), and BX/MD. These techniques will result in incomplete protocluster membership as they are biased towards strongly star-forming galaxies, and are likely to miss quiescent galaxies. In addition, their cuts in X-ray luminosities are higher than ours, possibly contributing to the (marginally) lower AGN fraction. We adopt their cuts in X ray luminosity, recalculate the protocluster AGN fraction, and plot these in Figure 3.7. Figure 3.8 shows that despite the lower cluster AGN fraction in these two protoclusters, the relative enhancement of cluster AGN over field AGN still increases with redshift. This may be because the luminosity cuts and the methods used for identifying galaxies are the same in the cluster and the field within each sample, and so studying the relative enhancement may be more appropriate for comparison between different studies.

The AGN fraction in clusters at $z > 1.5$ is 10–20%. This could mean that each massive protocluster galaxy is frequently "switched on" in terms of AGN activity,

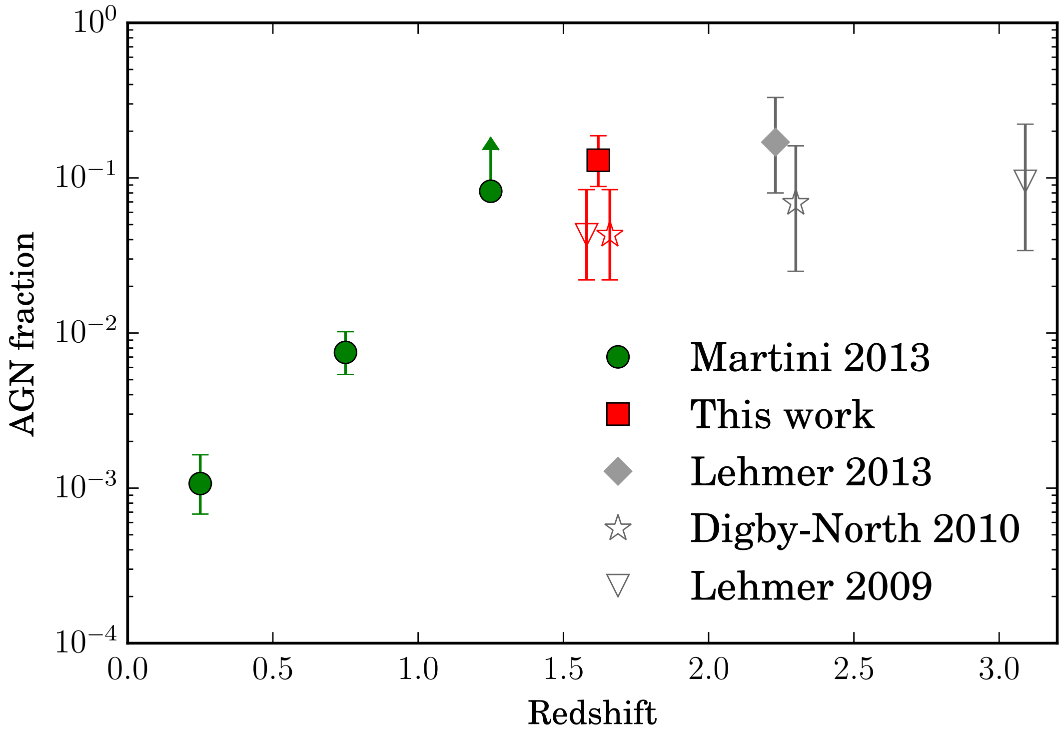

Figure 3.7. Cluster AGN fraction ($L_X > 10^{43}$ erg s^{-1}) as a function of redshift. Data points from literature at $z < 1.5$ are represented as green circles, and our work is represented as the red filled square. We plot the AGN fraction ($0.130^{+0.041}_{-0.021}$) using the hard band X-ray luminosity (2–10 keV) here to be consistent with other works. The data at redshifts $0.25, 0.75, 1.25, 2.23, 2.30$ and 3.09 are from Martini et al. (2013), Martini, Sivakoff & Mulchaey (2009), Martini et al. (2013, total AGN sample), Lehmer et al. (2013, HAE AGN sample), Digby-North et al. (2010, BX/MD AGN sample), and Lehmer et al. (2009, LBGs AGN sample) respectively. The three higher redshift studies are in grey as they do not sample the full protocluster galaxy population. The two highest redshift points are in open symbols as they use different luminosity cuts. We also calculate the AGN fraction at $z \sim 1.62$ according to the luminosity limits used by the two higher redshift studies and plot them as red points with symbols corresponding to the studies. These have been offset slightly in redshift for clarity.

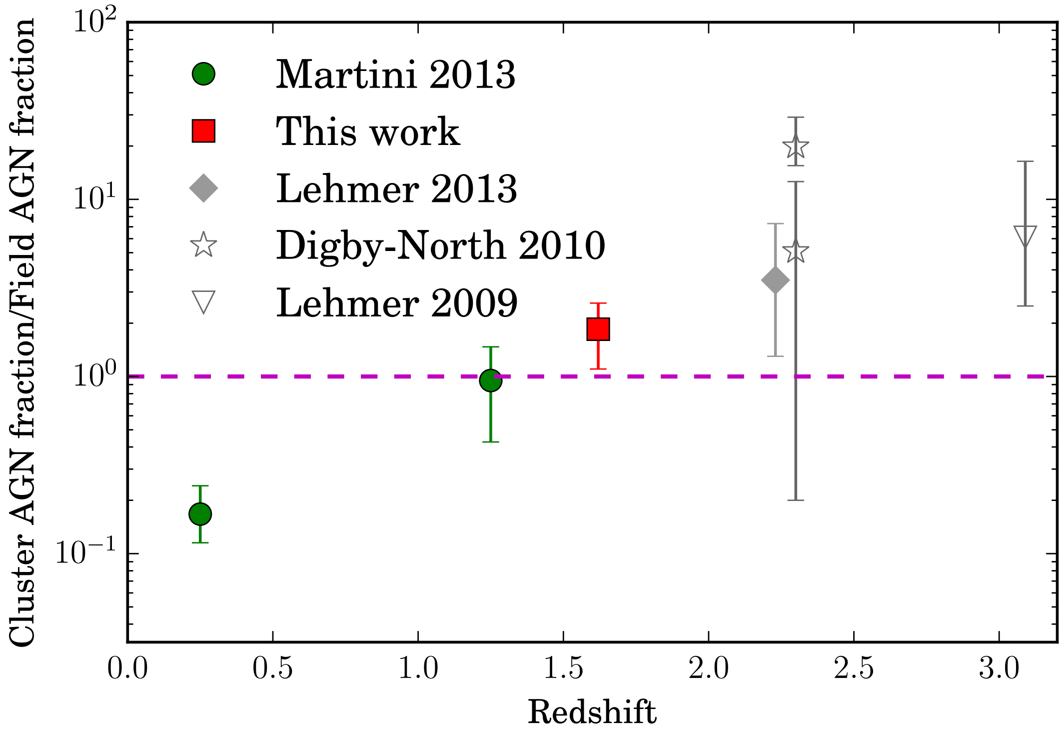

Figure 3.8. Cluster AGN fraction relative to field AGN fraction as a function of redshift. There is a reversal in the local anti-correlation after $z > 1.25$. The magenta dashed line indicates an equal cluster and field AGN fraction. As with Figure 3.7, data points from literature at $z < 1.5$ are represented as green circles, and this work (using the hard band X-ray luminosity) is represented as the red filled square. The three higher redshift studies are in grey as they do not sample the full protocluster galaxy population; Lehmer et al. (2013, HAE AGN sample), Digby-North et al. (2010, higher and lower points are BX/MD AGN and emission line AGN respectively) and Lehmer et al. (2009, mean AGN fraction among LBGs and LAEs). Open symbols denote that the luminosity cuts are different to $L_X > 10^{43}$ erg s^{-1}.

or that the phenomenon happens once but lasts for a longer time in the protocluster compared to the field. In Section 3.4, we found that there are no significant differences in the properties of AGN between the two different environments and interpreted that there is no evidence suggesting that the mechanisms responsible for triggering/fuelling AGN are different in the protocluster compared to the field. Therefore, the mechanisms responsible may simply be more frequent in the protocluster environment than the field.

Mergers and interactions such as galaxy harassment (Moore et al. 1996) have been suggested as the mechanisms responsible for triggering AGN activity (Springel, Di Matteo & Hernquist 2005). These processes may provide the instabilities required to funnel gas towards the SMBH. The decrease in the overall AGN fraction over cosmic time could be due to a decrease in frequency of fuelling mechanisms or due to a decrease in the amount of fuel available. It has been found that the frequency of mergers involving massive galaxies ($M_* > 10^{10}\,\mathrm{M}_\odot$) decreases as the Universe ages (Conselice, Rajgor & Myers 2008). The cold gas supply is also depleted as the Universe ages as it forms stars and accretes on to black holes. The suppression of AGN activity in mature clusters relative to the field in the local Universe may be due to virialization, as this has been suggested to halt merger rates (Lotz et al. 2013). It has been found by van Breukelen et al. (2009) that AGN are triggered by galaxy interaction and merging events during the pre-virialization evolutionary stage.

Lotz et al. (2013) explore the frequency of mergers in the Cl 0218.3–0510 protocluster, and find that the merger rate for galaxies in the protocluster is $\sim$ 2–4 mergers per Gyr per galaxy, as compared to ~ 0.5 mergers per Gyr per galaxy in the field. This increased merger rate may be responsible for the increase in AGN rates.

To test whether mergers and interactions are more frequent in the protocluster AGN compared to the field AGN, we used CANDELS-UDS visual classifications to calculate merger fractions using both the fraction of galaxies classed as "irregular", and those classed as "disturbed" (i.e. mergers or interactions). These morphologies were visually identified by a team of astronomers within the CANDELS collaboration (Kartaltepe et al. 2015). We impose that $> 50\%$ of classifiers must agree in order to accept the classification. We find that 4/6 protocluster AGN are "disturbed", compared to 3/18 field AGN ($67^{+16}_{-20}\%$ in the protocluster AGN as opposed to $17^{+10}_{-7}\%$ in the field AGN). The "irregular" fraction is 2/6 in the protocluster AGN and 0/20 in the field AGN ($33^{+20}_{-16}\%$ in the protocluster AGN and an upper limit of 5% in the field AGN). Errors are calculated following Wilson (1927) as described in Section 3.3.2. We note that morphologies may be subjective, and thus conclude that there is tentative evidence that mergers and interactions are fuelling AGN in the $z \sim 1.62$ protocluster. However, we also find that among the inactive galaxies in the protocluster, $18^{+14}_{-9}\%$ were classified as "disturbed", and an upper limit of 8% were classified as "irregular". This provides more evidence to support the hypothesis that the enhancement in AGN correlates with mergers and environmental interactions. We also find that, among the "disturbed" galaxies, 4/6 are AGN in the protocluster ($67^{+16}_{-20}\%$), while 3/28 are AGN in the field ($11^{+7}_{-5}\%$). This may suggest that the protocluster environment enhances the probability that a merger/interaction triggers an AGN.

We find that the AGN enhancement in the $z \sim 1.62$ protocluster lies mainly in its central regions. An excess of AGN has also been found by Galametz et al. (2009) in the central regions of clusters at lower redshifts. We find a larger excess in our study, however this is expected as the cluster AGN fraction increases with redshift as shown in Figure 3.7. Star formation in clusters also increases with redshift, and this could point towards a co-evolution between star-formation activity and AGN activity. This may be expected because they share the same gas source that becomes depleted as the Universe ages. However, Hatch et al. (2017) find that the central regions of the same protocluster at $z \sim 1.62$ have suppressed sSFR compared to outer regions, and one of many possibilities is that AGN feedback quenches star formation. We note that at higher redshift ($z \sim 3$), an enhancement of SFR has been reported in a protocluster instead (Umehata et al. 2015; Alexander et al. 2016).

The high AGN fraction in protoclusters at high redshift may have important implications for our understanding of galaxy evolution. A key ingredient in regulating star formation in current galaxy formation models is feedback from AGN (e.g., Croton et al. 2006). Therefore, the high protocluster AGN fraction at $z \sim 1.62$ could imply more rapid quenching of star formation in dense environments at high redshift. Yet in models of galaxy formation, no direct prescription for environmental dependence is applied to AGN feedback. Prescriptions of AGN feedback in some semi-analytic models do indirectly depend on environment, since (a) clusters have larger halo masses so there is more gas mass available for fuelling AGN, and (b) there is an environmental dependence of mergers, which stimulate accretion onto SMBHs (Henriques et al. 2016). However, environmental interactions such as harassment (Moore et al. 1996) could also disturb protocluster environments to funnel gas onto the SMBH (without a merger), and subsequently mass-quench galaxies in denser environments. It has been proposed that "mass quenching" (e.g. AGN feedback) and "environmental quenching" (e.g. mergers) are mechanisms that extinguish star formation independent of each other (e.g., Peng et al. 2010). However, in this work we find evidence for environmental dependence of AGN activity, consistent with recent work (Darvish et al. 2016) that finds an environmental dependence on mass quenching efficiency. This may therefore be evidence that a more direct environmental dependence of AGN feedback must be applied in galaxy formation models, as quenching mechanisms are crucial in determining galaxy formation and evolution.

3.7 Summary

In this work we study the prevalence of X-ray AGN in the Cl 0218.3–0510 protocluster at $z = 1.6233$, and compare them to a control field sample at $1.5 < z < 1.7$. We investigate the properties of field and protocluster AGN, and study the evolution of AGN activity in dense environments over cosmic time. We confirm a reversal of the local anti-correlation between galaxy density and AGN activity, as suggested by Martini et al. (2013). To summarise our findings:

1. We find an overdensity of AGN in the protocluster relative to the field; 23 ± 9 times the number of AGN per unit volume. The AGN fraction of massive galaxies in the protocluster is 2.1 ± 0.7 times that of massive galaxies in the

control field.

2. The AGN excess lies within 3 arcmin and mainly within the central arcmin of the protocluster. Therefore AGN activity is enhanced in the region of massive groups, where the sSFR of the galaxies is suppressed.

3. We find that the properties of field and protocluster AGN are not significantly different in terms of stellar mass distribution, hardness ratio, and X-ray luminosity. In terms of colours and stellar masses, field and protocluster AGN are not significantly different to typical field and protocluster galaxies, respectively. We conclude that there is no evidence suggesting that AGN in different environments are triggered/fuelled in different ways, and infer that the processes that trigger/fuel AGN are simply more frequent in denser environments.

4. We use CANDELS visually classified morphologies to test whether environmental interactions could be triggering AGN. The morphologically classified disturbed and irregular fractions are higher in cluster AGN than field AGN. The more frequent mergers and environmental interactions in the protocluster could explain the enhancement of AGN activity.

5. We combine our study with recent literature and find that the overall AGN fraction decreases with cosmic time. We find that the relative enhancement of cluster AGN and field AGN decreases as the Universe ages.

Chapter 4

The clustering of X-ray AGN at $0.5 < z < 4.5$: host galaxies dictate dark matter halo mass

In this chapter we investigate the relationship between AGN and dark matter halo mass using statistical clustering techniques. We present evidence that AGN do not reside in "special" environments, but instead show large-scale clustering determined by the properties of their host galaxies. Our study is based on a cross-correlation analysis applied to X-ray selected AGN in the COSMOS and UDS fields, spanning redshifts from $z \sim 4.5$ to $z \sim 0.5$. Consistent with previous studies, we find that AGN at all epochs are on average hosted by galaxies in dark matter halos of $10^{12} - 10^{13}$ $M_{\odot}$, intermediate between star-forming and passive galaxies. These form some of the most overdense environments at high redshift, suggesting that AGN activity may shift to overdense environments at high redshift, consistent with our smaller-scale findings in Chapter 3. We find that the same clustering signal can be produced by inactive (i.e. non-AGN) galaxies closely matched to the AGN in spectral class, stellar mass and redshift. We therefore argue that the inferred bias for AGN lies in between the star-forming and passive galaxy populations because AGN host galaxies are comprised of a mixture of the two populations. Although AGN hosted by higher mass galaxies are more clustered than lower mass galaxies, this stellar mass dependence disappears when passive host galaxies are removed. The strength of clustering is also largely independent of AGN X-ray luminosity. We conclude that the most important property that determines the clustering in a given AGN population is the fraction of passive host galaxies. We also infer that AGN luminosity is likely not driven by environmental triggering, and further hypothesise that AGN may be a stochastic phenomenon without a strong dependence on large-scale environment.

Most of the work presented in this chapter is submitted for publication (Krishnan et al. submitted).

4.1 Introduction

Numerous lines of observational evidence point towards a tight correlation between the evolution of galaxies and that of their SMBHs. For instance, the total star formation rate density and the total AGN accretion density appear to follow similar trends from $z \sim 2$ to $z \sim 0$ (e.g. Boyle et al. 1998; Franceschini et al. 1999; Silverman et al. 2008; Kormendy & Ho 2013 for a recent review), implying a link between the mass growth of SMBHs and their host galaxies. The properties of galaxies are also correlated with their environment (e.g., Gisler 1978; Dressler et al. 1999; De Lucia et al. 2006; Conselice 2014), which suggests that supermassive black holes may also be linked to their large-scale environment. Indeed, several studies have found correlations between the abundance of AGN and their environment. For example, Kauffmann et al. (2004) showed there is an enhancement of AGN in low-density regions compared to high-density regions in the local Universe, whilst at higher redshift the opposite is found, with an enhanced fraction of AGN in high-redshift protoclusters relative to the field (Lehmer et al. 2009; Digby-North et al. 2010; Krishnan et al. 2017).

A useful tool to examine the possible connection between AGN and the large scale environment in a statistical manner is the angular and spatial clustering of AGN. As SMBHs populate collapsed dark matter halos in the ΛCDM paradigm, they can be assumed to reflect the peaks in the spatial distribution of dark matter in the Universe. The 2-point correlation function (2pcf) is the most commonly used tool for large-scale clustering analysis (Peebles 1980). The 2pcf of galaxies expresses the excess probability of finding pairs of galaxies, above a random distribution. Comparison of the observed 2pcf to that of dark matter from the outputs of detailed dark matter simulations allows the determination of the dark matter halo masses of galaxies hosting AGN. In theory, the typical large-scale environments of AGN can then be inferred as a function of cosmic time, providing potential insights into the connection between AGN and their large-scale environments.

The 2pcf of quasars has been studied extensively in the literature and are found to reside in $10^{12-12.7}$ M$_\odot$ halos out to $z \sim 4$ (e.g., Croom et al. 2005; Shen et al. 2007; Ross et al. 2009; Eftekharzadeh et al. 2015; Ikeda et al. 2015; García-Vergara et al. 2017). Similarly, lower-luminosity broad line AGN out to $z \sim 0.5$ are hosted by dark matter halos of 10^{13} M$_\odot$ (Miyaji et al. 2011; Krumpe et al. 2012), and X-ray AGN across a wide range of redshifts ($z \sim 0.05$, $z \sim 0.1$, $z \sim 0.98$, $z \sim 1.25$, $z \sim 3.4$) inhabit halos of $\sim 10^{13}$ M$_\odot$ (Powell et al. 2018; Mountrichas & Georgakakis 2012; Koutoulidis et al. 2013; Bradshaw et al. 2011; Allevato et al. 2016, respectively). Many of these studies interpret the 10^{12-13} M$_\odot$ halo mass as evidence that groups are the ideal environment in which AGN are triggered through galaxy-galaxy interactions (e.g., Miyaji et al. 2011; Ikeda et al. 2015). Inconsistent with this interpretation, however, is the lack of evidence for an enhancement of AGN in groups relative to the field (Shen et al. 2007; Arnold et al. 2009; Oh et al. 2014; Tzanavaris et al. 2014) at low redshift.

Interpretation of the halo mass derived from clustering is complicated because it may not necessarily represent the environments of AGN, unless AGN are a consistent population inhabiting a single environment. If AGN are comprised of different populations of galaxies, each inhabiting a different environment, then the clustering of AGN will indicate the average of these environments. In fact, recent studies at $z \lesssim 1$ suggest that host galaxies play a major role in clustering measurements of AGN. For example, at $z \sim 0.7$, Mendez et al. (2016) find significant differences in the clustering measurements of X-ray, mid-IR and radio AGN, and that these differences are driven by differences in host galaxy properties (such as stellar mass and star-formation rate). Furthermore, at $z < 0.1$, Powell et al. (2018) find that, when accounting for host galaxy properties, AGN occupy dark matter halos consistent with the overall inactive galaxy population.

Drawing a consistent picture of the clustering of AGN is difficult because previous studies select AGN in various methods with different surveys and telescope sensitivities, thus sampling different distributions of host galaxy properties. Furthermore, the clustering is quantified using differing methods (e.g. angular, projected, real-space correlation functions) and a diverse range of models to estimate halo masses. While several works derive bias values of AGN/quasars using a broad redshift range, it has not been possible as yet for a single study to measure the *evolution* of the AGN bias with redshift from $z \sim 4.5$ to $z \sim 0.5$, due to the large samples required to obtain reliable bias measurements from the AGN auto-correlation function. In this work, we are able to use the cross-correlation function using the more numerous underlying galaxy sample from UDS and COSMOS, as these surveys provide the unique combination of depth and area required to detect large numbers of galaxies out to $z \sim 4$. This cross-correlation technique allows us to then reliably infer the auto-correlation functions of AGN, affording us the opportunity to split our X-ray AGN sample into several redshift intervals. In this study we are also able to investigate potential interpretations of the clustering signal of AGN by considering the influence of host galaxy properties such as mass and star-formation characteristics.

This chapter is structured as follows. We describe our sample selection in Section 4.2. Section 4.3 explains the methodology of our clustering analysis, and we present our results in Section 4.4. A discussion of our results is presented in Section 4.5. We adopt a WMAP9 cosmology (Hinshaw et al. 2013), with $\Omega_{\mathrm{m}} = 0.3$, $\Omega_{\Lambda} = 0.7$, and $h = 0.7$. All X-ray luminosities quoted are calculated in rest-frame bands using a power-law model with a photon index $\Gamma = 2$. We note that the effect of Galactic absorption on our fluxes is negligible.

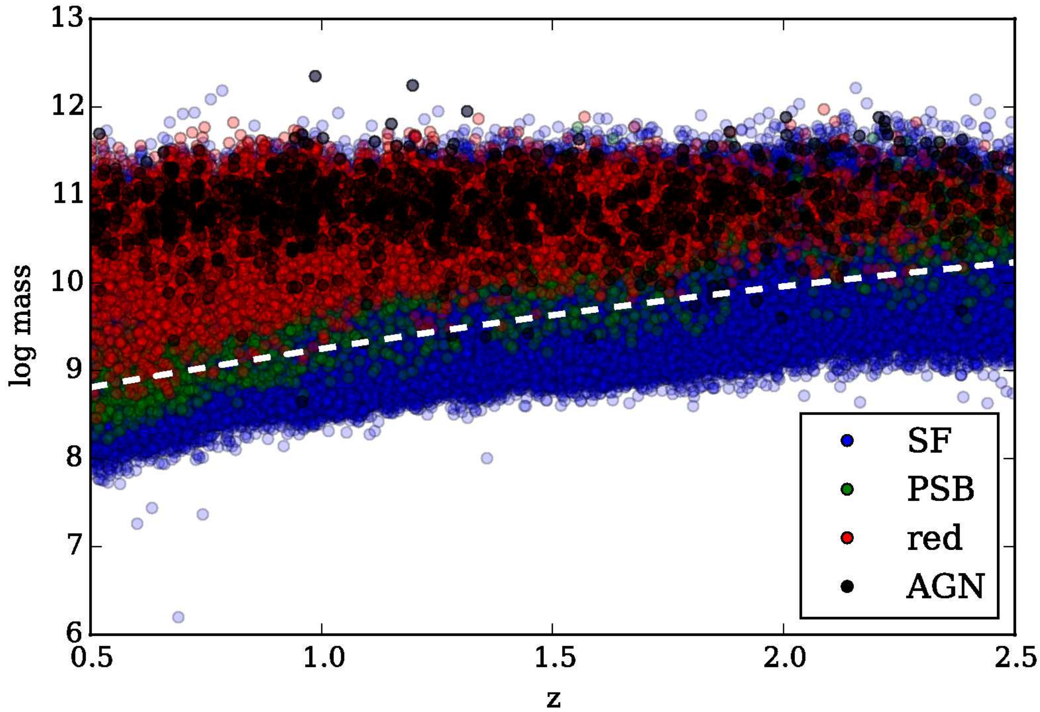

Figure 4.1. Stellar mass of AGN and galaxy samples (for which supercolour classifications are available) as a function of redshift, highlighting the different galaxy types as classified by the PCA technique, including PSBs (green), star-forming galaxies (blue), red galaxies (red) and AGN (black). The stellar mass completeness limit as derived by the Pozzetti method (see Section 2.5) is denoted by the white dashed line.

4.2 Sample selection

In this section we describe our sample selection. We make use of two deep and wide near-infrared surveys for our galaxy samples (UDS and COSMOS described in Chapter 2 in Section 2.1 and Section 2.2 respectively) with *Chandra* and *XMM-Newton* X-ray coverage.

4.2.1 Spectral class

We determine the spectral class of our AGN and galaxy samples using supercolour classifications that utilise the principal component analysis (PCA) technique outlined in Section 2.4, which separates galaxies by spectral class (such as star-forming, passive, post-starburst). Due to deeper data in the UDS field, galaxies can robustly be classified to $z = 3$, but galaxies in COSMOS are limited to $z = 2.5$ so we adopt a uniform cut in redshift when investigating the role of host galaxy properties. Figure 4.1 shows the stellar mass of the galaxy and AGN samples as a function of redshift.

4.2.2 Galaxy samples

To study the evolution of clustering of AGN as a function of cosmic time, we split our AGN and galaxy samples in redshift intervals of $0.5 < z < 0.8$, $0.8 < z < 1.3$, $1.3 < z < 2.1$, $2.1 < z < 4.5$ corresponding to equal cosmic time intervals of 1.8 Gyr. In order to maximise the quality of our galaxy sample, we apply a maximum limit to the minimum χ^2 values associated with fitting photometric redshifts. We also apply a K-band magnitude limit of $K = 23.7$ to our galaxy sample. After applying these quality cuts, our galaxy sample consists of ~ 60000 and ~ 170000 galaxies between $0.5 < z < 4.5$ in the UDS and COSMOS fields, respectively. In addition, we use the methodology from Pozzetti et al. (2010) to apply redshift-dependent 90% mass completeness limits to the galaxy sample. We do not apply a mass completeness cut to our AGN sample to maximise the sample size, but we note that 95% of our AGN are above the 90% mass completeness limit of $10^{10.2}\,\mathrm{M}_{\odot}$ at $z = 2.5$. The clustering measurements are robust to more conservative cuts in the K-band magnitude and mass completeness, as results are consistent within error-bars, albeit with larger uncertainties. The redshift distribution of the galaxy samples are shown by the solid lines in Figure 4.2.

4.2.3 AGN samples

It is important to select AGN detected to a uniform flux limit to ensure that the clustering measurements are not biased by the varying source density with exposure. We select our hard band AGN to a flux limit of 3.55×10^{-15} erg s^{-1} cm^{-2}. AGN outside the area corresponding to this flux limit are removed, as well as AGN within the region that have fainter fluxes than the flux limit. This limit was chosen to maximise the number of AGN, and applied to AGN in both the UDS and COSMOS fields. In the UDS, the X-UDS coverage is deeper but limited to the central ~ 0.33 deg^2. Outside this *Chandra*-covered region, we therefore supplement our X-UDS data with *XMM-Newton* data.

While the UDS achieves greater depths in both K-band and X-rays, the larger number of AGN in the COSMOS field effectively dictates our flux limit. To ensure a consistent depth, we therefore discard the fainter data in the UDS and adopt a shallower X-ray flux limit and K-band magnitude limit. We also make maximum use of the UDS field by computing the optimum flux limit for the UDS field independently (1.25×10^{-15} erg s^{-1} cm^{-2}) and measuring the clustering of AGN in this field. The results are consistent with the measurements using a flux limit of 3.55×10^{-15} erg s^{-1} cm^{-2}, with smaller uncertainties. The redshift distributions of the AGN selected to the latter flux limit are shown in Figure 4.2. Figure 4.3 and Figure 4.4 show the respective spatial distribution of the AGN in the UDS and COSMOS fields. The flux limit contours optimised for UDS and COSMOS are overlaid in green and light

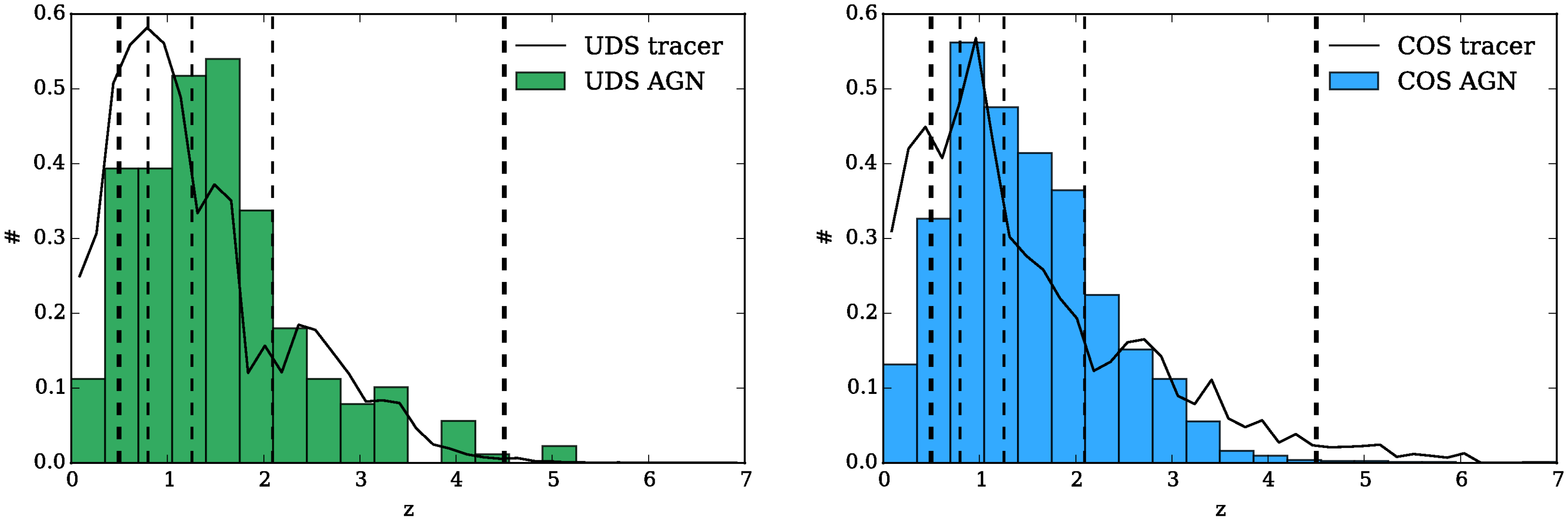

Figure 4.2. Redshift distribution of the AGN in the UDS (left) and COSMOS (right) fields are shown by the green and blue histograms, respectively. The galaxy redshift distributions within these two fields are shown by the solid black lines. The black dashed lines represent our redshift intervals of $0.5 < z < 0.8$, $0.8 < z < 1.3$, $1.3 < z < 2.1$, $2.1 < z < 4.5$, and the thicker lines denote the redshift limits of our study.

blue respectively. AGN selected to these flux limits are highlighted by the respective colours.

In our study of the links between clustering and AGN luminosity, we divide AGN into X-ray luminosity and redshift bins (see boxes in Figure 4.5). To the AGN in each bin, we apply a flux limit computed with the lower end of the luminosity bin and median redshift of the AGN within the bin. The diagonal lines traced out by missing points in the bottom right hand corners of the boxes in Figure 4.5 correspond to the sources that have been removed as their fluxes were lower than the applied flux limit.

4.3 Clustering methods

In this section, we describe the clustering methods used. We first measure the angular two point correlation function of AGN (Section 4.3.1) and that of the underlying dark matter (Section 4.3.1). We then measure the strength of clustering, using the "bias" parameter we describe in Section 4.3.2, by scaling the dark matter CF to the AGN CF and minimising χ^2. In this section we also derive the dark matter halo masses of AGN as a function of redshift.

4.3.1 Two point correlation functions

AGN correlation functions

The most commonly used statistical estimator of galaxy clustering uses the two-point auto-correlation function (ACF). The angular ACF, $w(\theta)$, measures the excess probability, above a random distribution, of finding a galaxy at an angular separation θ from another galaxy. We use the Landy & Szalay (1993) estimator, described by

$$w(\theta) = \frac{DD(\theta) - 2DR(\theta) + RR(\theta)}{RR(\theta)}, \tag{4.1}$$

where $DD(\theta)$, $DR(\theta)$ and $RR(\theta)$ are the galaxy-galaxy, galaxy-random and random-random normalised pair counts, respectively. We choose this estimator because it is more robust to effects that can affect clustering measurements, such as the size of the random catalogue and edge corrections (Coil 2013).

While the clustering of AGN and quasars have been studied using the ACF, this method requires large sample sizes to provide tight constraints on AGN host halo masses. As our AGN sample sizes are limited, we can make use of a close cousin of the ACF; the two-point cross-correlation function (CCF). We measure the CCF of the AGN with respect to K-band selected galaxy samples provided by the UDS and COSMOS surveys.

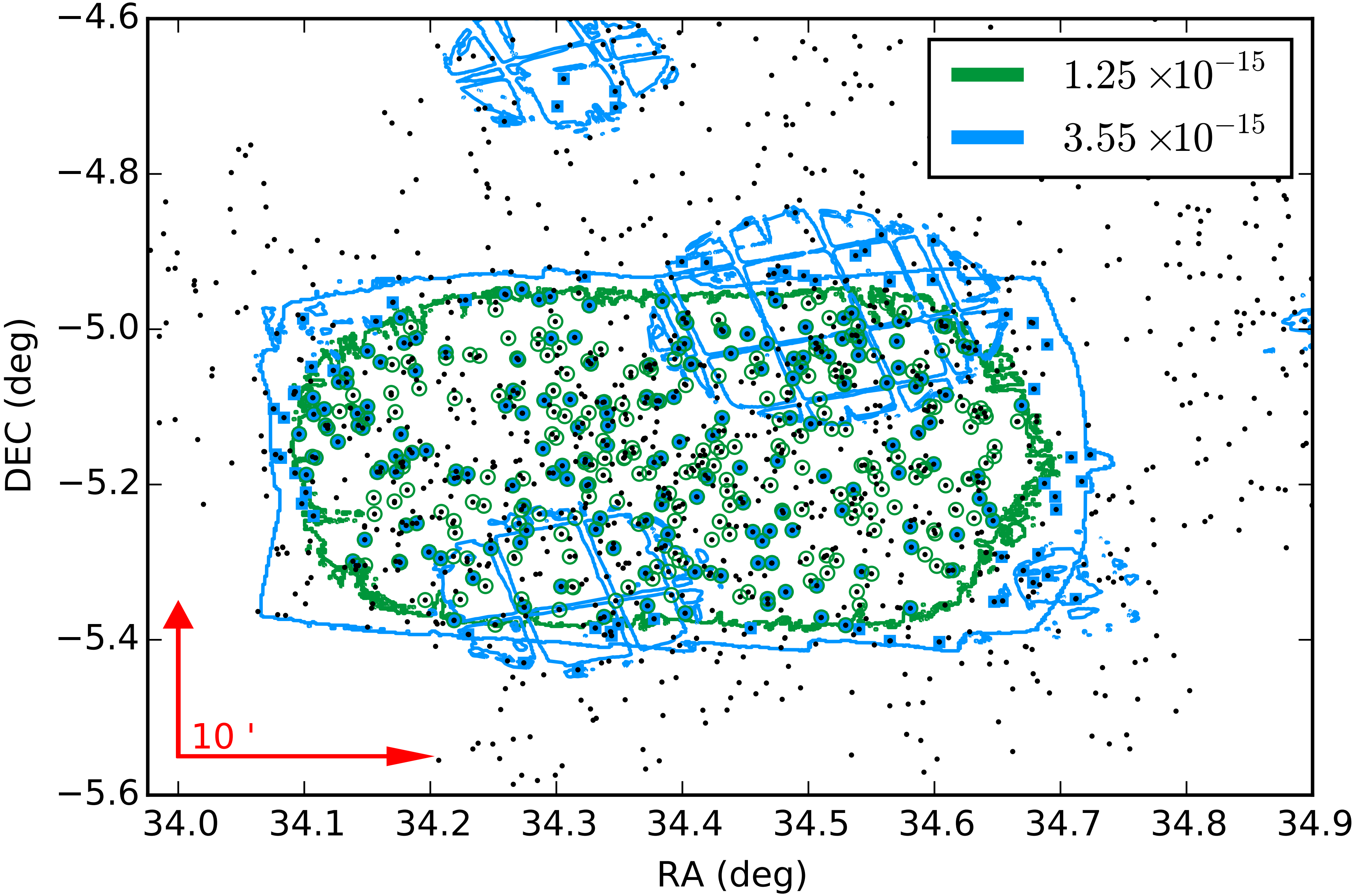

Figure 4.3. Hard-band X-ray AGN in UDS *Chandra* and *XMM-Newton*. All X-ray sources with optical/near-infrared counterparts are shown as black points, AGN with a flux limit of $\geq 1.25 \times 10^{-15}$ erg s^{-1} cm^{-2} and $\geq 3.55 \times 10^{-15}$ erg s^{-1} cm^{-2} are highlighted in green circles and blue squares, respectively. The contours corresponding to these flux limits are also shown in the respective colours. For reference, the red arrows in the bottom left corner of the plot shows a scale of $10'$.

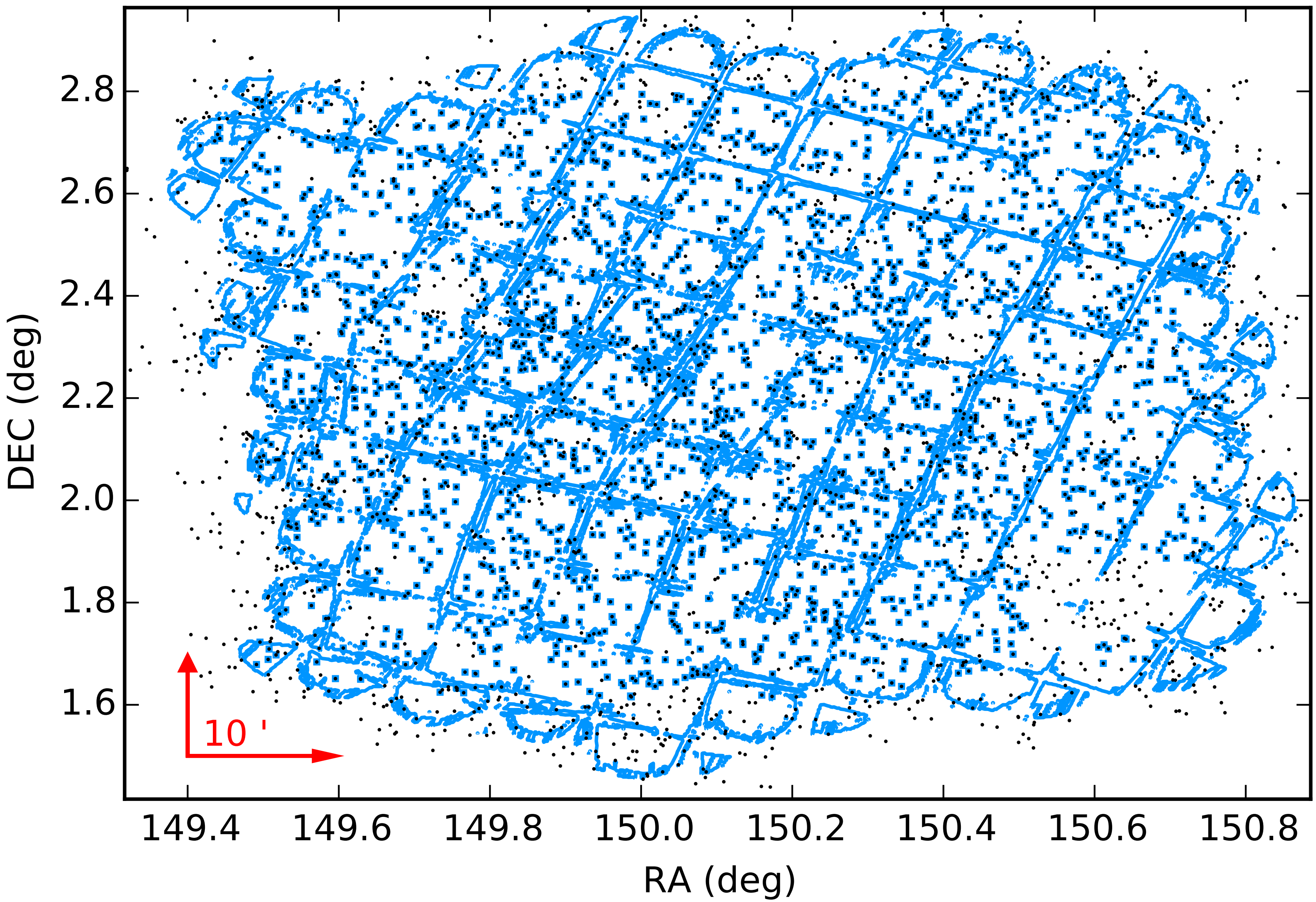

Figure 4.4. Hard-band X-ray AGN in COSMOS. All X-ray sources with optical/near-infrared counterparts are shown as black points, AGN with a flux limit of $\geq 3.55 \times 10^{-15}$ erg s^{-1} cm^{-2} are highlighted in blue squares, respectively. The contour corresponding to this flux limit is also shown in blue. Note that the larger size of the COSMOS field may give an appearance of a higher density of sources, but this does not reflect reality. For reference, the red arrows in the bottom left corner of the plot shows a scale of 10'.

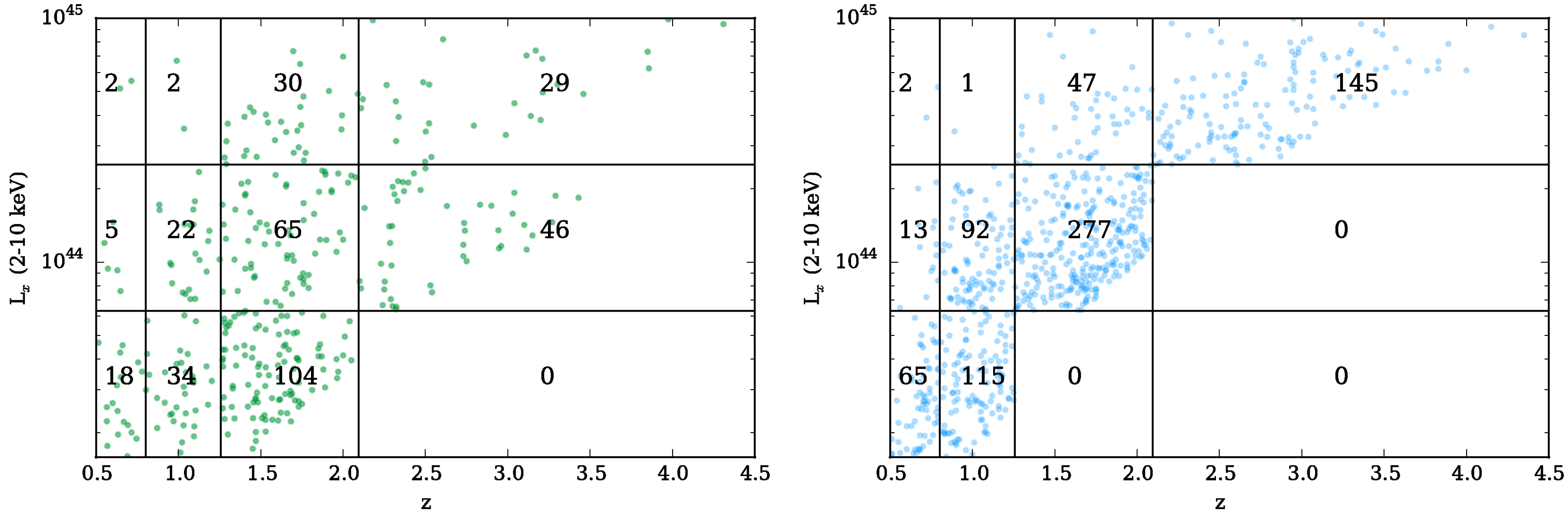

Figure 4.5. Number of AGN as a function of luminosity and redshift in UDS (left) and COSMOS (right). We apply a flux limit computed with the lower end of the luminosity bin and the median redshift of the AGN within the box. The diagonal line traced out by missing points in the bottom right hand corners of the boxes correspond to the sources that have been removed as their fluxes were lower than the applied flux limit.

We cross-correlate our AGN ($D_{\rm A}$) with a full volume-limited 90% mass-complete tracer galaxy population ($D_{\rm G}$), using:

$$w(\theta) = \frac{D_{\rm A}D_{\rm G}(\theta) - D_{\rm A}R_{\rm G}(\theta) - D_{\rm G}R_{\rm A}(\theta) + R_{\rm A}R_{\rm G}(\theta)}{R_{\rm A}R_{\rm G}(\theta)}, \tag{4.2}$$

where each term is normalised by the total pair counts. $R_{\rm A}$ and $R_{\rm G}$ denote the random source catalogues that populate the regions from which we select AGN (see Figures 4.3 and 4.4) and tracer galaxies respectively. For the tracer galaxy catalogues, we populate random catalogues corresponding to the "good" regions of UDS and COSMOS with artefacts such as stars and cross-talk masked out. For our AGN catalogues in UDS and COSMOS, we mask for the bad regions of the relevant optical/near-infrared images, as well as the regions of the X-ray image for which the flux limit is shallower than 3.55×10^{-15} erg s^{-1} cm^{-2}. For the study of luminosity-dependent clustering, we compute different random catalogues for each of the flux limits derived from the different luminosity and redshift bins.

In order to ensure that our clustering measurements are reliable, we impose a lower limit of 30 AGN in a given sample to qualify for our analysis. We ensure that the sample size of the random points is at least 10 times larger than that of the tracer population, and that these random catalogues map out the same regions as each of our galaxy catalogues.

As the clustering measured using the CCF is underestimated due to the limited observed field size, we apply a correction factor for the integral constraint C following Roche & Eales (1999),

$$C_{\rm CCF} = \frac{\sum R_{\rm A}R_{\rm G}(\theta)w(\theta)}{\sum R_{\rm A}R_{\rm G}(\theta)}. \tag{4.3}$$

The integral constraint for the ACF of our tracer sample is similarly defined as,

$$C_{\rm ACF} = \frac{\sum R_{\rm G}R_{\rm G}(\theta)w(\theta)}{\sum R_{\rm G}R_{\rm G}(\theta)}. \tag{4.4}$$

We assume that $w(\theta)$ of AGN traces the angular correlation function of the underlying dark matter distribution, following the method of Hartley et al. (2013) and Wilkinson et al. (2017).

Dark matter correlation functions

In order to interpret our angular correlation functions, we compute the angular correlation function of the matter distribution (dominated by dark matter) over the same volume as our tracer sample. We do this following the formalism of Smith et al. (2003) to compute the non-linear dark matter power spectrum at the mean redshift of the sample. This is then Fourier transformed to obtain the 3D non-linear dark matter angular correlation function; i.e. the sum of the correlation functions in the

1-halo regime (pair counts within the same halo) and the 2-halo regime (pair counts in different halos). Finally, we project this onto 2D using the redshift distribution of the sample and the Limber equation (Limber 1953). This routine therefore allows us to obtain synthetic $\mathrm{w}_{\mathrm{dm}}(\theta)$ from the halo model that can be fit to the observed AGN correlation functions.

4.3.2 Bias fitting and halo masses

Galaxies are biased tracers of the underlying dark matter density field. The linear galaxy bias parameter b, defined as the ratio of the overdensity of galaxies to the (δ_g) to the mean overdensity of matter,

$$b = \delta_g/\delta, \tag{4.5}$$

where δ is the overdensity, given by $\delta = \rho/\bar{\rho} - 1$ where $\bar{\rho}$ is in turn the mean mass density (e.g., Peebles 1980). Therefore galaxies with higher bias have a higher degree of clustering and are more likely to be found near the highest density peaks in the dark matter mass distribution.

We therefore use the bias b to indicate how strongly clustered our AGN sample is with respect to the underlying dark matter distribution. On linear scales, we can compute this parameter as the square root of the measured observed galaxy correlation function divided by the 2D dark matter correlation function following the definition,

$$w_{\mathrm{obs}}(\theta) = b^2 \times w_{\mathrm{dm}}(\theta), \tag{4.6}$$

where w_{obs} denotes the observed AGN cross-correlation function and w_{dm} denotes the projected correlation function of the dark matter distribution (e.g., Benson et al. 2000).

We therefore fit the dark matter correlation functions multiplied by b^2 to the observed AGN correlation function, and calculate the optimum value of b using χ^2 minimisation with weights corresponding to the inverse of the uncertainties on the observed correlation function. These uncertainties are calculated using the bootstrap method with 50 repetitions. We therefore resample the tracer/target sample with replacement 50 times, and evaluate $w(\theta)$ for each of the 50 bootstrap samples. The uncertainties are then given by the standard deviation of resampled values of $w(\theta)$. To obtain a combined bias measurement using two separate fields (UDS and COSMOS), we obtain individual χ^2 measurements of the two fields (using two independent AGN and dark matter correlation functions) and minimise the total χ^2.

We assume that both AGN and tracer galaxy populations trace the dark matter distribution, and that both populations are linearly biased. This implies that we expect the correlation function to be well described by linear gravity theory. This assumption holds true at large scales where both the linear ($w_{\rm linear}$) and non-linear ($w_{\rm non-linear}$) correlation functions are mutually consistent. However, the two CFs deviate at small scales, (Zehavi et al. 2005), so it is no longer appropriate to assume that the galaxy population traces the dark matter distribution. We therefore adopt a lower limit to θ corresponding to $w_{\rm non-linear} < 3 \times w_{\rm linear}$ between the linear and non-linear regimes in order to accurately constrain our bias measurements, following Wilkinson et al. (2017). We choose this limit as a trade-off between minimising the non-linear effects on small scales as well as maximising the scales over which we can use the correlation functions. We also employ an upper limit and do not consider pair counts at scales larger than $\theta = 0.4$ degrees as the finite field of view results in unreliable $w(\theta)$ measurements at large θ.

We thus determine the absolute bias of the AGN cross-correlated with tracer galaxies (CCF bias, $b_{\rm AG}$) and of the tracer galaxy auto correlation function (ACF bias, $b_{\rm G}$) with respect to the dark matter. These two absolute bias measurements can then be used to infer the relative bias of the target AGN sample $b_{\rm A}$ following $b_{\rm A} = b_{\rm AG}^2/b_{\rm G}$.

The ACF of the target AGN sample can be inferred by multiplying the cross-correlation functions by $(b_{\rm AG}^2/b_{\rm G}^2)$. The inferred ACFs of UDS and COSMOS X-ray AGN are plotted in Figure 4.6 along with their fitted bias.

Finally, we obtain dark matter halo mass estimates using the formalism of Mo & White (2002). The bias of dark matter halos is dependent on its mass and given epoch. We thus assign dark matter halo masses to our AGN samples by matching our bias measurements at a given redshift to the bias of dark matter halos of various masses.

4.4 Results

4.4.1 Interpreting the bias of X-ray AGN

We calculate cross-correlation functions in the UDS and COSMOS fields to obtain measurements of the bias and infer the dark matter halo masses of galaxies hosting X-ray AGN as a function of redshift. We plot our measurements in Figure 4.7, where the individual COSMOS and UDS measurements are presented, in addition to the combined estimate of the bias. As shown by Figure 4.7, the clustering of X-ray AGN suggest that they preferentially reside in "group-like" environments of $10^{12-13}\,\mathrm{M}_{\odot}$ irrespective of redshift, in agreement with previous studies (Croom et al. 2005; Ross et al. 2009; Shen et al. 2009; Krumpe et al. 2012; Allevato et al. 2016; Powell et al. 2018).

In Figure 4.8, we compare the bias of AGN to that of star-forming and passive galaxy populations in the UDS and COSMOS fields, selected using the supercolour

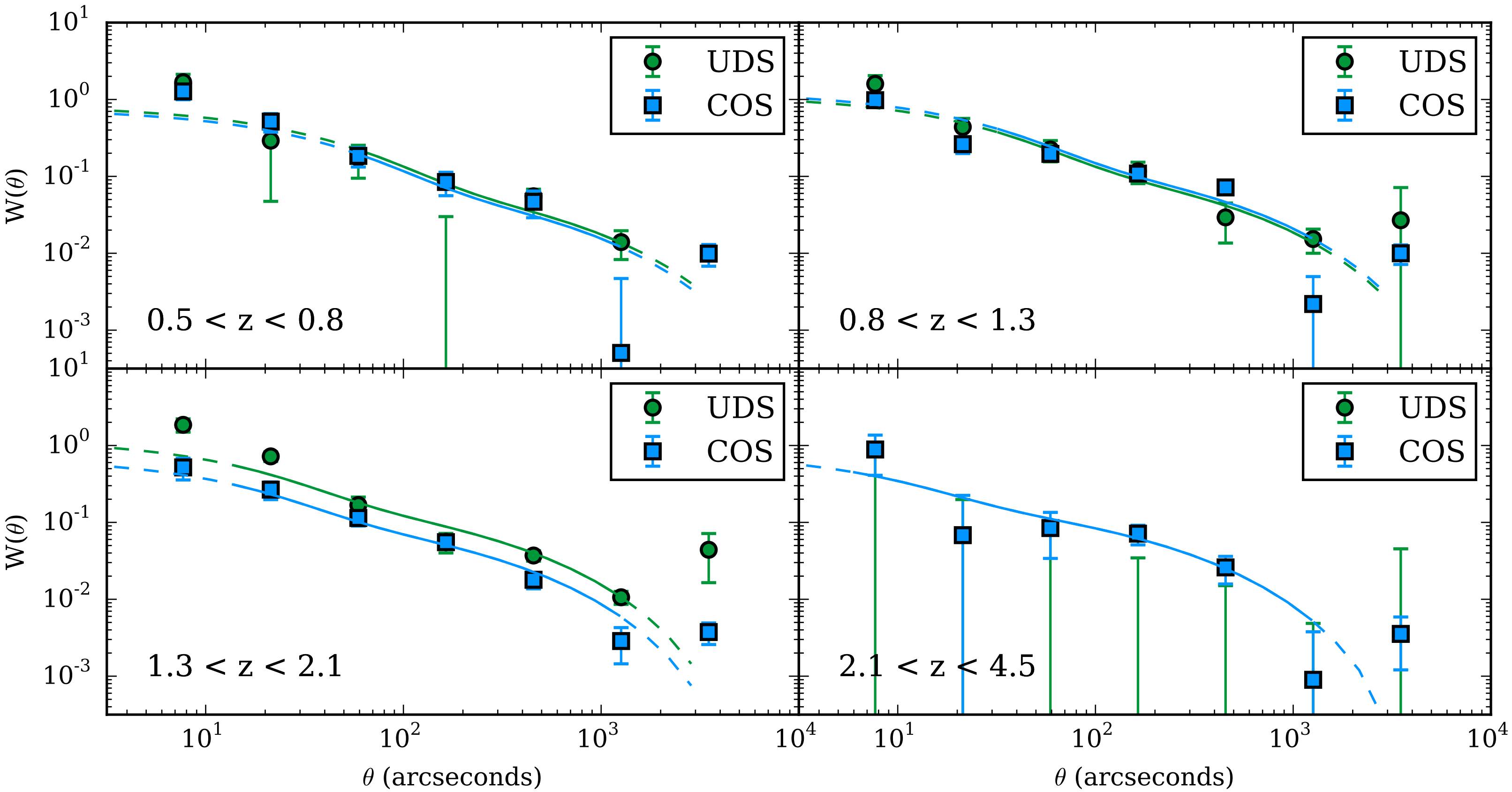

Figure 4.6. Inferred auto-correlation functions of X-ray AGN in the UDS (green) and COSMOS (light blue), as a function of redshift. We present the bias measurement with a flux limit optimised separately for each field. Uncertainties are derived from the standard deviation in resampled $w(\theta)$. We note that low number statistics can formally lead to negative $w(\theta)$ in certain bins, resulting in an underestimation of the bias. The combined measurements in these cases will not be affected by this problem as these points will have larger uncertainties and hence lower weights in the χ^2 minimisation. The dashed lines represent the fits of the dark matter correlation functions to the observed correlation functions (scaled by the square of the bias), and the over-plotted solid lines highlight the scales over which the observed correlation function is used in the fitting routine.

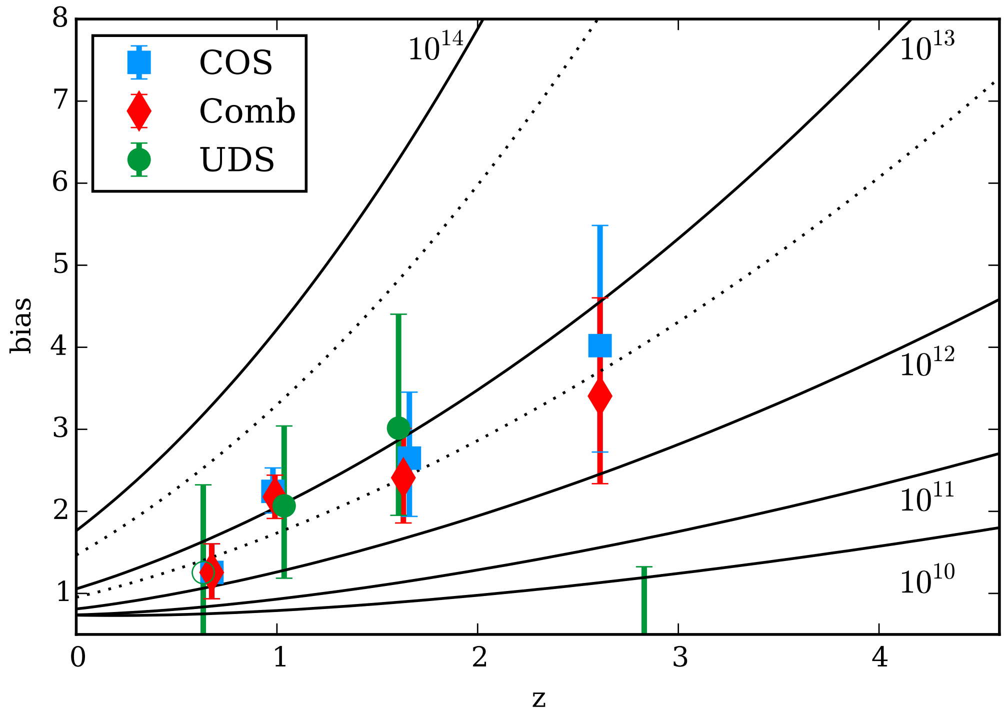

Figure 4.7. Redshift evolution of AGN bias in the UDS (green) and COSMOS (light blue). We present the bias measurement with a flux limit chosen to maximise the number of AGN in each field separately, as well as the combined measurement in red optimised for both fields. If fewer than 50 AGN are present in the sample, we plot them in open symbols as these points are potentially less reliable. The redshift evolution of dark matter halos corresponding to given masses are shown by the solid black lines, and are annotated by their corresponding halo masses in solar mass units. The dotted black lines show the evolution of $5 \times 10^{12}\,\mathrm{M}_{\odot}$ and $5 \times 10^{13}\,\mathrm{M}_{\odot}$. On average, therefore, AGN appear to inhabit $10^{12-13}\,\mathrm{M}_{\odot}$ halos with no evolution in redshift.

technique (see Section 2.4 and Wilkinson et al. in prep for more details), matched in mass and redshift distributions to the AGN population[1]. As this technique is only reliable out to $z \sim 2.5$, we truncate our final redshift bin to $z = 2.5$. We find that AGN are more clustered than star-forming galaxies, but less clustered than passive galaxies of the same mass. As it is well known that AGN are a composite population of star-forming and passive galaxies (e.g., Aird, Coil & Georgakakis 2017), the clustering signal may indicate this is a mixed population, or possibly a population transitioning from star-forming to passive.

To explore this issue, we compare the clustering of AGN to the clustering of an analogous mixed population of star-forming and passive inactive galaxies. To construct this matched control sample, for each AGN we find an inactive (i.e. non-

[1]We note that Wilkinson et al. (in prep) use the full redshift probability distribution to project the 3D dark matter correlation function, whereas we use a top hat redshift probability distribution for consistency with the method we use for our AGN sample.

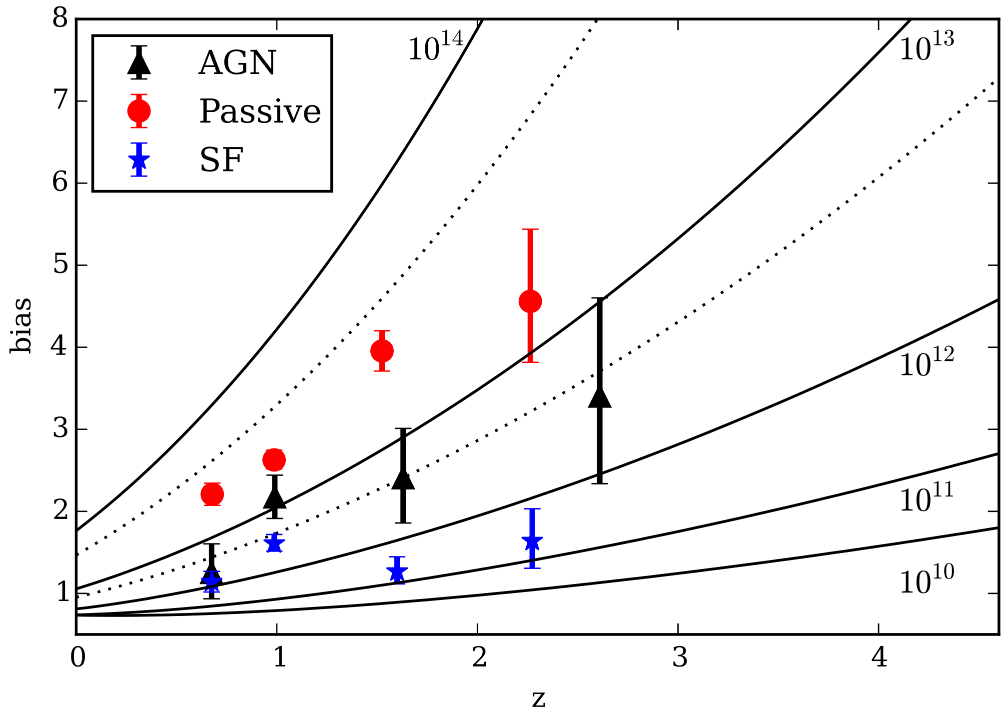

Figure 4.8. Redshift evolution of the bias of AGN (black), along with SF (blue) and passive (red) galaxies, as defined by the supercolour technique, matched in mass and redshift. X-ray AGN inhabit intermediate halo masses relative to star-forming and passive galaxies of the same mass distribution. The solid lines denote the evolution of dark matter halos, as in Figure 4.7.

AGN) "pair" that is the closest inactive galaxy in terms of redshift, spectral class as determined by its supercolours (SC1, SC2 and SC3), and stellar mass. We present the bias of this mixed galaxy population in Figure 4.9 and find that the AGN bias measurements in all redshift bins are entirely consistent with inactive galaxies of similar mass and spectral class.

The clustering of the non-AGN control galaxy population is intermediate between passive and star-forming galaxies (see Figure 4.8), as expected for a mixed sample, with an average clustering signal consistent with "group" mass halos. It is therefore possible that the intermediate clustering signal of AGN (corresponding to a halo mass of 10^{12-13} $M_{\odot}$) is produced by an averaging of the clustering signal from the mixed host galaxy population, and that the clustering of AGN predominantly reflects the mix of passive and star-forming host galaxies that occupy a range of different environments.

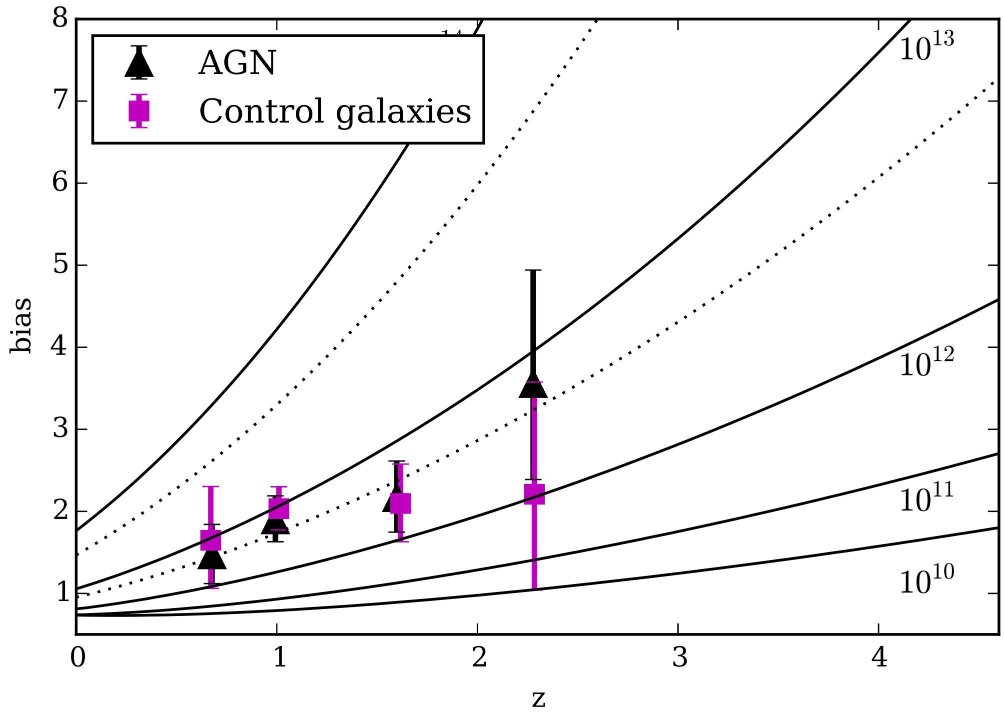

Figure 4.9. Redshift evolution of bias of X-ray AGN (for which supercolour classifications are available) in black triangles, compared to a control sample of inactive galaxies (in magenta squares), matched in stellar mass, spectral class (from supercolours), and redshift. The star-formation characteristics (i.e. spectral class) of star-forming galaxies in the non-AGN sample matches that of Figure 4.8. The solid lines denote the evolution of dark matter halos, as in Figure 4.7. The clustering of AGN is entirely consistent with the clustering of inactive galaxies with similar host galaxy properties.

4.4.2 The role of host galaxy properties on AGN clustering

We now investigate which properties of AGN host galaxies have the dominant influence on the AGN clustering signal. To disentangle the effects of stellar mass and host galaxy spectral class on clustering, we split our AGN into high and low host galaxy stellar mass subsamples around the median mass ($10^{10.75}$ $M_\odot$). In Figure 4.10(a), we plot our clustering measurements of the AGN and find that AGN in high mass galaxies are more strongly clustered and appear to reside in halos that are almost an order of magnitude (0.9 dex) more massive than AGN in low mass hosts out to $z \sim 2$ (at 2σ). This is consistent with expectations from the galaxy stellar mass-halo mass relation (e.g., Li et al. 2006; Meneux et al. 2008; Wake et al. 2011; Leauthaud et al. 2012; Marulli et al. 2013; Conselice et al. 2018).

We next consider how host galaxy spectral class affects the clustering strength. To do this, we define the passive fraction as the fraction of a given sample that are classified as either post-starburst or red-sequence (based on super-colours). In Figure 4.11 we plot the passive fractions of AGN and non-AGN galaxies, within our

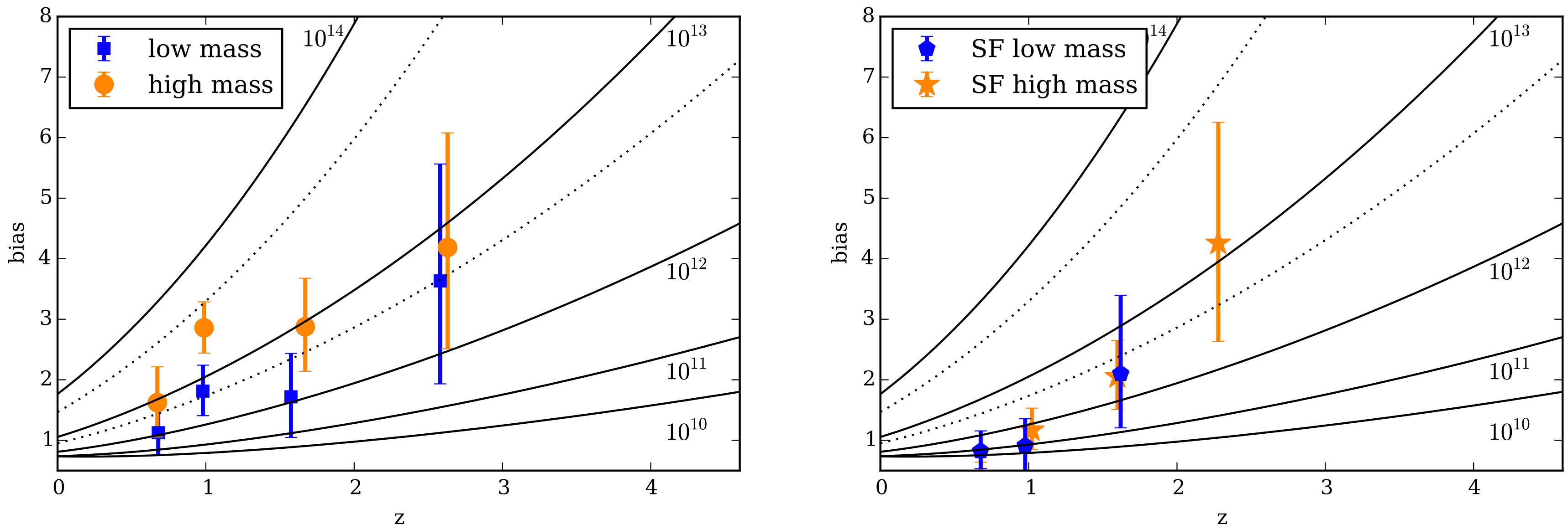

Figure 4.10. Left: (a) Redshift evolution of X-ray AGN bias in low ($M_* < 10^{10.75}\,\mathrm{M}_\odot$) and high ($M_* > 10^{10.75}\,\mathrm{M}_\odot$) mass host galaxies (blue squares and orange circles respectively). The solid lines denote the evolution of dark matter halos, as in Figure 4.7. AGN in more massive hosts appear to reside in more massive halos. **Right:** (b) Bias of X-ray AGN in low ($M_* < 10^{10.75}\,\mathrm{M}_\odot$ and high ($M_* > 10^{10.75}\,\mathrm{M}_\odot$) mass star-forming hosts (blue pentagons and orange stars respectively). There is now no significant difference between the bias measurements of AGN in low and high mass galaxies, indicating that star-forming activity is a more important driver of clustering than stellar mass.

two mass bins. We only select galaxies above the highest-redshift 90% completeness limit of $10^{10.2}$ $M_\odot$ to construct the low mass galaxy sample. This plot shows that (a) AGN have significantly lower passive fractions than galaxies of the same mass, and (b) AGN in high mass hosts, like high mass galaxies, have higher passive fractions than their low mass counterparts. Since passive hosts are more clustered than star-forming hosts (see Figure 4.8, and Hartley et al. 2013, Coil et al. 2017), the difference in the measured bias between AGN in low and high mass hosts may be due to different host spectral class. There appears to be a general correlation between the difference between the passive fractions and clustering signal of AGN in high and low mass bins (e.g. the most significant difference between the passive fractions of AGN in low and high mass galaxies is at $z \sim 1$, as is the most significant difference in bias of the two samples).

To explore this further, we would ideally measure the clustering of star-forming and passive AGN separately. Although we lack the sample sizes to explore the clustering of AGN hosted by passive galaxies, we measure the clustering of AGN in star-forming galaxies split around the same median mass, and plot our result in Figure 4.10(b). We find tentative evidence for a shift in the environments of AGN in star-forming host galaxies from higher halo masses at high redshift to field at low redshift. This is consistent with the effect of galaxy downsizing, where star-formation activity shifts from high mass halos to low mass halos as the Universe ages (Wilkinson et al. 2017). Although the increasing X-ray luminosity limit with redshift implies that we are only sensitive to higher mass black holes at higher redshifts at a given Eddington ratio, we do not expect this to affect our results significantly since we see no correlation between X-ray luminosity and halo mass (see Section 4.4.3). Figure 4.10(b) also shows that we find no difference between the dark matter halo masses of AGN in star-forming host galaxies in low and high mass bins, so the excess bias in Figure 4.10(a) is likely driven by the higher passive fractions in the high mass sample. We therefore find evidence that stellar mass is not the fundamental parameter that drives the excess clustering of AGN in higher mass host galaxies relative to AGN in lower mass host galaxies. Similar results have been obtained for the galaxy population, such as Coil et al. (2017), who find that galaxy clustering does not depend on stellar mass at a given sSFR. This may imply that the stellar mass-halo mass relation is driven by the correlation between passive fraction and stellar mass.

We caution that this analysis could be affected by the possibility that blue light from the AGN contaminates the SEDs and leads to an incorrect star-forming assignment of a passive galaxy. However, this effect is not expected to be significant as super-colour classifications are derived based on filters focussed on the rest-frame 4000 Å break region. AGN light may also contaminate the mass measurements, but our AGN have fairly low X-ray luminosities, while we only expect the most lumi-

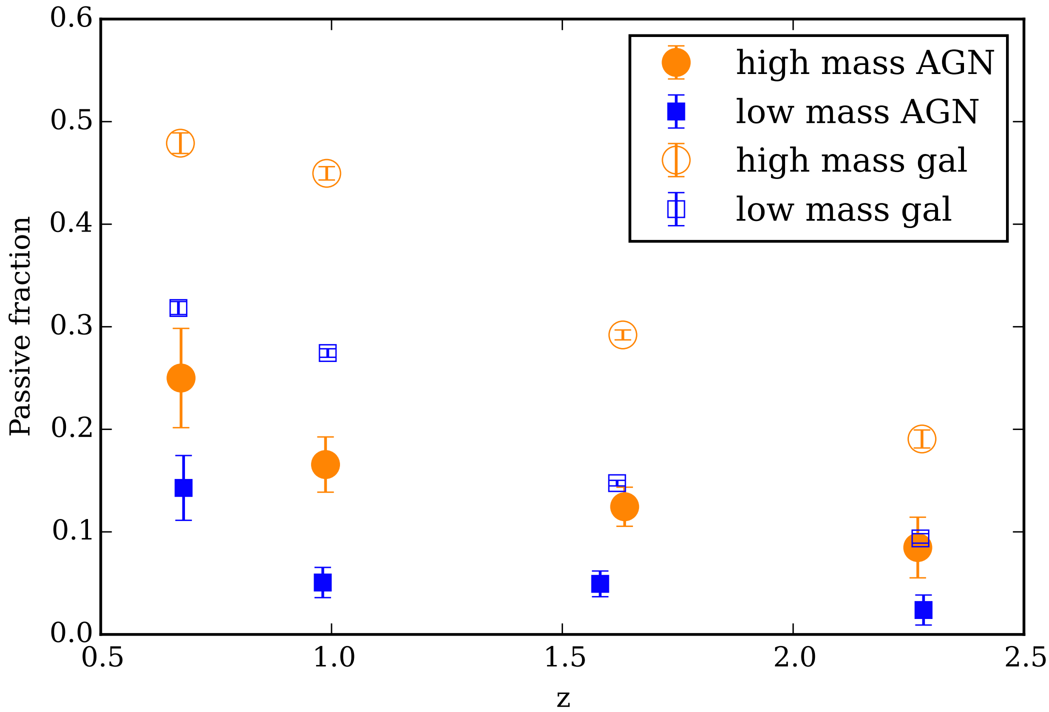

Figure 4.11. Passive fractions of AGN and galaxies split by stellar mass. AGN have significantly lower passive fractions than galaxies of the same mass. AGN in high mass galaxies ($M_* > 10^{10.75}\,\mathrm{M}_\odot$; filled orange circles) have higher passive fractions than those in low mass galaxies ($M_* < 10^{10.75}\,\mathrm{M}_\odot$; filled blue squares). In general, the high mass galaxy population (open orange circles) also has higher passive fractions than the low mass counterparts (open blue squares). There is a lower passive fraction among AGN hosts than the general galaxy population, so star forming galaxies are more likely to host AGN than passive galaxies.

nous AGN to have a significant impact on galaxy classifications and stellar masses (Almaini et al. in prep). In addition, Kocevski et al. (2017) report that color contamination by lower luminosity AGN in their study is negligible, and Santini et al. (2012) find that only 1.3% of their lower-luminosity sources had a difference in their stellar mass larger than a factor of two. We have tested the results in Figure 7 by removing the most luminous AGN ($L_X > 10^{44.4}$) from our sample, creating a new control sample, and repeating the clustering analysis. We find that the results are consistent within error-bars, and thus conclude that any contaminating AGN light does not have a major impact on our results.

4.4.3 Links between clustering and AGN luminosity

In this section we investigate whether the clustering of AGN is dependent on the power of the AGN determined through the proxy of X-ray luminosity. We study the correlation between the power of the black hole and the inferred dark matter

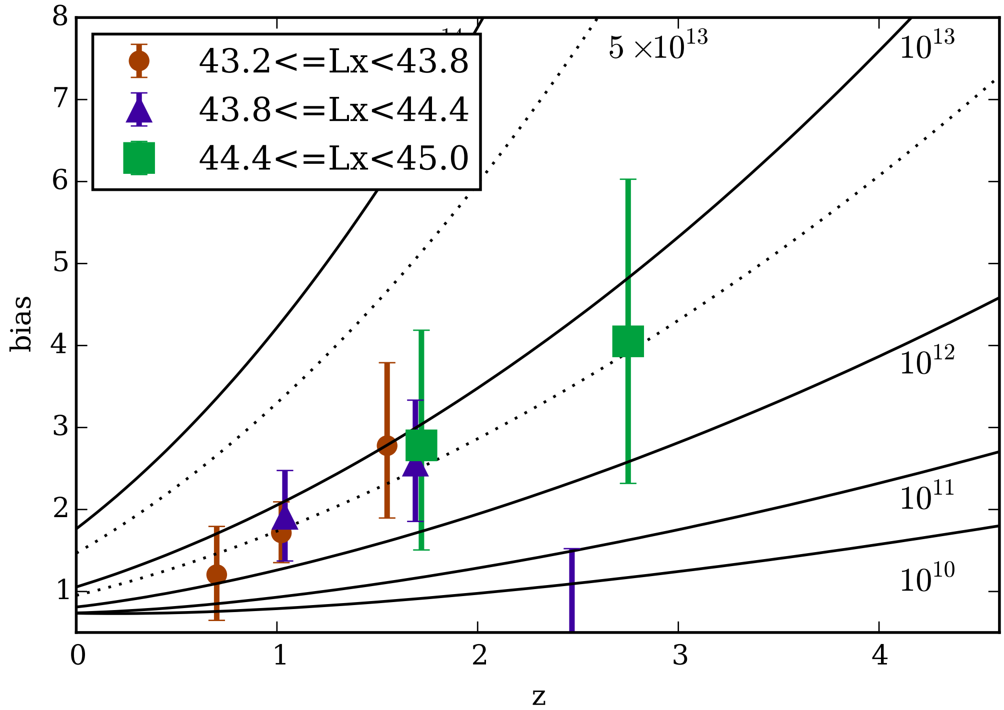

Figure 4.12. Bias measurements of AGN with hard band (2–10 keV) X-ray luminosities measured in erg s^{-1} in bins of $10^{43.2} \leq L_X < 10^{43.8}$, $10^{43.8} \leq L_X < 10^{44.4}$, and $10^{44.4} \leq L_X < 10^{45.0}$ in red circles, purple triangles, and green squares respectively. There is no correlation between redshift or luminosity and dark matter halo mass. The solid lines denote the evolution of dark matter halos, as in Figure 4.7.

halo mass by splitting our AGN into low, medium, and high X-ray luminosity bins, corresponding to $10^{43.2} \leq L_X < 10^{43.8}$, $10^{43.8} \leq L_X < 10^{44.4}$, and $10^{44.4} \leq L_X < 10^{45.0}$ erg s^{-1}. We cross-check passive fractions and mass distributions between the different luminosity bins and find no significant differences between the different luminosity populations. Passive fractions vary between $5 - 20\%$ at all redshifts and luminosities.

While previous studies across a wide range of AGN luminosities have found similar "group-like" halo masses, we are able to explore this in a robust manner by splitting our AGN sample by X-ray luminosity and redshift to obtain self-consistent estimates of the bias. In Figure 4.12, we show that there is no correlation between the power of the black hole on the clustering of the AGN, which is consistent with previous results (e.g., Magliocchetti et al. 2017). Since low, medium, and high X-ray luminosity AGN occupy similar mass halos, this implies that there may not be an environmental influence on the accretion rate of gas into the central black hole. This also implies that the environments of AGN of all luminosities are driven by the mixed population of their hosts.

4.4.4 Clustering and Eddington ratio

In this section we investigate whether the clustering of AGN is correlated with the efficiency of the radiative bolometric output of the black hole relative to the Eddington limit. The Eddington ratio $\lambda_{\rm Edd}$, relates the AGN luminosity to the Eddington limit as follows,

$$\lambda_{\rm Edd} = \frac{L_{\rm AGN}}{L_{\rm Edd}}, \tag{4.7}$$

where $L_{\rm AGN}$ is the total AGN luminosity and $L_{\rm Edd}$ is the Eddington luminosity. We assume that $\sim 10\%$ of the AGN's luminosity is emitted in X-rays (i.e. $L_{\rm AGN} \simeq 10L_X$). We also make use of $L_{\rm Edd} = 1.26 \times 10^{38}(\frac{M_{BH}}{M_\odot})$ erg s^{-1} and assume that the mass of the black hole, M_{BH}, is $\sim 0.15\%$ of the galaxy's stellar mass M_* (Kormendy 2000). It therefore follows that $\lambda_{\rm Edd} \propto \frac{L_X}{M_*}$.

We normalise the power of each galaxy's black hole (L_X) by its stellar mass, and split our AGN around the L_X:M_* median of 10^{33} erg s^{-1} M$_\odot^{-1}$ (corresponding to $\lambda_{\rm Edd} \simeq 0.05$). Figure 4.13(a) shows the bias of lower and higher Eddington ratio objects (low $\lambda_{\rm Edd}$ and high $\lambda_{\rm Edd}$ respectively)[2]. At $0.5 < z < 0.8$ and $1.3 < z < 2.1$, the clustering results of the two sub-groups are mutually consistent. At $z \sim 1$ however, low $\lambda_{\rm Edd}$ objects appear to reside in slightly more massive dark matter halos than high $\lambda_{\rm Edd}$ objects, consistent with radio-mode AGN (Bradshaw et al. 2011).

Since we find significant differences between the passive fractions and mass distributions of AGN with low and high $\lambda_{\rm Edd}$ (see Figure 4.14), we use the technique outlined in Section 4.4.2 to test whether the excess clustering in the low $\lambda_{\rm Edd}$ sample seen at $z \sim 1$ is due to their significantly higher passive fractions. The clustering of star-forming low $\lambda_{\rm Edd}$ and high $\lambda_{\rm Edd}$ objects is shown in Figure 4.13(b), where a marginal excess at $z \sim 1$ still exists. We lack sample sizes to test whether this excess is due to the difference in stellar mass distributions, although we note that we do not find evidence for a significant stellar-mass dependence (see Section 4.4.2), once the passive fraction is taken into account.

Similar to our findings, lower accretion rate radio AGN appear to reside in higher mass halos (e.g. Bradshaw et al. 2011), and higher accretion rate infrared AGN in lower mass halos (e.g. Hickox et al. 2009; Mendez et al. 2016). Although this could be interpreted as a dependence of accretion rate on halo mass (e.g. more massive structures at $z \sim 1$ heating cold accretionable gas and preventing efficient accretion onto the black hole), Mendez et al. (2016) find that the excess clustering

[2]We note that we are able to probe lower luminosity AGN at low redshift since AGN at all redshifts are selected to the same flux limit. This could imply that AGN in high mass galaxies at low redshift are probing lower accretion rates than the AGN in high mass galaxies at high redshift. We test this with a luminosity limited sample and find that the results are consistent within error-bars of the flux-limited sample.

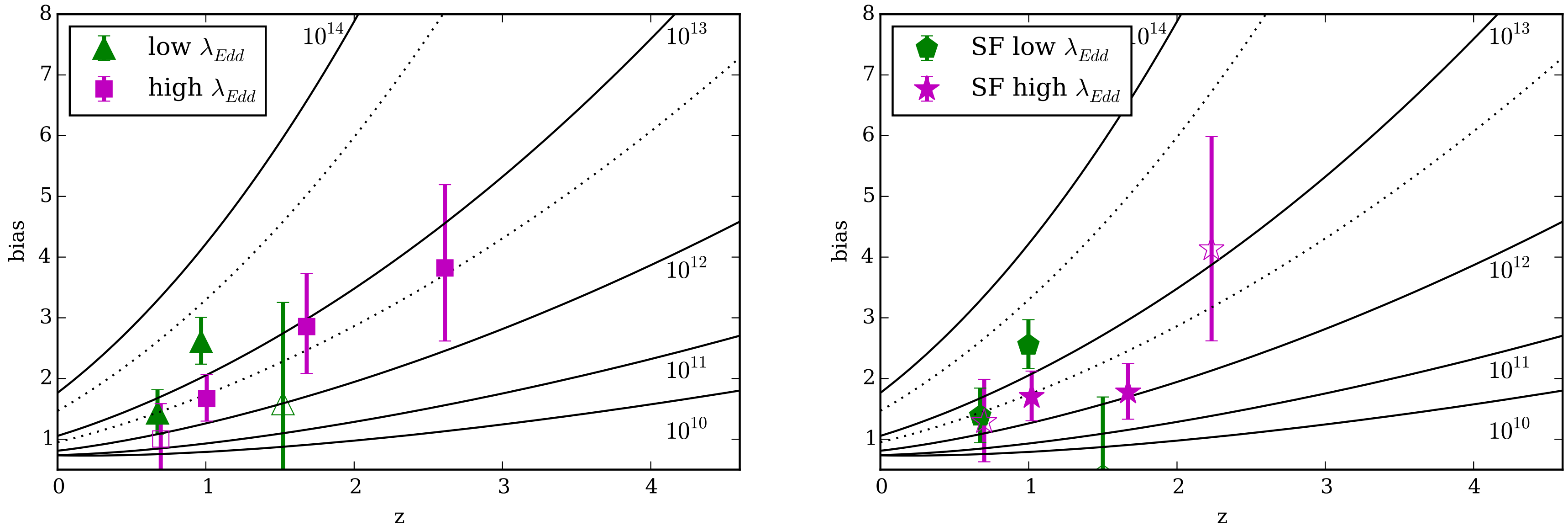

Figure 4.13. Left: (a) Bias of X-ray AGN with low (green triangles) and high (purple squares) $\lambda_{\rm Edd}$, in the UDS and COSMOS, as a function of redshift. **Right:** (b) Bias of star-forming low and high $\lambda_{\rm Edd}$ AGN in green pentagons and purple stars respectively. The marginal excess at $z \sim 1$ still stands and is unlikely to be due to a higher passive fraction. The solid lines denote the evolution of dark matter halos, as in Figure 4.7.

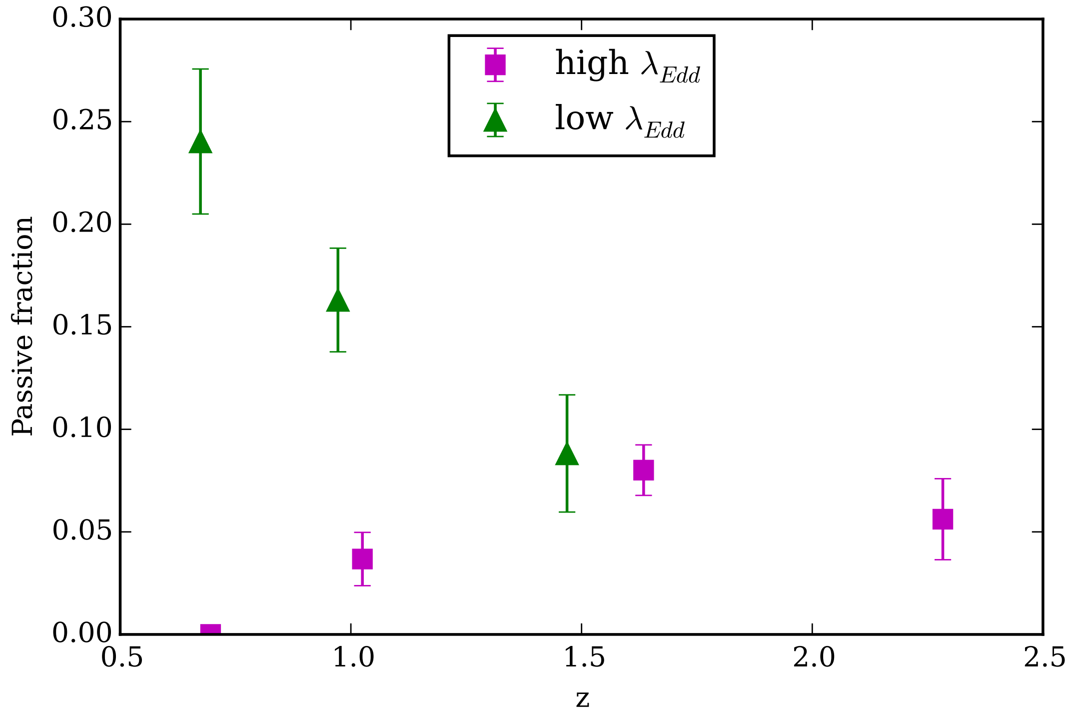

Figure 4.14. Passive fraction of low (green triangles) and high (magenta squares) λ_{Edd} AGN as a function of redshift. There is a higher passive fraction among low λ_{Edd} AGN at low redshifts.

of low accretion rate objects could be due to a difference in the host galaxy stellar masses and SFRs. We do not have sample sizes to disentangle whether the different clustering properties are due to different host galaxy properties or an underlying correlation with accretion rate, so more studies with larger samples are needed.

4.4.5 Clustering and hardness ratio

In this section we investigate whether there are correlations between AGN obscuration and clustering measurements. We use the hardness ratio (HR), defined by,

$$\mathrm{HR} = \frac{h - s}{h + s}, \tag{4.8}$$

where h is the count rate in the hard band (2–10 keV) and s is the count rate in the soft band (0.5–2 keV). We separate our AGN sample into hard (HR> 0) and soft (HR< 0), and study the clustering properties of each sample as a function of redshift. As shown by Figure 4.15, we find no significant difference in the bias of hard and soft AGN between $1.3 < z < 4.5$, and there is a slight excess in the clustering of hard AGN at $0.5 < z < 0.8$, and a slight excess in the clustering of soft AGN at $0.8 < z < 1.3$. There are no significant differences in the passive fractions and mass

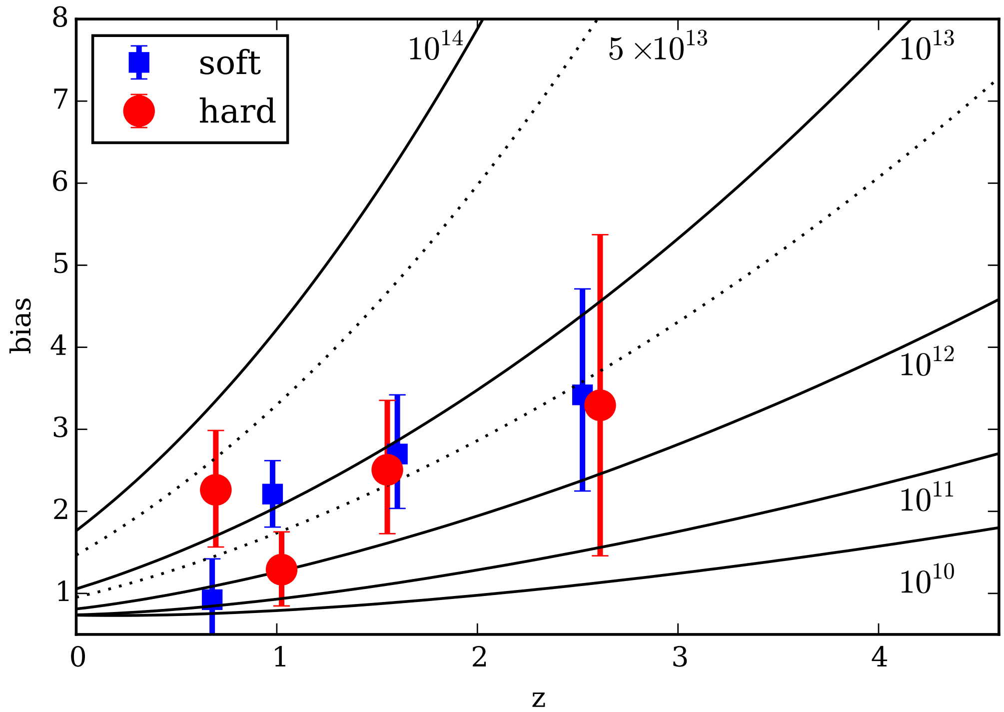

Figure 4.15. Redshift evolution of bias for hard (red circles) and soft (blue squares) X-ray AGN. There is no distinct correlation between clustering and hardness ratio. The solid lines denote the evolution of dark matter halos, as in Figure 4.7.

distributions of hard and soft AGN samples.

Previous studies on the clustering of obscured vs unobscured AGN have found contradictory results. Some report that hard/obscured AGN are more clustered (e.g Koutoulidis et al. 2018), while others suggest that soft/unobscured AGN are more clustered (e.g., Allevato et al. 2014), or that there is no significant difference between the two populations (e.g., Mendez et al. 2016). While it has been proposed that obscured and unobscured AGN have the same clustering in accordance with unification theory, there is also literature in favour of the two populations residing in different environments due to different accretion histories or different triggering mechanisms (Powell et al. 2018). Overall we find no significant trends in the clustering properties of hard and soft AGN, but more studies with larger sample sizes are clearly needed in order to obtain a tighter grasp on the subject. Larger sample sizes would also allow us to use a more physically motivated sample of hard and soft AGN (separated by a given column density threshold) and study the clustering of these samples in the different redshift bins used.

4.5 Discussion

We have investigated the clustering of AGN with X-ray luminosities between $43.2 < \log L_X < 45.0$ and redshifts between $0.5 < z < 4.5$, and measured a bias corresponding to dark matter halos of mass 10^{12-13} $M_\odot$. Similar results have previously been interpreted to indicate a preference for AGN to reside in group-like environments (e.g., Ikeda et al. 2015), but we have shown (see Figure 4.9) that the same clustering signal can be obtained from a mix of non-AGN star forming and passive galaxies that populate a range of halo masses. Based on this evidence, we suggest that AGN do not preferentially reside within a particular halo mass, and infer that AGN triggering is not primarily driven by the large-scale environment.

We find corroborating evidence when we divide the AGN by host galaxy property. The clustering of AGN hosted by star-forming galaxies (the dominant host type) have a bias corresponding to only 10^{11-12} $M_\odot$ halos at $z < 1.5$, comparable to the bias obtained for non-AGN star-forming galaxies of similar mass and redshift. Although we do not have a sufficiently large sample to measure the clustering of AGN in passive host galaxies, we note that the clustering of this minor component of the AGN population must be significantly stronger than the AGN in star-forming hosts, because the clustering strength of the combined population average to a halo mass of 10^{12-13} $M_\odot$. Thus AGN do not preferentially reside within halos of a certain mass.

Our interpretation of the clustering signal is supported by other observational evidence, such as the lack of enhanced AGN fractions in group-like environments (e.g., Shen et al. 2007; Arnold et al. 2009; Oh et al. 2014; Tzanavaris et al. 2014). Furthermore, if AGN preferentially reside in groups, we would expect the AGN host galaxy properties to vary with redshift since the fraction of star forming group galaxies increases with redshift (Butcher & Oemler 1978; Giodini et al. 2012; Popesso et al. 2012). Instead we find that the AGN host spectral class does not vary significantly from $z = 2.5$ to $z = 0.5$. We therefore suggest that large-scale environment (e.g. halo mass) is not the dominant factor in triggering an AGN, although it may play a minor role. We also note that the richest and rarest cluster environments (of halo mass $\sim 10^{15}\,M_\odot$) are not probed by the UDS/COSMOS fields, so we are unable to determine if AGN triggering is enhanced or suppressed in this specific regime.

Models of galaxy evolution, on the other hand, point to an important link between large-scale environment and triggering AGN activity. For instance, less massive groups have been proposed as the ideal environment for AGN activity due to an increased likelihood of mergers (Hopkins et al. 2008a,b). Our finding is in tension with the expectation that AGN should be preferentially triggered in groups if mergers trigger AGN activity. However, we also note that observational evidence that mergers are linked to AGN triggering remains inconclusive (Ellison et al. 2013;

Kocevski et al. 2015; Villforth et al. 2017; Hewlett et al. 2017).

Whilst AGN do not typically reside in a special environment, we find that AGN populate special host galaxies. We have shown that the AGN hosts are not a random subset of the underlying galaxy population within the UDS and COSMOS surveys. Instead, the passive fraction of AGN is lower than the underlying galaxy population at the same stellar mass (Figure 4.11), implying that AGN are preferentially hosted by star forming galaxies, consistent with the findings of other studies (Kauffmann et al. 2003; Alexander et al. 2005; Mullaney et al. 2012; Rosario et al. 2013; Aird, Coil & Georgakakis 2018e.g.,). We infer, therefore, that the probability of triggering an AGN is correlated with some properties of the host galaxy. Consistent with this inference, Kocevski et al. (2017) find evidence for a relationship between compactness and AGN triggering. We conclude that the triggering of AGN is likely not a simple single process, but is in fact a complex set (or sets) of conditions.

The set of conditions that trigger AGN are not likely to change drastically across $z = 2.5$ to $z = 0.5$ because we find that the stellar mass distribution and class of AGN host galaxies remain approximately constant in this redshift range. On the other hand, the Universe evolves drastically across this period, resulting in a significant change in galaxy properties: star formation declines (Madau & Dickinson 2014), galaxies grow in mass, and the morphological mix of galaxies evolves from predominantly irregulars to spirals and a larger fraction of early types (Mortlock et al. 2013). The passive fraction of AGN and galaxies both increase by a factor of $2 - 3$ from $z = 2.5$ to $z = 0.5$ (see Figure 4.11). This indicates that the fractions of star-forming and passive galaxies that host AGN do not change significantly with redshift (although we note that Aird, Coil & Georgakakis 2018 find evidence that quiescent galaxies are more likely to host AGN at higher redshifts).

The lack of dependence of the clustering signal on AGN power, as probed by the X-ray luminosity (Figure 4.12), suggests that the accretion rate of AGN does not have a simple dependence or correlation with its large-scale environment. This is in agreement with recent results from Yang et al. (2018). Furthermore, since we have shown that the clustering signal of AGN is primarily driven by the clustering properties of the AGN host population, and the mixture of host spectral classes, we infer indirectly that there is also no strong link between host spectral class and the AGN instantaneous accretion rate.

A correlation between host spectral class and AGN accretion rate is expected because of the evidence for a correlation between the growth of stellar mass and supermassive black holes (Boyle et al. 1998; Franceschini et al. 1999; Silverman et al. 2008). Given that the growth of stellar and black hole mass both rely on the availability of gas, we might expect to find higher accretion rates (through the proxy of X-ray luminosity) for star forming galaxies compared to passive galaxies of the same stellar mass. Since we find that the clustering strength of an AGN is primarily driven by its host spectral class, we would therefore expect the clustering signal of more luminous AGN to be lower than less luminous AGN, in discord with our findings.

We can explain the lack of variation in the clustering strengths for high and low luminosity AGN with the same phenomenon behind the flat SFR-L_X relationship for AGN found in previous work Stanley et al. (e.g., 2015). Hickox et al. (2014) proposed that large X-ray AGN variability on short timescales (relative to that of star-formation) dilutes the intrinsic correlation between SFR and L_X. To reproduce the underlying relation we must average over the most variable quantity (L_X in this case). High X-ray variability on short-timescales could also dilute any intrinsic L_X-host spectral class correlation, which would then dilute any variation in the clustering of AGN of different power. We note that a similar result may also be obtained if star-formation and black hole accretion are not coeval (Wild, Heckman & Charlot 2010).

Drawing our interpretations together, the triggering of AGN activity likely depends on a complex set of conditions. We find a lack of correlation between AGN power and clustering signal, and that a mix of non-AGN star-forming and passive galaxies can reproduce the same clustering signal as AGN. Together these suggest that large scale environment plays at most a minor role in triggering AGN activity. Availability of fuel may be inferred to play a major role since star-forming galaxies are more likely to host AGN at all epochs. This is supported by the well-known increased prevalence of high luminosity AGN at high redshift compared to low redshift (e.g. Figure 4.12). However, environment may be a relevant factor if mergers only trigger the most luminous AGN, as merger rates decline as the Universe ages (Conselice, Rajgor & Myers 2008). Furthermore, disks and bars may trigger nuclear activity (e.g., Knapen, Shlosman & Peletier 2000) as disk instabilities have been proposed to enhance gas flow to the nuclei of galaxies (Dekel, Sari & Ceverino 2009). Therefore, multiple mechanisms could be at play in the triggering of AGN, unlikely to be defined by solely large-scale environment or availability of fuel.

We note that our work is limited to X-ray selection, which tends to select more powerful and rapidly accreting AGN. Selection effects may play an important role in the interpretations and conclusions from AGN clustering results. Previous studies have found that X-ray and radio AGN are more clustered than mid-IR-selected AGN (e.g., Hickox et al. 2009; Mendez et al. 2016). However, when each AGN sample was studied using galaxy samples matched in stellar mass, star-formation rate, and redshift, Mendez et al. (2016) find no significant differences between the clustering properties of the AGN samples. They find that AGN selected in different wavelengths appear to have different clustering properties simply because they are sampling different host populations with different stellar mass and SFR distributions. Therefore, the method of AGN selection introduces inherent biases in the host galaxy properties and likely determines the clustering signal. Our study could be repeated using optical, near-infrared, and radio selected AGN with samples matched in mass, (s)SFR, and redshift to obtain a clearer picture of the impact of host galaxies on AGN clustering measurements. The implication for future AGN clustering studies is that samples must be divided by host galaxy properties as the clustering signal from AGN likely represents that of host galaxies.

To summarise our interpretations, the triggering of AGN activity likely depends on a complex set of conditions that do not depend solely on large-scale environment or availability of fuel. The parameters that define the triggering of AGN could have important implications for our understanding of galaxy evolution, particularly as our most sophisticated galaxy evolution models invoke AGN feedback as a key ingredient in reproducing the stellar mass functions of galaxies.

4.6 Conclusions

In this work we study the clustering properties of a flux-limited sample of hard X-ray selected AGN from $z \sim 4.5$ to $z \sim 0.5$, using the COSMOS and UDS multi-wavelength surveys. We compare them to a control galaxy sample designed to have similar distributions of stellar mass, spectral class, and redshift. We investigate the role of properties of host galaxies (e.g. stellar mass) and of the central AGN (X-ray luminosity) as a function of redshift. We find that the clustering properties of AGN cannot be naively linked to large-scale environments as host galaxy properties play a significant role in the clustering measurements. To summarise our findings:

1. We find that hard X-ray selected AGN in the UDS and COSMOS fields have a bias parameter corresponding to a typical halo mass of $10^{12-13}\,\mathrm{M}_{\odot}$.

2. We compare the clustering of AGN to star-forming and passive galaxy populations matched in mass and redshift distributions, and find that the clustering of AGN lies in between the star-forming and passive populations.

3. We can reproduce the clustering signal of AGN with an inactive galaxy population closely matched in spectral class, mass, and redshift distributions to the AGN host galaxies. We thus find that the mixed population of star-forming and passive AGN host galaxies drives the clustering properties of AGN.

4. We split AGN by host galaxy stellar mass and find an excess clustering in the high mass sample. The stellar mass dependence of clustering disappears once passive galaxies are removed from the samples, as we find no difference in their clustering properties. Therefore, we conclude that AGN clustering depends more strongly on the spectral class of the host galaxies than stellar mass.

5. We find no difference in the clustering properties of low, medium and high X-ray luminosity AGN. The triggering of AGN activity is likely determined by a complex set of conditions that do not depend solely on large-scale environment or availability of fuel.

Chapter 5

The small-scale environments of X-ray selected AGN at $0.5 < z < 2.5$

In this chapter we present a preliminary analysis of the properties of galaxy neighbours within 500 kpc of X-ray selected AGN between $z \sim 2.5$ and $z \sim 0.5$ in the UDS and COSMOS fields. At all epochs, we find consistent number densities of neighbours around AGN and control galaxies, suggesting that AGN do not live in special environments, in agreement with our results from Chapter 4. We find evidence that the neighbours of AGN are indistinguishable from those of control galaxies at $1.5 < z < 2.5$, since the properties of neighbours around AGN in passive/star-forming hosts are consistent with control passive/star-forming galaxies. The results at this epoch are thus consistent with the hypothesis that AGN are stochastically triggered with no significant environmental influences. We do not find this to be true at lower redshifts, however, since we find that the star-formation activity of neighbours of AGN varies significantly across redshift, displaying opposite trends below and above $z = 1$. At $1.0 < z < 1.5$ we find that the star-formation activity of the neighbours of AGN is enhanced (at 2.3σ) with respect to control galaxies, while this is reversed at $0.5 < z < 1.0$ (at 4.3σ). At $1.0 < z < 1.5$, the suppression of the passive neighbour fraction of AGN is found to be driven by that of AGN in passive hosts (which is significantly lower than that of control passive galaxies), while at $0.5 < z < 1.0$, the enhancement of the passive neighbour fraction of AGN is found to be driven by that of star-forming hosts (which is significantly higher than that of control star-forming galaxies). The drastic reversal of the trends between AGN and control galaxies clearly needs further investigation. In order to understand the trends further and draw robust conclusions, this study must be repeated in smaller redshift intervals, calling for larger sample sizes.

The preliminary work presented in this chapter is unpublished.

5.1 Introduction

There is growing observational evidence for the correlation between the star-formation properties of central galaxies and those of their satellites. The correlation has been reported since the 1980s (Wirth 1983; Ramella et al. 1987). With the advent of wide-field imaging surveys such as the Sloan Digital Sky Survey (SDSS, York et al. 2000), it has been possible for the identification of this effect in a systematic manner, as first discovered by Weinmann et al. (2006). They found that red central galaxies have a higher fraction of red satellites and coined the term "galactic conformity".

The SDSS has been widely used by several works to provide evidence for these trends from multiple angles. Using a clustering analysis, Ross & Brunner (2009) find that the fraction of late type satellites decreases as halo mass increases. Similar correlations have been discovered, at separations well beyond the virial radius (Kauffmann et al. 2013), in the alignment of the distribution of satellites within halos with centrals (Wang et al. 2008), and even in spectroscopically confirmed systems (Phillips et al. 2014). Conformity also appears to exist in terms of morphology since the morphologies of central and satellite galaxies appear to be correlated (Ann, Park & Choi 2008), as well as gas content since neighbours of red galaxies are likely deficient in star-forming gas (Papastergis et al. 2013). Deeper optical/near-infrared surveys such as the UDS and COSMOS have allowed for the detection of this effect out to $z \sim 2$–3 (albeit to a lower significance, e.g. Kawinwanichakij et al. 2014; Hartley et al. 2015).

These correlations are curious because it implies a causal connection between the centrals and satellites. The presence of satellite galaxies is unlikely to impact the star-formation in the central galaxy, except in rare, close encounters. Satellites are thought to stop forming stars due to gas removal processes such as tidal interactions and ram-pressure stripping (e.g. Socolovsky et al. 2018), but these mechanisms operate predominantly on smaller satellite galaxies and leave the interstellar medium of the central galaxy largely undisturbed.

There are several proposed explanations for the conformity phenomenon. Yang, Mo & van den Bosch (2006) suggest that galactic conformity is simply a direct result of hierarchical structure formation. Also known as "assembly bias", the argument is that a halo that assembled a significant fraction of its mass at early times would have accreted its satellites at higher redshifts than a similar halo that assembled at a later epoch. Wang & White (2012) show that conformity in semi-analytic models arises because red central galaxies inhabit more massive dark matter haloes than blue galaxies of the same stellar mass.

There is also literature in favour of hydrodynamical effects playing a crucial role. For example, Kauffmann, Li & Heckman (2010) suggest that conformity depends on gas accretion, and that the ability of both satellites and centrals to form stars depends upon the underlying reservoir of ionised gas that spans large spatial scales. Ann, Park & Choi (2008) propose that feedback processes (due to star-formation or AGN) during the formation of the central galaxy has an impact on the star-formation ability of nearby galaxies. Hartley et al. (2015) favour the latter scenario following analysis out to $z \sim 2$, although there are observations in direct conflict with this scenario, such as the abundance of passive dwarf galaxy satellites around massive star-forming galaxies such as our own Milky Way and M31.

The role that AGN host galaxies play in the conformity picture has not been tested thus far. Galaxies that host AGN are in a somewhat unique position in that their relationship with nearby galaxies is complex; they can both influence their neighbours via feedback, as well as be influenced by their neighbours via environmental triggering. AGN feedback plays an integral part in reproducing the stellar mass functions of galaxies in the latest models of galaxy evolution (e.g. Benson et al. 2003; Croton et al. 2006). Models also suggest that AGN are triggered via mergers and environmental interactions (e.g. Hopkins et al. 2006), although the observational evidence remains mixed (Ellison et al. 2013; Kocevski et al. 2015; Villforth et al. 2017; Hewlett et al. 2017). It is therefore unclear whether AGN are environmentally triggered or stochastic as suggested by recent works (Aird, Coil & Georgakakis 2019, Krishnan et al. submitted, see Chapter 4).

Studying the nearby neighbours of AGN would enable us to distinguish between the scenarios of stochasticity vs environmental triggering. If AGN are stochastic and do not influence their neighbours, we would expect to see that the relationship between the star-forming properties of AGN and their neighbours to be consistent with the expected conformity trends of control galaxies and their neighbours. If AGN are not stochastic and indeed environmentally linked, then we would expect a difference in the neighbour properties of AGN and control galaxies, such as the radial distributions of their passive neighbour fractions.

In Chapter 4, we found that the large-scale clustering signal of AGN are identical to those of control galaxies precisely matched in stellar mass, star-formation properties, and redshift. With this in mind one would expect that the conformity trends continue, and that AGN would be consistent with the control sample. The wealth of multi-wavelength and X-ray imaging of the square-degree scale fields of UDS and COSMOS allow us to test this hypothesis for the first time.

This chapter presents a preliminary analysis on the neighbours of AGN as a function of redshift, and is organised as follows. In Section 5.2 we describe our sample selection. Section 5.3 explains the methodology of our small-scale environment analysis, and we present our results in Section 5.4. Our discussion is presented in Section 5.5, and we summarise our results in Section 5.7. We adopt a WMAP9 cosmology (Hinshaw et al. 2013), with $\Omega_{\mathrm{m}} = 0.3$, $\Omega_{\Lambda} = 0.7$, and $h = 0.7$.

5.2 Sample selection

Please refer to Chapter 2 for details of the data sets used. We use the AGN and galaxy catalogues with available supercolour classifications (Wilkinson et al. in prep). Our sample selection is similar to Chapter 4, and we outline the differences below.

5.2.1 Galaxy samples

To study the evolution of the neighbours of AGN as a function of cosmic time, we split our AGN and galaxy samples in redshift intervals of $0.5 < z < 1.0$, $1.0 < z < 1.5$, and $1.5 < z < 2.5$. We apply a K-band magnitude limit of $K = 23.7$ to our galaxy sample to ensure high completeness. In addition, we use the methodology from Pozzetti et al. (2010) to apply redshift-dependent 90% mass completeness limits to the galaxy sample. Since passive galaxies are more incomplete at a given stellar mass, we apply a conservative completeness cut corresponding to the passive galaxy sample. After applying these quality cuts, our galaxy sample consists of ~ 19000 and ~ 54000 galaxies between $0.5 < z < 2.5$ in the UDS and COSMOS fields, respectively.

5.2.2 AGN samples

While there is very deep Chandra X-UDS coverage of the UDS field, it is limited to the central ~ 0.33 deg^2. Outside this Chandra-covered region, we supplement our X-UDS data with XMM-Newton data. For our data in both fields (UDS and COSMOS), we do not apply a flux limit to our X-ray sources. We do not apply a mass completeness cut to our AGN sample to maximise the sample size, but we note that 95% of our AGN are above the 90% mass completeness limit of $10^{10.05}\,\mathrm{M}_\odot$ at $z = 1.5$.

5.2.3 Control galaxies

As described in Section 2.4, the "spectral class" of our AGN and galaxy samples can be determined using supercolour classifications that utilise a principal component analysis (PCA) of the optical/near-infrared photometric data in the UDS and COSMOS fields (Wild et al. 2014; Wild et al. 2016). For example, the "spectral class" of a given galaxy may be star-forming, passive, or post-starburst. We create a control galaxy sample that is precisely matched in host galaxy properties to our AGN sample. For each AGN, we identify the closest matching galaxy in a 3-dimensional space of stellar mass, spectral class, and redshift. In Figure 5.1 we plot the resulting distributions of mass, sSFR and redshift, demonstrating the precise matching of control galaxies to AGN.

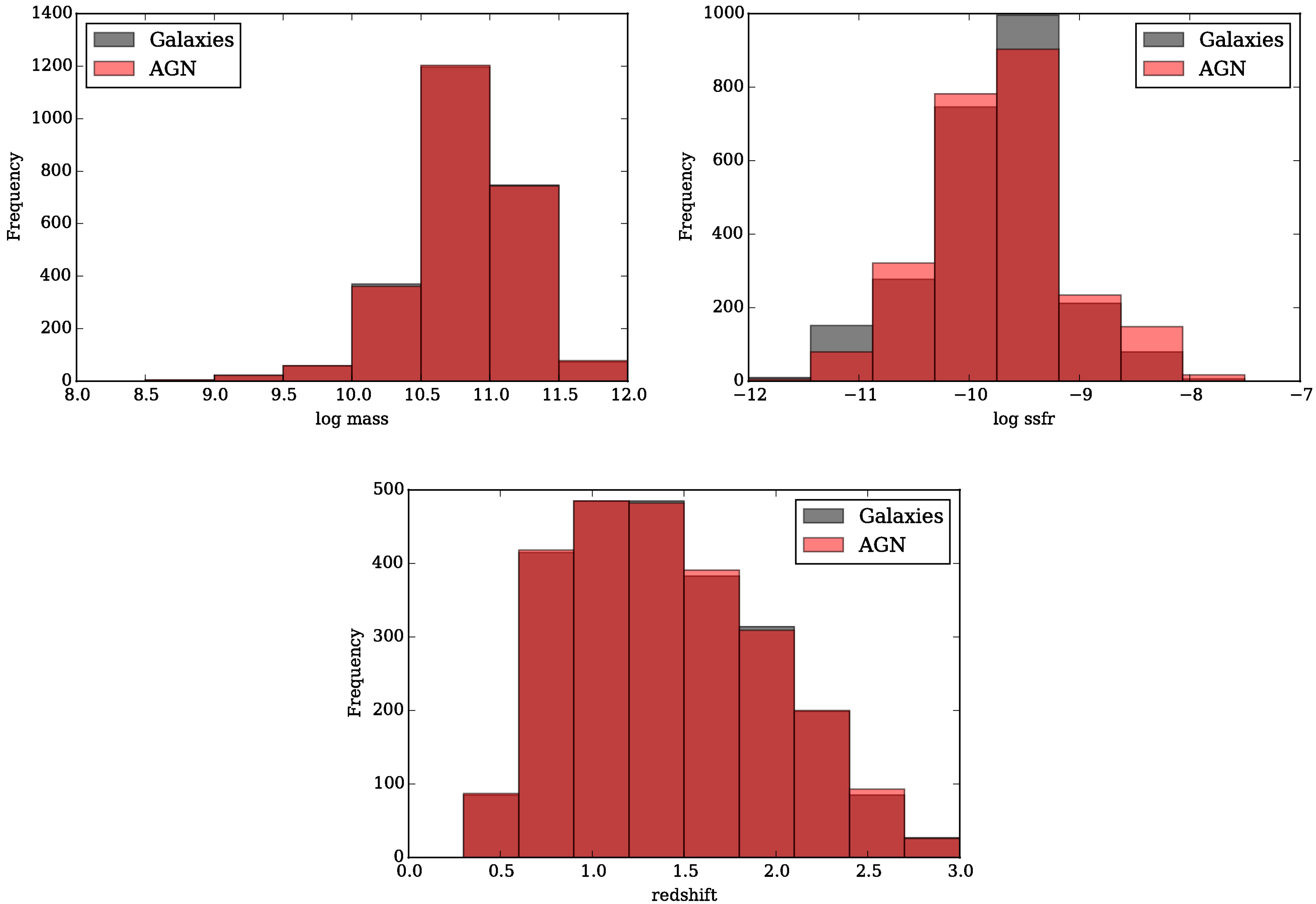

Figure 5.1. Distributions of mass, sSFR and redshift of AGN (red) compared to control galaxies (black). The sSFR distributions do not match as perfectly as mass and redshift, since the controls are matched to the AGN in spectral class (which correlates with sSFR).

5.3 Methods

In order to study their neighbours, we place apertures centred on AGN and control galaxies. We count neighbours in annuli from 100 kpc to 500 kpc in bins of 100 kpc. Since photometric redshifts have inherent uncertainties, we take into consideration the accuracy of redshifts by selecting neighbours within $\pm 3\sigma$ of the redshift dispersion (e.g. ± 0.1 at $0.5 < z < 1.0$).

We reject neighbours within a certain physical aperture/annulus with stellar masses below the redshift-dependent completeness limit (which correspond to passive galaxies and the upper end of the redshift bin following the Pozzetti et al. 2010 method). Other works studying "galactic conformity" (e.g. Kawinwanichakij et al. 2014; Hartley et al. 2015) reject satellites more massive than a certain limit requiring that the central object (on which apertures are placed) is the most massive object within the radius and redshift tolerance. Since we are interested in neighbours, not necessarily satellites, we do not impose this criterion.

Using this method, we essentially select neighbours within cylinders centred around AGN/control galaxies. These cylinders therefore have physical radius of the aperture and length of the redshift tolerance. In addition to the "true neighbours", however, we expect significant contamination from foreground and background galaxies that happen to lie along the line of sight within the cylinders. We note that there can also be contamination in the form of contribution from 2-halo (large-scale) clustering, but on such small scales (< 500 kpc), "true" neighbours are likely to dominate the counts. This can be seen in halo occupation decompositions of clustering data (Zheng, Coil & Zehavi 2007).

We subtract the background and foreground contamination in the following way. For each AGN, we construct a random catalogue of 10 positions, assigned the redshift of their parent AGN host galaxy. We count all neighbouring galaxies within 500 kpc and within the redshift tolerance of these 10 random pointings. We then scale the number of neighbours in the random pointing by the ratio of area of the annulus to the area of the 500 kpc aperture. The choice of the number of randoms per AGN was somewhat arbitrary, although we ensure that the uncertainties are dominated by the real galaxy counts and not the background estimation. This method is demonstrated in Figure 5.2.

It is important to account for the masked regions of the image (due to image artefacts such as cross-talk). To do this we place an aperture on the mask image at the location of each AGN/control galaxy/random pointing, with a pixel radius corresponding to the aperture physical radius of interest. For each AGN/control galaxy/random pointing, we then divide our neighbour counts by the "good" fraction of pixels to obtain the mask-corrected number of neighbours.

Number densities are then calculated as the number of neighbours around cen-

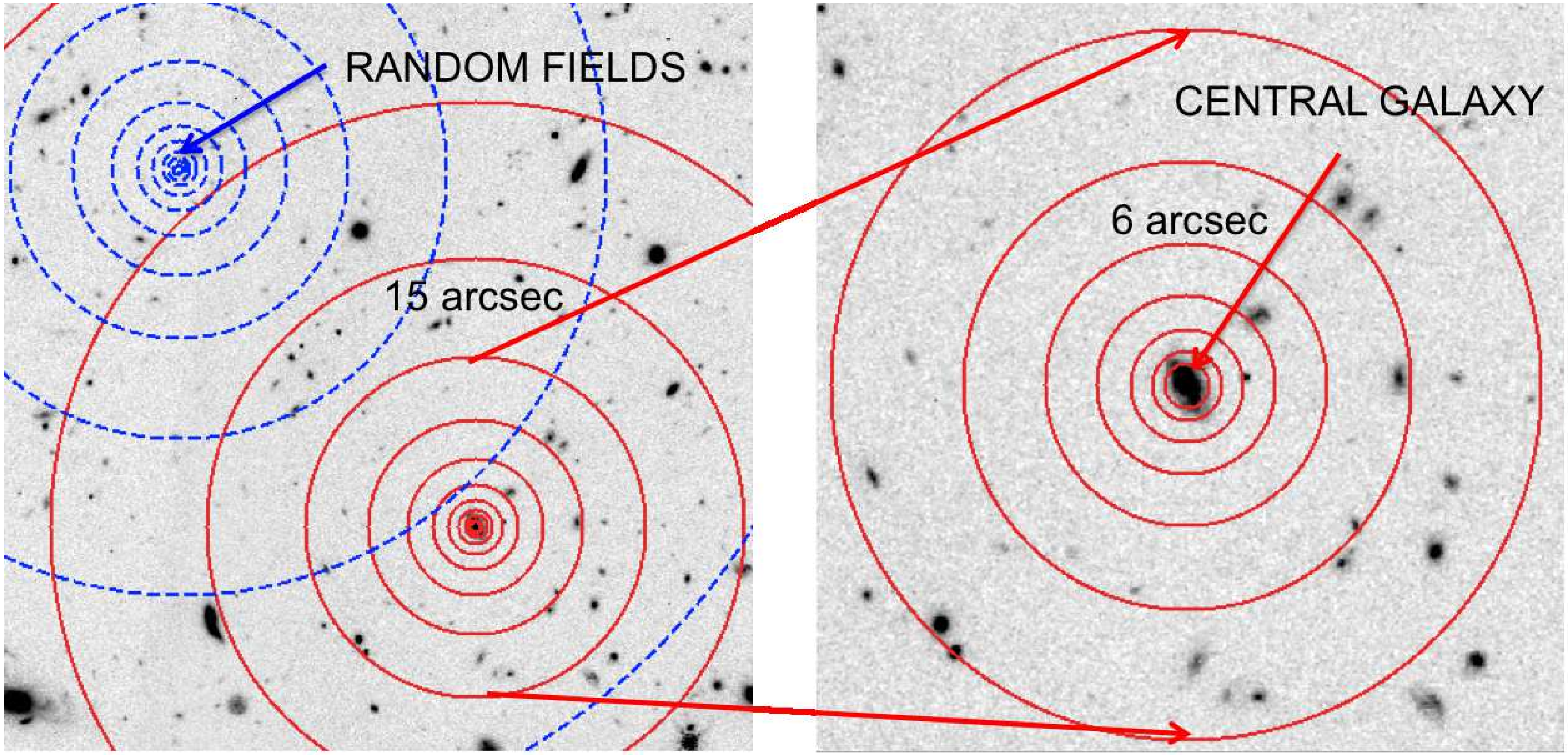

Figure 5.2. Figure from Kawinwanichakij et al. (2014) demonstrating the technique used to statistically estimate the contaminant foreground and background objects. Neighbours are counted in annuli from the AGN/control galaxies and random pointings. The random field measurements are then subtracted from those of the AGN/control galaxies to obtain the "true" distribution of neighbours around AGN and control galaxies.

trals (after mask-correction), normalised by the number of centrals and by the area of the annulus.

We use the spectral class from supercolour classifications to select passive neighbours (galaxies with a spectral class of "red" or "post-starburst"), after which we perform mask-correction and background-correction. We then divide this by the total neighbours (after mask-correction and background-correction). We define this ratio as the passive fraction of neighbours and study its dependence on radius for AGN, control galaxies, and randoms. The passive fraction of neighbours, f_{pass} is thus given by,

$$f_{pass} = \frac{N_{pass\_mask\_corr} - (\frac{1}{N_{rand}}) \times N_{pass\_mask\_corr\_rand}}{N_{tot\_mask\_corr} - (\frac{1}{N_{rand}}) \times N_{tot\_mask\_corr\_rand}}, \tag{5.1}$$

where N_{rand} is the number of random pointings per central (10), $N = N_{UDS} + N_{COS}$ in all cases, $mask\_corr$ indicates mask corrected counts, $pass$ indicates passive and tot indicates total.

As expected, we find that the number densities and the passive fractions of neighbours converge to that of randoms at large radii. We note that we study the distributions of properties of neighbours truncated at 300 kpc.

5.4 Results

To gain insight into the small scale environments of AGN, we first investigate the numbers of neighbours around AGN and control galaxies. We cross-check our analysis by computing these number densities for satellites of central galaxies following the method of Kawinwanichakij et al. (2014), and obtain consistent results.

In Figure 5.3, we plot the radial dependence of the projected number densities of neighbours around AGN, control galaxies, and measured in random pointings. The panels (a), (b), and (c) represent the redshift evolution of the number densities at $0.5 < z < 1.0$, $1.0 < z < 1.5$, and $1.5 < z < 2.5$ respectively. Consistent with expectations from galaxy clustering, there is a strong statistical excess of neighbours around AGN and control galaxies over random positions, extending to 500 kpc and beyond. These panels also show that we find no significant difference between the projected number densities of neighbours around AGN and control galaxies, independent of redshift. The projected number densities overall decrease by approximately an order of magnitude from $z \sim 0.5$ to $z \sim 2.5$, although this effect is predominantly due to the inclusion of fainter galaxies in the lower redshift bins. The small scale galaxy densities of the neighbours around AGN are therefore similar to those of galaxies matched in stellar mass, spectral class, and redshift. As galaxy properties are correlated with environment and redshift, we can determine whether the typical small scale environments of AGN differ from non-active galaxies with similar masses and star-forming properties, by comparing the properties of the neighbours of AGN to those of control galaxies as a function of redshift.

5.4.1 Low redshift

We compute the passive fraction of passive and star-forming centrals in order to compare to Hartley et al. (2015), and reproduce the "galactic conformity" trends, where satellites of passive centrals have significantly higher passive fractions compared to the field, and satellites of star-forming centrals have consistent passive fractions with the field. We also reproduce the radial decline in the enhancement of the passive satellite fraction of passive centrals. Having tested the reliability of our method, we proceed to repeat the analysis for the neighbours of AGN.

We first investigate the spectral class of the neighbours of AGN vs control galaxies. We plot our $0.5 < z < 1.0$ results in Figure 5.4, where panels (a) and (b) show the passive fraction of neighbours in the UDS and COSMOS fields respectively, of AGN, control galaxies, and random pointings. We note that the UDS has higher average passive fractions than COSMOS. We combine the measurements from these two fields and plot our results in Figure 5.5(a). As there are more AGN in the COSMOS field, the combined measurements are more influenced by the COSMOS data. These plots show that the passive fraction of neighbours is significantly (at 2.3σ within 300 kpc) higher for AGN centrals at $0.5 < z < 1.0$, compared to control galaxies. In both COSMOS and UDS data sets, the passive fractions of neighbours around AGN and control galaxies decrease with distance from the central. The enhancement of passive fraction in neighbours around AGN with respect to controls, is most significant in the central 300 kpc.

To investigate the role of host galaxy spectral class in the fraction of passive neighbours, we split our AGN and control galaxy samples into passive and star-forming. Figure 5.5(b) shows the fraction of passive neighbours of AGN in passive hosts and control passive galaxies, compared to neighbours of AGN in star-forming hosts and control star-forming galaxies. It can be seen that the fraction of passive neighbours of AGN in passive hosts at $0.5 < z < 1.0$ is *slightly* higher than that of passive control galaxies. However, the fraction of passive neighbours around AGN in star-forming hosts is *significantly* higher than control star-forming galaxies. Therefore this excess in the star-forming AGN population likely drives the excess of passive neighbours around AGN in Figure 5.5(a). This is in discord with usual galactic conformity trends (Weinmann et al. 2006; Ann, Park & Choi 2008; Kauffmann et al. 2013; Kawinwanichakij et al. 2014; Hartley et al. 2015). This may suggest that AGN either affect, or are affected by, their neighbours. Alternatively, AGN may correlate with the properties of their neighbours due to external factors (such

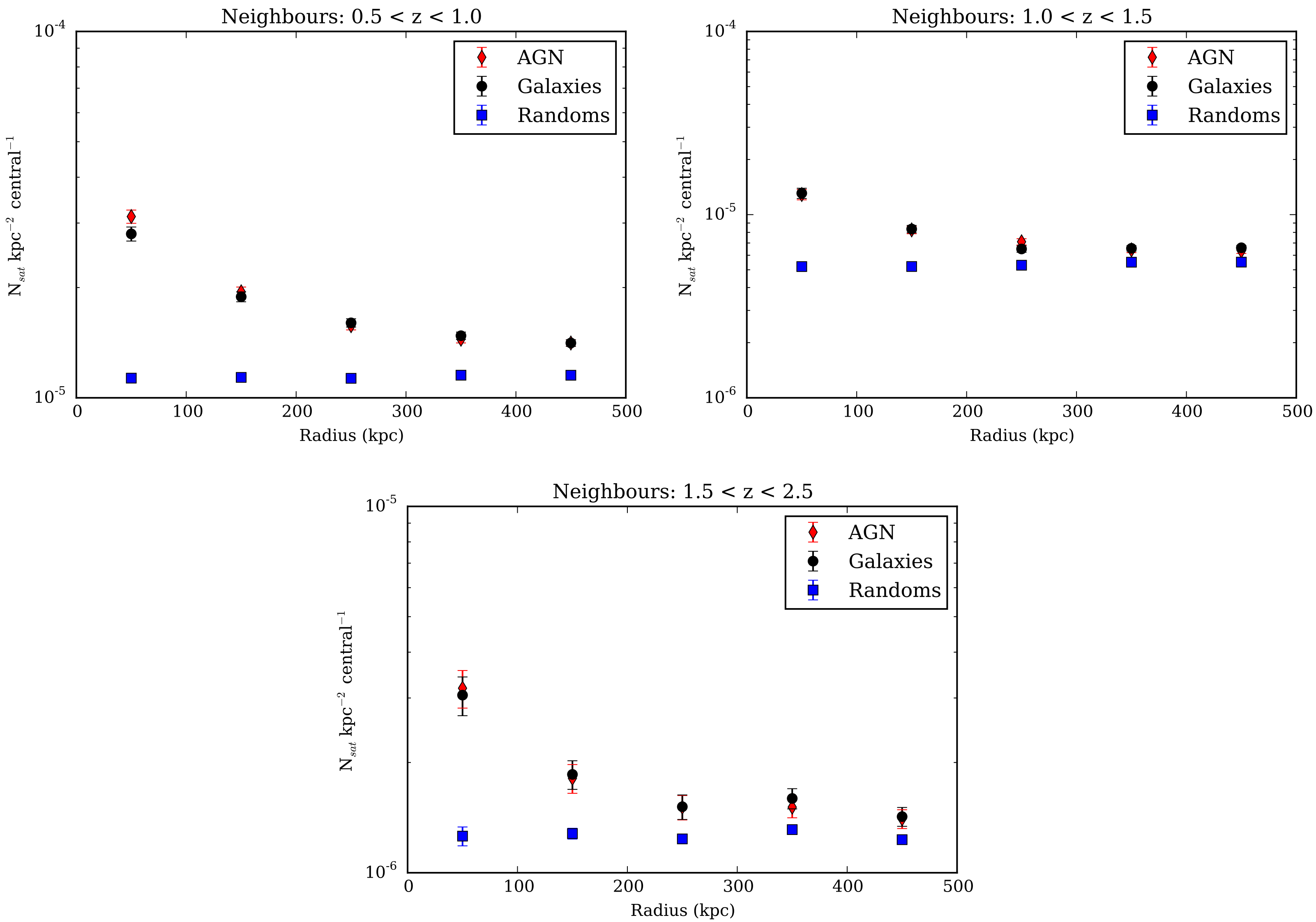

Figure 5.3. The projected number density of neighbours around AGN (red), control galaxies (black), and in random pointings (blue) as a function of radius (kpc) in three different redshift bins. Top left panel (a), top right panel (b) and bottom panel (c) show results at $0.5 < z < 1.0$, $1.0 < z < 1.5$, and $1.5 < z < 2.5$ respectively. The AGN and control galaxy population have no significant differences in their projected number densities (per kpc^{-2} per central) at all redshifts.

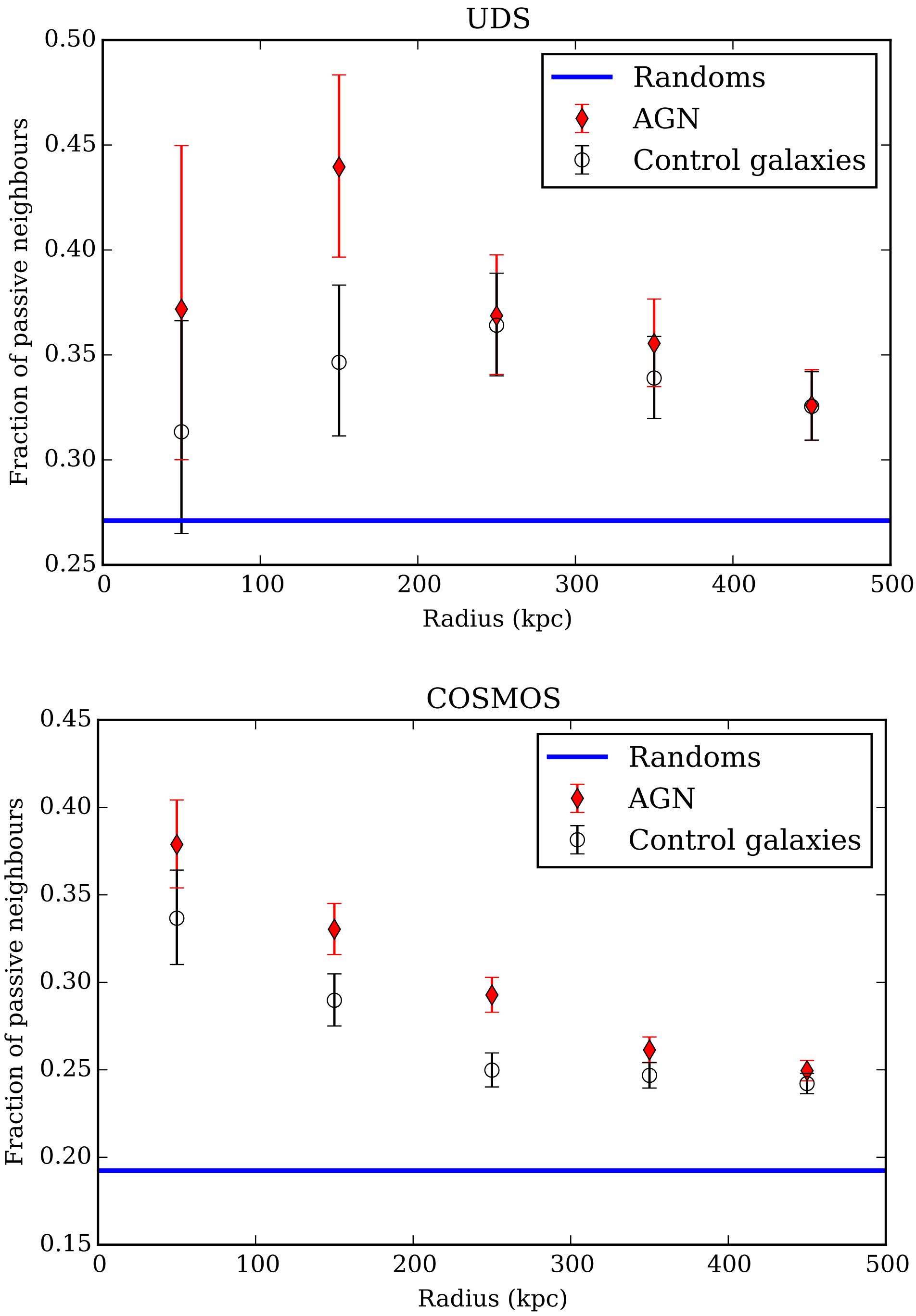

Figure 5.4. $0.5 < z < 1.0$: Radial plots of the fraction of neighbours classified as passive, around AGN, control galaxies, and in random pointings in the UDS in the upper panel (a) and COSMOS in the lower panel (b).

as the availability of gas or the formation time of the halo).

To further determine whether the stellar mass and star-formation properties are different between the neighbours of AGN and control galaxies at $0.5 < z < 1.0$, we investigate the mass, sSFR and $U - B$ colour distributions of neighbours within 300 kpc of AGN, control galaxies, and random positions in Figure 5.6 (a), (b), and (c) respectively.

Figure 5.6(a) shows that the neighbours of both AGN and galaxies are more massive than random apertures, as expected. There is no significant difference between the masses of the neighbours of AGN and those of control galaxies.

Figure 5.6(b) shows that the neighbours of both AGN and galaxies have lower sSFRs than random apertures, as expected due to their higher masses. The neighbours of AGN appear to have slightly lower sSFRs than control galaxies, consistent with Figure 5.5. Similarly, Figure 5.6(c) shows that the neighbours of both AGN and galaxies have redder colours than random apertures, also expected from their higher masses and lower sSFRs. The neighbours of AGN appear to have redder colours than control galaxies, consistent with Figure 5.5 and Figure 5.6(b). There is a small excess of redder neighbours around AGN as compared to those of control galaxies. The properties of the immediate neighbours of AGN are thus different to the neighbours of control galaxies.

5.4.2 Intermediate redshift

We now investigate the environments of AGN at slightly higher redshift of $1.0 < z < 1.5$. We plot our passive fractions of neighbours of AGN and galaxies at $1.0 < z < 1.5$ in Figure 5.7. The panels represent UDS and COSMOS as in Figure 5.4. In both UDS and COSMOS fields, control galaxies clearly have significantly higher passive fractions of neighbours than AGN (at 4.3σ). The combined results are displayed in Figure 5.8(a). We see that the neighbours of AGN have passive fractions similar to random apertures. Therefore at $1.0 < z < 1.5$ we find a reversal of the enhancement of passive neighbours around AGN found at $0.5 < z < 1.0$.

In Figure 5.8(b), we separate the AGN and control galaxy population into star-forming and passive hosts and study the fraction of passive neighbours. At low redshift, we found that the passive fraction of neighbours around AGN in passive hosts and control passive galaxies are only slightly different, but this figure shows the contrast between the passive neighbour fractions of AGN in passive hosts and control passive galaxies at $1.0 < z < 1.5$. Control passive galaxies show the expected conformity trends (see Weinmann et al. 2006; Ann, Park & Choi 2008; Kauffmann et al. 2013; Kawinwanichakij et al. 2014; Hartley et al. 2015). However, neighbours around AGN in passive hosts are consistent with the field and AGN in star-forming hosts and control star-forming galaxies. We would expect neighbours around AGN

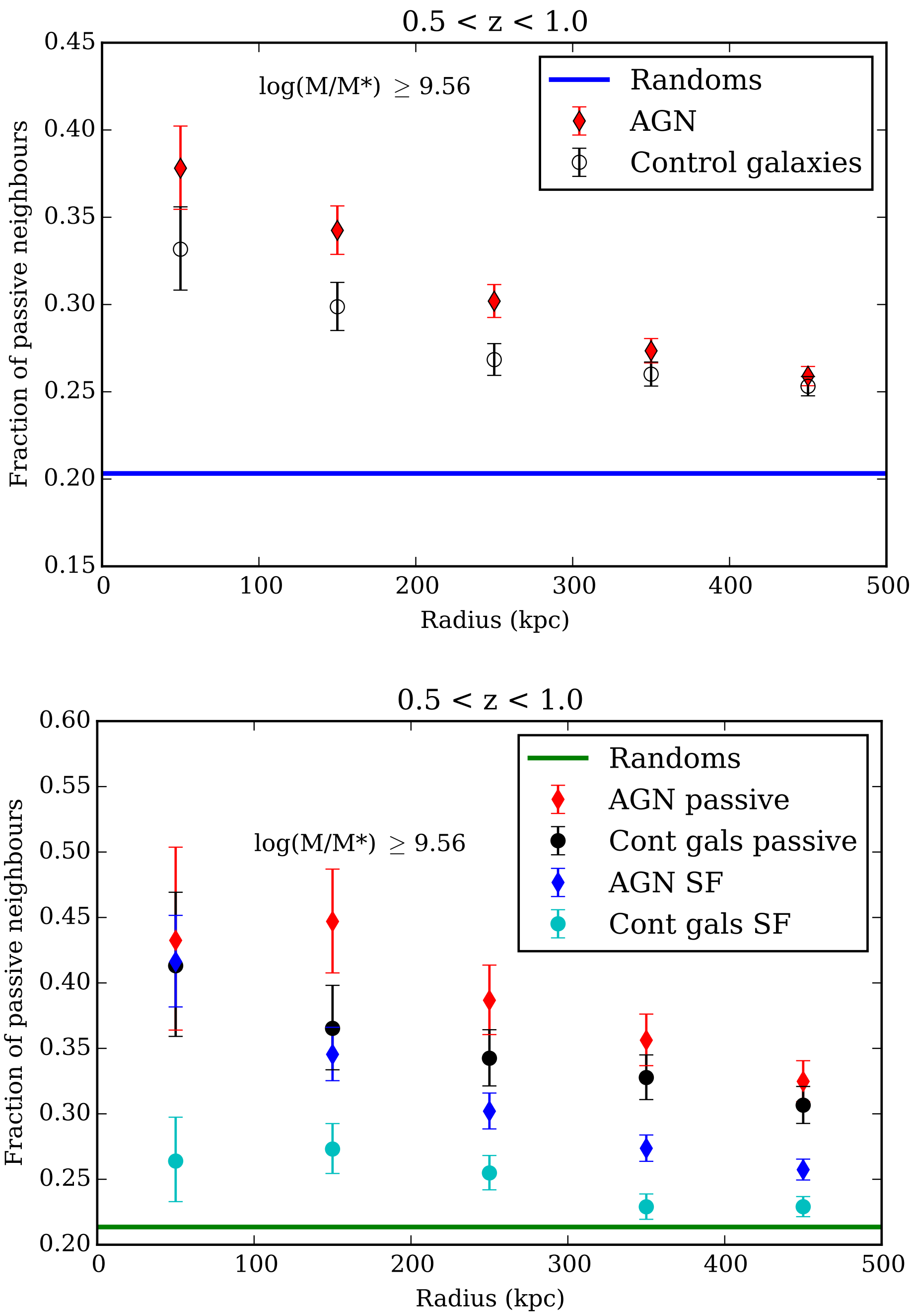

Figure 5.5. $0.5 < z < 1.0$: Radial plots of the fraction of neighbours classified as passive, around AGN (combined UDS and COSMOS), control galaxies, and in random pointings in the upper panel (a). The lower panel (b) shows the AGN and control galaxy sample split into star-forming and passive.

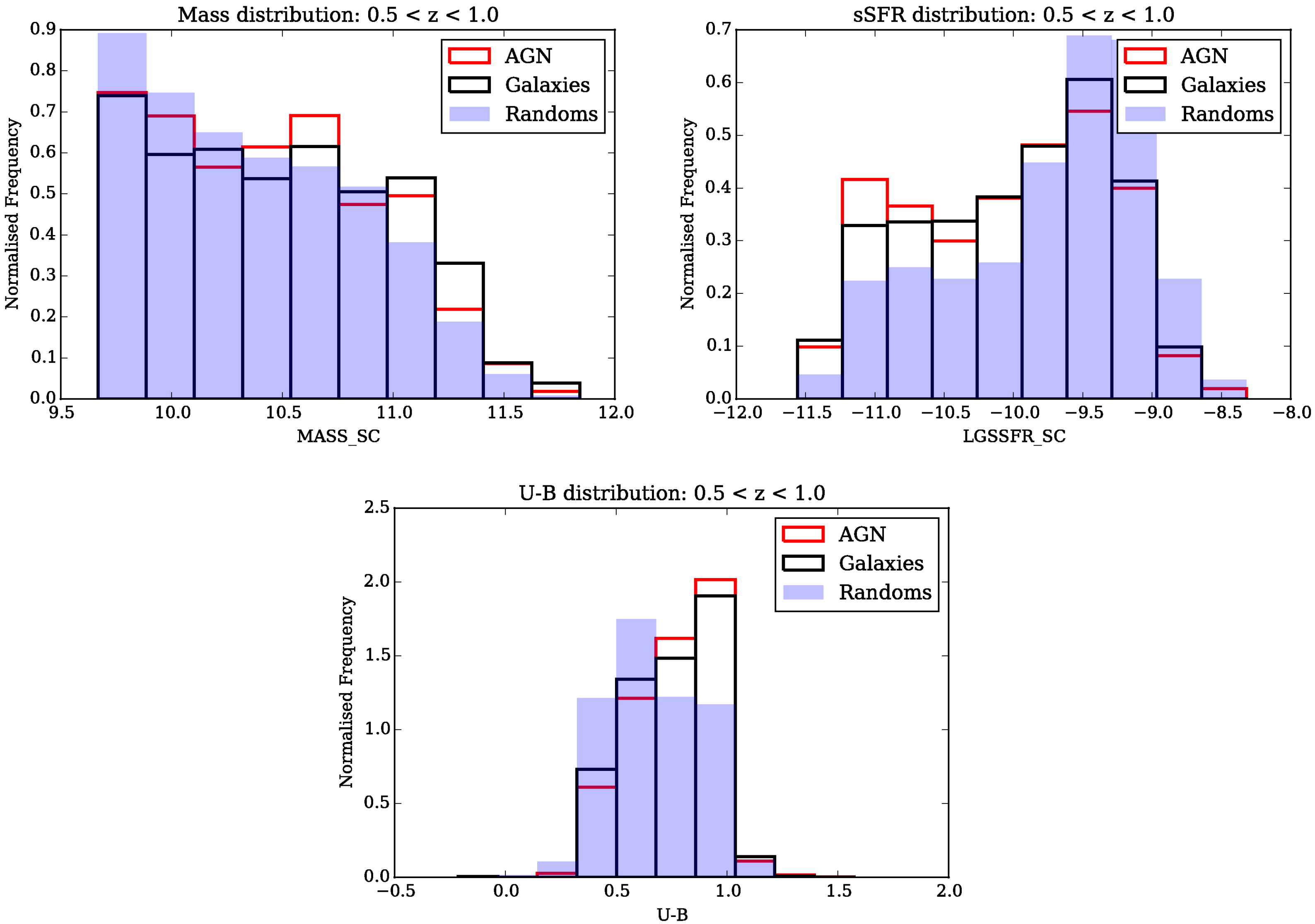

Figure 5.6. $0.5 < z < 1.0$:Distributions of the properties of neighbours within 300 kpc of AGN (red), control galaxies (black), and randoms (blue). Top left panel (a), top right panel (b) and bottom panel (c) show the distributions of mass, sSFR and $U - B$ colour, respectively.

in passive hosts to have similar passive fractions to those of control passive galaxies, but the neighbours are far more star-forming than expected. This may imply that AGN trigger star-forming activity in a high fraction of the neighbours, or that star-forming neighbours indicate a higher likelihood of triggering AGN in the central galaxy.

We investigate the star-formation and stellar mass properties of the neighbours around AGN and control galaxies at $1.0 < z < 1.5$. We plot the mass, sSFR and $U - B$ colour distributions of neighbours within 300 kpc of AGN, control galaxies, and random positions in Figure 5.9 (a), (b), and (c) respectively. Figure 5.9(a) shows that the neighbours of AGN are similar to random apertures. The neighbours of AGN appear slightly less massive compared to those of control galaxies, consistent with expectations given the neighbour passive fractions.

Figure 5.9(b) shows that the neighbours of AGN have higher sSFRs than galaxies, as expected from their passive fractions. Similarly, Figure 5.9(c) shows that the neighbours of AGN are very similar in colour to random apertures, consistent with Figure 5.8(a). The neighbours of AGN have much bluer colours than control galaxies, expected from their slightly lower masses and higher sSFRs. Therefore, the comparison between the neighbours of AGN and control galaxies seems altogether reversed at $1.0 < z < 1.5$. Bradshaw et al. (2011) find slightly different results as they find that the $U - B$ colour distributions of the neighbours of X-ray selected AGN and those of the general galaxy population are consistent with being drawn from the same underlying distribution as checked with a KS test. However, we note that this test was done on the unbinned mass distributions without background/foreground subtraction, so the neighbour populations of both AGN and control galaxies would be dominated by the randoms.

5.4.3 High redshift

Finally, we investigate our highest redshift bin of $1.5 < z < 2.5$. We plot our results for both UDS and COSMOS fields in Figure 5.10. In the first panel, the UDS data points appear to show an enhancement in the passive fraction of neighbours around AGN compared to control galaxies. However we find that the trend is opposite/non-existent in the COSMOS field as shown by the second panel. We note that this difference is not very significant, and could be due to cosmic variance.

The combined measurements from these fields are presented in Figure 5.11(a), where there is no significant difference between the passive neighbour fractions of AGN and control galaxies. The second panel (b) shows the AGN and control galaxies split by spectral type, which shows that the neighbours of AGN are consistent with galaxies of the same type. The trend of "galactic conformity" is observed where passive galaxies (and AGN in passive hosts) have higher passive fractions of

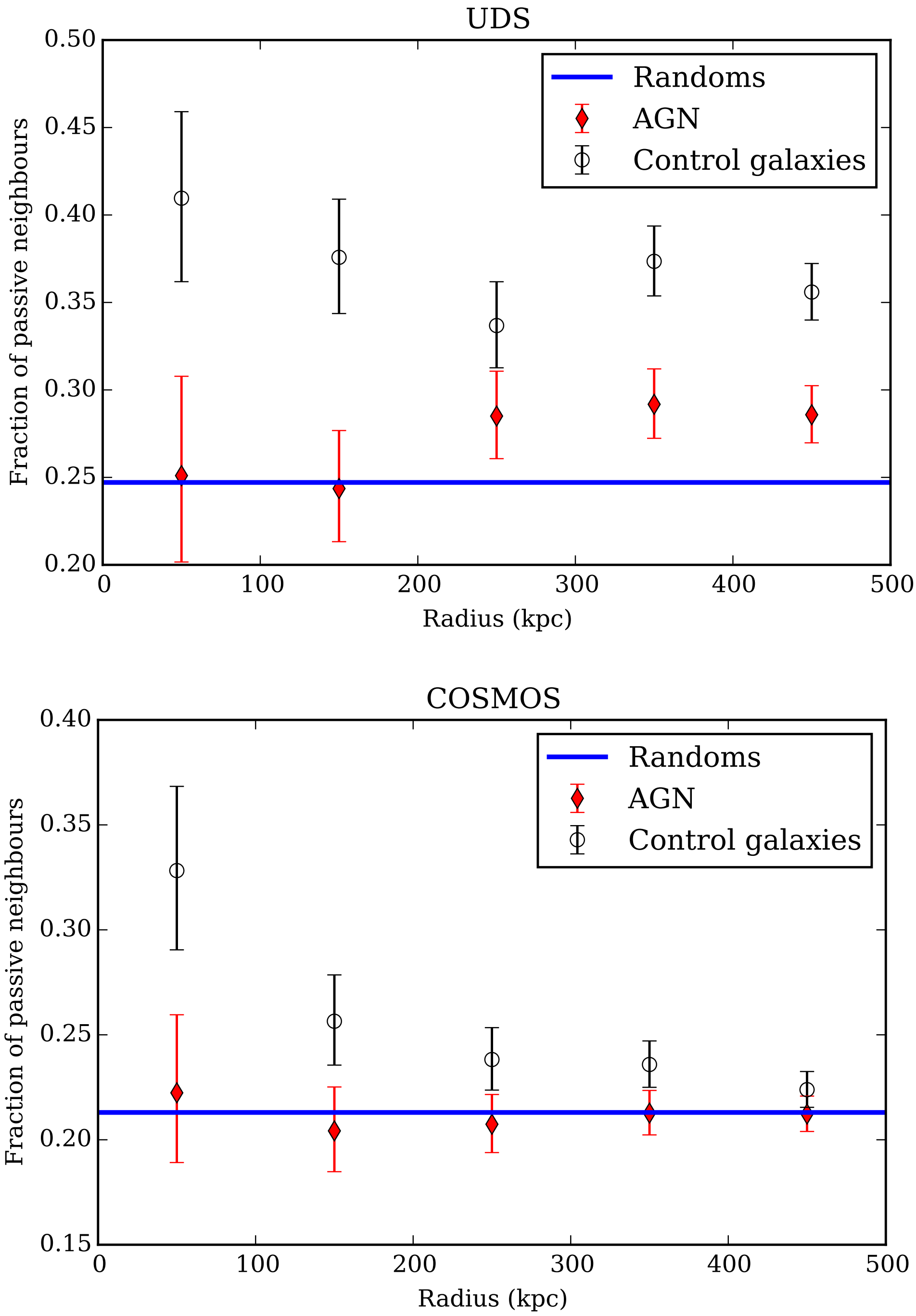

Figure 5.7. $1.0 < z < 1.5$: Radial plots of the fraction of neighbours classified as passive, around AGN, control galaxies, and in random pointings in the UDS in the upper panel (a) and COSMOS in the lower panel (b).

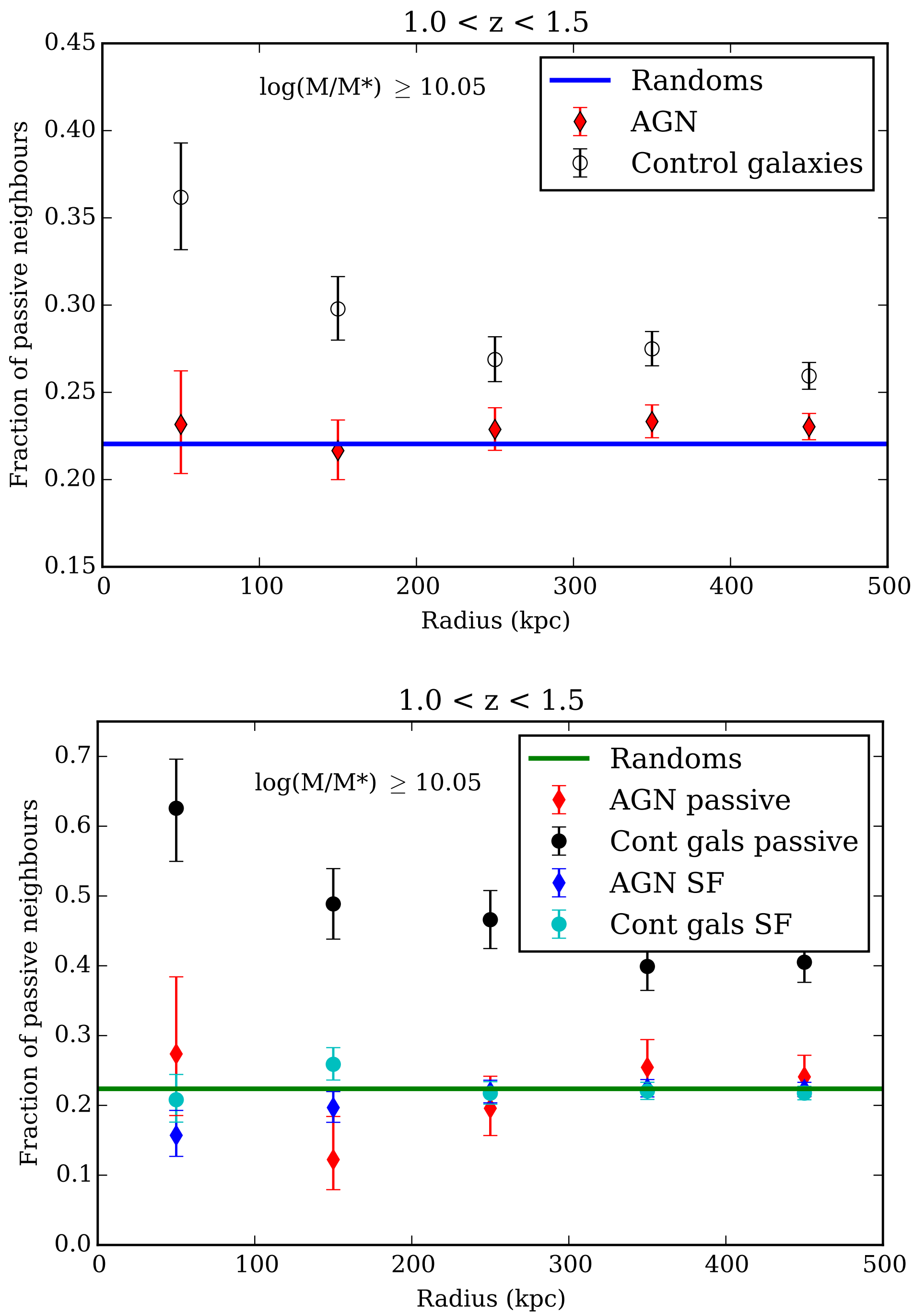

Figure 5.8. $1.0 < z < 1.5$: Radial plots of the fraction of neighbours classified as passive (combined UDS and COSMOS), around AGN, control galaxies, and in random pointings in the upper panel (a). The lower panel (b) shows the AGN and control galaxy sample split into star-forming and passive.

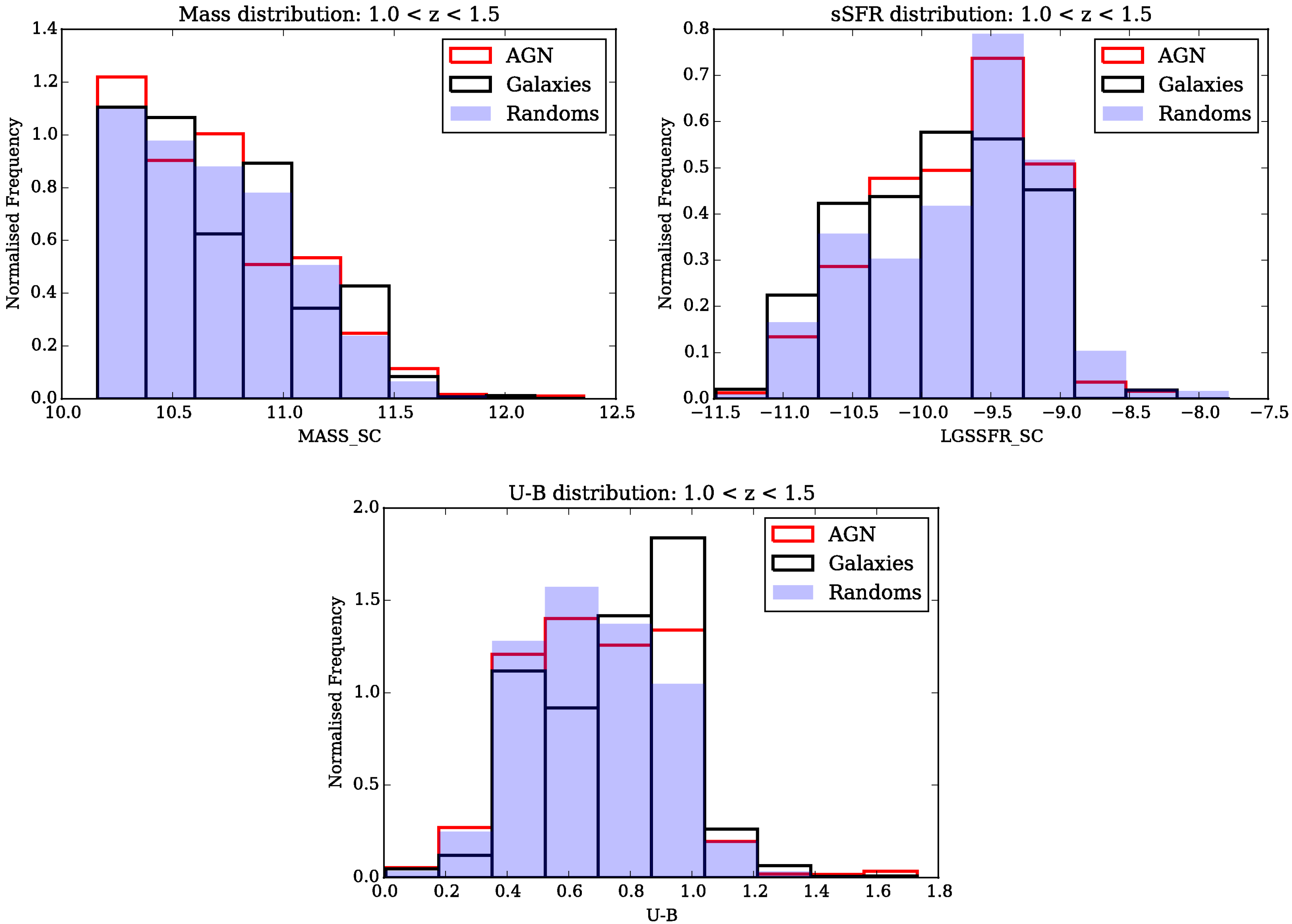

Figure 5.9. $1.0 < z < 1.5$: Distributions of the properties of neighbours within 300 kpc of AGN (red), control galaxies (black), and randoms (blue). Top left panel (a), top right panel (b) and bottom panel (c) show the distributions of mass, sSFR and $U - B$ colour, respectively.

neighbours than star-forming galaxies (and AGN in star-forming hosts). This plot suggests that there is no significant difference between AGN and control galaxies of the same type, consistent with Figure 5.11(a).

For completeness, we present the star-formation and stellar mass properties of the neighbours around AGN and control galaxies at $1.5 < z < 2.5$. We plot the mass, sSFR and $U - B$ colour distributions of neighbours within 300 kpc of AGN, control galaxies, and random positions in Figure 5.12 (a), (b), and (c) respectively. Figure 5.12(a) shows that the neighbours of AGN and control galaxies are more massive than random apertures.

5.5 Discussion

In this section we present a preliminary discussion of our results.

We find that AGN and control galaxies have consistent numbers of galaxy neighbours (per central per kpc^2), irrespective of redshift. If AGN were preferentially found in denser environments than control galaxies, we might expect an excess in the number of neighbours with respect to control galaxies. However, we find no significant differences in the two neighbour populations, suggesting that AGN do not prefer a "special" small-scale galaxy density. This might also imply that AGN are not primarily triggered by massive mergers or harassment, although comparison with a detailed model prediction would be required to make more definitive conclusions.

At all redshifts, the control galaxy population shows the expected trend of "galactic conformity" where passive galaxies have a higher fraction of passive neighbours than star-forming galaxies. We are thus confident that the results for AGN are reliable and representative (as the control population would suffer from effects such as number statistics in the same way that the AGN would).

Based on Chapter 4, we expected that the conformity trends would hold for the AGN sample at all redshifts, and that the AGN trends would be consistent with control galaxies. This has proved not to be the case. Only at $1.5 < z < 2.5$ do we find that AGN in star-forming/passive hosts are consistent with control star-forming/passive galaxies. At this epoch, the interpretation that AGN are stochastically triggered with no significant environmental effects, is consistent with our results.

We find significant variation in the star-formation properties of AGN neighbours compared to control galaxies at $z < 1.5$, as opposite trends are seen below and above $z = 1$. At $1.0 < z < 1.5$, the neighbours of AGN have low passive fractions regardless of whether the host is passive or star-forming, and AGN in passive hosts have significantly lower passive fractions than control passive galaxies. Thus the three possibilities are that the triggering of AGN is: (a) stochastic and AGN have

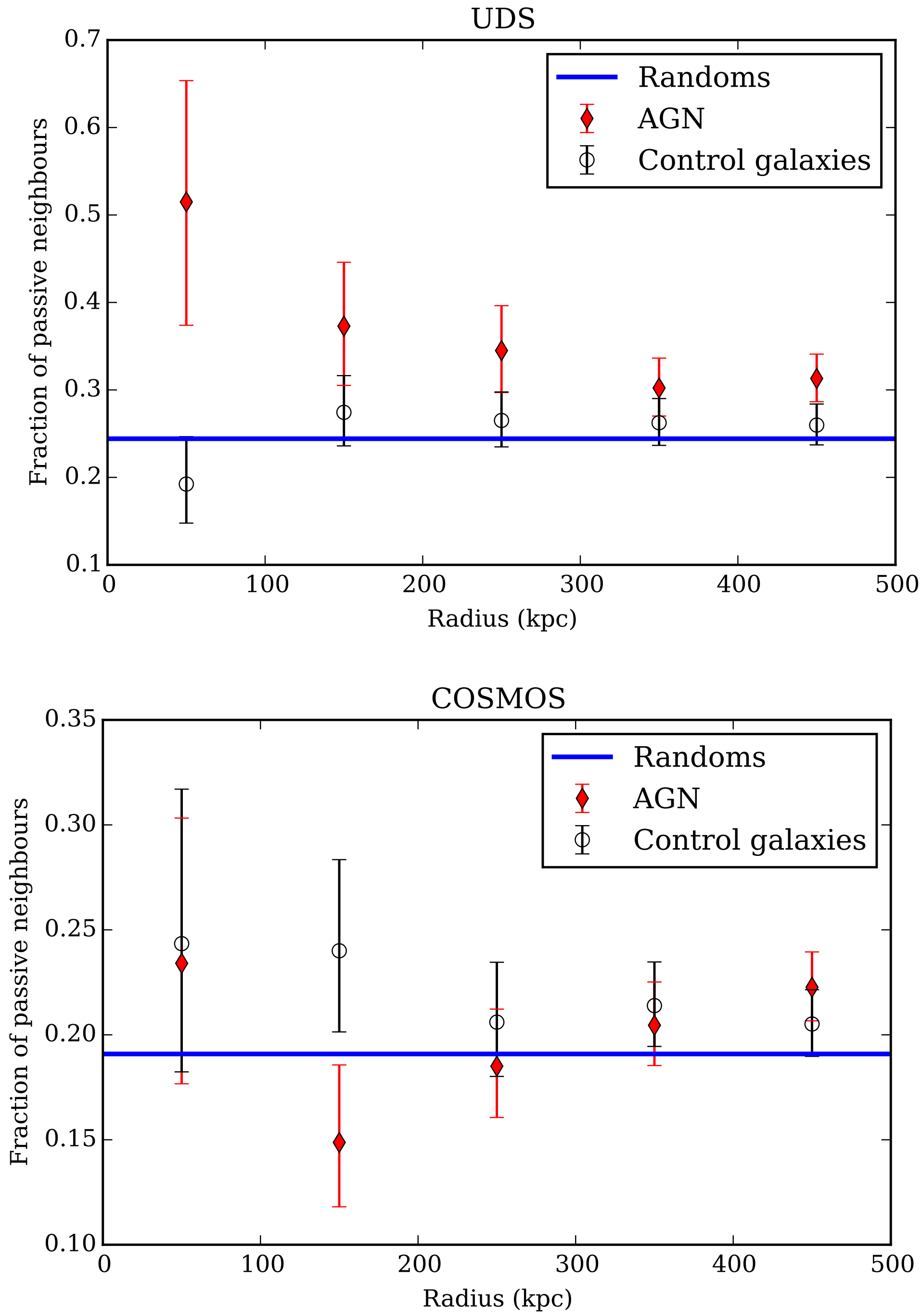

Figure 5.10. $1.5 < z < 2.5$: Radial plots of the fraction of neighbours classified as passive, around AGN, control galaxies, and in random pointings in the UDS in the upper panel (a) and COSMOS in the lower panel (b).

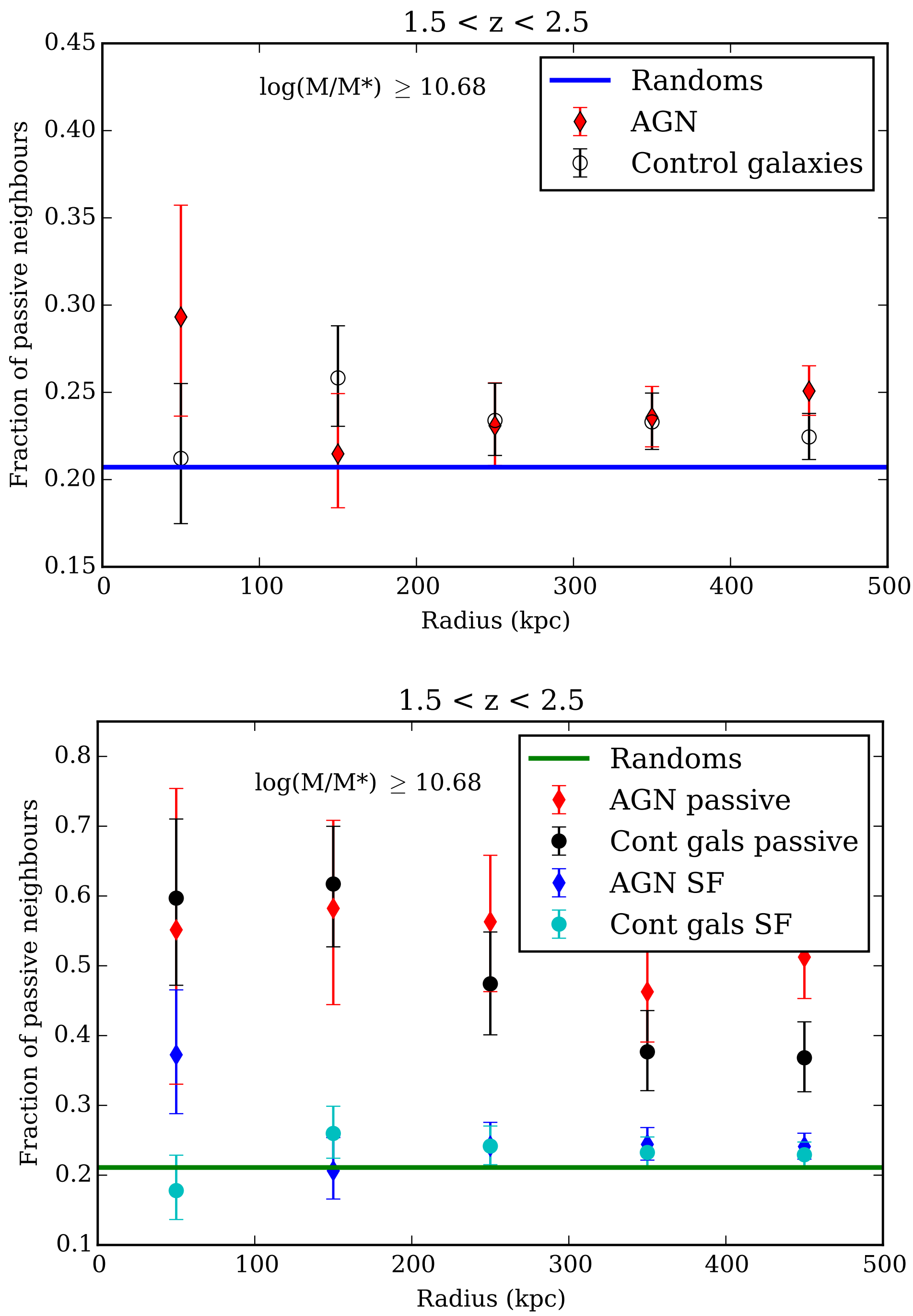

Figure 5.11. $1.5 < z < 2.5$: Radial plots of the fraction of neighbours classified as passive (combined UDS and COSMOS), around AGN, control galaxies, and in random pointings in the upper panel (a). The lower panel (b) shows the AGN and control galaxy sample split into star-forming and passive.

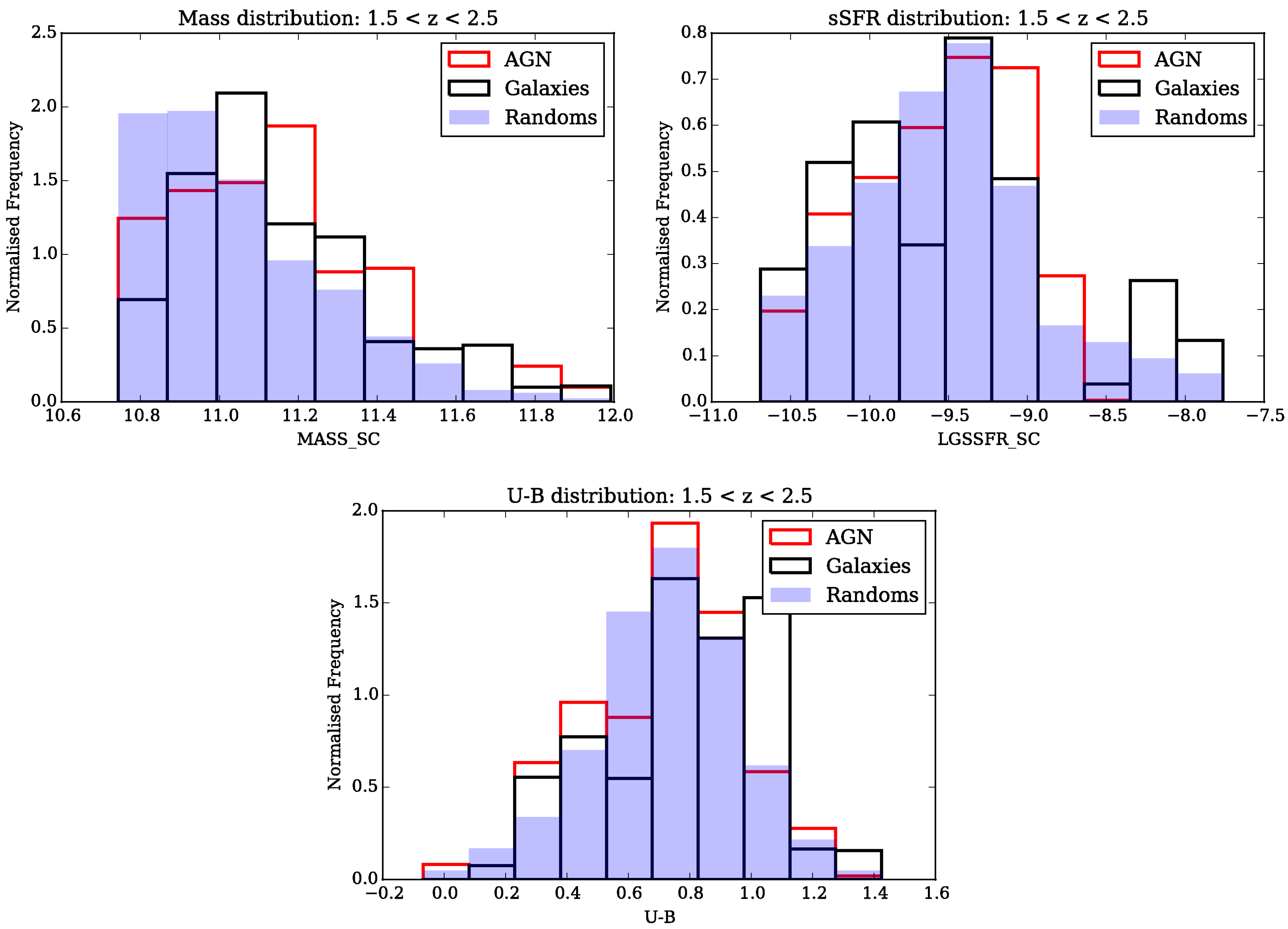

Figure 5.12. $1.5 < z < 2.5$:Distributions of the properties of neighbours within 300 kpc of AGN (red), control galaxies (black), and randoms (blue). Top left panel (a), top right panel (b) and bottom panel (c) show the distributions of mass, sSFR and $U - B$ colour, respectively.

an influence over their neighbours, (b) stochastic depending on the availability of fuel, or (c) not stochastic and has an environmental dependence.

Consistent with (a), AGN may be triggering star-formation in neighbours by compressing gas (positive feedback). However, AGN in passive hosts are unlikely to simultaneously remain quenched and trigger star-formation in nearby galaxies. Scenario (b) could be explained by the increased availability of gas at higher redshifts in dense environments, since a relatively small amount of gas is required to fuel the central black hole, whereas significantly larger amounts are required to fuel star-formation. Consistent with this scenario, AGN activity at this epoch could be correlated with star-forming activity in the same halo. Finally, possibility (c) could involve a wet merger that triggers star-formation and AGN in several neighbouring galaxies. However, we find that there is no statistically significant difference in the number density of neighbours of AGN and control galaxies, so this may be less likely to be the case.

While the scenario that AGN feedback quenches star-forming host galaxies (with lower likelihoods of proximity to passive galaxies) at $1.0 < z < 1.5$ is consistent with our results, we do not expect the periods of radiatively efficient AGN activity to linger as long as the expected quenching timescales of star-formation. Under the most rapid scenarios, quenching timescales are expected to be $\sim 100 - 500$ Myr (e.g. Wild et al. 2009; Barro et al. 2013; Wild et al. 2016; Herrera-Camus et al. 2019), whereas literature based on theoretical arguments (e.g., King & Nixon 2015) and observations (e.g., Schawinski et al. 2015) suggest that radiatively efficient AGN activity is unlikely to remain stable on timescales $\gtrsim 0.1$ Myr. Thus, it is highly unlikely that our results at $1.0 < z < 1.5$ are due to AGN feedback quenching star-forming host galaxies.

We acknowledge the potential caveat that dust-obscuration affects the classification and makes AGN in star-forming galaxies appear passive, which would also lead to our observed result. However, we would not expect this to affect AGN in passive hosts significantly more than control passive galaxies.

At lower redshifts of $0.5 < z < 1.0$, the fraction of passive neighbours of AGN is enhanced compared to neighbours of control galaxies. We find that this difference is likely driven by the neighbours around AGN in star-forming hosts, as their passive fraction is significantly higher than control star-forming galaxies. At this epoch, relating the possibilities (a), (b), and (c) as previously outlined, leads to entirely different scenarios. The possibility (a) relates to jets from the SMBH affecting the host galaxy environment on scales of hundreds of kpc, where gas heating could then switch off star-formation in nearby galaxies. However, our AGN are fairly low in luminosity and not expected to have powerful jets. In addition, AGN feedback is unlikely to affect the neighbours without quenching its own host galaxy first. This is inconsistent with Figure 5.11, which shows that AGN in star-forming hosts have a high fraction of passive neighbours as compared to those of control star-forming galaxies.

Passive galaxies (with a higher likelihood of proximity to other passive galaxies) may have had a renewed period of star-formation, either due to rejuvenation (b) or merging with a younger/gas-rich population (c). This might provide the gas required to funnel into the central engine, thereby triggering AGN. Cooling flows in the centres of galaxy clusters could also lead to star-forming galaxies with nuclear activity. Since we find no evidence for a difference in the number density of neighbours and control galaxies, it is uncertain whether wet mergers are a likely explanation.

We investigate whether the strong redshift dependence of the passive neighbour fraction between the AGN and control galaxies is due to systematic effects. We conclude that possible differences in X-ray luminosity and stellar mass with redshift are unlikely to play an important role as we find that the trends reported in this chapter are robust to uniform cuts in X-ray luminosity and stellar mass across the three redshift bins, as shown by Figure 5.13. We have also taken into consideration that at lower redshifts, AGN tend to have lower accretion rates for a given stellar mass. This implies that we are probing AGN with lower Eddington ratios at low redshift, with a higher passive likelihood of host galaxies, thus likely to be surrounded by other passive hosts. However, this effect is unlikely to explain the redshift dependence of our results, since Figure 5.5(b) shows that it is the star-forming host galaxies that have a more significant difference in the passive neighbour fraction compared to star-forming controls, as compared to the difference between that of passive host galaxies and passive controls.

It is important to address the potential concern that AGN in passive host galaxies are misclassified as star-forming galaxies by the super-colour technique due to contaminating AGN light. The population of AGN in star-forming hosts may have been contaminated by AGN in passive hosts that are misclassified due to nuclear light, leading to a similar result. We do not expect this effect to be significant due to multiple reasons. Firstly, super-colour classifications are derived based on filters focussed on the rest-frame 4000 Å break region. Secondly, a population of AGN in passive hosts that are misclassified as star-forming would be unlikely to have the same clustering properties as star-forming galaxies (as we find in Figure 4.10). Thirdly, only the most luminous AGN are expected to impact supercolour classifications of spectral class in a significant manner (Almaini et al. in prep). Kocevski et al. (2017) report that colour contamination by lower luminosity AGN in their study is negligible, and Santini et al. (2012) find that only 1.3% of their lower-luminosity sources had a difference in their stellar mass larger than a factor of two. In our sample at $0.5 < z < 1.0$, only 4.7% of our AGN are above $L_X > 10^{44}$. Finally, we would also not expect this effect to only manifest itself at $0.5 < z < 1.0$. Nevertheless, we have repeated the study after removing the most luminous AGN ($L_X > 10^{44.4}$)

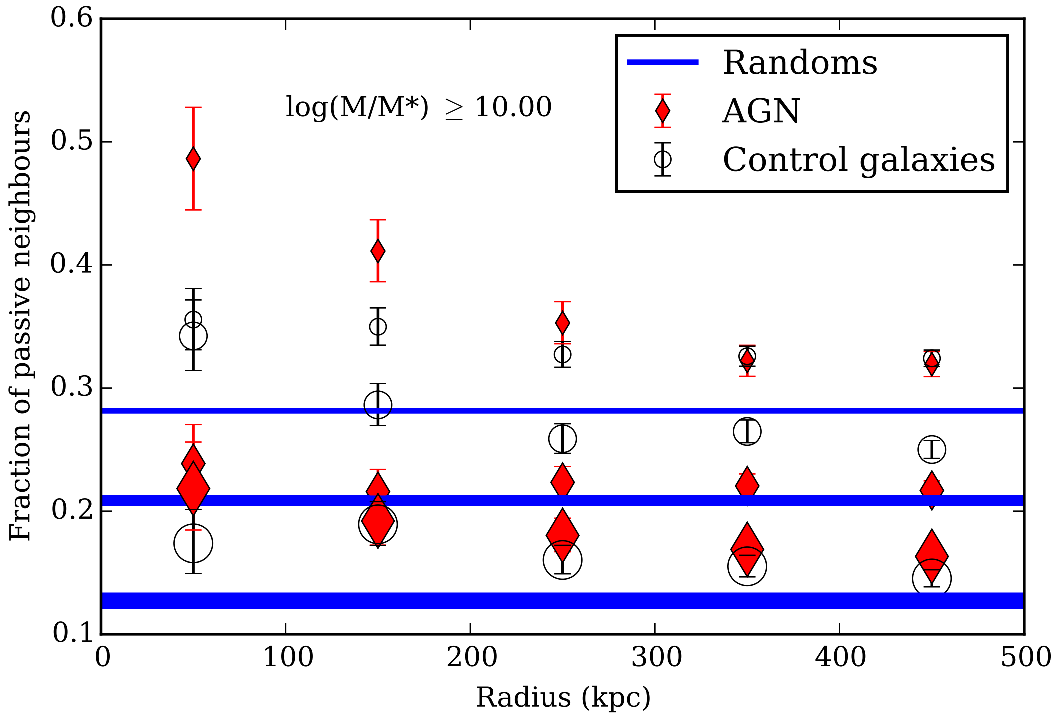

Figure 5.13. Radial plots of the fraction of neighbours classified as passive, around AGN, control galaxies, and in random pointings in the UDS and COSMOS as a function of redshift. The sizes of the points denote the three redshift bins, with small points corresponding to $0.5 < z < 1.0$, medium points corresponding to $1.0 < z < 1.5$, and large points corresponding to $1.5 < z < 2.5$. The AGN samples across the three redshift bins are subject to uniform cuts in X-ray luminosity and stellar mass, and the trends reported in Section 5.4 remain the same.

and found that AGN in star-forming hosts at $0.5 < z < 1.0$ still have higher passive fractions of neighbours, suggesting that the trends do not stem from misclassification. This result could further be checked for robustness after removing sources with point-like emission at their centres, which can be done using both visual inspection of the host galaxy morphologies and surface brightness profile fitting and modelling.

It is intriguing that at $0.5 < z < 1.0$ we find that the passive neighbour fractions of AGN are significantly higher than those of control galaxies, and that these trends drastically reverse at $1.0 < z < 1.5$. This clearly needs further investigation, and this study could be repeated in smaller redshift intervals to draw more robust conclusions. A tighter understanding of the redshift at which the star-formation properties of AGN neighbours changes, can enable us to interpret our results and further our grasp of the relationship between AGN activity and small-scale environment. Larger sample sizes are required to do so, as well as to split AGN in star-forming and passive hosts further by mass and obtain reliable results (we have investigated the impact of stellar mass on Figures 5.5, 5.8, and 5.11, but we found no significant differences or trends).

5.6 Future work

In our study we have focused on the small scale environments based on the host galaxy properties of AGN. The next step is to study the correlations between the properties of AGN themselves and the properties of neighbours (such as mass, colour, sSFR, passive fractions). The AGN sample can be split by luminosity, hardness ratio, and Eddington ratio to study correlations between the power, obscuration, and Eddington-relative accretion rate of AGN and the properties of neighbouring galaxies.

Another avenue for future work would be to investigate the expected neighbour distribution under the assumption that mergers or interactions trigger AGN activity, in order to provide a detailed comparison with our findings.

We could also pursue the study of whether the AGN fraction of nearby galaxies is correlated with the presence of a given AGN. Both pairs and compact groups have been found to host an enhancement in AGN activity (Ellison et al. 2011; Tzanavaris et al. 2014). We can use our data to investigate whether similar environments trigger AGN in multiple nearby galaxies. The AGN fraction can be studied as a function of distance from the AGN, and compared to control galaxies.

Finally, we could compare our results to neighbours of star-forming, passive, post-starburst, and sub-millimetre galaxy populations. It would also be interesting to investigate other properties of neighbours such as morphologies, sizes, and metallicities.

5.7 Summary

In this work we study the galaxy neighbours within 500 kpc of a sample of X-ray selected AGN between $z \sim 2.5$ and $z \sim 0.5$, using the COSMOS and UDS multi-wavelength surveys. We compare them to a control galaxy sample designed to have similar distributions of stellar mass, spectral class, and redshift. To summarise our findings:

1. We detect no statistically significant increase or decrease in the number densities of neighbours around AGN and control galaxies across all redshifts. It appears that AGN do not preferentially reside in denser environments than control galaxies, as we might expect an excess in the number of neighbours with respect to control galaxies. This may also suggest that AGN are not triggered by massive mergers or harassment.

2. We find evidence that the neighbours of AGN are indistinguishable from control galaxies at $1.5 < z < 2.5$, where the passive neighbour fractions of AGN in passive/star-forming hosts are consistent with control passive/star-forming galaxies. The results at this epoch are consistent with AGN being triggered via stochastic accretion of cold gas.

3. At lower redshifts, however, we find different trends:

4. We find that X-ray selected AGN between $1.0 < z < 1.5$ have a lower passive fraction of neighbours than the control sample at 4.3σ significance. We find that this is mostly driven by the passive neighbour fraction of AGN in passive hosts being significantly lower than that of the control passive sample.

5. In contrast, we find that X-ray selected AGN between $0.5 < z < 1.0$ in the UDS and COSMOS fields have a higher passive fraction of neighbours than the control sample at 2.3σ significance. We find that this is mostly driven by a higher fraction of passive neighbours of AGN in star-forming hosts compared to that of the control star-forming sample.

Chapter 6

Conclusions and future outlook

In this thesis we investigate the interplay between AGN activity and host galaxy environment using three complementary methods, making use of recently available state-of-the-art data. In this concluding chapter, we briefly summarise the main results of my PhD in Section 6.1, discuss our conclusions in Section 6.2, and suggest relevant future work in Section 6.3.

6.1 Review of major results

We outlined the motivations of this thesis in Section 1.3.3, identifying three main questions:

- *What happens to AGN activity in dense structures at high redshift?*

  In Chapter 3, we find an AGN overdensity in the Cl 0218.3–0510 protocluster at $z \sim 1.6$ of 23 ± 9 times the field density. This AGN overdensity is centrally concentrated, above and beyond the overdensity of massive galaxies. The AGN fraction among massive protocluster galaxies is enhanced by a factor 2.1 ± 0.7 compared to the field. We find that the properties of field and protocluster AGN are not significantly different in terms of stellar mass distribution, hardness ratio, and X-ray luminosity. Field and protocluster AGN are also not significantly different in colour and stellar mass to typical field and protocluster galaxies, respectively. In terms of morphologies, however, we find that the "irregular" and "interacting" fractions of galaxies in the protocluster are higher than the field.

- *What role do host galaxies play in the connection between AGN and large-scale structure?*

  In Chapter 4, we show using cross-correlation analyses that large-scale clustering of AGN is likely determined by the properties of their host galaxies.

Although we find that AGN at all epochs from $z \sim 4.5$ to $z \sim 0.5$ are on average hosted by galaxies in "group-like" dark matter halos of $10^{12} - 10^{13}$ $M_{\odot}$, the same clustering signal can be produced by inactive (i.e. non-AGN) galaxies closely matched to the AGN in spectral class, stellar mass and redshift. We find that AGN hosted by higher mass galaxies are more clustered than lower mass galaxies, but this stellar mass dependence disappears when passive host galaxies are removed. The strength of clustering is also largely independent of AGN X-ray luminosity. We conclude that the most important property that determines the clustering in a given AGN population is the fraction of passive host galaxies.

- *What can the small scale environments of AGN tell us about triggering?*

  In Chapter 5, we find consistent number densities of neighbours around AGN and control galaxies at all epochs between $z \sim 2.5$ and $z \sim 0.5$. These small-scale results reinforce the large-scale clustering results from Chapter 4, suggesting that AGN do not reside in "special" environments. A more complex picture emerges when we investigate the type of galaxies neighbouring AGN. The results of this chapter are preliminary, but we find evidence that the neighbours of AGN are consistent with those of a carefully constructed control galaxy sample at $1.5 < z < 2.5$, and the star-forming activity of neighbours around AGN in passive/star-forming hosts is consistent with control passive/star-forming galaxies. At $1.0 < z < 1.5$ we find that the star-formation activity of the neighbours of AGN is enhanced (at 2.3σ) with respect to control galaxies. At this epoch, AGN in passive galaxies have significantly lower passive neighbour fractions than passive controls, while AGN in star-forming hosts have consistent passive neighbour fractions with star-forming controls. At lower redshifts of $0.5 < z < 1.0$, we find a suppression of star-forming neighbours as compared to control galaxies (at 4.3σ). AGN in star-forming galaxies at this epoch have *significantly* higher passive fractions than star-forming control galaxies, whereas AGN in passive hosts have *slightly* higher passive fractions than passive control galaxies.

6.2 Conclusions

6.2.1 The evolution of AGN environments with redshift

In Chapter 3, we discussed the scarcity of AGN in the local Universe, and their higher incidence in lower density field environments (e.g. Dressler, Thompson & Shectman 1985; Kauffmann et al. 2004). This suppression of AGN in clusters is more significant in the cores (e.g., Alberts et al. 2016), suggesting an anti-correlation between galaxy density and AGN activity. In contrast, we show in Chapter 3 that the AGN fraction is enhanced by a factor of two relative to the field in a well-identified protocluster at $z \sim 1.6$, and that this enhancement is centrally concentrated. Therefore the high redshift Universe appears to paint an entirely different picture of the relationship between AGN and galaxy density.

Several studies found that the cluster AGN fraction increases with redshift (Galametz et al. 2009; Martini et al. 2013; Alberts et al. 2016; Bufanda et al. 2017), although the AGN fraction in the general galaxy population shows a similar increase with redshift (e.g., Merloni & Heinz 2013). To study the evolution of AGN environments with redshift, we presented the ratio between the cluster AGN fraction:field AGN fraction in Figure 3.8 by combining our results with those from recent literature. As expected, this ratio is much below unity at low redshift (i.e. AGN are scarce in local galaxy clusters). As we turn to higher redshift however, this ratio approaches unity at $z \sim 1.25$, and then increases to 2 for our protocluster at $z \sim 1.6$. While the luminosity limits are lower and selection methods are more biased at $z > 2$, current estimates show that this value continues to increase out to $z \sim 3$.

This suggests that AGN environments shift to denser environments at higher redshift. Similarly, in Chapter 4, we find that the typical dark matter halo mass of AGN host galaxies is $10^{12} - 10^{13}$ $M_{\odot}$ at all epochs, which form some of the most overdense environments at high redshift. We find that this clustering signal can be reproduced by a control galaxy sample closely matched in stellar mass, spectral class, and redshift, suggesting that host galaxies may drive the clustering signal and that AGN do not live in special environments.

This picture becomes more complex in our preliminary study of the properties of neighbours of AGN in Chapter 5, which provides yet another complementary view of the environments of AGN. We find that the number densities of neighbours around AGN and control galaxies are similar at all epochs, suggesting that AGN do not live in special environments, consistent with our findings from Chapter 4. No strong conclusions can be made based on our study of the passive neighbour fraction of AGN and control galaxies.

6.2.2 The influence of environment on AGN & host galaxy properties

AGN properties

We find no evidence for an environmental impact on the nuclear properties of AGN. In Chapter 3, we investigate the relationship between properties of AGN as a function of environment. We show that the environment does not appear to impact most of the properties of AGN. We do not find evidence for a significant difference between the properties of field and protocluster AGN in terms of hardness ratio, X-ray luminosities, and Eddington ratio.

In Chapter 4, we find no correlation between AGN luminosity and typical dark matter halo mass. This suggests that the accretion rate of AGN does not have a simple dependence or correlation with its large-scale environment. This is in agreement with recent results from Yang et al. (2018). We also find no significant correlations between the typical halo mass and other properties of AGN such as hardness ratio and Eddington ratio. We therefore conclude that the environment does not affect the nuclear properties of AGN.

Host galaxy properties

We do find correlations between the host galaxy properties and environment. In Chapter 3, we find that the colour of the AGN host galaxy depends on the environment, as there is a significant difference between the colours of AGN in the protocluster and the field. However, we also find that the colours of field and protocluster AGN are not significantly different from typical field and protocluster galaxies, so these properties appear to randomly sample their parent distributions.

We also find a significant difference between AGN in the protocluster and field in terms of galaxy morphologies. We find that $67^{+16}_{-20}\%$ of protocluster AGN are classified as "disturbed" as opposed to $17^{+10}_{-7}\%$ in the field AGN. Similarly, $33^{+20}_{-16}\%$ of protocluster AGN are "irregular" compared to an upper limit of 5% in the field AGN. However, we also find that among the inactive galaxies in the protocluster, $18^{+14}_{-9}\%$ were classified as "disturbed", and an upper limit of 8% were classified as "irregular".

In Chapter 4, we find that the typical halo mass depends on both stellar mass and star-formation activity of the host galaxy. We find that the difference in the halo mass of AGN hosted by low and high stellar mass galaxies disappears when passive galaxies are removed, suggesting that star-formation activity has a more important connection to the environment than stellar mass. In conclusion, the environment does affect host galaxies, but we find no evidence that the environment affects AGN hosts differently to other galaxies.

6.2.3 The triggering of AGN

Stochastic cold gas accretion onto SMBH

AGN triggering has been proposed to result from the stochastic accretion of cold gas on to the black hole (e.g., Kocevski et al. 2012; Aird, Coil & Georgakakis 2018), without a strong dependence on host galaxy environment. One of our key conclusions in Chapter 4 was the lack of correlation between AGN X-ray luminosity and clustering strength, suggesting that X-ray luminosity of the AGN was not driven by environmental triggering. We also found an independence of AGN properties (X-ray luminosity, hardness ratio, and Eddington ratio) on environment in Chapter 3. Furthermore, in Chapter 4, we found that clustering signal of AGN was consistent with a closely matched control galaxy sample, indicating that the large scale environment of AGN is likely driven by host galaxy properties. As presented in Chapter 5, the number densities of neighbours around AGN and control galaxies are similar, indicating no strong environmental preference of AGN. Taken together, these results point towards the lack of a critical association of the dominant AGN triggering mechanisms with host galaxy environment.

There is much evidence for "stochastic accretion" scenario, both in our work, and in the literature. We investigate the typical host galaxy properties of AGN in Chapter 4 and find that AGN hosts are typically massive and star-forming, consistent with expectations given the shared availability of gas. Several studies also report that AGN are more prevalent among star-forming galaxies (Kauffmann et al. 2003; Alexander et al. 2005; Mullaney et al. 2012; Rosario et al. 2013), pointing towards a co-evolution between the growth of black holes and their hosts. Similarly, Aird, Coil & Georgakakis (2018) find that the probability that a quiescent galaxy hosting AGN (a) is much lower than a star-forming galaxy of the same mass, and (b) increases with redshift, consistent with cold gas availability in such systems. Furthermore, the morphologies of AGN hosts, at large, have been found to be disk-like and relatively undisturbed at $z \sim 2$ (Kocevski et al. 2012). AGN have also been observed to display a broad distribution of accretion rates (Aird, Coil & Georgakakis 2018), likely reflecting the magnitude of AGN accretion variability (Hickox et al. 2014) due to stochasticity in the accretion process. In addition, Aird, Coil & Georgakakis (2019) find that the majority of AGN lie on the star-forming main-sequence, and find that the average SFR is linearly correlated with the AGN fraction across a broad range in stellar mass and redshift. Finally, the increased prevalence of high luminosity AGN at high redshift compared to low redshift (e.g. Figure 4.12) could also be a manifestation of the increased availability of gas.

The role of mergers and galaxy interactions

The "stochastic accretion" scenario explains the increase with redshift in both cluster and field AGN fractions (see Figure 3.7) with the decrease in the availability of cold gas with cosmic time, as well as relating the suppression of AGN activity in low-redshift clusters with the lack of available cold gas in such environments. However, it does not explain why in Chapter 3 we find an enhancement of AGN activity in regions of the $z \sim 1.6$ protocluster associated with a suppression of sSFR. The enhancement of AGN in this Cl 0218.3–0510 protocluster (also see, Lehmer et al. 2009; Digby-North et al. 2010; Lehmer et al. 2013; Saez et al. 2015), is also surprising in the context of stochastic accretion, considering that the host galaxies in this environment are red, with likely less access to cold gas than their field counterparts (that tend to be bluer). In addition, we find direct (but tentative) evidence in Chapter 3 that this AGN enhancement correlates with an enhancement of merger and interaction fraction. Therefore, it appears that interactions do play a role in triggering AGN activity in this specific environment.

The low velocity dispersions and increased likelihoods of environmental interactions in the cores of protoclusters could explain the increase in the AGN fraction towards the centre of protocluster, as observed in Figure 3.3. These interactions would be expected to subside as the clusters mature and virialise, and indeed it has been suggested that AGN are triggered by galaxy interaction and merging events during the *pre-virialisation* evolutionary stage (van Breukelen et al. 2009). As clusters age, their galaxies tend to have access to neither cold gas nor environmental triggers, and therefore become less likely to host AGN than field galaxies. In a reversal to the picture at high redshift, the cores of these clusters at low redshift would be expected to have a lower likelihood of hosting AGN activity than their outskirts (due to the lower rates of interactions such as harassment), matching observations (e.g. Alberts et al. 2016).

The observational evidence on the subject of AGN activity and its links to galaxy interactions remains inconclusive (Ellison et al. 2013; Kocevski et al. 2015; Villforth et al. 2017; Hewlett et al. 2017). Therefore, the most likely explanation appears to be that mergers do not *always* trigger AGN activity, nor can AGN *only* be triggered via mergers and interactions. However, there is indeed evidence in favour of an association between AGN activity and environmental interactions. Both pairs and compact groups have been found to host an enhancement in AGN activity (Ellison et al. 2011; Tzanavaris et al. 2014). Recently, Aird, Coil & Georgakakis (2019) found that the most rapidly accreting AGN occur in starburst galaxies. They suggest that this cannot be explained solely by the copious amounts of available gas in such galaxies, and that mergers also play a role in triggering AGN in starburst galaxies.

Environmental interactions may also preferentially increase the probability of triggering AGN in passive galaxies, with lower amounts of gas than star-forming galaxies, by providing an extra kick of turbulence aiding the funnelling of gas into the central engine. In Chapter 4, we found that AGN in star forming hosts reside in low mass halos, and inferred that AGN in passive hosts must live in clusters (in order to produce the observed clustering signal averaged into an intermediate halo mass). We also found in Chapter 3 that protocluster AGN are red while AGN in blue hosts make up majority of the field sample (see Figure 3.6(a)). Furthermore, within the "irregular" galaxies of the protocluster, $67^{+16}_{-20}\%$ are AGN, compared to $11^{+7}_{-5}\%$ in the field. This implies that galaxy interactions are significantly less likely to be an important triggering mechanism in the field, where stochastic accretion of gas may be more likely. In order to ascertain whether dense environments enhance the triggering of AGN in passive galaxies, future studies can calculate the fraction of red galaxies that host AGN in clusters and field as a function of redshift.

The majority of AGN are hosted by normal, star-forming main-sequence galaxies (Aird, Coil & Georgakakis 2019, also see Figure 4.11). These galaxies are likely triggered by the stochastic accretion of cold gas, without a dominant influence from the environment. We conclude that although galaxy mergers and interactions *can* indeed play a role in triggering AGN, particularly in passive galaxies, they are not a crucial parameter for the (star-forming main-sequence) majority of the AGN population.

The role of additional physical processes

While galaxy mergers may directly trigger AGN activity by disturbing the cold gas and funnelling gas into the central engine, it is also possible that they simply lead to the formation of a bulge. This could in turn trigger AGN activity through secular processes of bulge growth, including gas accretion into the centres of galaxies and star-formation (increasing the central mass density). This bulge can also form without a merger, and grow via secular mechanisms, leading to an increased probability of triggering AGN. This possibility is consistent with the well-known correlation between the masses of the bulges and those of the black holes (e.g., Ferrarese & Merritt 2000; Gebhardt et al. 2000). In addition, there is recent evidence that the compactness is correlated with a high incidence of AGN (Barro et al. 2013; Kocevski et al. 2017). This bulge build-up scenario is also favoured by Aird, Coil & Georgakakis (2019), to explain the enhancement of the AGN fraction among star-forming galaxies that lie below the main sequence in comparison to main-sequence galaxies (with more gas).

Disks and bars may also play a role in triggering nuclear activity (e.g., Knapen, Shlosman & Peletier 2000) as disk instabilities have been proposed to enhance gas flow to the nuclei of galaxies (Dekel, Sari & Ceverino 2009).

Triggering in a nutshell

To summarise our understanding of AGN triggering:

- The vast majority of AGN are hosted by normal, star-forming galaxies and are likely triggered stochastically.
- Mergers *can* trigger AGN by providing turbulence and funnelling gas into the central engine.
- Mergers do not *necessarily* trigger AGN, and AGN do not *need* mergers to be triggered.

- AGN triggering is likely to depend on additional physical processes.

6.3 Future outlook

6.3.1 Short-term follow-up

Despite efforts from the astronomical community (including our own), the links between AGN and environment remain unclear. Evidently, the prevalence of AGN must be studied in more protoclusters at high redshift, to confirm the trends reported in Chapter 3 to a higher significance. Having shown in Chapter 4 the importance of controlling for host galaxy properties, these protocluster studies must ideally compare to a control galaxy sample matched in stellar mass, (s)SFR, and redshift. Since the cluster galaxy properties change significantly as the Universe ages, one can disentangle the AGN dependence on host galaxies vs environment by measuring the AGN fraction as a function of local galaxy density at fixed redshift, mass and (s)SFR. Larger galaxy and AGN sample sizes are required to enable the study of the redshift evolution of AGN activity as a function of galaxy environment.

From Chapter 4, we inferred that AGN hosted by passive galaxies must live in higher mass halos. Larger AGN sample sizes will enable us to test this inference and directly measure the clustering properties of AGN hosted by passive galaxies. Furthermore, the dependence (if any) of hardness ratio and Eddington ratio on large-scale environment can be more clearly understood. Since our work is limited to X-ray selection, which tends to select more powerful and rapidly accreting AGN, we must bear in mind the caveat that the method of AGN selection introduces inherent biases in the host galaxy properties and likely drives the clustering signal. Therefore, our clustering analyses of AGN could be repeated using optical, near-infrared, and radio selected AGN with samples matched in mass, (s)SFR, and redshift to obtain a tighter grasp on the impact of host galaxies on AGN clustering measurements. Since the clustering signal from AGN likely depends on the properties of the host galaxies, the implication for future AGN clustering studies is then that samples must be divided by host galaxy properties.

The apparent reversal of the relationship found in Chapter 5 between the star-formation properties of AGN neighbours above and below $z = 1$ clearly requires deeper inspection. This will also be made possible with larger sample sizes, allowing for the investigation of trends in finer redshift bins. In order to study correlations between the power, obscuration, and Eddington-relative accretion rate of AGN and the properties of neighbouring galaxies, the study could be repeated after splitting AGN sample by nuclear properties (such as X-ray luminosity, hardness ratio, and Eddington ratio).

These studies could also use additional data from X-ray surveys with comparable wavebands such as the *Chandra* Deep Field North/South and the All-wavelength Extended Groth strip International Survey (AEGIS) to increase source statistics. The range in AGN luminosity can be improved using NuSTAR Legacy Survey observations such as the Swift-BAT AGN survey.

6.3.2 Long-term outlook

Looking beyond the study of AGN activity as a function of environment, several related fields (e.g. the study of AGN outflows, variability) are left wanting for more data. To our rescue comes several impending surveys and telescopes:

The *James Webb Space Telescope (JWST)*, currently planned for March 2021, will allow for unprecedented observations of the high-redshift Universe. It is frequently volunteered as the next breakthrough of galaxy evolution, and the range of near-infrared filters on its Near Infrared Camera (NIRCam) will allow us to reliably classify large numbers of galaxies (e.g. using PCA) out to $z \sim 5$.

At the time of writing, *the extended ROentgen Survey with an Imaging Telescope Array (eROSITA)*, is due to launch later this year. *eROSITA* will perform the first all-sky X-ray imaging survey in the medium energy range (up to 10 keV) and aims to systematically detect up to $\sim 10^6$ distant AGN. These large numbers of AGN can then be complemented with follow-up using deeper *Chandra* X-ray imaging, overlapping spectroscopic and mid-infrared surveys such as the 4-metre Multi-Object Spectroscopic Telescope (4MOST) and the Wide-field Infrared Survey Explorer (WISE), as well as optical and near-infrared surveys from Hyper-Suprime Cam (HSC) and Euclid.

The *Advanced Telescope for High Energy Astrophysics (ATHENA)*, is a future X-ray telescope, currently under development for launch around 2031. *ATHENA* will possess unparalleled capabilities compared to its cousins in the present (and future). The expected plane of X-ray luminosity and redshift space probed by *ATHENA* (as compared to *Chandra*, *XMM-Newton*, and *eROSITA*) is shown in Figure 6.1, which portrays the impressive and exciting potential that lies before us. The field of active galactic nuclei looks ahead to a rosy future.

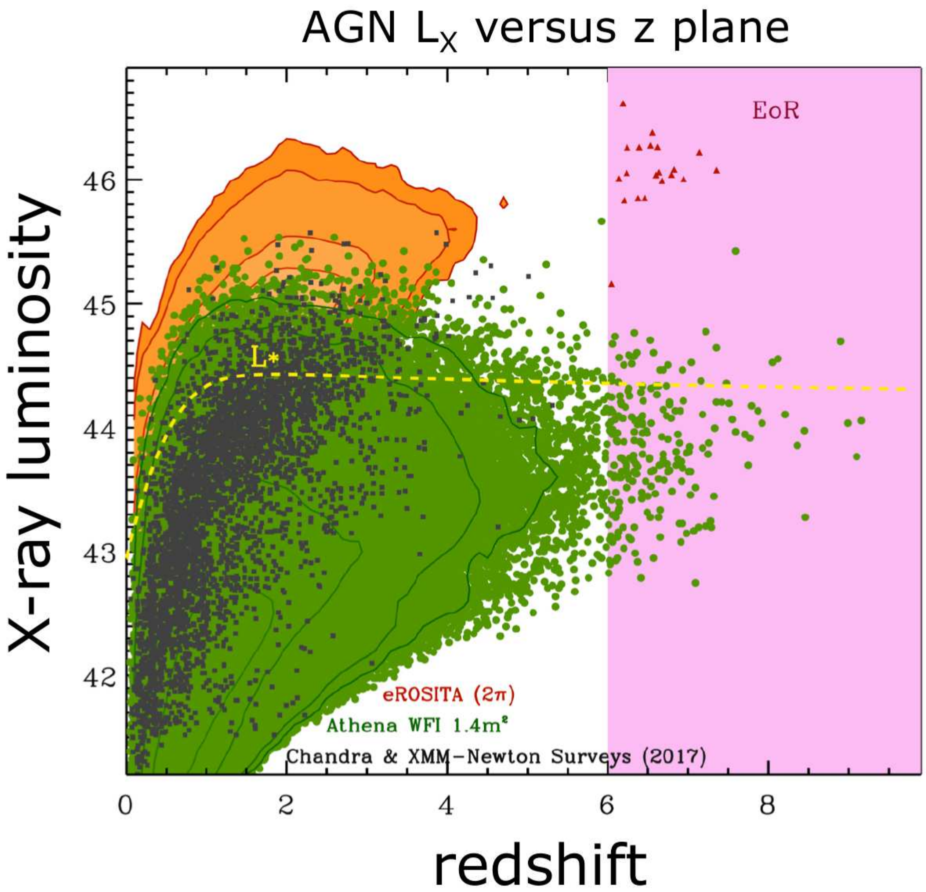

Figure 6.1. The X-ray luminosity - redshift plane of AGN as probed by *Chandra* and *XMM-Newton* (black points), *eROSITA* (orange shaded region with red contours), and *ATHENA* (green points and green contours) from Aird et al. (2013). While the intermediate future with *eROSITA* will provide large numbers of AGN with which we can obtain *Chandra* follow-up, *ATHENA* is expected to revolutionise the field altogether over the next couple of decades.

Bibliography

Abbott B. P., Abbott R., Abbott T. D., Abernathy M. R., Acernese F., Ackley K., Adams C., Adams T., Addesso P., Adhikari R. X., et al., 2016. *Physical Review Letters*, **116(6)**, 061102. *Observation of Gravitational Waves from a Binary Black Hole Merger.*

Abell G. O., 1965. ARA&A, **3**, 1. *Clustering of Galaxies.*

Adelberger K. L., Steidel C. C., Shapley A. E., Hunt M. P., Erb D. K., Reddy N. A., Pettini M., 2004. ApJ, **607**, 226. *Optical Selection of Star-forming Galaxies at Redshifts 1 ¡ z ¡ 3.*

Aird J., Coil A. L., Georgakakis A., 2017. MNRAS, **465**, 3390. *X-rays across the galaxy population - I. Tracing the main sequence of star formation.*

Aird J., Coil A. L., Georgakakis A., 2018. MNRAS, **474**, 1225. *X-rays across the galaxy population - II. The distribution of AGN accretion rates as a function of stellar mass and redshift.*

Aird J., Coil A. L., Georgakakis A., 2019. MNRAS, **484**, 4360. *X-rays across the galaxy population - III. The incidence of AGN as a function of star formation rate.*

Aird J., Nandra K., Laird E. S., Georgakakis A., Ashby M. L. N., Barmby P., Coil A. L., Huang J.-S., Koekemoer A. M., Steidel C. C., Willmer C. N. A., 2010. MNRAS, **401**, 2531. *The evolution of the hard X-ray luminosity function of AGN.*

Aird J., Comastri A., Brusa M., Cappelluti N., Moretti A., Vanzella E., Volonteri M., Alexander D., Afonso J. M., Fiore F., Georgantopoulos I., Iwasawa K., Merloni A., Nandra K., Salvaterra R., Salvato M., Severgnini P., Schawinski K., Shankar F., Vignali C., Vito F., 2013. *arXiv e-prints. The Hot and Energetic Universe: The formation and growth of the earliest supermassive black holes.*

Akiyama M., Ueda Y., Watson M. G., Furusawa H., Takata T., Simpson C., Morokuma T., Yamada T., Ohta K., Iwamuro F., Yabe K., Tamura N., Moritani Y., Takato N., Kimura M., Maihara T., Dalton G., Lewis I., Lee H., Curtis-Lake E., Macaulay E., Clarke F., Silverman J. D., Croom S., Ouchi M., Hanami H., Díaz Tello J., Yoshikawa T., Fujishiro N., Sekiguchi K., 2015. PASJ, **67**, 82. *The Subaru-XMM-Newton Deep Survey (SXDS). VIII. Multi-wavelength identification, optical/NIR spectroscopic properties, and photometric redshifts of X-ray sources.*

Alberts S., Pope A., Brodwin M., Chung S. M., Cybulski R., Dey A., Eisenhardt P. R. M., Galametz A., Gonzalez A. H., Jannuzi B. T., Stanford S. A., Snyder

G. F., Stern D., Zeimann G. R., 2016. ApJ, **825**, 72. *Star Formation and AGN Activity in Galaxy Clusters from z=1-2: a Multi-Wavelength Analysis Featuring Herschel/PACS.*

Alexander D. M., Hickox R. C., 2012. New A Rev., **56**, 93. *What drives the growth of black holes?*

Alexander D. M., Bauer F. E., Chapman S. C., Smail I., Blain A. W., Brandt W. N., Ivison R. J., 2005. ApJ, **632**, 736. *The X-Ray Spectral Properties of SCUBA Galaxies.*

Alexander D. M., Simpson J. M., Harrison C. M., Mullaney J. R., Smail I., Geach J. E., Hickox R. C., Hine N. K., Karim A., Kubo M., Lehmer B. D., Matsuda Y., Rosario D. J., Stanley F., Swinbank A. M., Umehata H., Yamada T., 2016. MNRAS, **461(3)**, 2944. *ALMA observations of a $z \approx 3.1$ protocluster: star formation from active galactic nuclei and Lyman-alpha blobs in an overdense environment.*

Allevato V., Finoguenov A., Civano F., Cappelluti N., Shankar F., Miyaji T., Hasinger G., Gilli R., Zamorani G., Lanzuisi G., Salvato M., Elvis M., Comastri A., Silverman J., 2014. ApJ, **796**, 4. *Clustering of Moderate Luminosity X-Ray-selected Type 1 and Type 2 AGNS at Z ˜ 3.*

Allevato V., Civano F., Finoguenov A., Marchesi S., Shankar F., Zamorani G., Hasinger G., Salvato M., Miyaji T., Gilli R., Cappelluti N., Brusa M., Suh H., Lanzuisi G., Trakhtenbrot B., Griffiths R., Vignali C., Schawinski K., Karim A., 2016. ApJ, **832**, 70. *The Chandra COSMOS Legacy Survey: Clustering of X-Ray-selected AGNs at 2.9 ¡= z ¡= 5.5 Using Photometric Redshift Probability Distribution Functions.*

Ann H. B., Park C., Choi Y.-Y., 2008. MNRAS, **389**, 86. *Galactic satellite systems: radial distribution and environment dependence of galaxy morphology.*

Antonucci R., 1993. ARA&A, **31**, 473. *Unified models for active galactic nuclei and quasars.*

Arnold T. J., Martini P., Mulchaey J. S., Berti A., Jeltema T. E., 2009. ApJ, **707**, 1691. *Active Galactic Nuclei in Groups and Clusters of Galaxies: Detection and Host Morphology.*

Arnouts S., Moscardini L., Vanzella E., Colombi S., Cristiani S., Fontana A., Giallongo E., Matarrese S., Saracco P., 2002. MNRAS, **329**, 355. *Measuring the redshift evolution of clustering: the Hubble Deep Field South.*

Ashby M. L. N., Willner S. P., Fazio G. G., Huang J.-S., Arendt R., Barmby P., Barro G., Bell E. F., Bouwens R., Cattaneo A., Croton D., Davé R., Dunlop J. S., Egami E., Faber S., Finlator K., Grogin N. A., Guhathakurta P., Hernquist L., Hora J. L., Illingworth G., Kashlinsky A., Koekemoer A. M., Koo D. C., Labbé I., Li Y., Lin L., Moseley H., Nandra K., Newman J., Noeske K., Ouchi M., Peth M., Rigopoulou D., Robertson B., Sarajedini V., Simard L., Smith H. A., Wang Z., Wechsler R., Weiner B., Wilson G., Wuyts S., Yamada T., Yan H., 2013. ApJ, **769**, 80. *SEDS: The Spitzer Extended Deep Survey. Survey Design, Photometry, and Deep IRAC Source Counts.*

Asquith R., Pearce F. R., Almaini O., Knebe A., Gonzalez-Perez V., Benson A., Blaizot J., Carretero J., Castander F. J., Cattaneo A., Cora S. A., Croton D. J., Devriendt J. E., Fontanot F., Gargiulo I. D., Hartley W., Henriques B., Lee J., Mamon G. A., Onions J., Padilla N. D., Power C., Srisawat C., Stevens A. R. H., Thomas P. A., Vega-Martínez C. A., Yi S. K., 2018. MNRAS, **480**, 1197. *Cosmic CARNage II: the evolution of the galaxy stellar mass function in observations and galaxy formation models.*

Baldry I. K., Balogh M. L., Bower R. G., Glazebrook K., Nichol R. C., Bamford S. P., Budavari T., 2006. MNRAS, **373**, 469. *Galaxy bimodality versus stellar mass and environment.*

Baldwin J. A., Phillips M. M., Terlevich R., 1981. PASP, **93**, 5. *Classification parameters for the emission-line spectra of extragalactic objects.*

Bardeen J. M., Bond J. R., Kaiser N., Szalay A. S., 1986. ApJ, **304**, 15. *The statistics of peaks of Gaussian random fields.*

Barro G., Faber S. M., Pérez-González P. G., Koo D. C., Williams C. C., Kocevski D. D., Trump J. R., Mozena M., McGrath E., van der Wel A., Wuyts S., Bell E. F., Croton D. J., Ceverino D., Dekel A., Ashby M. L. N., Cheung E., Ferguson H. C., Fontana A., Fang J., Giavalisco M., Grogin N. A., Guo Y., Hathi N. P., Hopkins P. F., Huang K.-H., Koekemoer A. M., Kartaltepe J. S., Lee K.-S., Newman J. A., Porter L. A., Primack J. R., Ryan R. E., Rosario D., Somerville R. S., Salvato M., Hsu L.-T., 2013. ApJ, **765**, 104. *CANDELS: The Progenitors of Compact Quiescent Galaxies at z 2.*

Bell E. F., Wolf C., Meisenheimer K., Rix H.-W., Borch A., Dye S., Kleinheinrich M., Wisotzki L., McIntosh D. H., 2004. ApJ, **608**, 752. *Nearly 5000 Distant Early-Type Galaxies in COMBO-17: A Red Sequence and Its Evolution since z˜1.*

Benson A. J., Cole S., Frenk C. S., Baugh C. M., Lacey C. G., 2000. MNRAS, **311**, 793. *The nature of galaxy bias and clustering.*

Benson A. J., Bower R. G., Frenk C. S., Lacey C. G., Baugh C. M., Cole S., 2003. ApJ, **599**, 38. *What Shapes the Luminosity Function of Galaxies?*

Bertin E., Arnouts S., 1996. A&AS, **117**, 393. *SExtractor: Software for source extraction.*

Bertone G., Hooper D., Silk J., 2005. Phys. Rep., **405(5-6)**, 279. *Particle dark matter: evidence, candidates and constraints.*

Best P. N., Heckman T. M., 2012. MNRAS, **421**, 1569. *On the fundamental dichotomy in the local radio-AGN population: accretion, evolution and host galaxy properties.*

Birnboim Y., Dekel A., 2003. MNRAS, **345**, 349. *Virial shocks in galactic haloes?*

Blanton M. R., Hogg D. W., Bahcall N. A., Baldry I. K., Brinkmann J., Csabai I., Eisenstein D., Fukugita M., Gunn J. E., Ivezić Ž., Lamb D. Q., Lupton R. H., Loveday J., Munn J. A., Nichol R. C., Okamura S., Schlegel D. J., Shimasaku K., Strauss M. A., Vogeley M. S., Weinberg D. H., 2003. ApJ, **594**, 186. *The Broadband Optical Properties of Galaxies with Redshifts 0.02 ¡ z ¡ 0.22.*

Blanton M. R., Eisenstein D., Hogg D. W., Schlegel D. J., Brinkmann J., 2005. ApJ, **629**, 143. *Relationship between Environment and the Broadband Optical Properties of Galaxies in the Sloan Digital Sky Survey.*

Bower R. G., Benson A. J., Crain R. A., 2012. MNRAS, **422**, 2816. *What shapes the galaxy mass function? Exploring the roles of supernova-driven winds and active galactic nuclei.*

Bower G. A., Green R. F., Danks A., Gull T., Heap S., Hutchings J., Joseph C., Kaiser M. E., Kimble R., Kraemer S., Weistrop D., Woodgate B., Lindler D., Hill R. S., Malumuth E. M., Baum S., Sarajedini V., Heckman T. M., Wilson A. S., Richstone D. O., 1998. ApJ, **492(2)**, L111. *Kinematics of the Nuclear Ionized Gas in the Radio Galaxy M84 (NGC 4374).*

Boyle B. J., Fong R., Shanks T., Peterson B. A., 1990. MNRAS, **243**, 1. *A catalogue of faint, UV-excess objects.*

Boyle B. J., Georgantopoulos I., Blair A. J., Stewart G. C., Griffiths R. E., Shanks T., Gunn K. F., Almaini O., 1998. MNRAS, **296**, 1. *ASCA observations of deep ROSAT fields - II. The 2-10keV AGN luminosity function.*

Bradshaw E. J., Almaini O., Hartley W. G., Chuter R. W., Simpson C., Conselice C. J., Dunlop J. S., McLure R. J., Cirasuolo M., 2011. MNRAS, **415**, 2626. *Environments of active galactic nuclei at z ¡ 1.5 in the UKIDSS Ultra-Deep Survey.*

Brinchmann J., Charlot S., White S. D. M., Tremonti C., Kauffmann G., Heckman T., Brinkmann J., 2004. MNRAS, **351**, 1151. *The physical properties of star-forming galaxies in the low-redshift Universe.*

Brown L. D., Cai T. T., DasGupta A., 2001. *Statist. Sci.*, **16(2)**, 101. *Interval Estimation for a Binomial Proportion.*

Bruzual G., Charlot S., 2003. MNRAS, **344**, 1000. *Stellar population synthesis at the resolution of 2003.*

Bufanda E., Hollowood D., Jeltema T. E., Rykoff E. S., Rozo E., Martini P., Abbott T. M. C., Abdalla F. B., Allam S., Banerji M., Benoit-Lévy A., Bertin E., Brooks D., Carnero Rosell A., Carrasco Kind M., Carretero J., Cunha C. E., da Costa L. N., Desai S., Diehl H. T., Dietrich J. P., Evrard A. E., Fausti Neto A., Flaugher B., Frieman J., Gerdes D. W., Goldstein D. A., Gruen D., Gruendl R. A., Gutierrez G., Honscheid K., James D. J., Kuehn K., Kuropatkin N., Lima M., Maia M. A. G., Marshall J. L., Melchior P., Miquel R., Mohr J. J., Ogando R., Plazas A. A., Romer A. K., Rooney P., Sanchez E., Santiago B., Scarpine V., Sevilla-Noarbe I., Smith R. C., Soares-Santos M., Sobreira F., Suchyta E., Tarle G., Thomas D., Tucker D. L., Walker A. R., DES Collaboration, 2017. MNRAS, **465**, 2531. *The evolution of active galactic nuclei in clusters of galaxies from the Dark Energy Survey.*

Buitrago F., Trujillo I., Conselice C. J., Häußler B., 2013. MNRAS, **428**, 1460. *Early-type galaxies have been the predominant morphological class for massive galaxies since only z 1.*

Butcher H., Oemler, Jr. A., 1978. ApJ, **219**, 18. *The evolution of galaxies in clusters. I - ISIT photometry of C1 0024+1654 and 3C 295.*

Capak P., Aussel H., Ajiki M., McCracken H. J., Mobasher B., Scoville N., Shopbell P., Taniguchi Y., Thompson D., Tribiano S., Sasaki S., Blain A. W., Brusa M., Carilli C., Comastri A., Carollo C. M., Cassata P., Colbert J., Ellis R. S., Elvis M., Giavalisco M., Green W., Guzzo L., Hasinger G., Ilbert O., Impey C., Jahnke K., Kartaltepe J., Kneib J.-P., Koda J., Koekemoer A., Komiyama Y., Leauthaud A., Le Fevre O., Lilly S., Liu C., Massey R., Miyazaki S., Murayama T., Nagao T., Peacock J. A., Pickles A., Porciani C., Renzini A., Rhodes J., Rich M., Salvato M., Sanders D. B., Scarlata C., Schiminovich D., Schinnerer E., Scodeggio M., Sheth K., Shioya Y., Tasca L. A. M., Taylor J. E., Yan L., Zamorani G., 2007. ApJS, **172**, 99. *The First Release COSMOS Optical and Near-IR Data and Catalog.*

Casali M., Adamson A., Alves de Oliveira C., Almaini O., Burch K., Chuter T., Elliot J., Folger M., Foucaud S., Hambly N., Hastie M., Henry D., Hirst P., Irwin M., Ives D., Lawrence A., Laidlaw K., Lee D., Lewis J., Lunney D., McLay S., Montgomery D., Pickup A., Read M., Rees N., Robson I., Sekiguchi K., Vick A., Warren S., Woodward B., 2007. A&A, **467**, 777. *The UKIRT wide-field camera.*

Chabrier G., 2003. PASP, **115**, 763. *Galactic Stellar and Substellar Initial Mass Function.*

Chevalier R. A., Clegg A. W., 1985. Nature, **317**, 44. *Wind from a starburst galaxy nucleus.*

Chuter R. W., Almaini O., Hartley W. G., McLure R. J., Dunlop J. S., Foucaud S., Conselice C. J., Simpson C., Cirasuolo M., Bradshaw E. J., 2011. MNRAS, **413**, 1678. *Galaxy environments in the UKIDSS Ultra Deep Survey.*

Civano F., Elvis M., Brusa M., Comastri A., Salvato M., Zamorani G., Aldcroft T., Bongiorno A., Capak P., Cappelluti N., Cisternas M., Fiore F., Fruscione A., Hao H., Kartaltepe J., Koekemoer A., Gilli R., Impey C. D., Lanzuisi G., Lusso E., Mainieri V., Miyaji T., Lilly S., Masters D., Puccetti S., Schawinski K., Scoville N. Z., Silverman J., Trump J., Urry M., Vignali C., Wright N. J., 2012. ApJS, **201**, 30. *The Chandra COSMOS Survey. III. Optical and Infrared Identification of X-Ray Point Sources.*

Civano F., Marchesi S., Comastri A., Urry M. C., Elvis M., Cappelluti N., Puccetti S., Brusa M., Zamorani G., Hasinger G., Aldcroft T., Alexander D. M., Allevato V., Brunner H., Capak P., Finoguenov A., Fiore F., Fruscione A., Gilli R., Glotfelty K., Griffiths R. E., Hao H., Harrison F. A., Jahnke K., Kartaltepe J., Karim A., LaMassa S. M., Lanzuisi G., Miyaji T., Ranalli P., Salvato M., Sargent M., Scoville N. J., Schawinski K., Schinnerer E., Silverman J., Smolcic V., Stern D., Toft S., Trakhtenbrot B., Treister E., Vignali C., 2016. ApJ, **819**, 62. *The Chandra Cosmos Legacy Survey: Overview and Point Source Catalog.*

Clowe D., Bradač M., Gonzalez A. H., Markevitch M., Randall S. W., Jones C., Zaritsky D., 2006. ApJ, **648**, L109. *A Direct Empirical Proof of the Existence of Dark Matter.*

Coil A. L., Mendez A. J., Eisenstein D. J., Moustakas J., 2017. ApJ, **838**, 87. *PRIMUS+DEEP2: The Dependence of Galaxy Clustering on Stellar Mass and Specific Star Formation Rate at 0.2 ¡ z ¡ 1.2.*

Coil A. L. *The Large-Scale Structure of the Universe*, 387. 2013.

Conselice C. J., Twite J. W., Palamara D. P., Hartley W., 2018. ApJ, **863**, 42. *The Halo Masses of Galaxies to z 3: A Hybrid Observational and Theoretical Approach.*

Conselice C. J., Rajgor S., Myers R., 2008. MNRAS, **386**, 909. *The structures of distant galaxies - I. Galaxy structures and the merger rate to z ˜ 3 in the Hubble Ultra-Deep Field.*

Conselice C. J., 2014. ARA&A, **52**, 291. *The Evolution of Galaxy Structure Over Cosmic Time.*

Cooke E. A., Hatch N. A., Muldrew S. I., Rigby E. E., Kurk J. D., 2014. MNRAS, **440**, 3262. *A $z = 2.5$ protocluster associated with the radio galaxy MRC 2104-242: star formation and differing mass functions in dense environments.*

Cooper M. C., Newman J. A., Coil A. L., Croton D. J., Gerke B. F., Yan R., Davis M., Faber S. M., Guhathakurta P., Koo D. C., Weiner B. J., Willmer C. N. A., 2007. MNRAS, **376**, 1445. *The DEEP2 galaxy redshift survey: evolution of the colour-density relation at 0.4 ¡ z ¡ 1.35.*

Cowie L. L., Songaila A., 1977. Nature, **266**, 501. *Thermal evaporation of gas within galaxies by a hot intergalactic medium.*

Croom S. M., Boyle B. J., Shanks T., Smith R. J., Miller L., Outram P. J., Loaring N. S., Hoyle F., da Ângela J., 2005. MNRAS, **356**, 415. *The 2dF QSO Redshift Survey - XIV. Structure and evolution from the two-point correlation function.*

Croton D. J., Springel V., White S. D. M., De Lucia G., Frenk C. S., Gao L., Jenkins A., Kauffmann G., Navarro J. F., Yoshida N., 2006. MNRAS, **365**, 11. *The many lives of active galactic nuclei: cooling flows, black holes and the luminosities and colours of galaxies.*

Darvish B., Mobasher B., Sobral D., Rettura A., Scoville N., Faisst A., Capak P., 2016. ApJ, **825**, 113. *The Effects of the Local Environment and Stellar Mass on Galaxy Quenching to z 3.*

Davis M., Efstathiou G., Frenk C. S., White S. D. M., 1985. ApJ, **292**, 371. *The evolution of large-scale structure in a universe dominated by cold dark matter.*

De Lucia G., Springel V., White S. D. M., Croton D., Kauffmann G., 2006. MNRAS, **366**, 499. *The formation history of elliptical galaxies.*

Dekel A., Sari R., Ceverino D., 2009. ApJ, **703**, 785. *Formation of Massive Galaxies at High Redshift: Cold Streams, Clumpy Disks, and Compact Spheroids.*

Diamond-Stanic A. M., Moustakas J., Tremonti C. A., Coil A. L., Hickox R. C., Robaina A. R., Rudnick G. H., Sell P. H., 2012. ApJ, **755(2)**, L26. *High-velocity Outflows without AGN Feedback: Eddington-limited Star Formation in Compact Massive Galaxies.*

Digby-North J. A., Nandra K., Laird E. S., Steidel C. C., Georgakakis A., Bogosavljević M., Erb D. K., Shapley A. E., Reddy N. A., Aird J., 2010. MNRAS, **407**, 846. *Excess AGN activity in the $z = 2.30$ Protocluster in HS 1700+64.*

Dressler A., Smail I., Poggianti B. M., Butcher H., Couch W. J., Ellis R. S., Oemler, Jr. A., 1999. ApJS, **122**, 51. *A Spectroscopic Catalog of 10 Distant Rich Clusters of Galaxies.*

Dressler A., Thompson I. B., Shectman S. A., 1985. ApJ, **288**, 481. *Statistics of emission-line galaxies in rich clusters.*

Dressler A., 1980. ApJ, **236**, 351. *Galaxy morphology in rich clusters - Implications for the formation and evolution of galaxies.*

Efstathiou G., 2000. MNRAS, **317**, 697. *A model of supernova feedback in galaxy formation.*

Eftekharzadeh S., Myers A. D., White M., Weinberg D. H., Schneider D. P., Shen Y., Font-Ribera A., Ross N. P., Paris I., Streblyanska A., 2015. MNRAS, **453**, 2779. *Clustering of intermediate redshift quasars using the final SDSS III-BOSS sample.*

Einstein A., 1916. *Annalen der Physik*, **354**, 769. *Die Grundlage der allgemeinen Relativitätstheorie.*

Ellison S. L., Patton D. R., Mendel J. T., Scudder J. M., 2011. MNRAS, **418**, 2043. *Galaxy pairs in the Sloan Digital Sky Survey - IV. Interactions trigger active galactic nuclei.*

Ellison S. L., Mendel J. T., Scudder J. M., Patton D. R., Palmer M. J. D., 2013. MNRAS, **430**, 3128. *Galaxy pairs in the Sloan Digital Sky Survey - VII. The merger-luminous infrared galaxy connection.*

Elvis M., Maccacaro T., Wilson A. S., Ward M. J., Penston M. V., Fosbury R. A. E., Perola G. C., 1978. MNRAS, **183**, 129. *Seyfert galaxies as X-ray sources.*

Event Horizon Telescope Collaboration, Akiyama K., Alberdi A., Alef W., Asada K., Azulay R., Baczko A.-K., Ball D., Baloković M., Barrett J., et al., 2019. ApJ, **875**, L6. *First M87 Event Horizon Telescope Results. VI. The Shadow and Mass of the Central Black Hole.*

Faber S. M., Willmer C. N. A., Wolf C., Koo D. C., Weiner B. J., Newman J. A., Im M., Coil A. L., Conroy C., Cooper M. C., Davis M., Finkbeiner D. P., Gerke B. F., Gebhardt K., Groth E. J., Guhathakurta P., Harker J., Kaiser N., Kassin S., Kleinheinrich M., Konidaris N. P., Kron R. G., Lin L., Luppino G., Madgwick D. S., Meisenheimer K., Noeske K. G., Phillips A. C., Sarajedini V. L., Schiavon R. P., Simard L., Szalay A. S., Vogt N. P., Yan R., 2007. ApJ, **665**, 265. *Galaxy Luminosity Functions to z˜1 from DEEP2 and COMBO-17: Implications for Red Galaxy Formation.*

Farouki R., Shapiro S. L., 1981. ApJ, **243**, 32. *Computer simulations of environmental influences on galaxy evolution in dense clusters. II - Rapid tidal encounters.*

Fath E. A., 1909. *Lick Observatory Bulletin*, **5**, 71. *The spectra of some spiral nebulae and globular star clusters.*

Ferrarese L., Merritt D., 2000. ApJ, **539**, L9. *A Fundamental Relation between Supermassive Black Holes and Their Host Galaxies.*

Finkelstein D., 1958. *Phys. Rev.*, **110**, 965. *Past-Future Asymmetry of the Gravitational Field of a Point Particle.*

Fontanot F., Somerville R. S., De Lucia G., Monaco P., Santini P., 2009. *Monthly Notices of the Royal Astronomical Society*, **397(4)**, 1776. *The many manifestations of downsizing: hierarchical galaxy formation models confront observations.*

Ford H. C., Harms R. J., Tsvetanov Z. I., Hartig G. F., Dressel L. L., Kriss G. A., Bohlin R. C., Davidsen A. F., Margon B., Kochhar A. K., 1994. ApJ, **435**, L27. *Narrowband HST images of M87: Evidence for a disk of ionized gas around a massive black hole.*

Franceschini A., Hasinger G., Miyaji T., Malquori D., 1999. MNRAS, **310**, L5. *On the relationship between galaxy formation and quasar evolution.*

Furusawa H., Kosugi G., Akiyama M., Takata T., Sekiguchi K., Tanaka I., Iwata I., Kajisawa M., Yasuda N., Doi M., Ouchi M., Simpson C., Shimasaku K., Yamada T., Furusawa J., Morokuma T., Ishida C. M., Aoki K., Fuse T., Imanishi M., Iye M., Karoji H., Kobayashi N., Kodama T., Komiyama Y., Maeda Y., Miyazaki S., Mizumoto Y., Nakata F., Noumaru J., Ogasawara R., Okamura S., Saito T., Sasaki T., Ueda Y., Yoshida M., 2008. ApJS, **176**, 1. *The Subaru/XMM-Newton Deep Survey (SXDS). II. Optical Imaging and Photometric Catalogs.*

Galametz A., Stern D., Eisenhardt P. R. M., Brodwin M., Brown M. J. I., Dey A., Gonzalez A. H., Jannuzi B. T., Moustakas L. A., Stanford S. A., 2009. ApJ, **694**, 1309. *The Cosmic Evolution of Active Galactic Nuclei in Galaxy Clusters.*

García-Vergara C., Hennawi J. F., Barrientos L. F., Rix H.-W., 2017. ApJ, **848**, 7. *Strong Clustering of Lyman Break Galaxies around Luminous Quasars at Z 4.*

Gebhardt K., Bender R., Bower G., Dressler A., Faber S. M., Filippenko A. V., Green R., Grillmair C., Ho L. C., Kormendy J., Lauer T. R., Magorrian J., Pinkney J., Richstone D., Tremaine S., 2000. ApJ, **539**, L13. *A Relationship between Nuclear Black Hole Mass and Galaxy Velocity Dispersion.*

Gillessen S., Eisenhauer F., Trippe S., Alexander T., Genzel R., Martins F., Ott T., 2009. ApJ, **692**, 1075. *Monitoring Stellar Orbits Around the Massive Black Hole in the Galactic Center.*

Giodini S., Finoguenov A., Pierini D., Zamorani G., Ilbert O., Lilly S., Peng Y., Scoville N., Tanaka M., 2012. A&A, **538**, A104. *The galaxy stellar mass function of X-ray detected groups. Environmental dependence of galaxy evolution in the COSMOS survey.*

Giovanelli R., Haynes M. P., 1985. ApJ, **292**, 404. *Gas deficiency in cluster galaxies - A comparison of nine clusters.*

Gisler G. R., 1978. MNRAS, **183**, 633. *Clusters of galaxies and the statistics of emission-line galaxies.*

Gómez P. L., Nichol R. C., Miller C. J., Balogh M. L., Goto T., Zabludoff A. I., Romer A. K., Bernardi M., Sheth R., Hopkins A. M., Castander F. J., Connolly A. J., Schneider D. P., Brinkmann J., Lamb D. Q., SubbaRao M., York D. G., 2003. ApJ, **584**, 210. *Galaxy Star Formation as a Function of Environment in the Early Data Release of the Sloan Digital Sky Survey.*

Goulding A. D., Alexander D. M., 2009. MNRAS, **398**, 1165. *Towards a complete census of AGN in nearby Galaxies: a large population of optically unidentified AGN.*

Goulding A. D., Forman W. R., Hickox R. C., Jones C., Murray S. S., Paggi A., Ashby M. L. N., Coil A. L., Cooper M. C., Huang J.-S., Kraft R., Newman J. A., Weiner B. J., Willner S. P., 2014. ApJ, **783**, 40. *Tracing the Evolution of Active Galactic Nuclei Host Galaxies over the Last 9 Gyr of Cosmic Time.*

Grogin N. A., Kocevski D. D., Faber S. M., Ferguson H. C., Koekemoer A. M., Riess A. G., Acquaviva V., Alexander D. M., Almaini O., Ashby M. L. N., Barden M., Bell E. F., Bournaud F., Brown T. M., Caputi K. I., Casertano S., Cassata P., Castellano M., Challis P., Chary R.-R., Cheung E., Cirasuolo M., Conselice C. J., Roshan Cooray A., Croton D. J., Daddi E., Dahlen T., Davé R., de Mello D. F., Dekel A., Dickinson M., Dolch T., Donley J. L., Dunlop J. S., Dutton A. A., Elbaz D., Fazio G. G., Filippenko A. V., Finkelstein S. L., Fontana A., Gardner J. P., Garnavich P. M., Gawiser E., Giavalisco M., Grazian A., Guo Y., Hathi N. P., Häussler B., Hopkins P. F., Huang J.-S., Huang K.-H., Jha S. W., Kartaltepe J. S., Kirshner R. P., Koo D. C., Lai K., Lee K.-S., Li W., Lotz J. M., Lucas R. A., Madau P., McCarthy P. J., McGrath E. J., McIntosh D. H., McLure R. J., Mobasher B., Moustakas L. A., Mozena M., Nandra K., Newman J. A., Niemi S.-M., Noeske K. G., Papovich C. J., Pentericci L., Pope A., Primack J. R., Rajan A., Ravindranath S., Reddy N. A., Renzini A., Rix H.-W., Robaina A. R., Rodney S. A., Rosario D. J., Rosati P., Salimbeni S., Scarlata C., Siana B., Simard L., Smidt J., Somerville R. S., Spinrad H., Straughn A. N., Strolger L.-G., Telford O., Teplitz H. I., Trump J. R., van der Wel A., Villforth C., Wechsler R. H., Weiner B. J., Wiklind T., Wild V., Wilson G., Wuyts S., Yan H.-J., Yun M. S., 2011. ApJS, **197**, 35. *CANDELS: The Cosmic Assembly Near-infrared Deep Extragalactic Legacy Survey.*

Groth E. J., Peebles P. J. E., 1977. ApJ, **217**, 385. *Statistical analysis of catalogs of extragalactic objects. VII - Two- and three-point correlation functions for the high-resolution Shane-Wirtanen catalog of galaxies.*

Gunn J. E., Gott, III J. R., 1972. ApJ, **176**, 1. *On the Infall of Matter Into Clusters of Galaxies and Some Effects on Their Evolution.*

Guo Q., White S., Boylan-Kolchin M., De Lucia G., Kauffmann G., Lemson G., Li C., Springel V., Weinmann S., 2011. MNRAS, **413**, 101. *From dwarf spheroidals to cD galaxies: simulating the galaxy population in a ΛCDM cosmology.*

Hardcastle M. J., Evans D. A., Croston J. H., 2007. MNRAS, **376**, 1849. *Hot and cold gas accretion and feedback in radio-loud active galaxies.*

Harrison C., 2014. *PhD thesis*, Durham University ¡EMAIL¿c.m.harrison@durham.ac.uk¡/EMAIL¿.

Hartley W. G., Almaini O., Mortlock A., Conselice C. J., Grützbauch R., Simpson C., Bradshaw E. J., Chuter R. W., Foucaud S., Cirasuolo M., Dunlop J. S., McLure R. J., Pearce H. J., 2013. MNRAS, **431**, 3045. *Studying the emergence of the red sequence through galaxy clustering: host halo masses at z ¿ 2.*

Hartley W. G., Conselice C. J., Mortlock A., Foucaud S., Simpson C., 2015. MNRAS, **451**, 1613. *Galactic conformity and central/satellite quenching, from the satellite profiles of M* galaxies at 0.4 ¡ z ¡ 1.9 in the UKIDSS UDS.*

Hatch N. A., Kurk J. D., Pentericci L., Venemans B. P., Kuiper E., Miley G. K., Röttgering H. J. A., 2011. MNRAS, **415**, 2993. *Hα emitters in z 2 protoclusters: evidence for faster evolution in dense environments.*

Hatch N. A., Wylezalek D., Kurk J. D., Stern D., De Breuck C., Jarvis M. J., Galametz A., Gonzalez A. H., Hartley W. G., Mortlock A., Seymour N., Stevens J. A., 2014. MNRAS, **445**, 280. *Why z ¿ 1 radio-loud galaxies are commonly located in protoclusters.*

Hatch N. A., Muldrew S. I., Cooke E. A., Hartley W. G., Almaini O., Simpson C. J., Conselice C. J., 2016. MNRAS, **459**, 387. *The structure and evolution of a forming galaxy cluster at z = 1.62.*

Hatch N. A., Cooke E. A., Muldrew S. I., Hartley W. G., Almaini O., Conselice C. J., Simpson C. J., 2017. MNRAS, **464**, 876. *The impact of protocluster environments at z = 1.6.*

Heckman T. M., Best P. N., 2014. ARA&A, **52**, 589. *The Coevolution of Galaxies and Supermassive Black Holes: Insights from Surveys of the Contemporary Universe.*

Henriques B. M. B., White S. D. M., Thomas P. A., Angulo R. E., Guo Q., Lemson G., Wang W., 2016. *ArXiv e-prints. Galaxy formation in the Planck cosmology - IV. Mass and environmental quenching, conformity and clustering.*

Herrera-Camus R., Tacconi L., Genzel R., Förster Schreiber N., Lutz D., Bolatto A., Wuyts S., Renzini A., Lilly S., Belli S., Übler H., Shimizu T., Davies R., Sturm E., Combes F., Freundlich J., García-Burillo S., Cox P., Burkert A., Naab T., Colina L., Saintonge A., Cooper M., Feruglio C., Weiss A., 2019. ApJ, **871**, 37. *Molecular and Ionized Gas Phases of an AGN-driven Outflow in a Typical Massive Galaxy at z 2.*

Hewett P. C., Warren S. J., Leggett S. K., Hodgkin S. T., 2006. MNRAS, **367(2)**, 454. *The UKIRT Infrared Deep Sky Survey ZY JHK photometric system: passbands and synthetic colours.*

Hewlett T., Villforth C., Wild V., Mendez-Abreu J., Pawlik M., Rowlands K., 2017. MNRAS, **470**, 755. *The redshift evolution of major merger triggering of luminous AGNs: a slight enhancement at z 2.*

Hickox R. C., Jones C., Forman W. R., Murray S. S., Kochanek C. S., Eisenstein D., Jannuzi B. T., Dey A., Brown M. J. I., Stern D., Eisenhardt P. R., Gorjian V., Brodwin M., Narayan R., Cool R. J., Kenter A., Caldwell N., Anderson M. E., 2009. ApJ, **696**, 891. *Host Galaxies, Clustering, Eddington Ratios, and Evolution of Radio, X-Ray, and Infrared-Selected AGNs.*

Hickox R. C., Mullaney J. R., Alexander D. M., Chen C.-T. J., Civano F. M., Goulding A. D., Hainline K. N., 2014. ApJ, **782**, 9. *Black Hole Variability and the Star Formation-Active Galactic Nucleus Connection: Do All Star-forming Galaxies Host an Active Galactic Nucleus?*

Hinshaw G., Larson D., Komatsu E., Spergel D. N., Bennett C. L., Dunkley J., Nolta M. R., Halpern M., Hill R. S., Odegard N., Page L., Smith K. M., Weiland J. L., Gold B., Jarosik N., Kogut A., Limon M., Meyer S. S., Tucker G. S., Wollack E., Wright E. L., 2013. ApJS, **208**, 19. *Nine-year Wilkinson Microwave Anisotropy Probe (WMAP) Observations: Cosmological Parameter Results.*

Hodgkin S. T., Irwin M. J., Hewett P. C., Warren S. J., 2009. MNRAS, **394**, 675. *The UKIRT wide field camera ZYJHK photometric system: calibration from 2MASS.*

Hopkins P. F., Hernquist L., Cox T. J., Di Matteo T., Robertson B., Springel V., 2006. ApJS, **163**, 1. *A Unified, Merger-driven Model of the Origin of Starbursts, Quasars, the Cosmic X-Ray Background, Supermassive Black Holes, and Galaxy Spheroids.*

Hopkins P. F., Cox T. J., Kereš D., Hernquist L., 2008a. ApJS, **175**, 390. *A Cosmological Framework for the Co-Evolution of Quasars, Supermassive Black Holes, and Elliptical Galaxies. II. Formation of Red Ellipticals.*

Hopkins P. F., Hernquist L., Cox T. J., Kereš D., 2008b. ApJS, **175**, 356. *A Cosmological Framework for the Co-Evolution of Quasars, Supermassive Black Holes, and Elliptical Galaxies. I. Galaxy Mergers and Quasar Activity.*

Hubble E., Humason M. L., 1931. ApJ, **74**, 43. *The Velocity-Distance Relation among Extra-Galactic Nebulae.*

Hubble E. P., 1925. ApJ, **62**. *NGC 6822, a remote stellar system.*

Hubble E. P., 1926. ApJ, **64**. *Extragalactic nebulae.*

Hubble E. P., 1936. *Realm of the Nebulae.*

Icke V., 1985. A&A, **144**, 115. *Distant encounters between disk galaxies and the origin of S 0 spirals.*

Ikeda H., Nagao T., Taniguchi Y., Matsuoka K., Kajisawa M., Akiyama M., Miyaji T., Kashikawa N., Morokuma T., Shioya Y., Enoki M., Capak P., Koekemoer A. M., Masters D., Salvato M., Sanders D. B., Schinnerer E., Scoville N. Z., 2015. ApJ, **809**, 138. *The Quasar-LBG Two-point Angular Cross-correlation Function at z˜4 in the COSMOS Field.*

Ilbert O., Arnouts S., McCracken H. J., Bolzonella M., Bertin E., Le Fèvre O., Mellier Y., Zamorani G., Pellò R., Iovino A., Tresse L., Le Brun V., Bottini D., Garilli B., Maccagni D., Picat J. P., Scaramella R., Scodeggio M., Vettolani G., Zanichelli A., Adami C., Bardelli S., Cappi A., Charlot S., Ciliegi P., Contini T., Cucciati O., Foucaud S., Franzetti P., Gavignaud I., Guzzo L., Marano B., Marinoni C., Mazure A., Meneux B., Merighi R., Paltani S., Pollo A., Pozzetti L., Radovich M., Zucca E., Bondi M., Bongiorno A., Busarello G., de La Torre S., Gregorini L., Lamareille F., Mathez G., Merluzzi P., Ripepi V., Rizzo D., Vergani D., 2006. A&A, **457**, 841. *Accurate photometric redshifts for the CFHT legacy survey calibrated using the VIMOS VLT deep survey.*

Ilbert O., McCracken H. J., Le Fèvre O., Capak P., Dunlop J., Karim A., Renzini M. A., Caputi K., Boissier S., 2013. *Mass assembly in quiescent and star-forming galaxies since z 4 from UltraVISTA DR1 in the COSMOS field.*

Ivezić Ž., Menou K., Knapp G. R., Strauss M. A., Lupton R. H., Vanden Berk D. E., Richards G. T., Tremonti C., Weinstein M. A., Anderson S., Bahcall N. A., Becker R. H., Bernardi M., Blanton M., Eisenstein D., Fan X., Finkbeiner D., Finlator K., Frieman J., Gunn J. E., Hall P. B., Kim R. S. J., Kinkhabwala A., Narayanan V. K., Rockosi C. M., Schlegel D., Schneider D. P., Strateva I., SubbaRao M., Thakar A. R., Voges W., White R. L., Yanny B., Brinkmann J., Doi M., Fukugita M., Hennessy G. S., Munn J. A., Nichol R. C., York D. G., 2002. AJ, **124**, 2364. *Optical and Radio Properties of Extragalactic Sources Observed by the FIRST Survey and the Sloan Digital Sky Survey.*

Jarvis M. J., Bonfield D. G., Bruce V. A., Geach J. E., McAlpine K., McLure R. J., González-Solares E., Irwin M., Lewis J., Yoldas A. K., Andreon S., Cross N. J. G., Emerson J. P., Dalton G., Dunlop J. S., Hodgkin S. T., Le F. O., Karouzos M., Meisenheimer K., Oliver S., Rawlings S., Simpson C., Smail I., Smith D. J. B., Sullivan M., Sutherland W., White S. V., Zwart J. T. L., 2013. MNRAS, **428**, 1281. *The VISTA Deep Extragalactic Observations (VIDEO) survey.*

Kaiser N., 1984. ApJ, **284**, L9. *On the spatial correlations of Abell clusters.*

Kartaltepe J. S., Mozena M., Kocevski D., McIntosh D. H., Lotz J., Bell E. F., Faber S., Ferguson H., Koo D., Bassett R., Bernyk M., Blancato K., Bournaud F., Cassata P., Castellano M., Cheung E., Conselice C. J., Croton D., Dahlen T., de Mello D. F., DeGroot L., Donley J., Guedes J., Grogin N., Hathi N., Hilton M., Hollon B., Koekemoer A., Liu N., Lucas R. A., Martig M., McGrath E., McPartland C., Mobasher B., Morlock A., O'Leary E., Peth M., Pforr J., Pillepich A., Rosario D., Soto E., Straughn A., Telford O., Sunnquist B., Trump J., Weiner B., Wuyts S., Inami H., Kassin S., Lani C., Poole G. B., Rizer Z., 2015. ApJS, **221**, 11. *CANDELS Visual Classifications: Scheme, Data Release, and First Results.*

Kauffmann G., Heckman T. M., Tremonti C., Brinchmann J., Charlot S., White S. D. M., Ridgway S. E., Brinkmann J., Fukugita M., Hall P. B., Ivezić Ž., Richards G. T., Schneider D. P., 2003. MNRAS, **346**, 1055. *The host galaxies of active galactic nuclei.*

Kauffmann G., White S. D. M., Heckman T. M., Ménard B., Brinchmann J., Charlot S., Tremonti C., Brinkmann J., 2004. MNRAS, **353**, 713. *The environmental dependence of the relations between stellar mass, structure, star formation and nuclear activity in galaxies.*

Kauffmann G., Li C., Zhang W., Weinmann S., 2013. MNRAS, **430**, 1447. *A re-examination of galactic conformity and a comparison with semi-analytic models of galaxy formation.*

Kauffmann G., Li C., Heckman T. M., 2010. MNRAS, **409**, 491. *The accretion of gas on to galaxies as traced by their satellites.*

Kawinwanichakij L., Papovich C., Quadri R. F., Tran K.-V. H., Spitler L. R., Kacprzak G. G., Labbé I., Straatman C. M. S., Glazebrook K., Allen R., Cowley M., Davé R., Dekel A., Ferguson H. C., Hartley W. G., Koekemoer A. M., Koo D. C., Lu Y., Mehrtens N., Nanayakkara T., Persson S. E., Rees G., Salmon B., Tilvi V., Tomczak A. R., van Dokkum P., 2014. ApJ, **792**, 103. *The Distribution of Satellites around Massive Galaxies at 1 ¡ z ¡ 3 in ZFOURGE/CANDELS: Dependence on Star Formation Activity.*

Kellermann K. I., Sramek R., Schmidt M., Shaffer D. B., Green R., 1989. AJ, **98**, 1195. *VLA observations of objects in the Palomar Bright Quasar Survey.*

Kereš D., Katz N., Weinberg D. H., Davé R., 2005. MNRAS, **363**, 2. *How do galaxies get their gas?*

King A., Nixon C., 2015. MNRAS, **453**, L46. *AGN flickering and chaotic accretion.*

Knapen J. H., Shlosman I., Peletier R. F., 2000. ApJ, **529**, 93. *A Subarcsecond Resolution Near-Infrared Study of Seyfert and "Normal" Galaxies. II. Morphology.*

Kocevski D. D., Lubin L. M., Gal R., Lemaux B. C., Fassnacht C. D., Squires G. K., 2009. ApJ, **690**, 295. *Chandra Observations of the cl1604 Supercluster at z = 0.9: Evidence for an Overdensity of Active Galactic Nuclei.*

Kocevski D. D., Faber S. M., Mozena M., Koekemoer A. M., Nandra K., Rangel C., Laird E. S., Brusa M., Wuyts S., Trump J. R., Koo D. C., Somerville R. S., Bell E. F., Lotz J. M., Alexander D. M., Bournaud F., Conselice C. J., Dahlen T., Dekel A., Donley J. L., Dunlop J. S., Finoguenov A., Georgakakis A., Giavalisco M., Guo Y., Grogin N. A., Hathi N. P., Juneau S., Kartaltepe J. S., Lucas R. A., McGrath E. J., McIntosh D. H., Mobasher B., Robaina A. R., Rosario D., Straughn A. N., van der Wel A., Villforth C., 2012. ApJ, **744**, 148. *CANDELS: Constraining the AGN-Merger Connection with Host Morphologies at z ˜ 2.*

Kocevski D. D., Brightman M., Nandra K., Koekemoer A. M., Salvato M., Aird J., Bell E. F., Hsu L.-T., Kartaltepe J. S., Koo D. C., Lotz J. M., McIntosh D. H., Mozena M., Rosario D., Trump J. R., 2015. ApJ, **814**, 104. *Are Compton-thick AGNs the Missing Link between Mergers and Black Hole Growth?*

Kocevski D. D., Barro G., Faber S. M., Dekel A., Somerville R. S., Young J. A., Williams C. C., McIntosh D. H., Georgakakis A., Hasinger G., Nandra K., Civano F., Alexander D. M., Almaini O., Conselice C. J., Donley J. L., Ferguson H. C., Giavalisco M., Grogin N. A., Hathi N., Hawkins M., Koekemoer A. M., Koo D. C., McGrath E. J., Mobasher B., Pérez González P. G., Pforr J., Primack J. R., Santini P., Stefanon M., Trump J. R., van der Wel A., Wuyts S., Yan H., 2017. ApJ, **846**, 112. *CANDELS: Elevated Black Hole Growth in the Progenitors of Compact Quiescent Galaxies at z 2.*

Kocevski D. D., Hasinger G., Brightman M., Nandra K., Georgakakis A., Cappelluti N., Civano F., Li Y., Li Y., Aird J., Alexander D. M., Almaini O., Brusa M., Buchner J., Comastri A., Conselice C. J., Dickinson M. A., Finoguenov A., Gilli R., Koekemoer A. M., Miyaji T., Mullaney J. R., Papovich C., Rosario D., Salvato M., Silverman J. D., Somerville R. S., Ueda Y., 2018. ApJS, **236**, 48. *X-UDS: The Chandra Legacy Survey of the UKIDSS Ultra Deep Survey Field.*

Kodama T., Smail I., Nakata F., Okamura S., Bower R. G., 2001. ApJ, **562**, L9. *The Transformation of Galaxies within the Large-Scale Structure around a z=0.41 Cluster.*

Koekemoer A. M., Faber S. M., Ferguson H. C., Grogin N. A., Kocevski D. D., Koo D. C., Lai K., Lotz J. M., Lucas R. A., McGrath E. J., Ogaz S., Rajan A., Riess A. G., Rodney S. A., Strolger L., Casertano S., Castellano M., Dahlen T., Dickinson M., Dolch T., Fontana A., Giavalisco M., Grazian A., Guo Y., Hathi N. P., Huang K.-H., van der Wel A., Yan H.-J., Acquaviva V., Alexander D. M., Almaini O., Ashby M. L. N., Barden M., Bell E. F., Bournaud F., Brown T. M., Caputi K. I., Cassata P., Challis P. J., Chary R.-R., Cheung E., Cirasuolo M., Conselice C. J., Roshan Cooray A., Croton D. J., Daddi E., Davé R., de Mello D. F., de Ravel L., Dekel A., Donley J. L., Dunlop J. S., Dutton A. A., Elbaz D., Fazio G. G., Filippenko A. V., Finkelstein S. L., Frazer C., Gardner J. P., Garnavich P. M., Gawiser E., Gruetzbauch R., Hartley W. G., Häussler B., Herrington J., Hopkins P. F., Huang J.-S., Jha S. W., Johnson A., Kartaltepe J. S., Khostovan A. A., Kirshner R. P., Lani C., Lee K.-S., Li W., Madau P., McCarthy P. J., McIntosh D. H., McLure R. J., McPartland C., Mobasher B., Moreira H., Mortlock A., Moustakas L. A., Mozena M., Nandra K., Newman J. A., Nielsen J. L., Niemi S., Noeske K. G., Papovich C. J., Pentericci L., Pope A., Primack J. R., Ravindranath S., Reddy N. A., Renzini A., Rix H.-W., Robaina A. R., Rosario D. J., Rosati P., Salimbeni S., Scarlata C., Siana B., Simard L., Smidt J., Snyder D., Somerville R. S., Spinrad H., Straughn A. N., Telford O., Teplitz H. I., Trump J. R., Vargas C., Villforth C., Wagner C. R., Wandro P., Wechsler R. H., Weiner B. J., Wiklind T., Wild V., Wilson G., Wuyts S., Yun M. S., 2011. ApJS, **197**, 36. *CANDELS: The Cosmic Assembly Near-infrared Deep Extragalactic Legacy Survey - The Hubble Space Telescope Observations, Imaging Data Products, and Mosaics.*

Kormendy J., Ho L. C., 2013. ARA&A, **51**, 511. *Coevolution (Or Not) of Supermassive Black Holes and Host Galaxies.*

Kormendy J., 2000. *ArXiv Astrophysics e-prints. Monsters at the Heart of Galaxy Formation.*

Koutoulidis L., Plionis M., Georgantopoulos I., Fanidakis N., 2013. MNRAS, **428**, 1382. *Clustering, bias and the accretion mode of X-ray-selected AGN.*

Koutoulidis L., Georgantopoulos I., Mountrichas G., Plionis M., Georgakakis A., Akylas A., Rovilos E., 2018. MNRAS, **481**, 3063. *Dependence of clustering of X-ray AGN on obscuration.*

Krishnan C., Hatch N. A., Almaini O., Kocevski D., Cooke E. A., Hartley W. G., Hasinger G., Maltby D. T., Muldrew S. I., Simpson C., 2017. MNRAS, **470**, 2170. *Enhancement of AGN in a protocluster at $z = 1.6$.*

Krumpe M., Miyaji T., Coil A. L., Aceves H., 2012. ApJ, **746**, 1. *The Spatial Clustering of ROSAT All-Sky Survey Active Galactic Nuclei. III. Expanded Sample and Comparison with Optical Active Galactic Nuclei.*

Lacey C., Cole S., 1993. MNRAS, **262**, 627. *Merger rates in hierarchical models of galaxy formation.*

Laigle C., McCracken H. J., Ilbert O., Hsieh B. C., Davidzon I., Capak P., Hasinger G., Silverman J. D., Pichon C., Coupon J., Aussel H., Le Borgne D., Caputi K., Cassata P., Chang Y.-Y., Civano F., Dunlop J., Fynbo J., Kartaltepe J. S., Koekemoer A., Le Fèvre O., Le Floc'h E., Leauthaud A., Lilly S., Lin L., Marchesi S., Milvang-Jensen B., Salvato M., Sanders D. B., Scoville N., Smolcic V., Stockmann M., Taniguchi Y., Tasca L., Toft S., Vaccari M., Zabl J., 2016. ApJS, **224**, 24. *The COSMOS2015 Catalog: Exploring the 1 ¡ z ¡ 6 Universe with Half a Million Galaxies.*

Landy S. D., Szalay A. S., 1993. ApJ, **412**, 64. *Bias and variance of angular correlation functions.*

Larson R. B., Tinsley B. M., Caldwell C. N., 1980. ApJ, **237**, 692. *The evolution of disk galaxies and the origin of S0 galaxies.*

Lawrence A., Warren S. J., Almaini O., Edge A. C., Hambly N. C., Jameson R. F., Lucas P., Casali M., Adamson A., Dye S., Emerson J. P., Foucaud S., Hewett P., Hirst P., Hodgkin S. T., Irwin M. J., Lodieu N., McMahon R. G., Simpson C., Smail I., Mortlock D., Folger M., 2007. MNRAS, **379**, 1599. *The UKIRT Infrared Deep Sky Survey (UKIDSS).*

Leauthaud A., Tinker J., Bundy K., Behroozi P. S., Massey R., Rhodes J., George M. R., Kneib J.-P., Benson A., Wechsler R. H., Busha M. T., Capak P., Cortês M., Ilbert O., Koekemoer A. M., Le Fèvre O., Lilly S., McCracken H. J., Salvato M., Schrabback T., Scoville N., Smith T., Taylor J. E., 2012. ApJ, **744**, 159. *New Constraints on the Evolution of the Stellar-to-dark Matter Connection: A Combined Analysis of Galaxy-Galaxy Lensing, Clustering, and Stellar Mass Functions from z = 0.2 to z =1.*

Lehmer B. D., Alexander D. M., Geach J. E., Smail I., Basu-Zych A., Bauer F. E., Chapman S. C., Matsuda Y., Scharf C. A., Volonteri M., Yamada T., 2009. ApJ, **691**, 687. *The Chandra Deep Protocluster Survey: Evidence for an Enhancement of AGN Activity in the SSA22 Protocluster at z = 3.09.*

Lehmer B. D., Lucy A. B., Alexander D. M., Best P. N., Geach J. E., Harrison C. M., Hornschemeier A. E., Matsuda Y., Mullaney J. R., Smail I., Sobral D., Swinbank A. M., 2013. ApJ, **765**, 87. *Concurrent Supermassive Black Hole and Galaxy Growth: Linking Environment and Nuclear Activity in z = 2.23 Hα Emitters.*

Lewis I., Balogh M., De Propris R., Couch W., Bower R., Offer A., Bland-Hawthorn J., Baldry I. K., Baugh C., Bridges T., Cannon R., Cole S., Colless M., Collins C., Cross N., Dalton G., Driver S. P., Efstathiou G., Ellis R. S., Frenk C. S., Glazebrook K., Hawkins E., Jackson C., Lahav O., Lumsden S., Maddox S., Madgwick D., Norberg P., Peacock J. A., Percival W., Peterson B. A., Sutherland W., Taylor K., 2002. MNRAS, **334**, 673. *The 2dF Galaxy Redshift Survey: the environmental dependence of galaxy star formation rates near clusters.*

Li C., Kauffmann G., Jing Y. P., White S. D. M., Börner G., Cheng F. Z., 2006. MNRAS, **368**, 21. *The dependence of clustering on galaxy properties.*

Lidman C., Iacobuta G., Bauer A. E., Barrientos L. F., Cerulo P., Couch W. J., Delaye L., Demarco R., Ellingson E., Faloon A. J., Gilbank D., Huertas-Company M., Mei S., Meyers J., Muzzin A., Noble A., Nantais J., Rettura A., Rosati P., Sánchez-Janssen R., Strazzullo V., Webb T. M. A., Wilson G., Yan R., Yee H. K. C., 2013. MNRAS, **433(1)**, 825. *The importance of major mergers in the build up of stellar mass in brightest cluster galaxies at z = 1.*

Limber D. N., 1953. ApJ, **117**, 134. *The Analysis of Counts of the Extragalactic Nebulae in Terms of a Fluctuating Density Field.*

Lintott C. J., Schawinski K., Slosar A., Land K., Bamford S., Thomas D., Raddick M. J., Nichol R. C., Szalay A., Andreescu D., Murray P., Vandenberg J., 2008. MNRAS, **389**, 1179. *Galaxy Zoo: morphologies derived from visual inspection of galaxies from the Sloan Digital Sky Survey.*

Lotz J. M., Papovich C., Faber S. M., Ferguson H. C., Grogin N., Guo Y., Kocevski D., Koekemoer A. M., Lee K.-S., McIntosh D., Momcheva I., Rudnick G., Saintonge A., Tran K.-V., van der Wel A., Willmer C., 2013. ApJ, **773**, 154. *Caught in the Act: The Assembly of Massive Cluster Galaxies at* $z = 1.62$.

Madau P., Dickinson M., 2014. ARA&A, **52**, 415. *Cosmic Star-Formation History.*

Madau P., Rees M. J., 2001. ApJ, **551**, L27. *Massive Black Holes as Population III Remnants.*

Magliocchetti M., Popesso P., Brusa M., Salvato M., Laigle C., McCracken H. J., Ilbert O., 2017. MNRAS, **464**, 3271. *The clustering properties of radio-selected AGN and star-forming galaxies up to redshifts z 3.*

Malmquist K. G., 1922. *Meddelanden fran Lunds Astronomiska Observatorium Serie I*, **100**, 1. *On some relations in stellar statistics.*

Malmquist K. G., 1925. *Meddelanden fran Lunds Astronomiska Observatorium Serie I*, **106**, 1. *A contribution to the problem of determining the distribution in space of the stars.*

Marchesi S., Civano F., Elvis M., Salvato M., Brusa M., Comastri A., Gilli R., Hasinger G., Lanzuisi G., Miyaji T., Treister E., Urry C. M., Vignali C., Zamorani G., Allevato V., Cappelluti N., Cardamone C., Finoguenov A., Griffiths R. E., Karim A., Laigle C., LaMassa S. M., Jahnke K., Ranalli P., Schawinski K., Schinnerer E., Silverman J. D., Smolcic V., Suh H., Trakhtenbrot B., 2016. ApJ, **817**, 34. *The Chandra COSMOS Legacy survey: optical/IR identifications.*

Martini P., Miller E. D., Brodwin M., Stanford S. A., Gonzalez A. H., Bautz M., Hickox R. C., Stern D., Eisenhardt P. R., Galametz A., Norman D., Jannuzi B. T., Dey A., Murray S., Jones C., Brown M. J. I., 2013. ApJ, **768**, 1. *The Cluster and Field Galaxy Active Galactic Nucleus Fraction at* $z = 1\text{-}1.5$*: Evidence for a Reversal of the Local Anticorrelation between Environment and AGN Fraction.*

Martini P., Sivakoff G. R., Mulchaey J. S., 2009. ApJ, **701**, 66. *The Evolution of Active Galactic Nuclei in Clusters of Galaxies to Redshift 1.3.*

Marulli F., Bolzonella M., Branchini E., Davidzon I., de la Torre S., Granett B. R., Guzzo L., Iovino A., Moscardini L., Pollo A., Abbas U., Adami C., Arnouts S., Bel J., Bottini D., Cappi A., Coupon J., Cucciati O., De Lucia G., Fritz A., Franzetti P., Fumana M., Garilli B., Ilbert O., Krywult J., Le Brun V., Le Fèvre O., Maccagni D., Małek K., McCracken H. J., Paioro L., Polletta M., Schlagenhaufer H., Scodeggio M., Tasca L. A. M., Tojeiro R., Vergani D., Zanichelli A., Burden A., Di Porto C., Marchetti A., Marinoni C., Mellier Y., Nichol R. C., Peacock J. A., Percival W. J., Phleps S., Wolk M., Zamorani G., 2013. A&A, **557**, A17.

The VIMOS Public Extragalactic Redshift Survey (VIPERS) . Luminosity and stellar mass dependence of galaxy clustering at 0.5 ¡ z ¡ 1.1.

Masters K. L., Mosleh M., Romer A. K., Nichol R. C., Bamford S. P., Schawinski K., Lintott C. J., Andreescu D., Campbell H. C., Crowcroft B., Doyle I., Edmondson E. M., Murray P., Raddick M. J., Slosar A., Szalay A. S., Vandenberg J., 2010. MNRAS, **405**, 783. *Galaxy Zoo: passive red spirals.*

McCracken H. J., Milvang-Jensen B., Dunlop J., Franx M., Fynbo J. P. U., Le Fèvre O., Holt J., Caputi K. I., Goranova Y., Buitrago F., Emerson J. P., Freudling W., Hudelot P., López-Sanjuan C., Magnard F., Mellier Y., Møller P., Nilsson K. K., Sutherland W., Tasca L., Zabl J., 2012. A&A, **544**, A156. *UltraVISTA: a new ultra-deep near-infrared survey in COSMOS.*

Mendez A. J., Coil A. L., Aird J., Skibba R. A., Diamond-Stanic A. M., Moustakas J., Blanton M. R., Cool R. J., Eisenstein D. J., Wong K. C., Zhu G., 2016. ApJ, **821**, 55. *PRIMUS + DEEP2: Clustering of X-Ray, Radio, and IR-AGNs at z0̃.7.*

Meneux B., Guzzo L., Garilli B., Le Fèvre O., Pollo A., Blaizot J., De Lucia G., Bolzonella M., Lamareille F., Pozzetti L., Cappi A., Iovino A., Marinoni C., McCracken H. J., de la Torre S., Bottini D., Le Brun V., Maccagni D., Picat J. P., Scaramella R., Scodeggio M., Tresse L., Vettolani G., Zanichelli A., Abbas U., Adami C., Arnouts S., Bardelli S., Bongiorno A., Charlot S., Ciliegi P., Contini T., Cucciati O., Foucaud S., Franzetti P., Gavignaud I., Ilbert O., Marano B., Mazure A., Merighi R., Paltani S., Pellò R., Radovich M., Vergani D., Zamorani G., Zucca E., 2008. A&A, **478**, 299. *The VIMOS-VLT Deep Survey (VVDS). The dependence of clustering on galaxy stellar mass at z ˜ 1.*

Merloni A., Heinz S., 2007. MNRAS, **381**, 589. *Measuring the kinetic power of active galactic nuclei in the radio mode.*

Merloni A., Heinz S. *Evolution of Active Galactic Nuclei*, 503. 2013.

Merritt D., 1983. ApJ, **264**, 24. *Relaxation and tidal stripping in rich clusters of galaxies. I. Evolution of the mass distribution.*

Mihos J. C., Hernquist L., 1996. ApJ, **464**, 641. *Gasdynamics and Starbursts in Major Mergers.*

Miyaji T., Zamorani G., Cappelluti N., Gilli R., Griffiths R. E., Comastri A., Hasinger G., Brusa M., Fiore F., Puccetti S., Guzzo L., Finoguenov A., 2007. ApJS, **172**, 396. *The XMM-Newton Wide-Field Survey in the COSMOS Field. V. Angular Clustering of the X-Ray Point Sources.*

Miyaji T., Krumpe M., Coil A. L., Aceves H., 2011. ApJ, **726**, 83. *The Spatial Clustering of ROSAT All-sky Survey AGNs. II. Halo Occupation Distribution Modeling of the Cross-correlation Function.*

Mo H. J., White S. D. M., 1996. MNRAS, **282**, 347. *An analytic model for the spatial clustering of dark matter haloes.*

Mo H. J., White S. D. M., 2002. MNRAS, **336**, 112. *The abundance and clustering of dark haloes in the standard ΛCDM cosmogony.*

Moore B., Katz N., Lake G., Dressler A., Oemler A., 1996. Nature, **379**, 613. *Galaxy harassment and the evolution of clusters of galaxies.*

Mortlock A., Conselice C. J., Hartley W. G., Ownsworth J. R., Lani C., Bluck A. F. L., Almaini O., Duncan K., van der Wel A., Koekemoer A. M., Dekel A., Davé R., Ferguson H. C., de Mello D. F., Newman J. A., Faber S. M., Grogin N. A., Kocevski D. D., Lai K., 2013. MNRAS, **433**, 1185. *The redshift and mass dependence on the formation of the Hubble sequence at z ¿ 1 from CANDELS/UDS.*

Mountrichas G., Georgakakis A., 2012. MNRAS, **420**, 514. *The clustering of X-ray-selected active galactic nuclei at z= 0.1.*

Mullaney J. R., Alexander D. M., Goulding A. D., Hickox R. C., 2011. MNRAS, **414**, 1082. *Defining the intrinsic AGN infrared spectral energy distribution and measuring its contribution to the infrared output of composite galaxies.*

Mullaney J. R., Pannella M., Daddi E., Alexander D. M., Elbaz D., Hickox R. C., Bournaud F., Altieri B., Aussel H., Coia D., Dannerbauer H., Dasyra K., Dickinson M., Hwang H. S., Kartaltepe J., Leiton R., Magdis G., Magnelli B., Popesso P., Valtchanov I., Bauer F. E., Brandt W. N., Del Moro A., Hanish D. J., Ivison R. J., Juneau S., Luo B., Lutz D., Sargent M. T., Scott D., Xue Y. Q., 2012. MNRAS, **419**, 95. *GOODS-Herschel: the far-infrared view of star formation in active galactic nucleus host galaxies since z 3.*

Nair P. B., Abraham R. G., 2010. ApJS, **186**, 427. *A Catalog of Detailed Visual Morphological Classifications for 14,034 Galaxies in the Sloan Digital Sky Survey.*

Oh S., Mulchaey J. S., Woo J.-H., Finoguenov A., Tanaka M., Cooper M. C., Ziparo F., Bauer F. E., Matsuoka K., 2014. ApJ, **790**, 43. *The Active Galactic Nucleus Population in X-Ray-selected Galaxy Groups at 0.5 ¡ z ¡ 1.1.*

Ostriker J. P., 1980. *Comments on Astrophysics*, **8**, 177. *Elliptical Galaxies are not Made by Merging Spiral Galaxies.*

Pacucci F., Natarajan P., Volonteri M., Cappelluti N., Urry C. M., 2017. *The Astrophysical Journal*, **850(2)**, L42. *Conditions for Optimal Growth of Black Hole Seeds.*

Padovani P., Alexander D. M., Assef R. J., De Marco B., Giommi P., Hickox R. C., Richards G. T., Smolčić V., Hatziminaoglou E., Mainieri V., Salvato M., 2017. A&A Rev., **25**, 2. *Active galactic nuclei: what's in a name?*

Papastergis E., Giovanelli R., Haynes M. P., Rodríguez-Puebla A., Jones M. G., 2013. ApJ, **776**, 43. *The Clustering of ALFALFA Galaxies: Dependence on H I Mass, Relationship with Optical Samples, and Clues of Host Halo Properties.*

Papovich C., Momcheva I., Willmer C. N. A., Finkelstein K. D., Finkelstein S. L., Tran K.-V., Brodwin M., Dunlop J. S., Farrah D., Khan S. A., Lotz J., McCarthy P., McLure R. J., Rieke M., Rudnick G., Sivanandam S., Pacaud F., Pierre M., 2010. ApJ, **716**, 1503. *A Spitzer-selected Galaxy Cluster at z = 1.62.*

Park K., Ricotti M., Natarajan P., Bogdanović T., Wise J. H., 2016. ApJ, **818**, 184. *Bulge-driven Fueling of Seed Black Holes.*

Peacock J. A., 1999. *Cosmological Physics.*

Peebles P. J. E., Schramm D. N., Turner E. L., Kron R. G., 1991. Nature, **352**, 769. *The case for the relativistic hot big bang cosmology.*

Peebles P. J. E., 1980. *The large-scale structure of the universe.*

Peng Y.-j., Lilly S. J., Kovač K., Bolzonella M., Pozzetti L., Renzini A., Zamorani G., Ilbert O., Knobel C., Iovino A., Maier C., Cucciati O., Tasca L., Carollo C. M., Silverman J., Kampczyk P., de Ravel L., Sanders D., Scoville N., Contini T., Mainieri V., Scodeggio M., Kneib J.-P., Le Fèvre O., Bardelli S., Bongiorno A., Caputi K., Coppa G., de la Torre S., Franzetti P., Garilli B., Lamareille F., Le Borgne J.-F., Le Brun V., Mignoli M., Perez Montero E., Pello R., Ricciardelli E., Tanaka M., Tresse L., Vergani D., Welikala N., Zucca E., Oesch P., Abbas U., Barnes L., Bordoloi R., Bottini D., Cappi A., Cassata P., Cimatti A., Fumana M., Hasinger G., Koekemoer A., Leauthaud A., Maccagni D., Marinoni C., McCracken H., Memeo P., Meneux B., Nair P., Porciani C., Presotto V., Scaramella R., 2010. ApJ, **721**, 193. *Mass and Environment as Drivers of Galaxy Evolution in SDSS and zCOSMOS and the Origin of the Schechter Function.*

Perlmutter S., Aldering G., Goldhaber G., Knop R. A., Nugent P., Castro P. G., Deustua S., Fabbro S., Goobar A., Groom D. E., Hook I. M., Kim A. G., Kim M. Y., Lee J. C., Nunes N. J., Pain R., Pennypacker C. R., Quimby R., Lidman C., Ellis R. S., Irwin M., McMahon R. G., Ruiz-Lapuente P., Walton N., Schaefer B., Boyle B. J., Filippenko A. V., Matheson T., Fruchter A. S., Panagia N., Newberg H. J. M., Couch W. J., Project T. S. C., 1999. ApJ, **517**, 565. *Measurements of* Ω *and* Λ *from 42 High-Redshift Supernovae.*

Phillips J. I., Wheeler C., Boylan-Kolchin M., Bullock J. S., Cooper M. C., Tollerud E. J., 2014. MNRAS, **437**, 1930. *A dichotomy in satellite quenching around L* galaxies.*

Planck Collaboration, Aghanim N., Akrami Y., Ashdown M., Aumont J., Baccigalupi C., Ballardini M., Banday A. J., Barreiro R. B., Bartolo N., Basak S., Battye R., Benabed K., Bernard J.-P., Bersanelli M., Bielewicz P., Bock J. J., Bond J. R., Borrill J., Bouchet F. R., Boulanger F., Bucher M., Burigana C., Butler R. C., Calabrese E., Cardoso J.-F., Carron J., Challinor A., Chiang H. C., Chluba J., Colombo L. P. L., Combet C., Contreras D., Crill B. P., Cuttaia F., de Bernardis P., de Zotti G., Delabrouille J., Delouis J.-M., Di Valentino E., Diego J. M., Doré O., Douspis M., Ducout A., Dupac X., Dusini S., Efstathiou G., Elsner F., Enßlin T. A., Eriksen H. K., Fantaye Y., Farhang M., Fergusson J., Fernandez-Cobos R., Finelli F., Forastieri F., Frailis M., Franceschi E., Frolov A., Galeotta S., Galli S., Ganga K., Génova-Santos R. T., Gerbino M., Ghosh T., González-Nuevo J., Górski K. M., Gratton S., Gruppuso A., Gudmundsson J. E., Hamann J., Handley W., Herranz D., Hivon E., Huang Z., Jaffe A. H., Jones W. C., Karakci A., Keihänen E., Keskitalo R., Kiiveri K., Kim J., Kisner T. S., Knox L., Krachmalnicoff N., Kunz M., Kurki-Suonio H., Lagache G., Lamarre J.-M., Lasenby A., Lattanzi M., Lawrence C. R., Le Jeune M., Lemos P., Lesgourgues J., Levrier F., Lewis A., Liguori M., Lilje P. B., Lilley M., Lindholm V., López-Caniego M., Lubin P. M., Ma Y.-Z., Macías-Pérez J. F., Maggio G., Maino D., Mandolesi N., Mangilli A., Marcos-Caballero A., Maris M., Martin P. G., Martinelli M., Martínez-González E., Matarrese S., Mauri N., McEwen J. D., Meinhold P. R., Melchiorri A., Mennella A., Migliaccio M., Millea M., Mitra S., Miville-Deschênes M.-A., Molinari D., Montier L., Morgante G., Moss A., Natoli P., Nørgaard-Nielsen H. U., Pagano L., Paoletti D., Partridge B., Patanchon G., Peiris H. V., Perrotta F., Pettorino V., Piacentini F., Polastri L., Polenta G., Puget J.-L., Rachen J. P., Reinecke M., Remazeilles M., Renzi A., Rocha G., Rosset C., Roudier G., Rubiño-Martín J. A., Ruiz-Granados B., Salvati L., Sandri M., Savelainen M., Scott D., Shellard E. P. S., Sirignano C., Sirri G., Spencer L. D., Sunyaev R., Suur-Uski A.-S., Tauber J. A., Tavagnacco D., Tenti M., Toffolatti L., Tomasi M., Trombetti T., Valenziano L., Valiviita J., Van Tent B., Vibert L., Vielva P., Villa F., Vittorio N., Wandelt B. D., Wehus I. K., White M., White S. D. M., Zacchei A., Zonca A., 2018. *arXiv e-prints. Planck 2018 results. VI. Cosmological parameters.*

Polletta M., Courvoisier T. J.-L., Hooper E. J., Wilkes B. J., 2000. A&A, **362**, 75. *The far-infrared emission of radio loud and radio quiet quasars.*

Polletta M., Tajer M., Maraschi L., Trinchieri G., Lonsdale C. J., Chiappetti L., Andreon S., Pierre M., Le Fèvre O., Zamorani G., Maccagni D., Garcet O., Surdej J., Franceschini A., Alloin D., Shupe D. L., Surace J. A., Fang F., Rowan-Robinson M., Smith H. E., Tresse L., 2007. ApJ, **663**, 81. *Spectral Energy Distributions of Hard X-Ray Selected Active Galactic Nuclei in the XMM-Newton Medium Deep Survey.*

Popesso P., Biviano A., Rodighiero G., Baronchelli I., Salvato M., Saintonge A., Finoguenov A., Magnelli B., Gruppioni C., Pozzi F., Lutz D., Elbaz D., Altieri B., Andreani P., Aussel H., Berta S., Capak P., Cava A., Cimatti A., Coia D., Daddi E., Dannerbauer H., Dickinson M., Dasyra K., Fadda D., Förster Schreiber N., Genzel R., Hwang H. S., Kartaltepe J., Ilbert O., Le Floch E., Leiton R., Magdis G., Nordon R., Patel S., Poglitsch A., Riguccini L., Sanchez Portal M., Shao L., Tacconi L., Tomczak A., Tran K., Valtchanov I., 2012. A&A, **537**, A58. *The evolution of the star formation activity per halo mass up to redshift ˜1.6 as seen by Herschel.*

Powell M. C., Cappelluti N., Urry C. M., Koss M., Finoguenov A., Ricci C., Trakhtenbrot B., Allevato V., Ajello M., Oh K., Schawinski K., Secrest N., 2018. ApJ, **858**, 110. *The Swift/BAT AGN Spectroscopic Survey. IX. The Clustering Environments of an Unbiased Sample of Local AGNs.*

Pozzetti L., Bolzonella M., Zucca E., Zamorani G., Lilly S., Renzini A., Moresco M., Mignoli M., Cassata P., Tasca L., Lamareille F., Maier C., Meneux B., Halliday C., Oesch P., Vergani D., Caputi K., Kovač K., Cimatti A., Cucciati O., Iovino A., Peng Y., Carollo M., Contini T., Kneib J.-P., Le Févre O., Mainieri V., Scodeggio M., Bardelli S., Bongiorno A., Coppa G., de la Torre S., de Ravel L., Franzetti P., Garilli B., Kampczyk P., Knobel C., Le Borgne J.-F., Le Brun V., Pellò R., Perez Montero E., Ricciardelli E., Silverman J. D., Tanaka M., Tresse L., Abbas U., Bottini D., Cappi A., Guzzo L., Koekemoer A. M., Leauthaud A., Maccagni D., Marinoni C., McCracken H. J., Memeo P., Porciani C., Scaramella R., Scarlata C., Scoville N., 2010. A&A, **523**, A13. *zCOSMOS - 10k-bright spectroscopic sample. The bimodality in the galaxy stellar mass function: exploring its evolution with redshift.*

Ramella M., Giuricin G., Mardirossian F., Mezzetti M., 1987. A&A, **188**, 1. *Morphological population and first-ranked galaxy morphology in loose groups of galaxies.*

Ravindranath S., Ferguson H. C., Conselice C., Giavalisco M., Dickinson M., Chatzichristou E., de Mello D., Fall S. M., Gardner J. P., Grogin N. A., Hornschemeier A., Jogee S., Koekemoer A., Kretchmer C., Livio M., Mobasher B., Somerville R., 2004. ApJ, **604**, L9. *The Evolution of Disk Galaxies in the GOODS-South Field: Number Densities and Size Distribution.*

Richstone D. O., 1976. ApJ, **204**, 642. *Collisions of galaxies in dense clusters. II - Dynamical evolution of cluster galaxies.*

Riess A. G., Filippenko A. V., Challis P., Clocchiatti A., Diercks A., Garnavich P. M., Gilliland R. L., Hogan C. J., Jha S., Kirshner R. P., Leibundgut B., Phillips M. M., Reiss D., Schmidt B. P., Schommer R. A., Smith R. C., Spyromilio J., Stubbs C., Suntzeff N. B., Tonry J., 1998. AJ, **116**, 1009. *Observational Evidence from Supernovae for an Accelerating Universe and a Cosmological Constant.*

Roche N., Eales S. A., 1999. MNRAS, **307**, 703. *The angular correlation function and hierarchical moments of ˜70000 faint galaxies to R=23.5.*

Rosario D. J., Burtscher L., Davies R., Genzel R., Lutz D., Tacconi L. J., 2013. ApJ, **778**, 94. *The Mid-infrared Emission of Narrow-line Active Galactic Nuclei: Star Formation, Nuclear Activity, and Two Populations Revealed by Wise.*

Ross A. J., Brunner R. J., 2009. MNRAS, **399**, 878. *Halo-model analysis of the clustering of photometrically selected galaxies from SDSS.*

Ross N. P., Shen Y., Strauss M. A., Vanden Berk D. E., Connolly A. J., Richards G. T., Schneider D. P., Weinberg D. H., Hall P. B., Bahcall N. A., Brunner R. J., 2009. ApJ, **697**, 1634. *Clustering of Low-redshift (z ¡= 2.2) Quasars from the Sloan Digital Sky Survey.*

Rubin V. C., Ford, Jr. W. K., Thonnard N., 1978. ApJ, **225**, L107. *Extended rotation curves of high-luminosity spiral galaxies. IV - Systematic dynamical properties, SA through SC.*

Rybicki G. B., Lightman A. P., 1979. *Radiative processes in astrophysics.*

Saez C., Lehmer B. D., Bauer F. E., Stern D., Gonzales A., Rreza I., Alexander D. M., Matsuda Y., Geach J. E., Harrison F. A., Hayashino T., 2015. MNRAS, **450**, 2615. *An extragalactic spectroscopic survey of the SSA22 field.*

Sanders D. B., Salvato M., Aussel H., Ilbert O., Scoville N., Surace J. A., Frayer D. T., Sheth K., Helou G., Brooke T., Bhattacharya B., Yan L., Kartaltepe J. S., Barnes J. E., Blain A. W., Calzetti D., Capak P., Carilli C., Carollo C. M., Comastri A., Daddi E., Ellis R. S., Elvis M., Fall S. M., Franceschini A., Giavalisco M., Hasinger G., Impey C., Koekemoer A., Le Fèvre O., Lilly S., Liu M. C., McCracken H. J., Mobasher B., Renzini A., Rich M., Schinnerer E., Shopbell P. L., Taniguchi Y., Thompson D. J., Urry C. M., Williams J. P., 2007. ApJS, **172**, 86. *S-COSMOS: The Spitzer Legacy Survey of the Hubble Space Telescope ACS 2 deg^2 COSMOS Field I: Survey Strategy and First Analysis.*

Santini P., Rosario D. J., Shao L., Lutz D., Maiolino R., Alexander D. M., Altieri B., Andreani P., Aussel H., Bauer F. E., Berta S., Bongiovanni A., Brandt W. N., Brusa M., Cepa J., Cimatti A., Daddi E., Elbaz D., Fontana A., Förster Schreiber N. M., Genzel R., Grazian A., Le Floc'h E., Magnelli B., Mainieri V., Nordon R., Pérez Garcia A. M., Poglitsch A., Popesso P., Pozzi F., Riguccini L., Rodighiero G., Salvato M., Sanchez-Portal M., Sturm E., Tacconi L. J., Valtchanov I., Wuyts S., 2012. A&A, **540**, A109. *Enhanced star formation rates in AGN hosts with respect to inactive galaxies from PEP-Herschel observations.*

Schawinski K., Lintott C., Thomas D., Sarzi M., Andreescu D., Bamford S. P., Kaviraj S., Khochfar S., Land K., Murray P., Nichol R. C., Raddick M. J., Slosar A., Szalay A., VandenBerg J., Yi S. K., 2009. MNRAS, **396**, 818. *Galaxy Zoo: a sample of blue early-type galaxies at low redshift*.*

Schawinski K., Koss M., Berney S., Sartori L. F., 2015. MNRAS, **451**, 2517. *Active galactic nuclei flicker: an observational estimate of the duration of black hole growth phases of* 10^5 *yr.*

Schmidt M., Green R. F., 1983. ApJ, **269**, 352. *Quasar evolution derived from the Palomar bright quasar survey and other complete quasar surveys.*

Schmidt M., 1963. Nature, **197**, 1040. *3C 273 : A Star-Like Object with Large Red-Shift.*

Schwarzschild K., 1916. *Sitzungsberichte der Königlich Preußischen Akademie der Wissenschaften (Berlin), 1916, Seite 189-196. Über das Gravitationsfeld eines Massenpunktes nach der Einsteinschen Theorie.*

Scoville N., Aussel H., Brusa M., Capak P., Carollo C. M., Elvis M., Giavalisco M., Guzzo L., Hasinger G., Impey C., Kneib J.-P., LeFevre O., Lilly S. J., Mobasher B., Renzini A., Rich R. M., Sanders D. B., Schinnerer E., Schminovich D., Shopbell P., Taniguchi Y., Tyson N. D., 2007. ApJS, **172**, 1. *The Cosmic Evolution Survey (COSMOS): Overview.*

Sérsic J. L., 1963. *Boletin de la Asociacion Argentina de Astronomia La Plata Argentina*, **6**, 41. *Influence of the atmospheric and instrumental dispersion on the brightness distribution in a galaxy.*

Seyfert C. K., 1943. ApJ, **97**, 28. *Nuclear Emission in Spiral Nebulae.*

Shapley H., 1933. *Proceedings of the National Academy of Science*, **19**, 591. *Luminosity Distribution and Average Density of Matter in Twenty-Five Groups of Galaxies.*

Shen Y., Mulchaey J. S., Raychaudhury S., Rasmussen J., Ponman T. J., 2007. ApJ, **654**, L115. *Differences in the AGN Populations of Groups and Clusters: Clues to AGN Evolution.*

Shen Y., Strauss M. A., Ross N. P., Hall P. B., Lin Y.-T., Richards G. T., Schneider D. P., Weinberg D. H., Connolly A. J., Fan X., Hennawi J. F., Shankar F., Vanden Berk D. E., Bahcall N. A., Brunner R. J., 2009. ApJ, **697**, 1656. *Quasar Clustering from SDSS DR5: Dependences on Physical Properties.*

Silk J., Mamon G. A., 2012. *Research in Astronomy and Astrophysics*, **12**, 917. *The current status of galaxy formation.*

Silk J., Rees M. J., 1998. A&A, **331**, L1. *Quasars and galaxy formation.*

Silverman J. D., Green P. J., Barkhouse W. A., Kim D.-W., Kim M., Wilkes B. J., Cameron R. A., Hasinger G., Jannuzi B. T., Smith M. G., Smith P. S., Tananbaum H., 2008. ApJ, **679**, 118. *The Luminosity Function of X-Ray-selected Active Galactic Nuclei: Evolution of Supermassive Black Holes at High Redshift.*

Simpson C., Westoby P., Arumugam V., Ivison R., Hartley W., Almaini O., 2013. MNRAS, **433**, 2647. *The prevalence of AGN feedback in massive galaxies at z 1.*

Smith R. E., Peacock J. A., Jenkins A., White S. D. M., Frenk C. S., Pearce F. R., Thomas P. A., Efstathiou G., Couchman H. M. P., 2003. MNRAS, **341**, 1311. *Stable clustering, the halo model and non-linear cosmological power spectra.*

Smolčić V., 2009. ApJ, **699**, L43. *The Radio AGN Population Dichotomy: Green Valley Seyferts Versus Red Sequence Low-Excitation Active Galactic Nuclei.*

Socolovsky M., Almaini O., Hatch N. A., Wild V., Maltby D. T., Hartley W. G., Simpson C., 2018. MNRAS, **476**, 1242. *The enhancement of rapidly quenched galaxies in distant clusters at 0.5 ¡ z ¡ 1.0.*

Springel V., Di Matteo T., Hernquist L., 2005. ApJ, **620**, L79. *Black Holes in Galaxy Mergers: The Formation of Red Elliptical Galaxies.*

Springel V., Frenk C. S., White S. D. M., 2006. Nature, **440**, 1137. *The large-scale structure of the Universe.*

Stanley F., Harrison C. M., Alexander D. M., Swinbank A. M., Aird J. A., Del Moro A., Hickox R. C., Mullaney J. R., 2015. MNRAS, **453**, 591. *A remarkably flat relationship between the average star formation rate and AGN luminosity for distant X-ray AGN.*

Steidel C. C., Adelberger K. L., Shapley A. E., Pettini M., Dickinson M., Giavalisco M., 2003. ApJ, **592**, 728. *Lyman Break Galaxies at Redshift z ˜ 3: Survey Description and Full Data Set.*

Steidel C. C., Shapley A. E., Pettini M., Adelberger K. L., Erb D. K., Reddy N. A., Hunt M. P., 2004. ApJ, **604**, 534. *A Survey of Star-forming Galaxies in the 1.4¡˜Z¡˜ 2.5 Redshift Desert: Overview.*

Strateva I., Ivezić Ž., Knapp G. R., Narayanan V. K., Strauss M. A., Gunn J. E., Lupton R. H., Schlegel D., Bahcall N. A., Brinkmann J., Brunner R. J., Budavári T., Csabai I., Castander F. J., Doi M., Fukugita M., Győry Z., Hamabe M., Hennessy G., Ichikawa T., Kunszt P. Z., Lamb D. Q., McKay T. A., Okamura S., Racusin J., Sekiguchi M., Schneider D. P., Shimasaku K., York D., 2001. AJ, **122**, 1861. *Color Separation of Galaxy Types in the Sloan Digital Sky Survey Imaging Data.*

Sutherland W., Saunders W., 1992. MNRAS, **259**, 413. *On the likelihood ratio for source identification.*

Tanaka M., Finoguenov A., Ueda Y., 2010. ApJ, **716**, L152. *A Spectroscopically Confirmed X-ray Cluster at z = 1.62 with a Possible Companion in the Subaru/XMM-Newton Deep Field.*

Toomre A., Toomre J., 1972. ApJ, **178**, 623. *Galactic Bridges and Tails.*

Tremaine S., Gebhardt K., Bender R., Bower G., Dressler A., Faber S. M., Filippenko A. V., Green R., Grillmair C., Ho L. C., Kormendy J., Lauer T. R., Magorrian J., Pinkney J., Richstone D., 2002. ApJ, **574**, 740. *The Slope of the Black Hole Mass versus Velocity Dispersion Correlation.*

Turner T. J., Weaver K. A., Mushotzky R. F., Holt S. S., Madejski G. M., 1991. ApJ, **381**, 85. *Einstein Observatory SSS and MPC observations of the complex X-ray spectra of Seyfert galaxies.*

Tzanavaris P., Gallagher S. C., Hornschemeier A. E., Fedotov K., Eracleous M., Brandt W. N., Desjardins T. D., Charlton J. C., Gronwall C., 2014. ApJS, **212**, 9. *A Chandra-Swift View of Point Sources in Hickson Compact Groups: High AGN Fraction but a Dearth of Strong AGNs.*

Ueda Y., Watson M. G., Stewart I. M., Akiyama M., Schwope A. D., Lamer G., Ebrero J., Carrera F. J., Sekiguchi K., Yamada T., Simpson C., Hasinger G., Mateos S., 2008. ApJS, **179**, 124. *The Subaru/XMM-Newton Deep Survey (SXDS). III. X-Ray Data.*

Umehata H., Tamura Y., Kohno K., Ivison R. J., Alexander D. M., Geach J. E., Hatsukade B., Hughes D. H., Ikarashi S., Kato Y., Izumi T., Kawabe R., Kubo M., Lee M., Lehmer B., Makiya R., Matsuda Y., Nakanishi K., Saito T., Smail I., Yamada T., Yamaguchi Y., Yun M., 2015. ApJ, **815(1)**, L8. *ALMA Deep Field in SSA22: A Concentration of Dusty Starbursts in a z = 3.09 Protocluster Core.*

Urry C. M., Padovani P., 1995. PASP, **107**, 803. *Unified Schemes for Radio-Loud Active Galactic Nuclei.*

van Breukelen C., Simpson C., Rawlings S., Akiyama M., Bonfield D., Clewley L., Jarvis M. J., Mauch T., Readhead T., Stobbart A.-M., Swinbank M., Watson M., 2009. MNRAS, **395**, 11. *Evidence of a link between the evolution of clusters and their AGN fraction.*

Villforth C., Hamilton T., Pawlik M. M., Hewlett T., Rowlands K., Herbst H., Shankar F., Fontana A., Hamann F., Koekemoer A., Pforr J., Trump J., Wuyts S., 2017. MNRAS, **466**, 812. *Host galaxies of luminous z 0.6 quasars: major mergers are not prevalent at the highest AGN luminosities.*

Volonteri M., Haardt F., Madau P., 2003. ApJ, **582**, 559. *The Assembly and Merging History of Supermassive Black Holes in Hierarchical Models of Galaxy Formation.*

Volonteri M., 2010. A&A Rev., **18**, 279. *Formation of supermassive black holes.*

Wake D. A., Whitaker K. E., Labbé I., van Dokkum P. G., Franx M., Quadri R., Brammer G., Kriek M., Lundgren B. F., Marchesini D., Muzzin A., 2011. ApJ, **728**, 46. *Galaxy Clustering in the NEWFIRM Medium Band Survey: The Relationship Between Stellar Mass and Dark Matter Halo Mass at 1 ¡ z ¡ 2.*

Wang W., White S. D. M., 2012. MNRAS, **424**, 2574. *Satellite abundances around bright isolated galaxies.*

Wang Y., Yang X., Mo H. J., Li C., van den Bosch F. C., Fan Z., Chen X., 2008. MNRAS, **385**, 1511. *Probing the intrinsic shape and alignment of dark matter haloes using SDSS galaxy groups.*

Weedman D. W., Hao L., Higdon S. J. U., Devost D., Wu Y., Charmandaris V., Brandl B., Bass E., Houck J. R., 2005. ApJ, **633**, 706. *Mid-Infrared Spectra of Classical AGNs Observed with the Spitzer Space Telescope.*

Weinmann S. M., van den Bosch F. C., Yang X., Mo H. J., 2006. MNRAS, **366**, 2. *Properties of galaxy groups in the Sloan Digital Sky Survey - I. The dependence of colour, star formation and morphology on halo mass.*

White S. D. M., Frenk C. S., Davis M., 1983. ApJ, **274**, L1. *Clustering in a neutrino-dominated universe.*

Wild V., Walcher C. J., Johansson P. H., Tresse L., Charlot S., Pollo A., Le Fèvre O., de Ravel L., 2009. MNRAS, **395**, 144. *Post-starburst galaxies: more than just an interesting curiosity.*

Wild V., Almaini O., Cirasuolo M., Dunlop J., McLure R., Bowler R., Ferreira J., Bradshaw E., Chuter R., Hartley W., 2014. MNRAS, **440**, 1880. *A new method for classifying galaxy SEDs from multiwavelength photometry.*

Wild V., Almaini O., Dunlop J., Simpson C., Rowlands K., Bowler R., Maltby D., McLure R., 2016. MNRAS, **463(1)**, 832. *The evolution of post-starburst galaxies from z=2 to 0.5.*

Wild V., Heckman T., Charlot S., 2010. MNRAS, **405**, 933. *Timing the starburst-AGN connection.*

Wilkinson A., Almaini O., Chen C.-C., Smail I., Arumugam V., Blain A., Chapin E. L., Chapman S. C., Conselice C. J., Cowley W. I., Dunlop J. S., Farrah D., Geach J., Hartley W. G., Ivison R. J., Maltby D. T., Michałowski M. J., Mortlock A., Scott D., Simpson C., Simpson J. M., van der Werf P., Wild V., 2017. MNRAS, **464**, 1380. *The SCUBA-2 Cosmology Legacy Survey: the clustering of submillimetre galaxies in the UKIDSS UDS field.*

Wilson E. B., 1927. *Journal of the American Statistical Association*, **22(158)**, 209. *Probable Inference, the Law of Succession, and Statistical Inference.*

Wirth A., 1983. ApJ, **274**, 541. *Galaxy content of selected southern groups - Elliptical galaxies at low density.*

Yang G., Brandt W. N., Darvish B., Chen C.-T. J., Vito F., Alexander D. M., Bauer F. E., Trump J. R., 2018. MNRAS, **480**, 1022. *Does black-hole growth depend on the cosmic environment?*

Yang X., Mo H. J., van den Bosch F. C., 2006. ApJ, **638**, L55. *Observational Evidence for an Age Dependence of Halo Bias.*

York D. G., Adelman J., Anderson, Jr. J. E., Anderson S. F., Annis J., Bahcall N. A., Bakken J. A., Barkhouser R., Bastian S., Berman E., Boroski W. N., Bracker S., Briegel C., Briggs J. W., Brinkmann J., Brunner R., Burles S., Carey L., Carr M. A., Castander F. J., Chen B., Colestock P. L., Connolly A. J., Crocker J. H., Csabai I., Czarapata P. C., Davis J. E., Doi M., Dombeck T., Eisenstein D., Ellman N., Elms B. R., Evans M. L., Fan X., Federwitz G. R., Fiscelli L., Friedman S., Frieman J. A., Fukugita M., Gillespie B., Gunn J. E., Gurbani V. K., de Haas E., Haldeman M., Harris F. H., Hayes J., Heckman T. M., Hennessy G. S., Hindsley R. B., Holm S., Holmgren D. J., Huang C.-h., Hull C., Husby D., Ichikawa S.-I., Ichikawa T., Ivezić Ž., Kent S., Kim R. S. J., Kinney E., Klaene M., Kleinman A. N., Kleinman S., Knapp G. R., Korienek J., Kron R. G., Kunszt P. Z., Lamb D. Q., Lee B., Leger R. F., Limmongkol S., Lindenmeyer C., Long D. C., Loomis C., Loveday J., Lucinio R., Lupton R. H., MacKinnon B., Mannery E. J., Mantsch P. M., Margon B., McGehee P., McKay T. A., Meiksin A., Merelli A., Monet D. G., Munn J. A., Narayanan V. K., Nash T., Neilsen E., Neswold R., Newberg H. J., Nichol R. C., Nicinski T., Nonino M., Okada N., Okamura S., Ostriker J. P., Owen R., Pauls A. G., Peoples J., Peterson R. L., Petravick D., Pier J. R., Pope A., Pordes R., Prosapio A., Rechenmacher R., Quinn T. R., Richards G. T., Richmond M. W., Rivetta C. H., Rockosi C. M., Ruthmansdorfer K., Sandford D., Schlegel D. J., Schneider D. P., Sekiguchi M., Sergey G., Shimasaku K., Siegmund W. A., Smee S., Smith J. A., Snedden S., Stone R., Stoughton C., Strauss M. A., Stubbs C., SubbaRao M., Szalay A. S., Szapudi I., Szokoly G. P., Thakar A. R., Tremonti C., Tucker D. L., Uomoto A., Vanden Berk D., Vogeley M. S., Waddell P., Wang S.-i., Watanabe M., Weinberg D. H., Yanny B., Yasuda N., SDSS Collaboration, 2000. AJ, **120**, 1579. *The Sloan Digital Sky Survey: Technical Summary.*

Younger J. D., Cox T. J., Seth A. C., Hernquist L., 2007. ApJ, **670**, 269. *Antitruncated Stellar Disks via Minor Mergers.*

Zehavi I., Zheng Z., Weinberg D. H., Frieman J. A., Berlind A. A., Blanton M. R., Scoccimarro R., Sheth R. K., Strauss M. A., Kayo I., Suto Y., Fukugita M., Nakamura O., Bahcall N. A., Brinkmann J., Gunn J. E., Hennessy G. S., Ivezić Ž., Knapp G. R., Loveday J., Meiksin A., Schlegel D. J., Schneider D. P., Szapudi I., Tegmark M., Vogeley M. S., York D. G., SDSS Collaboration, 2005. ApJ, **630**, 1. *The Luminosity and Color Dependence of the Galaxy Correlation Function.*

Zheng Z., Coil A. L., Zehavi I., 2007. ApJ, **667**, 760. *Galaxy Evolution from Halo Occupation Distribution Modeling of DEEP2 and SDSS Galaxy Clustering.*

Zwicky F., 1933. *Helvetica Physica Acta*, **6**, 110. *Die Rotverschiebung von extragalaktischen Nebeln.*

Zwicky F., 1937. ApJ, **86**, 217. *On the Masses of Nebulae and of Clusters of Nebulae.*